Acta Physica Hungarica

VOLUME 72 · NUMBER 1, 1992

Akadémiai Kiadó, Budapest

ACTA PHYS. HUNG. APAHAQ 72 (1) 1-122 (1992) HU ISSN 0231-4428

ACTA PHYSICA HUNGARICA

A JOURNAL OF THE HUNGARIAN ACADEMY OF SCIENCES

EDITED BY
I. KOVÁCS

Acta Physica publishes original papers on subjects in physics. Papers are accepted in English, French, German and Russian.

Acta Physica is published in two yearly volumes (4 issues each) by

AKADÉMIAI KIADÓ
Publishing House of the Hungarian Academy of Sciences
H–1117 Budapest, Prielle Kornélia u. 19–35.

Subscription information

Orders should be addressed to

AKADÉMIAI KIADÓ
H–1519 Budapest, P.O. Box 245

Acta Physica Hungarica is abstracted/indexed in Chemical Abstracts, Mathematical Reviews, Science Abstracts, Physics Briefs, Risk Abstracts, Engineering Information, Inc. EI Page One Database

CONTENTS

Acta Physica Hungarica 72 (1), pp. 3–5 (1992)

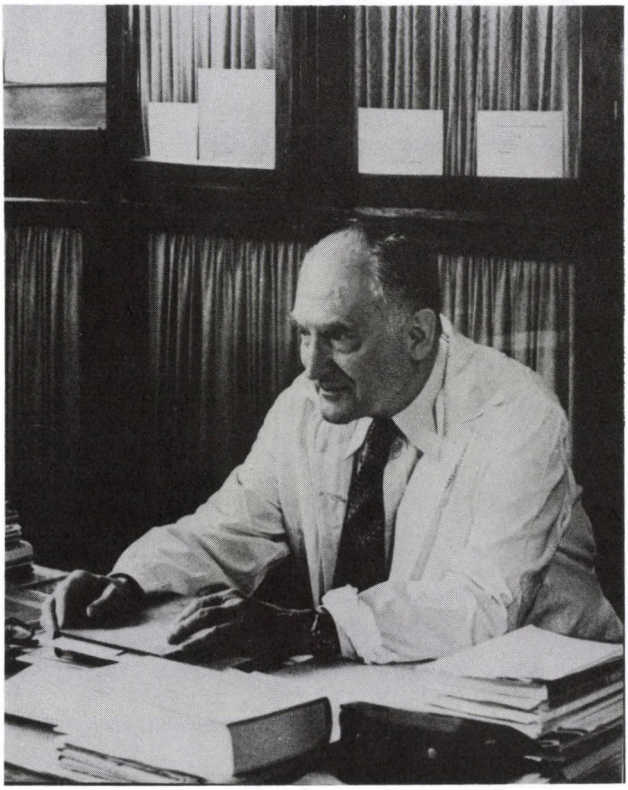

80th birthday of Professor Imre Tarján

Professor IMRE TARJÁN, Member of the Hungarian Academy of Sciences and former president of the Department for Mathematical and Physical Sciences, celebrated his 80th birthday on 26th of July, 1992.

Imre Tarján demonstrated his talent already as a secondary school student, winning the all-Hungarian competition in physics in 1930. An interesting fact: the winner of a similar competition several years before was Edward Teller, the Hungarian-born American physicist. At the University Imre Tarján was a member of the Eötvös College, an outstanding institution of the pre- and postwar period. Having graduated he began his scientific career working with the famous Hungarian physicist, Professor Zoltán Gyulai in Debrecen. This auspicious beginning was interrupted practically for ten years by World War II and the difficulties of the postwar reconstruction.

Acta Physica Hungarica 72, 1992
Akadémiai Kiadó, Budapest

Professor Tarján is a scientist who has achieved outstanding results in two apparently largely different fields; moreover, in both fields he founded scientific schools. One of his fields is solid state physics, or more precisely, crystal physics, the other is molecular biophysics. Professor Tarján was among the first to recognize and to carry out pioneering work in order to develop the idea that in solids (as well as in biological macromolecular systems) a basic understanding of the physical properties (biological functions) can be achieved only by a thorough knowledge of the atomic and molecular order and of the structural defects acting against this order.

While still a student of Zoltán Gyulai, in the thirties he began to investigate structural defects generated by ionizing radiation, especially by X-rays, in alkali halide crystals. Developing these studies he made conclusions concerning the mechanism of generation and the structure of crystal defects, their interaction with other lattice defects (dislocations, impurities), and he pointed out the role of the defect in some macroscopic properties. With his co-workers he was successful producing extremely pure alkali halide crystals; this success became the starting point for obtaining further interesting results both in Hungary and abroad.

One of his outstanding results was realized in the early fifties, when, together with Zoltán Gyulai, he was among the first in the world to grow artificial quartz crystals. At about the same time he and his co-workers produced NaI(Tl), anthracene, naphthalene, and other single crystals for the detection of nuclear radiation.

In the mid-sixties he extended methods and approaches usually applied in solid state physics to the investigation of biological macromolecular systems, e.g. he was one of the first to use stochastic models to characterize processes of photodamage in the nucleoproteins of bacteriophages and also to describe the interaction of ions or antibiotics with the membranes of bacteria. One of the conclusions of this work was that the protection against photodimerization of a nucleic acid having a double-helix structure is linked with the twisted arrangement of its structural elements.

Professor Tarján always considered the application of results obtained in basic research for solving practical problems as an important aspect of his work. He is one of the protagonists, on an international scale, to advocate application-oriented crystal growth. He contributed towards the foundation of nuclear medicine in Hungary and has been responsible for many of its developments. Some prime examples of this activity are the transfer to industry of the technology developed together with his co-workers for producing NaI(Tl) single crystals for gamma-ray detection, and the elaboration of models for a number of instruments in nuclear medicine. A result of particular importance obtained in the seventies by him and this team in applied biotechnology is the elaboration of a process for the last quantitative characterization of the phage–host bacteria interaction parameters and the development of an automatic equipment for measuring these quantities. This method, i.e. UV chemical dosimetry is applicable in environmental protection, in the pharmaceutics industry, food industry and in agriculture.

Scientific workers and physicians have a good reason to be grateful to Professor Tarján for his outstanding role in their education. He founded one of the bases of

crystal physics in Hungary, the Research Laboratory for Crystal Physics of the Hungarian Academy of Sciences. The leading scientific staff of this Laboratory acknowledges him as one of their former teachers. In the field of biophysics he had a pioneering role in the organization of interdisciplinary teams and in finding and shaping the ways and the attitudes in the collaboration of variously trained research workers. He was responsible for the founding of the Research Laboratory for Biophysics of the Hungarian Academy of Sciences where the leading scientists — experts in biology, physics and chemistry — were also his students. In the field of medical education he participated not only in the training of generations of physicians by inspiring an exact scientific way of thinking but also developed an internationally accepted system and textbook for the biophysical education of medical students.

Professor Tarján, in spite of his 80 years, is as active as few of the young in many areas including biophysical education, research of biological macromolecules and scientific public life.

His colleagues and students, Hungarian physicists and biophysicists, together with the Hungarian scientific and medical communities wish him good health and creative activity in the years to come.

József Janszky *Györgyi Rontó*

Acta Physica Hungarica 72 (1), pp. 7–12 (1992)

EFFECT OF TEMPERATURE ON THE GRAIN BOUNDARY MOVEMENTS DURING CREEP IN COPPER AND A COPPER–ZINC ALLOY

M. B. ZIKRY and K. H. GEORGY*

College for Girls, Ain-Shams University
Cairo, Egypt
**Solid State Physics Department, National Research Center*
Dokki, Cairo, Egypt

(Received 8 January 1991)

Previous work by the present authors [1] showed that the presence of second phase particles of zinc at the boundaries of copper grains blocked the absorption of lattice dislocations by these boundaries during sliding at steady state creep. This was detected from measuring the sensitivity parameter of the steady state creep rate to the applied stress at wide range, either for pure copper or for copper 28 wt% zinc solid solution. In this work we consider the effect of temperature and accordingly the redistribution and diffusion of these zinc atoms at the copper grain boundaries on this blocking phenomenon. It was found that changing the temperature from 200 °C to 400 °C did not alter the suppression of grain boundary movements and, accordingly, their cooperation to creep deformation was also suppressed.

Recently, the present authors [1] have observed that the presence of second phase particles of zinc at the boundaries of copper grains blocked the absorption of lattice dislocations by these boundaries during sliding at steady state creep, at the temperature of 200 °C. The changes of structure and the sliding of these grain boundaries during creep were found to be suppressed. In this work, we are interested in considering this observation at some other relatively high temperatures, namely 300 and 400 °C. The convenient method we used to detect this blocking effect at the boundaries is to measure the sensitivity parameter of the steady state creep rate to the applied stress at wide range, either for pure copper or for copper 28 wt% zinc solid solution.

The influence of solute atoms in alloys and solid solutions on the mobility of dislocations during sliding at high temperature creep were extensively studied and discussed previously [2–4]. The mechanisms controlling the creep rate of these materials were mainly considered to be based on dislocation dynamics. Unfortunately, little knowledge about grain boundary movements or changes of structure during creep processes were mentioned. In this work, direct experimental evidence based on measurements of the creep rate sensitivities is given to relate the interaction between the moving dislocations, the moving boundaries and the solute atoms. The role of temperature which can change the amount of solute atoms to segregate along the boundaries by diffusion was found to be of interest to be examined.

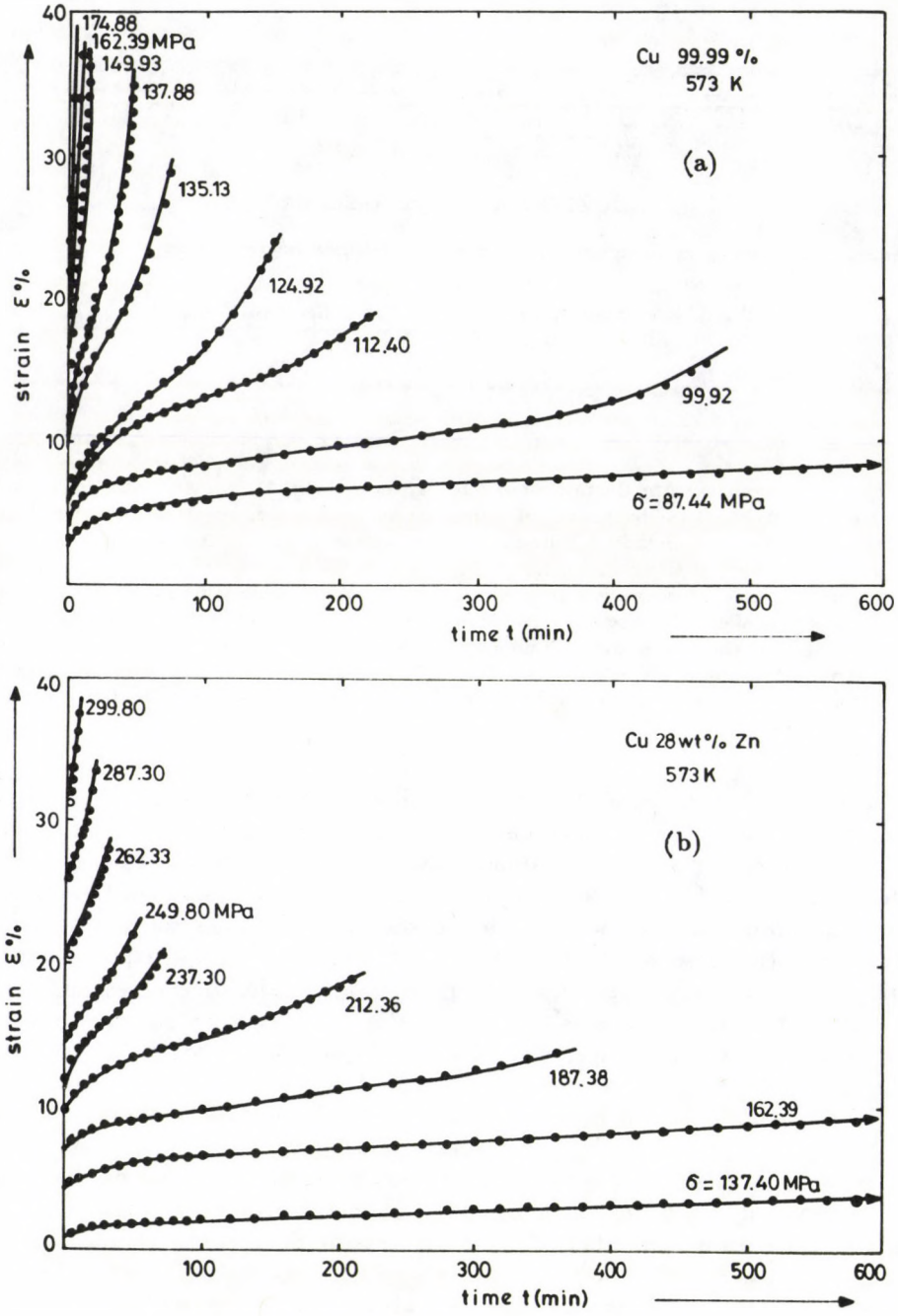

Fig. 1. Typical examples of creep curves tested at 300 °C: a) for pure copper; b) for Cu 28 wt% Zn solid solution

Samples of copper of purity 99.99 % and of alloys of homogenized composition of copper 28 wt% zinc, were used in the form of wires of circular cross section of a diameter of 1 mm. These samples were prepared carefully for creep tests and were first annealed under vacuum for 2 h at 723 K to eliminate the effect of pre-cold work. Creep tests were then carried out on both types of samples at the different temperatures, using a carefully adopted conventional type creep machine.

Figures 1a–b present typical sets of creep curves. These sets of curves are for:

a) pure copper tested at 300 °C and stress ranging from 87 to 175 MPa.

b) Cu 28 wt% Zn solid solution tested at 300 °C and applied stress ranging from 137 to 300 MPa.

All the stages of creep can be distinguished between these two sets of curves (a–b) and, accordingly, the hardening and strengthening between pure copper and the Cu–Zn solid solution at the comparable conditions of examination.

Figure 2 presents the relation between the logarithm of applied stress σ and the logarithm of steady state creep rate $\dot{\varepsilon}_s$, and allows us to determine the sensitivity parameter

$$m' = \left(\frac{\partial \ln \dot{\varepsilon}_s}{\partial \ln \sigma}\right)_T \tag{1}$$

at the different testing temperatures of 200, 300 and 400 °C, for

a) pure copper and

b) Cu 28 wt% Zn solid solution.

From the Figure it can be noticed that:

a) for pure copper the slope m' at any temperature is increasing with increasing stress and the change of temperature from 200 to 400 °C did not change this behaviour of m'.

b) for the solid solution the slope m' at any temperature is constant independent of stress, and the change of temperature from 200 to 400 °C has an effect on the values of m' considered to be negligible.

Figure 3 illustrates the change of m' with the applied stress σ. It represents an important relation concerning the sensitivity parameter of the creep rate. Figure 3a is for pure copper. It shows that m' increases regularly with stress at lower levels to reach about 5 at 100 MPa. It then begins to increase in an accelerating manner at higher stress levels to reach several orders of magnitude of about 30 at 170 MPa. This type of changes between the sensitivity parameter m' and the applied stress σ can be observed for all the testing temperatures and, generally, independent of temperature for pure copper.

In case of the Cu–Zn solid solution (Fig. 3b) quite different shape and magnitude of changes of m' with applied stress σ can be observed:

i) At any temperature in the range (200–400 °C), it is not possible to observe any change in the value of m' with the applied stress (m' = constant independent of stress).

ii) The maximum change in the values of m' with temperature in the range from 200 to 400 °C is between 4 and 7. It is not possible to estimate the exact reason illustrating this change of m' with temperature, which is considered negligible. The structural changes due to the absorption of slipping dislocations by

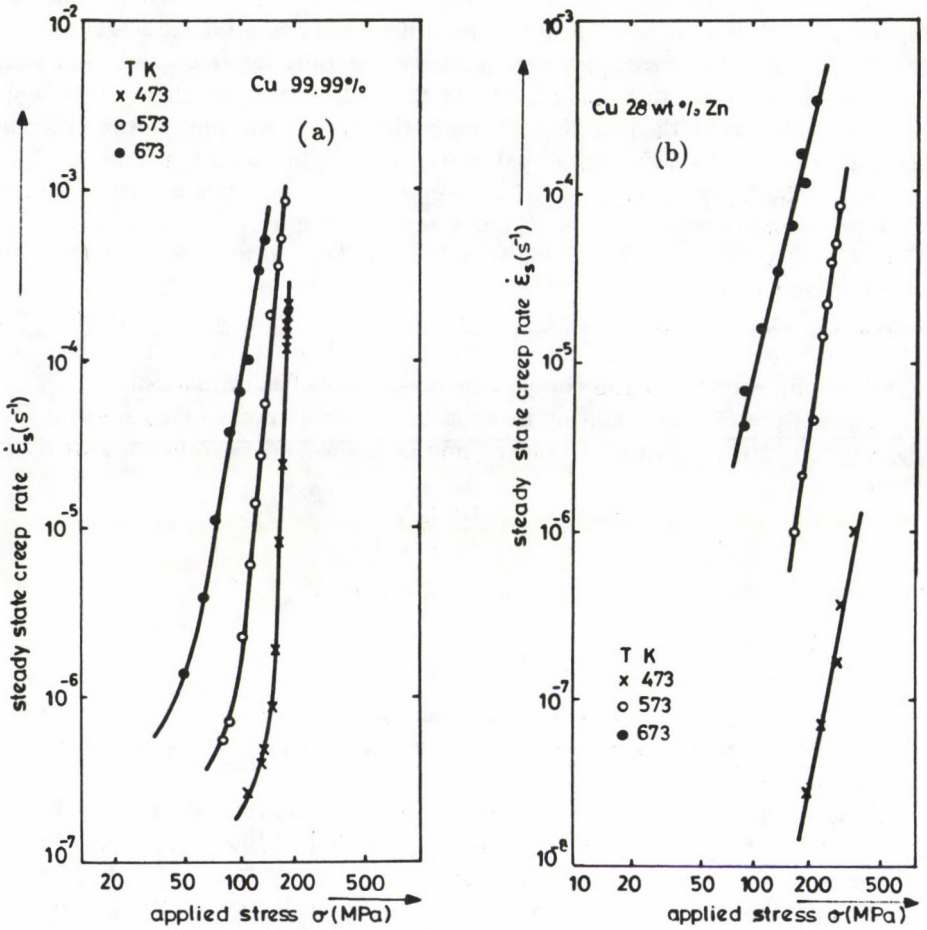

Fig. 2. Bilogarithmic relations between the steady state creep rate $\dot{\varepsilon}_s$ and the applied stress σ: a) for pure copper; b) for Cu 28 wt% Zn solid solution

grain boundaries during creep have previously been discussed [5, 6]. It was suggested that, as these moving dislocations are absorbed by grain boundaries, they dissociate into the boundaries structural dislocations and move along to cause grain boundary movements or slidings [7, 8]. Many factors affect this interaction between slipping dislocations and grain boundaries, and consequently affect the extent of boundaries cooperation in the creep process. One important factor of these that affects the rate of absorption of dislocations by grain boundaries is considered to depend on the lattice diffusion at the boundaries [9]. One important part of this diffusion at the boundaries involves the diffusion of the precipitated (or networks of) solute atoms at these boundaries.

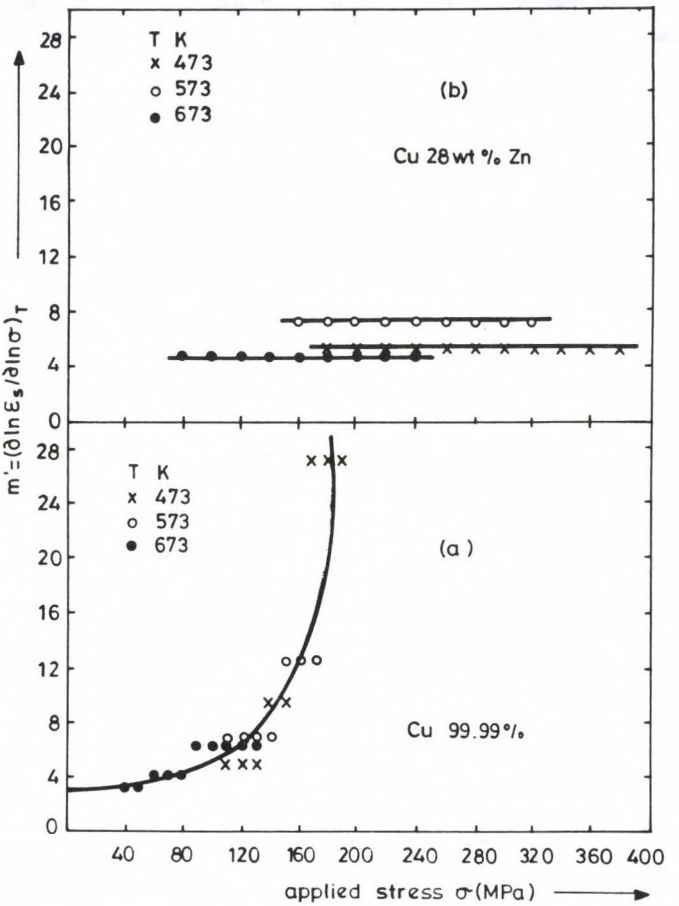

Fig. 3. Dependence of the sensitivity parameter m' on the applied stress σ: a) for pure copper; b) for Cu 28 wt% Zn solid solution

For this reason it is generally believed that in the range of temperature where the bulk diffusion is fast enough to transport a reasonable amount of solute atoms the segregation of these atoms along the boundaries can be enhanced [10]. However, although the beneficial effects of these segregated solute atoms have been well recognized since the early 1960's [11], the mechanisms through which these atoms or precipitates operate have not been completely defined, and little is known about their segregation or grain boundary precipitations and their combined effects on creep properties [10].

In a previous work on creep properties of an aluminium–copper solid solution [12] it was found that either the segregation or precipitations of copper atoms at

grain boundaries of aluminium did not prevent the moving dislocations from being absorbed and penetrating through these boundaries, which is the reason for the detectable movements and changing of structure of these boundaries during creep at any testing temperature.

In the present work on pure copper and on copper–zinc solid solution, another behaviour of zinc atoms at the grain boundaries of copper is detected. For pure copper the sensitivity parameter m' (Eq. (1)), increases first at a constant rate and then at a growing rate by increasing of applied stress σ, indicating a cooperation between grain boundary movements and creep process at any testing temperature especially at higher levels of applied stress. In case of copper–zinc solid solution, this observation differs. At any temperature, the value of the sensitivity parameter m' of the creep rate remains constant independent of stress levels. Changing of temperature in the range up to 400 °C did not change this phenomenon and its effect on the absolute values of m' was considered negligible. This was previously discussed [1] on the basis of blocking effects of grain boundaries movements as a result of the presence of zinc atoms. The zinc atoms act as pegs which suppress the displacements between boundaries [13]. At higher temperatures, the changes in the amount of zinc atoms segregated at the boundaries of copper grains by diffusion did not alter its beneficial influence in blocking the movements of these boundaries during creep. The applied stress sensitivity parameter of the steady state creep rate remains constant with the change of applied stress.

References

1. M. B. Zikry and K. H. Georgy, phys. stat. sol., *(a) 112*, K91, 1989.
2. S. Koda, K. Matsuura and S. Takahashi, J. Inst. Metals, *91*, 229, 1963.
3. M. Pahutová, T. Hostinský, J. Čadek and P. Ryš, Phil. Mag., 20, 375, 1969.
4. T. Hasegawa, S. Karashima and Y. Ikeuchi, Acta Met., *21*, 887, 1973.
5. H. Kokawa, T. Watanabe and S. Karashima, Phil. Mag., *A44*, 1239, 1981.
6. H. Kokawa, T. Watanabe and S. Karashima, Scripta Met., *17*, 1155, 1983.
7. C. A. P. Horton, J. M. Silock and G. R. Kegg, phys. stat. sol., *(a) 26*, 215, 1974.
8. R. C. Pond, D. A. Smith and P. W. J. Southerden, Phil. Mag., *A37*, 27, 1978.
9. M. Menyhárd and L. Uray, Scripta Met., *17*, 1195, 1983.
10. U. Franzoni, F. Marchetti and S. Sturlese, Scripta Met., *19*, 511, 1985.
11. R. F. Decker and J. W. Freeman, Trans. of the Met. Soc. of AIME, *218*, 277, 1960.
12. N. L. Tawfik, K. H. Georgy and T. H. Youssef, Czech. J. Physics, *41*, 855, 1991.
13. K. Suzuki, R. Tanaka and T. Mori, Scripta Met., *19*, 1005, 1985.

Acta Physica Hungarica 72 (1), pp. 13–22 (1992)

STABILITY OF TWO SUPERPOSED HOMOGENEOUS FLUIDS

R. P. SINGH and H. C. KHARE*

Department of Mathematics and Statistics, Ewing Christian College Allahabad, India

**Department of Mathematics and Statistics, University of Allahabad Allahabad, India*

(Received 2 April 1991)

The stability of two homogeneous fluids under gravitational force has been discussed. A general perturbation in the horizontal plane $z = 0$ has been taken with wave number k_x, k_y along and perpendicular to the streaming motion, respectively. It is found that critical wave number k^* lies on an ellipse in the first quadrant of k_x, k_y plane.

Introduction

Initially, Jeans [1] studied the problem of gravitational instability of a static infinite homogeneous medium. He found a critical wave number $k^*[= 4\pi G\rho/C^2]^{1/2}$ and showed that the system becomes unstable for all perturbations of wave numbers less than k^*. Here C stands for velocity of sound ρ for density of medium and G for gravitational constant. Ledoux [2] considered this problem of stability in an infinite isothermal medium and showed that the medium in unstable for perturbations propagating parallel to the plane of symmetry of the medium. Ficke [3] discussed this problem with effect of rotation. Chandrasekhar [4,5,6] reviewed the work of Jeans and showed that, when the medium is rotating with an angular velocity Ω and perturbation is propagating in perpendicular direction then the critical wave number k^* is given by

$$k^* = \left[\frac{4\pi G\rho - 4\Omega^2}{C^2}\right]^{1/2}.$$

Later Sharma and Thakur [7] considered the problem of two fluids in porous medium. Here, we propose to discuss the problem of instability of two superposed homogeneous fluids for general perturbation in horizontal plane $z = 0$. A general dispersion relation be obtained. Critical wave number k^* will be derived and some special cases will be discussed.

Mathematical formulation of the problem

The two streams of different densities are separated by the plane $z = 0$, such that in the region $z > 0$ the system is of density ρ_1 and in the region $z < 0$ the system is of density ρ_2. The streams are moving along the x axis with velocity V_1 in region $z > 0$ and V_2 in region $z < 0$. The external force on the system is the gravitational force.

Following Chandrasekhar [8] the linearized perturbation equations are

$$\rho_r \left(\frac{\partial}{\partial t} + V_r \frac{\partial}{\partial x}\right) u_r = -\frac{\partial}{\partial x}\delta p_r + \rho_r \frac{\partial}{\partial x}\delta\varphi_r, \tag{1}$$

$$\rho_r \left(\frac{\partial}{\partial t} + V_r \frac{\partial}{\partial x}\right) v_r = -\frac{\partial}{\partial y}\delta p_r + \rho_r \frac{\partial}{\partial y}\delta\varphi_r, \tag{2}$$

$$\rho_r \left(\frac{\partial}{\partial t} + V_r \frac{\partial}{\partial x}\right) w_r = -\frac{\partial}{\partial z}\delta p_r + \rho_r \frac{\partial}{\partial z}\delta\varphi_r, \tag{3}$$

$$\left(\frac{\partial}{\partial t} + V_r \frac{\partial}{\partial x}\right) \delta\rho_r = -\rho_r \left(\frac{\partial u_r}{\partial x} + \frac{\partial v_r}{\partial y} + \frac{\partial w_r}{\partial z}\right), \tag{4}$$

$$\left(\frac{\partial^2}{\partial x^2} + \frac{\partial^2}{\partial y^2} + \frac{\partial^2}{\partial z^2}\right) \delta\varphi_r = -4\pi G\delta\rho_r, \tag{5}$$

$$\left(\frac{\partial}{\partial t} + V_r \frac{\partial}{\partial x}\right) \delta\rho_r = C_r^2 \left(\frac{\partial}{\partial t} + V_r \frac{\partial}{\partial x}\right) \delta\rho_r. \tag{6}$$

Here the suffix r stands for the two regions. For $r = 1$ we have the region $z > 0$ and for $r = 2$ we have $z < 0$. (u, v, w) are components of perturbation of velocity along x, y, z axes, respectively. C_r is the velocity of sound in the medium and V_r is the streaming velocity in the region along x axis. Other symbols have their usual meanings.

We ascribe to all quantities describing the perturbation a dependence on x, y and t of the form

$$\Psi(z) e^{i(k_x x + k_y y) + nt}, \tag{7}$$

where

$$k = \sqrt{k_x^2 + k_y^2}. \tag{8}$$

Here k_x, k_y are the real numbers denoting the wave numbers of the propagation of the disturbance along x and y axes, respectively. k given by (8) is the wave number of the disturbance. $i = \sqrt{-1}$, t is symbol for time and $\psi(z)$ denotes some functions of z. n is a constant, in general a complex number, of the form $n = n_R + in_I$.

For the perturbation of the form (7) we have

$$\frac{\partial}{\partial t} = n, \quad \frac{\partial}{\partial x} = ik_x, \quad \frac{\partial}{\partial y} = ik_y, \quad \frac{\partial}{\partial z} = D$$

and

$$\frac{\partial^2}{\partial x^2} + \frac{\partial^2}{\partial y^2} + \frac{\partial^2}{\partial z^2} = D^2 - k^2. \tag{9}$$

Now writing

$$\sigma_r = n + ik_x V_r \tag{10}$$

and taking the perturbation of the form (7) we get linearized Eqs (1) to (6) as

$$\rho_r \sigma_r u_r = -ik_x \delta p_r + ik_x \rho_r \delta\phi_r, \tag{11}$$

$$\rho_r \sigma_r v_r = -ik_y \delta p_r + ik_y \rho_r \delta\phi_r, \tag{12}$$

$$\rho_r \sigma_r w_r = -D\,\delta p_r + \rho_r D\,\delta\phi_r, \tag{13}$$

$$\sigma_r \delta\rho_r = -\rho_r(ik_x u_r + ik_y v_r + Dw_r), \tag{14}$$

$$(D^2 - k^2)\delta\varphi_r = -4\pi G\delta\rho_r, \tag{15}$$

$$\delta p_r = C_r^2 \delta\rho_r. \tag{16}$$

Substituting the value of u_r, v_r and w_r from (11) and (13), respectively, in (14) and eliminating δp_r with the help of (16) we get

$$[\sigma_r^2 - (D^2 - k^2)C_r^2]\delta\rho_r = -\rho_r(D^2 - k^2)\delta\varphi_r. \tag{17}$$

Eliminating $\delta\rho_r$ from (15) and (17) we get a fourth order differential equation in $\delta\varphi_r$ as

$$(D^2 - k^2)(D^2 - \alpha_r^2)\delta\varphi_r = 0, \tag{18}$$

where

$$\alpha_r^2 = \frac{\sigma_r^2 + k^2 C_r^2 - 4\pi G\rho_r}{C_r^2}. \tag{19}$$

Solutions of the differential equation

The differential equations are solved subject to the physical conditions of the problem. The solutions are to be bounded in the two regions. This leads to the solution of (18) in the two regions giving $\delta\varphi_1$ in the region $z > 0$ and $\delta\varphi_2$ in the region $z < 0$, as

$$\delta\varphi_1 = \lambda_1 e^{-kz} + \mu_1 e^{-\alpha_1 z}, \tag{20}$$

$$\delta\varphi_2 = \lambda_2 e^{kz} + \mu_2 e^{\alpha_2 z}, \tag{21}$$

where α_1, α_2 are non-negative quantities. λ_1, μ_1, λ_2 and μ_2 are arbitrary constants in the above equations, to be determined with the help of the four boundary conditions.

Boundary condition 1:

Perturbed gravitational potential $\delta\varphi$ is continuous at $z = 0$, i.e.

$$\delta\varphi_1 = \delta\varphi_2 \quad \text{at} \quad z = 0,$$

this gives,

$$\lambda_1 + \mu_1 = \lambda_2 + \mu_2,$$

or

$$\lambda_1 + \mu_1 - \lambda_2 - \mu_2 = 0. \tag{22}$$

Boundary condition 2:
Normal derivative of the perturbed potential is continuous at $z = 0$, i.e.

$$D\delta\varphi_1 = D\delta\varphi_2 \quad \text{at} \quad z = 0,$$

this gives,

$$-k\lambda_1 - \alpha_1\mu_1 = k\lambda_2 + \alpha_2\mu_2,$$

or

$$k\lambda_1 + \alpha_1\mu_1 + k\lambda_2 + \alpha_2\mu_2 = 0. \tag{23}$$

Boundary condition 3:
Total perturbed pressure is continuous at $z = 0$, i.e.

$$\delta p_1 = \delta p_2 \quad \text{at} \quad z = 0,$$

this gives,

$$C_1^2\delta\rho_1 = C_2^2\delta\rho_2 \quad \text{at} \quad z = 0,$$

i.e.

$$C_1^2(D^2 - k^2)\delta\varphi_1 = C_2^2(D^2 - k^2)\delta\varphi_2 \quad \text{at} \quad z = 0,$$

i.e.

$$o\lambda_1 + C_1^2(\alpha_1^2 - k^2)\mu_1 + o\lambda_2 - C_2^2(\alpha_2^2 - k^2)\mu_2 = 0. \tag{24}$$

Boundary condition 4:
Normal displacement of any point is unique at the interface $z = 0$ equivalently,

$$\frac{w_1}{\sigma_1} = \frac{w_2}{\sigma_2} \quad \text{at} \quad z = 0.$$

Now from Eqs (1.13), (1.15) and (1.16) eliminating δp_r, and $\delta\rho_r$ we get

$$w_r = \frac{1}{\sigma_r}\left[1 + \frac{C_r^2}{4\pi G\rho_r}(D^2 - k^2)\right] D\delta\varphi_r.$$

Hence the above condition gives

$$\frac{1}{\sigma_1^2}\left[1 + \frac{C_1^2}{4\pi G\rho_1}(D^2 - k^2)\right] D\delta\varphi_1 = \frac{1}{\sigma_2^2}\left[1 + \frac{C_1^2}{4\pi G\rho_2}(D^2 - k^2)\right] D\delta\varphi_2 \quad \text{at} \quad z = 0,$$

i.e.

$$\frac{k}{\sigma_1^2}\lambda_1 + \frac{\alpha_1}{\sigma_1^2}\left[1 + \frac{C_1^2}{4\pi G\rho_1}(\alpha_1^2 - k^2)\right]\mu_1 + \frac{k}{\sigma_2^2}\lambda_2 + \frac{\alpha_2}{\sigma_2^2}\left[1 + \frac{C_2^2}{4\pi G\rho_2}(\alpha_2^2 - k^2)\right]\mu_2 = 0 \tag{25}$$

Writing the above linear equations in matrix form we get,

$$\begin{bmatrix} a_{11} & a_{12} & a_{13} & a_{14} \\ a_{21} & a_{22} & a_{23} & a_{24} \\ a_{31} & a_{32} & a_{33} & a_{34} \\ a_{41} & a_{42} & a_{43} & a_{44} \end{bmatrix} \begin{bmatrix} \lambda_1 \\ \mu_1 \\ \lambda_2 \\ \mu_2 \end{bmatrix} = \begin{bmatrix} 0 \\ 0 \\ 0 \\ 0 \end{bmatrix},$$

or, symbolically as

$$[a_{ij}][X_j] = [0], \tag{26}$$

where

$$\begin{aligned}
&X_1 = \lambda_1, && X_2 = \mu_1, && X_3 = \lambda_2, && X_4 = \mu_2, \\
&a_{11} = 1, && a_{12} = 1, && a_{13} = -1, && a_{14} = -1, \\
&a_{21} = k, && a_{22} = \alpha_1, && a_{23} = k, && a_{24} = \alpha_2, \\
&a_{31} = 0, && a_{32} = C_1^2(\alpha_1^2 - k^2), && a_{33} = 0, && a_{34} = -C_2^2(\alpha_2^2 - k^2), \\
&a_{41} = \frac{k}{\sigma_1^2}, && a_{42} = \frac{\alpha_1}{\sigma_1^2}\left[1 + \frac{C_1^2}{4\pi G\rho_1}(\alpha_1^2 - k^2)\right], \\
&a_{43} = \frac{k}{\sigma_2^2}, && a_{44} = \frac{\alpha_2}{\sigma_2^2}\left[1 + \frac{C_2^2}{4\pi G\rho_2}(\alpha_2^2 - k^2)\right].
\end{aligned}$$

For non trivial solutions of the Eq. (26) we must have the determinant of the coefficient equal to zero, i.e.

$$|a_{ij}| = 0. \tag{27}$$

Simplifying the above determinant we get

$$\begin{vmatrix} 2C_1^2(\alpha_1 + k), & C_2^2(\alpha_2 + k) + C_1^2(\alpha_1 + k) \\ \left(\frac{1}{\sigma_2^2} - \frac{1}{\sigma_1^2}\right) - \frac{2C_1^2\alpha_1(\alpha_1 + k)}{4\pi G\rho_1\sigma_1^2}, & \left(\frac{1}{\sigma_2^2} - \frac{1}{\sigma_1^2}\right) + \frac{1}{4\pi G}\left[\frac{C_2^2(\alpha_2 + k)}{\rho_2\sigma_2^2} - \frac{C_1^2\alpha_1(\alpha_1 + k)}{\rho_1\sigma_1^2}\right] \end{vmatrix} =$$

or

$$\left(\frac{1}{\sigma_2^2} - \frac{1}{\sigma_1^2}\right)\left[\frac{1}{C_1^2(\alpha_1 + k)} - \frac{1}{C_2^2(\alpha_2 + k)}\right] = \frac{1}{2\pi G}\left[\frac{\alpha_2}{\rho_2\sigma_2^2} + \frac{\alpha_1}{\rho_1\sigma_1^2}\right]. \tag{28}$$

Equation (28) is the dispersion relation for the problem in the most general case. Solving this and putting $n = 0$ we can get the critical wave number k^*. This k^* determines the criterion for instability. However, it is not possible, in general, to get the value of $k = k^*$ from the dispersion relation in closed form. The numerical value of k^* can be obtained in a specific physical problem. In order to get a feel of the solution, we do this in special cases of physical interest.

Special case 1:

Let the two streams be moving in opposite directions with equal velocities parallel to x axis, i.e. $\mathbf{V}_1 = V_1\mathbf{i}$, $\mathbf{V}_2 = -V_2\mathbf{i}$.

In this case

$$\sigma_1^2 = \sigma_2^2 = (n + ik_xV)^2.$$

Putting this value in Eq. (28) we get

$$\frac{\alpha_1}{\rho_1} + \frac{\alpha_2}{\rho_2} = 0. \tag{29}$$

Simplifying this equation and putting the value of α_1^2 and α_2^2 from (19) we have the above dispersion relation as

$$n(n + i2k_xV)\left[\rho_2^2C_2^2 - \rho_1^2C_1^2\right] + \left[\rho_2^2C_2^2(C_1^2 - V^2) - \rho_1^2C_1^2(C_2^2 - V^2)\right]k_x^2 + C_1^2C_2^2\left[\rho_2^2 - \rho_1^2\right]k_y^2 = 4\pi G\rho_1\rho_2\left[\rho_2C_2^2 - \rho_1C_1^2\right].$$

For discussing the marginal state when the instability sets in we put $n = 0$ in the above dispersion relation and obtain the critical wave number $k^*\left(= \sqrt{k_x^2 + k_y^2}\right)$. Thus

$$[\rho_2^2C_2^2(C_1^2 - V^2) - \rho_1^2C_1^2(C_2^2 - V^2)]k_x^2 + C_1^2C_2^2[\rho_2^2 - \rho_1^2]k_y^2 = 4\pi G\rho_1\rho_2[\rho_2C_2^2 - \rho_1C_1^2],$$

i.e.

$$\frac{k_x^2}{\Delta_1^2} + \frac{k_y^2}{\Delta_2^2} = 1, \tag{30}$$

where

$$\Delta_1^2 = \frac{4\pi G\rho_1\rho_2[\rho_2C_2^2 - \rho_1C_1^2]}{\rho_2^2C_2^2(C_1^2 - V^2) - \rho_1^2C_1^2(C_2^2 - V^2)},$$

$$\Delta_2^2 = \frac{4\pi G\rho_1\rho_2[\rho_2C_2^2 - \rho_1C_1^2]}{C_1^2C_1^2[\rho_2^2 - \rho_1^2]}.$$

We observe that when the perturbation propagates along both the axes x and y with wave numbers k_x and k_y, respectively, then the value of the critical wave number k^* lies on the elliptic orbit in the first quadrant given by Eq. (30) whose axes are $k_y = 0$ and $k_x = 0$. Thus the positive k_x, k_y plane is divided in two regions by the marginal state elliptic curve (30). One is the unstable region where $k < k^*$ and the other is the stable region where $k > k^*$.

We also see that if we have horizontal wave propagation of the perturbation along and perpendicular to the streaming motion then the criterion for the stability is different from those as it would be when the perturbation is propagating only along the streaming motion or perpendicular to the streaming motion. k_x, k_y play a combined role in deciding k^*, and it is not just by simple addition but by the rule of Eq. (30). For a given set of k_x, k_y the critical wave number $k^* = \sqrt{k_x^2 + k_y^2}$ does not mean that k_x and k_y are separately critical numbers. It is critical only when one of them is zero, i.e. when $k_x = 0$, $k^* = k_y$ or when $k_y = 0$, $k^* = k_x$.

Particular cases

1. When the perturbation is propagating only along the streaming motion, then $k_y = 0$ and $k_x = k^*$ is given by

$$k^* = \left[\frac{4\pi G\rho_1\rho_2(\rho_2 C_2^2 - \rho_1 C_1^2)}{\rho_2^2 C_2^2(C_1^2 - V^2) - \rho_1^2 C_1^2(C_2^2 - V^2)}\right]^{1/2}. \tag{31}$$

The above expression clearly shows that the determination of the stability is dependent on streaming velocity and it has destabilizing effect on the stability. k^* also depends on density and sound velocity in the medium. Similar results have been obtained by Sengar and Khare.

2. When the perturbation is propagating perpendicular to the direction of the streaming motion in the horizontal plane, then $k_x = 0$ and $k_y = k^*$ is given by

$$k^* = \left[\frac{4\pi G\rho_1\rho_2(\rho_2 C_2^2 - \rho_1 C_1^2)}{C_1^2 C_2^2(\rho_2^2 - \rho_1^2)}\right]. \tag{32}$$

This expression is free from streaming velocity showing that in this case the stability of the system is unaffected by the streaming motion.

Further considering Eq. (29) since α_1 and α_2 are non-negative, it follows that

$$\alpha_1 = \alpha_2 = 0, \tag{33}$$

i.e.

$$\frac{-k_x^2 V^2 + k^2 C_1^2 - 4\pi G\rho_1}{C_1^2} = \frac{-k_x^2 V^2 + k^2 C_2^2 - 4\pi G\rho_2}{C_2^2} = 0,$$

giving

$$\frac{k_x^2}{\frac{4\pi G\rho_1}{C_1^2 - V^2}} + \frac{k_y^2}{\frac{4\pi G\rho_1}{C_1^2}} = 1 \tag{34}$$

and

$$\frac{k_x^2}{\frac{4\pi G\rho_2}{C_2^2 - V^2}} + \frac{k_y^2}{\frac{4\pi G\rho_2}{C_2^2}} = 1. \tag{35}$$

Thus the two media become disentangled for the stability conditions in this case and the system becomes unstable for the wave number $k\left(\sqrt{k_x^2 + k_y^2}\right)$ whenever it is less than k^* given by (34) or (35) for the two regions, respectively. Particularly, when the perturbation is propagating only along the streaming motion, i.e. $k_x = k^*$, $k_y = 0$ we have

$$k^* = \frac{4\pi G\rho_1}{C_1^2 - V^2} \quad \text{and} \quad \frac{4\pi G\rho_2}{C_2^2 - V^2}. \tag{36}$$

When the perturbation is propagating in the perpendicular direction to the streaming motion in its plane, i.e. $k_y = k^*$, $k_x = 0$ we have

$$k^* = \frac{4\pi G\rho_1}{C_1^2} \quad \text{and} \quad \frac{4\pi G\rho_2}{C_2^2}. \tag{37}$$

The results (36) clearly show that k^* dependence is only on streaming velocity, medium density and velocity of sound in the medium. It is independent of the other medium density and sound velocity. Thus the values of k^* show that the system is decomposed.

Similarly in the case of (37) the system is decomposed with k^* depending only on the medium density and sound velocity. The streaming velocity has no effect on k^*.

This decomposition of the system in two separate media suggests that the two media may be treated independently for various results under consideration.

Special case 2:

For a single homogeneous medium when the two streams are moving in opposite direction with equal velocity v, (i.e. $\rho_1 = \rho_2 = \rho$, $C_1 = C_2 = C$, $V_1 = V$, $V_2 = -V$) we have Eq. (33) as

$$\alpha_1 = \alpha_2 = 0,$$

giving

$$\frac{k_x^2}{\frac{4\pi G\rho}{C^2 - V^2}} + \frac{k_y^2}{\frac{4\pi G\rho}{C^2}} = 1, \tag{38}$$

which determines the critical wave number k^* satisfying (38) and $k^* = \sqrt{k_x^2 + k_y^2}$.

In particular, for the perturbation along the streaming motion $k_y = 0$ and

$$k_x = k^* = \frac{4\pi G\rho}{C^2 - V^2} \tag{39}$$

and for the perturbation perpendicular to the streaming motion $k_x = 0$ and

$$k_y = k^* = \left[\frac{4\pi G\rho}{C^2}\right]^{1/2}. \tag{40}$$

Obviously, for the single static homogeneous medium

$$k^* = \left[\frac{4\pi G\rho}{C^2}\right]^{1/2}, \tag{41}$$

which is Jeans result. Talwar and Kalra have obtained a similar result.

Special case 3:

Let the two media be at rest, i.e. $V_1 = V_2 = 0$. Then $\sigma_r^2 = n^2$. Putting in dispersion relation (28) we get,

$$\frac{\alpha_1}{\rho_1} + \frac{\alpha_2}{\rho_2} = 0,$$

where

$$\alpha_r^2 = \frac{n^2 - 4\pi G\rho_r + k^2 C_r^2}{C_r^2}.$$

From these two relations we get

$$\rho_2^2 C_2^2[n^2 - 4\pi G\rho_r + k^2 C_1^2] = \rho_1^2 C_1^2[n^2 - 4\pi G\rho_2 + k^2 C_2^2],$$

i.e.

$$n^2 = \frac{4\pi G(\rho_1\rho_2^2 C_2^2 - \rho_2\rho_1^2 C_1^2) - k^2 C_1^2 C_2^2(\rho_2^2 - \rho_1^2)}{(\rho_2^2 C_2^2 - \rho_1^2 C_1^2)}.$$

For the critical wave number k^* we put $n = 0$ in the above equation and get

$$k^* = \sqrt{k_x^2 + k_y^2} = \left[\frac{4\pi G\rho_1\rho_2[\rho_2 C_2^2 - \rho_1 C_1^2]}{C_1^2 C_2^2(\rho_2^2 - \rho_1^2)}\right]^{1/2}, \tag{42}$$

which shows that k^* follows a circular path of radius

$$\left[\frac{4\pi G\rho_1\rho_2[\rho_2 C_2^2 - \rho_1 C_1^2]}{C_1^2 C_2^2(\rho_2^2 - \rho_1^2)}\right]^{1/2},$$

i.e. in every direction of perturbation propagation for the wave number $k < k^*$ given by (42) the system is unstable and for $k > k^*$ it is stable.

Conclusion

A general dispersion relation for horizontal propagation has been derived. The limitation of obtaining a general solution for k^* has been discussed and results obtained in special cases. It is suggested that numerical calculation may be made to get some results.

For some special cases the critical wave number has been obtained. In particular, we discussed the stability criteria for the perturbation propagation along the streaming motion, and perpendicular to the streaming motion separately. We found that the streaming motion has destabilizing effect when the perturbation is propagating along the streaming motion, but for perpendicular propagation the instability criterion is unaffected by the streaming motion. In general, k^* follows an elliptic path in first quadrant. The value of critical wave number k^* can be found for the perturbation propagation in any direction in horizontal plane $z = 0$. In case of static medium, i.e. in the absence of streaming motion, the value of k^* is the same in every direction. In other words, we find a circular path in first quadrant for k^*, of a radius equal to Jeans critical wave number k_j^*. But in the presence of streaming motion, because of destabilizing effect of streaming velocity, the value of k^* is increased from k_j^* for perturbation propagation in every direction of the horizontal plane $z = 0$ other than the transversal. As a result, the circular orbit changes into an elliptic one. We further observe that the stabilizing tendency is dependent on the wave number, therefore the system has maximum stabilizing tendency for the transversal perturbation propagation and minimum for the perturbations propagating parallel to the streaming velocity.

Acknowledgement

Thanks are due to the University Grants Commission for financial assistance.

References

1. J. H. Jeans, Phil. Trans. Roy. Soc. London, *199*, 1, 1902.
2. P. Ledoux, Annales d' Astrophys., *14*, 438, 1951.
3. W. Fricke, Astrophysics J., *120*, 356, 1954.
4. S. Chandrasekhar and E. Fermi, Astrophysics J., *118*, 1953.
5. S. Chandrasekhar, Astrophysics J., *119*, 7, 1954.
6. S. Chandrasekhar, Vistas in Astronomy, Vol. I, p. 344, Pergamon Press, Oxford, 1955.
7. R. C. Sharma and K. P. Thakur, Astrophysics and Space Science, *81*, 95, 1982.
8. S. Chandrasekhar, Hydrodynamic and Hydromagnetic Stability, Oxford University Press, Oxford, 1961.

Acta Physica Hungarica 72 (1), pp. 23–45 (1992)

HALL EFFECT IN THE VISCOUS FLOW OF AN IONIZED GAS BETWEEN TWO PARALLEL WALLS UNDER TRANSVERSE MAGNETIC FIELD IN A ROTATING SYSTEM

T. LINGA RAJU and V. V. RAMANA RAO

Department of Applied Mathematics, Andhra University
Visakhapatnam — 530003, India

(Received 21 August 1991)

The equations of motion accounting for rigid rotation about an axis perpendicular to the flow have been given and exact solutions have been obtained for both velocities such as the primary flow as well as the secondary flow corresponding to the cases of non-conducting and conducting walls, taking into account the Hall currents. In case of non-conducting walls, it is found that these solutions for u, w are all independent of the partial pressure of the electron gas, s. The induced magnetic field is neglected under the assumption that the magnetic Reynolds number is small.

1. Introduction

The study of flow problems of an electrically conducting fluid, particularly of an ionized gas, is currently receiving considerable interest. Such studies have been made for many years in connection with astronomical and geophysical problems, motion of the interstellar gas, etc. In the last few decades considerable interest has also been developed in the study of the interaction between magnetic field and the flow of an electrically conducting incompressible viscous fluid due its wide applications in modern technology. It is also well known that a number of astronomical bodies, viz., the sun, the planets, the magnetic stars, pulsars, etc., possess fluid interior and at least surface a magnetic field. Hence any flow phenomenon occurring in a celestial body takes place under the influence of an external magnetic field. In the presence of the strong magnetic field due to gyration and drift of charged particles the effect of resulting Hall currents is to be taken into consideration. These Hall effects introduce a cross flow of a double swirl pattern and tend to increase the rate of flow for a given pressure gradient [1].

The theory of rotating fluids is highly important because of its occurrence in various natural phenomena and for its applications in various technological situations which are directly governed by the actions of the Coriolis forces. Interactions of Coriolis forces with electromagnetic forces are met often in the planetary motions of various solar systems. Therefore, it is of considerable interest to study the effects of Coriolis forces on specific flow problems.

The study of the flow of a conducting fluid through a straight channel under a uniform transverse magnetic field presents one of the simplest problems in MHD.

The problems concerned with the effects of Hall currents on specific flow problems under the influence of a strong magnetic field have been studied by several authors notably, Broer et al [2], Sato [3], Sherman and Sutton [4], Tani [1], Yaminishi [5], Katagiri [6], Pop [7], Gupta [8], Datta and Jana [9], Jana and Datta [10], Jana et al [11], Krishnam Raju et al [12], etc. These effects in the unsteady case were discussed by Sakhnovskii [13], Vatazhin [14], Debnath et al [15], etc.

In this paper an attempt has been made to study the flow of a rotating electrically conducting viscous fluid in the presence of a uniform transverse magnetic field taking Hall effects into consideration following Sato's [3] analysis. The induced magnetic field is neglected under the assumption that the magnetic Reynolds number is small. Exact solutions are obtained for both primary and secondary velocity distributions and the discussion has been also made for various governing parameters such as Hall parameter α, Hartmann number H_a and the rotation parameter T.

2. Basic equations, boundary conditions and their solutions

The viscous flow of an ionized gas between two parallel walls in a rotating system is considered. Figure 1 illustrates the co-ordinate system used to write the equations of motion. The x-axis is taken in the direction of hydrodynamic pressure gradient in the plane parallel to the channel walls, not in the direction of flow. A parallel uniform magnetic field $\mathbf{B}_0$ is applied in the y-direction. The system is rotated about the y-axis perpendicular to the walls with an angular velocity Ω'. The height of the channel is denoted by $2h$ and the width is assumed to be very large compared with $2h$.

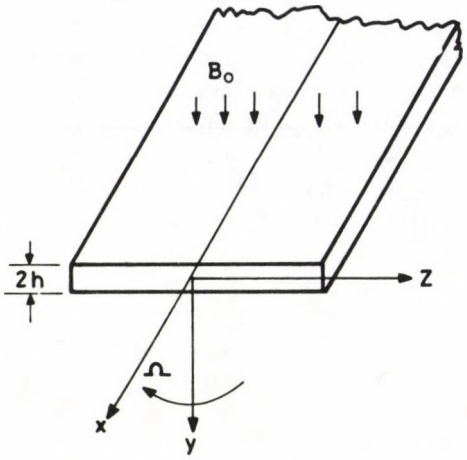

Fig. 1. The rotating system

The following assumptions are made:

1. The density of gas is everywhere constant.
2. The ionisation is in equilibrium, which is not affected by the applied electric and magnetic fields.
3. The effect of space charge is neglected.
4. The flow is fully developed and stationary, that is, $\partial/\partial t = 0$ and $\partial/\partial x = 0$, except $\partial p'/\partial x \neq 0$.
5. The magnetic Reynolds number R_m is small, namely, the induced magnetic field is small compared with the applied field. Therefore, components in the conductivity tensor are expressed in terms of $\mathbf{B}_0$.
6. The flow is two-dimensional, namely, $\partial/\partial z = 0$.

The fundamental equations to be solved are the equations of motion and current for the study flow of a neutral fully-ionized gas valid under the above assumptions and expressed as (see Spitzer [16]),

$$\mathbf{J} \times \mathbf{B} - \nabla p' + \rho\nu\nabla^2\mathbf{V} = 2\rho\overrightarrow{\Omega} \times \mathbf{V}, \tag{1}$$

$$\mathbf{E} + \mathbf{V} \times \mathbf{B} + \mathbf{E}_e - \frac{c}{en}\mathbf{J} \times \mathbf{B} - \frac{\mathbf{J}}{\sigma_0} = 0, \tag{2}$$

in which vectors $\mathbf{J}$, $\mathbf{B}$ and $\mathbf{E}$ are the current density, the magnetic flux density and the electric field, respectively. Also p' is pressure, ρ the density, ν the kinematic viscosity, $-e/c$ the electron charge in e.m.u. and n is the number density of ions which is equal to that of electrons, $\mathbf{E}_e$ denotes the equivalent electric field due to the gradient of electron pressure p_e, namely $\mathbf{E}_e = (\frac{c}{en})\nabla p_e$. The conductivity σ_0 is defined as a coefficient of proportionality between current density and the collision term in the equation of motion of charged particles as is shown in Spitzer [16].

The other fundamental equations are the continuity relations

$$\mathrm{div}\mathbf{V} = 0, \tag{3}$$

$$\mathrm{div}\mathbf{J} = 0. \tag{4}$$

The boundary conditions are

$$\mathbf{V} = 0 \quad \text{at} \quad y = \pm h. \tag{5}$$

Equations (1–4) are simplified by the above-mentioned assumptions and boundary conditions given by Eq. (5) as

$$-\frac{\partial p'}{\partial x}[1 - s(1 - \frac{\sigma_1}{\sigma_0})] + \rho\nu\frac{d^2u}{dy^2} + B_0[-\sigma_1(E_z + uB_0) + \sigma_2(E_x - wB_0)] = 2\rho\Omega w, \tag{6}$$

$$s\frac{\partial p'}{\partial x}\frac{\sigma_2}{\sigma_0} + \rho\nu\frac{d^2w}{dy^2} + B_0[\sigma_1(E_x - wB_0) + \sigma_2(E_z + uB_0)] = -2\rho\Omega u, \tag{7}$$

in which Ω represents the angular velocity with which the system is rotated about the y-axis and $s = \frac{p_e}{p'}$ is the ratio of the electron pressure to the total pressure. The value of s is $\frac{1}{2}$ for a neutral fully-ionized plasma and approximately zero for a weakly-ionized gas. u, w and E_x, E_z are the x and z components of velocity and electric field, respectively. Also

$$\sigma_1 = \frac{\sigma_0}{1+\alpha^2}, \tag{8}$$

$$\sigma_2 = \frac{\sigma_0 \alpha}{1+\alpha^2}, \tag{9}$$

$$\alpha = \frac{\omega_e}{[\frac{1}{\tau} + \frac{1}{\tau_e}]}, \tag{10}$$

where ω_e is the gyration frequency of the electron, τ and τ_e are the mean collision time between electron and ion, electron and neutral particle, respectively. The above expression for α which is valid in the case of a partially-ionized gas agrees with that of the fully-ionized gas when τ_e approaches zero.

The two Eqs (6,7) have been non-dimensionalised, using the characteristic length h and velocity $u_p = -\frac{\partial p'}{\partial x}(\frac{h^2}{\rho\nu})$. The same notation is used u, w for u/u_p and w/w_p and y for y/h.

Further introducing the Taylor number T, given by $T^2 = \frac{\Omega h^2}{\nu}$, we obtain the non-dimensional equations as

$$k_1 + \frac{d^2u}{dy^2} - \frac{\sigma_1}{\sigma_0}H_a^2(m_z + u) + \frac{\sigma_2}{\sigma_0}H_a^2(m_x - w) = 2\,T^2 w, \tag{11}$$

$$k_2 + \frac{d^2w}{dy^2} - \frac{\sigma_1}{\sigma_0}H_a^2(m_x - w) + \frac{\sigma_2}{\sigma_0}H_a^2(m_z + u) = -2\,T^2 u, \tag{12}$$

in which

$$k_1 = 1 - s(1 - \frac{\sigma_1}{\sigma_0}), \quad k_2 = -s\frac{\sigma_2}{\sigma_0}, \quad m_x = \frac{E_x}{B_0 u_p}, \quad m_z = \frac{E_z}{B_0 u_p}$$

and the Hartmann number H_a is defined as $H_a^2 = B_0^2 h^2 \sigma_0/\rho\nu$.

Introducing $q = u + iw$, $K = k_1 + ik_2$ and $M = m_x + im_z$; Eqs (11,12) can be written in complex form as:

$$\frac{d^2q}{dy} + \left\{ i\left(\frac{\sigma_2}{\sigma_0}H_a^2 + 2T^2\right) - \frac{\sigma_1}{\sigma_0}H_a^2 \right\} q = -H_a^2 M \left(\frac{\sigma_2}{\sigma_0} + i\frac{\sigma_1}{\sigma_0} + K\right), \tag{13}$$

which is to be solved subject to the boundary conditions $q(\pm 1) = 0$.

I_x and I_z defined in non-dimensional form as $J_x/(\sigma_0 B_0 u_p)$ and $J_z/(\sigma_0 B_0 u_p)$, respectively, are given in complex notation as

$$I = I_x + iI_z = \frac{\sigma_2 + i\sigma_1}{\sigma_0}\{q - iM - \frac{s}{H_a^2}\} + \frac{is}{H_a^2}. \tag{14}$$

The non-dimensional electric field M is to be determined by boundary conditions at large x and z.

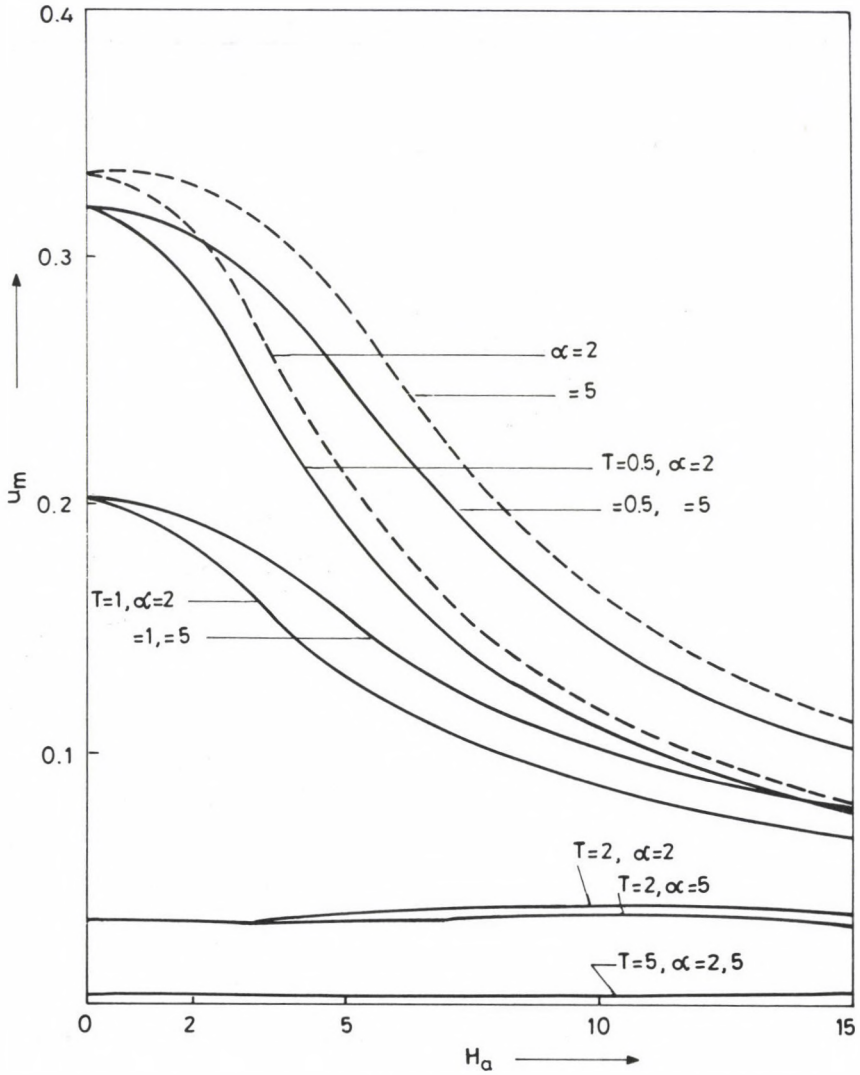

Fig. 2. Mean velocity u_m (non-conducting walls). Broken line: Sato's calculation ($T = 0$)

Non-conducting walls

When the side walls kept at large distance in z-direction are made up of the non-conducting material, the induced electric current does not go out of the channel

but circulates in the fluid. So an additional condition for the current defined in non-dimensional form is

$$\int I_x dy = 0.$$

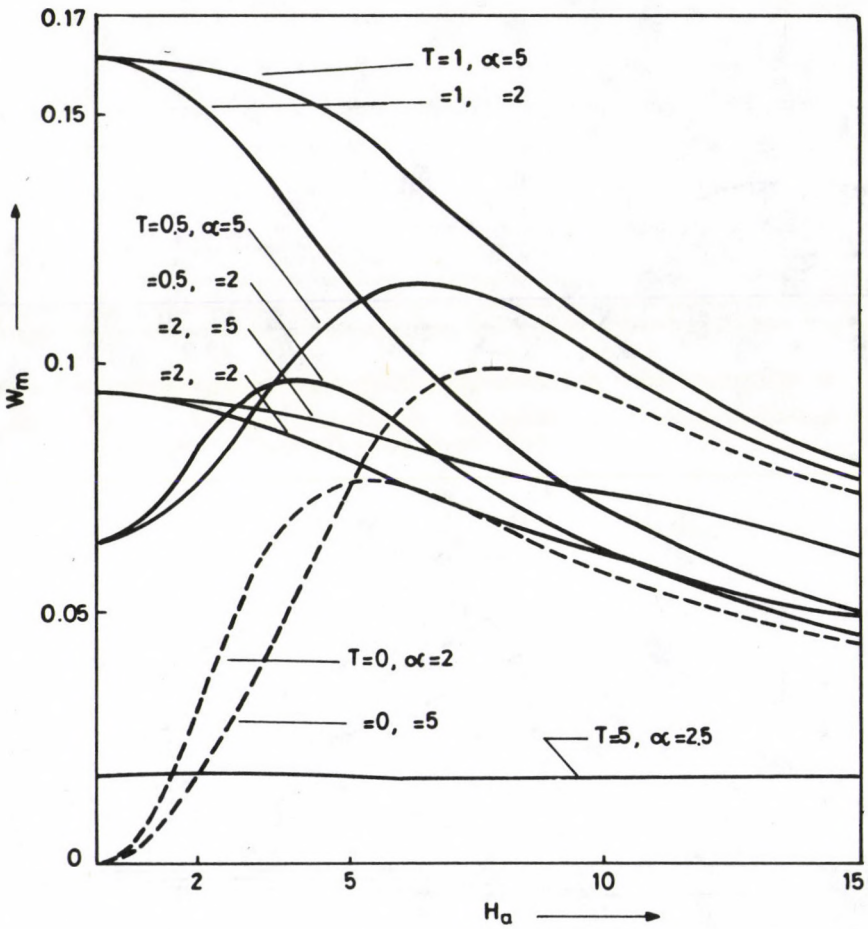

Fig. 3. Mean velocity w_m (non-conducting walls). Broken line: Sato's calculation ($T = 0$)

Similarly if the insulation at large x is also assumed, another relation is obtained as

$$\int I_x dy = 0.$$

The constants in the solution are determined by these two conditions. Solutions for q and I are all independent of the partial pressure of the electron gas s

and obtained as

$$q = q_m(p - iq)\frac{\{\mathrm{ch}(p - iq) - \mathrm{ch}(p - iq)y\}}{(p - iq)\mathrm{ch}(p - iq) - \mathrm{sh}(p - iq)}, \tag{15}$$

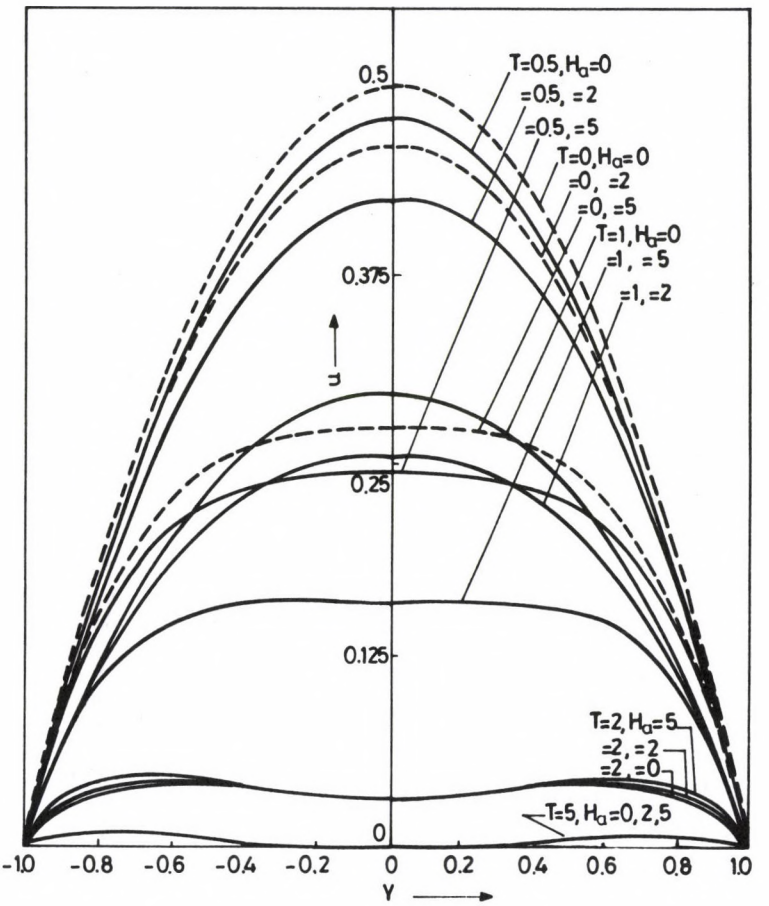

Fig. 4. Primary velocity distribution for $\alpha = 2$ (non-conducting walls). Broken line: Sato's calculation ($T = 0$)

$$I = \frac{\sigma_2 + i\sigma_1}{\sigma_0}\left[\frac{q}{q_m} - 1\right], \tag{16}$$

where

$$q_m = \int_0^1 q\,dy = \frac{(1 + i\alpha)\{(p - iq)\mathrm{ch}(p - iq) - \mathrm{sh}(p - iq)\}}{H_a^2\,\mathrm{sh}(p - iq) - i2T^2(1 + i\alpha)(p - iq)\mathrm{ch}(p - iq)}, \tag{17}$$

$$p \text{ or } q = \frac{1}{\sqrt{2}} \left[\sqrt{\left\{ \frac{\sigma_1^2}{\sigma_0^2} H_a^4 + \left(\frac{\sigma_2}{\sigma_0} H_a^2 + 2T^2 \right)^2 \right\}} \pm \frac{\sigma_1}{\sigma_0} H_a^2 \right]^{1/2} \tag{18}$$

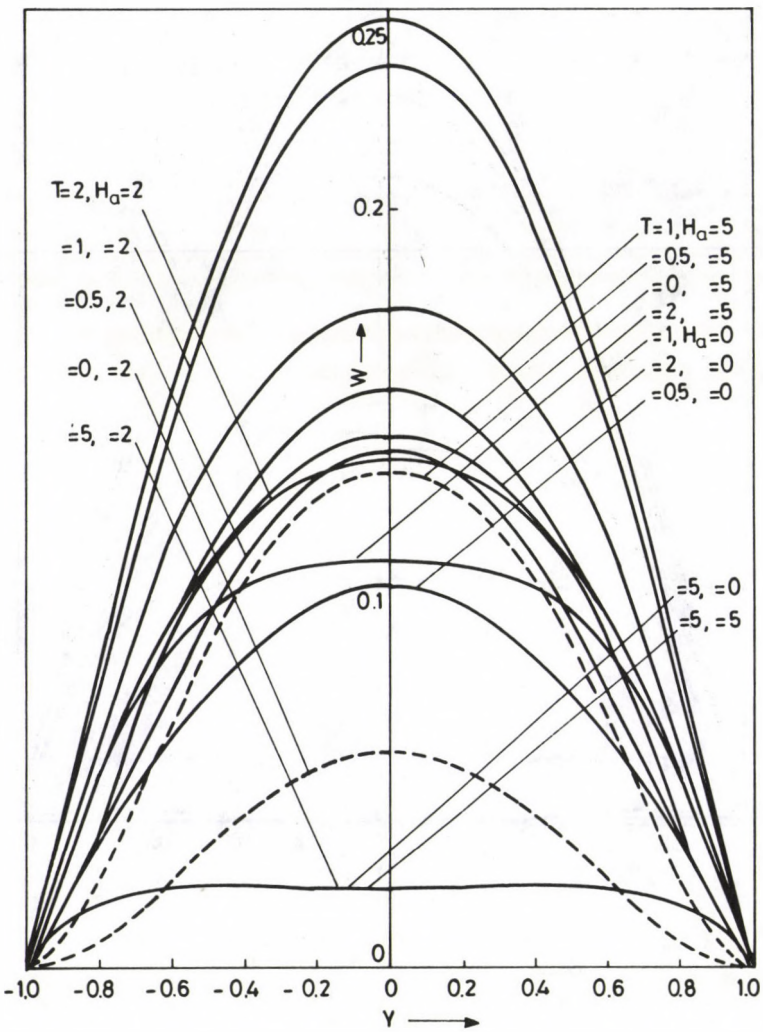

Fig. 5. Secondary velocity distribution for $\alpha = 2$ (non-conducting walls). Broken line: Sato's calculation ($T = 0$)

Separating real and imaginary parts of q and q_m from Eqs (15) and (18), we obtain the velocity distributions u, w and the mean velocities u_m and w_m over

the cross section; discussion has been also made for various governing parameters involved.

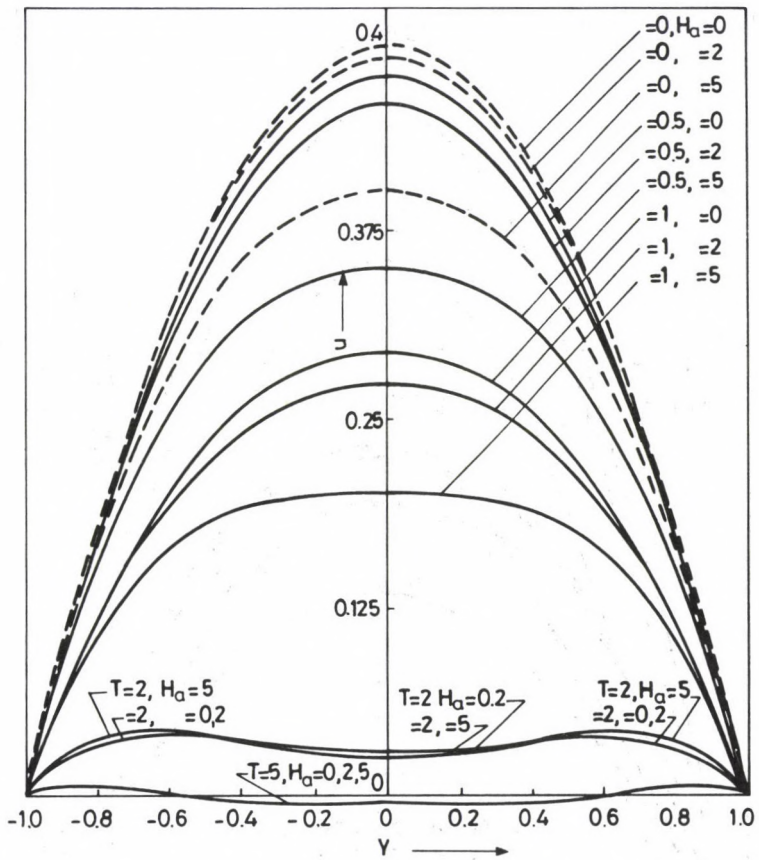

Fig. 6. Primary velocity distribution for $\alpha = 5$ (non-conducting walls). Broken line: Sato's calculation ($T = 0$)

Conducting walls

When the side walls are made up of conducting material and short-circuited by an external conductor, the induced electric current flows out of the channel. In this case no electric potential exists between the side walls. If we assume zero electric field also in the x-direction, we have

$$m_x = 0, \quad m_z = 0.$$

These conditions are realised, for instance for the flow between two concentric cylinders under the radial magnetic field with the pressure gradient parallel to the axis of cylinder.

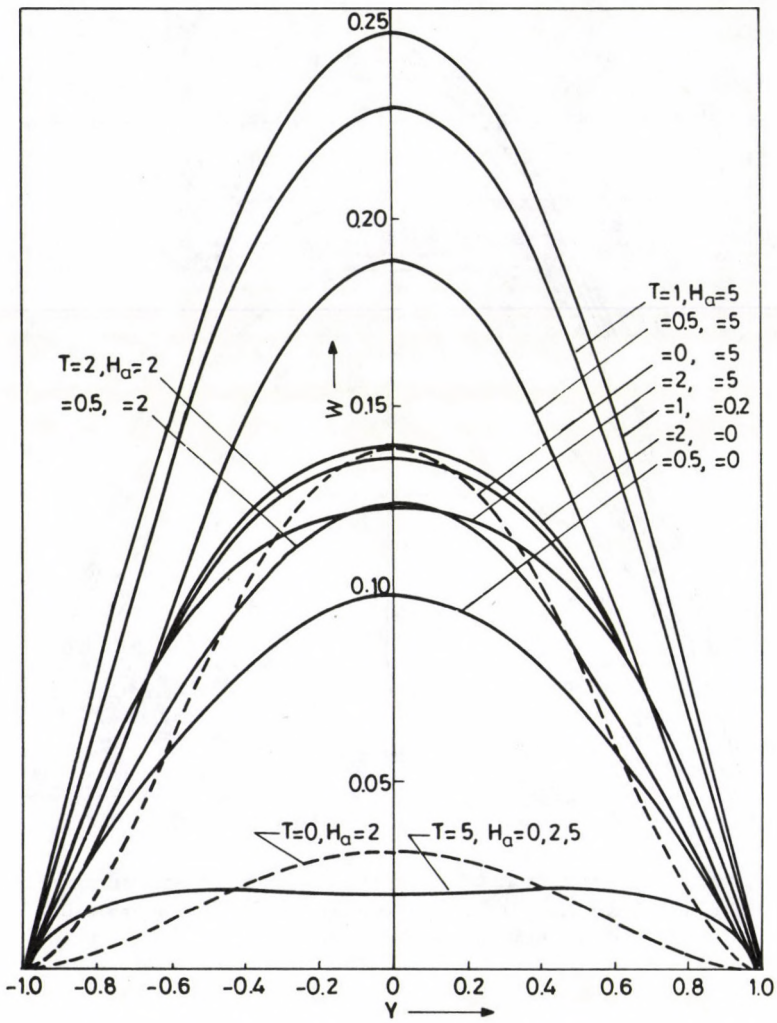

Fig. 7. Secondary velocity distribution for $\alpha = 5$ (non-conducting walls). Broken line: Sato's calculation ($T = 0$)

Constants in the solution are determined by these two conditions. Solutions for q and I depend on s and are obtained as Eq. (15) and

$$I = \left(\frac{\sigma_2 + i\sigma_1}{\sigma_0}\right)\left(q - \frac{s}{H_a^2}\right) + \frac{is}{H_a^2}, \tag{19}$$

where

$$q_m = \frac{1 - s + \frac{s(\sigma_1 - i\sigma_2)}{\sigma_0}}{(\frac{\sigma_1 - i\sigma_2}{\sigma_0})H_a^2 - 2iT^2} \left[\frac{(p - iq)\mathrm{ch}(p - iq) - \mathrm{sh}(p - iq)}{(p - iq)\mathrm{ch}(p - iq)}\right]. \tag{20}$$

p and q are the same as in Eq. (18).

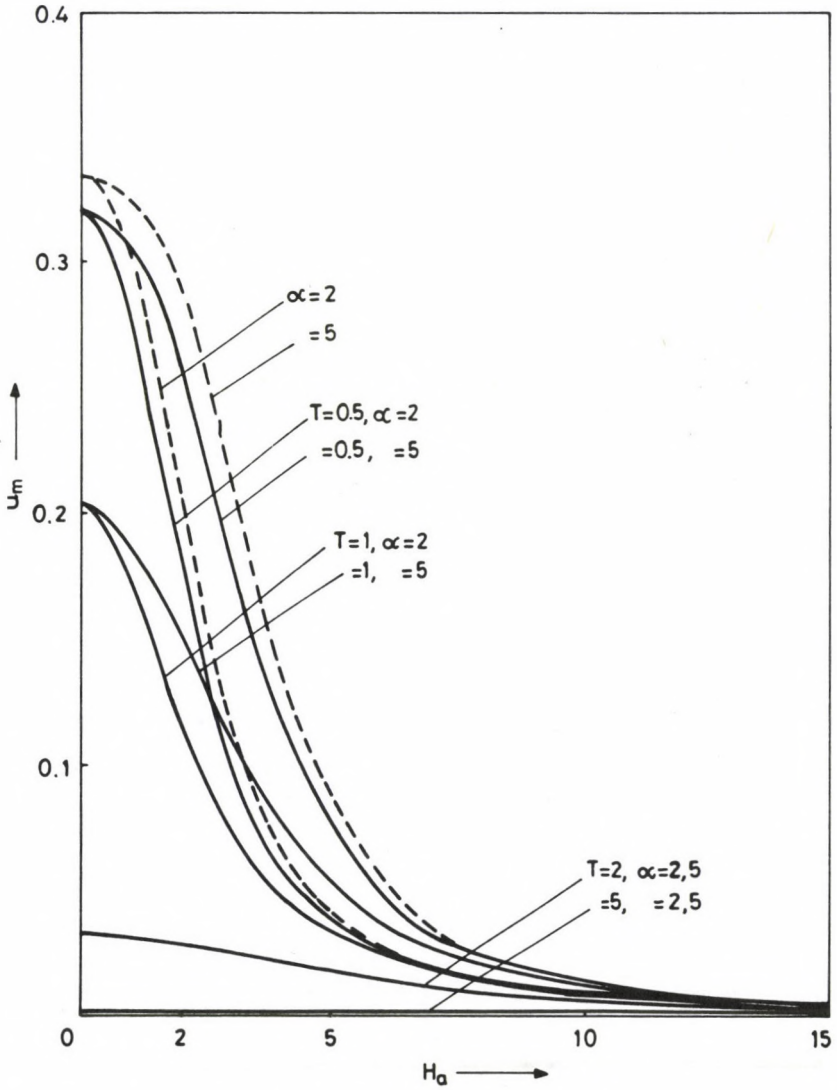

Fig. 8. Mean velocity u_m (conducting walls). $s = 0$. Broken line: Sato's calculation ($T = 0$)

In this case also by separating real and imaginary parts of q and q_m from Eqs (15) and (20), we obtain the velocity distributions and the mean velocities. Discussion has also been made for the governing parameters, viz., α, T and H_a.

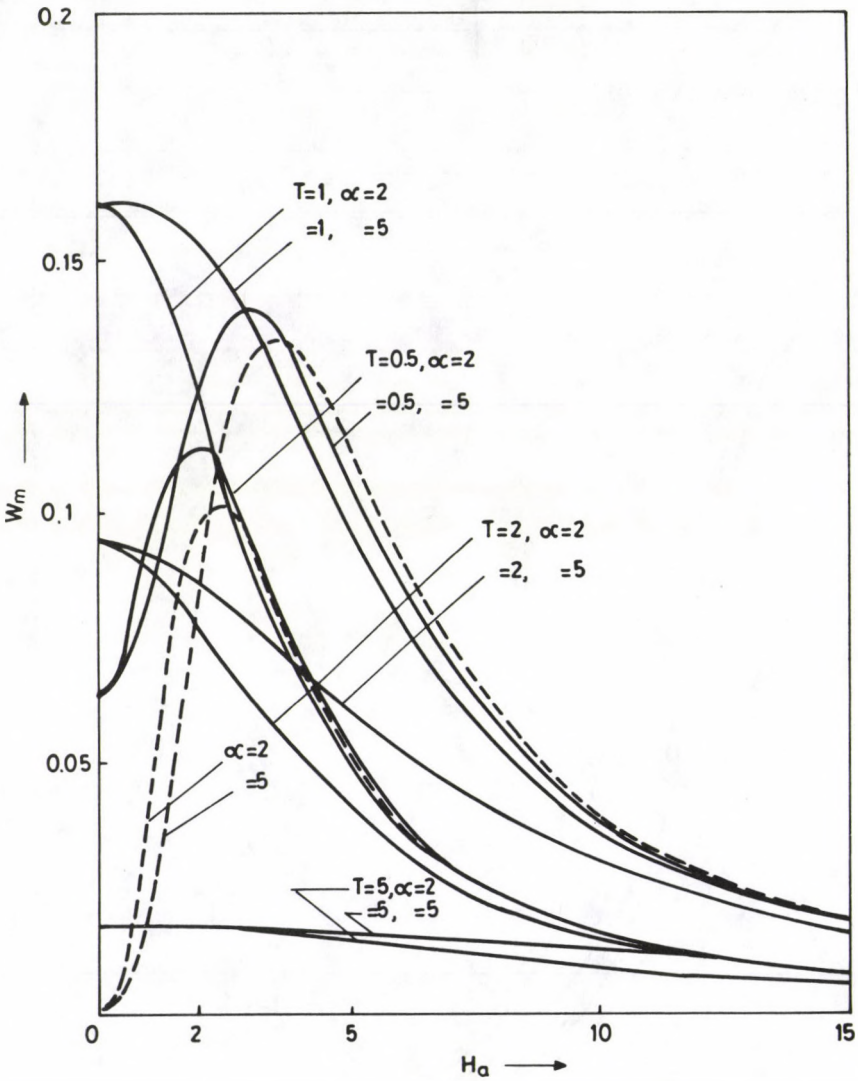

Fig. 9. Mean velocity w_m (conducting walls). $s = 0$. Broken line: Sato's calculation ($T = 0$)

3. Results and discussion

Non-conducting walls

The mean velocity profiles have been plotted against the Hartmann number H_a in Figs 2 and 3, respectively, for different values of the Hall parameter α and

Taylor number T. For fixed values of α and H_a it is concluded that the primary mean velocity u_m decreases as Taylor number T increases. When $T = 0$, we recover the work of Sato [3]. The conclusion that for fixed H_a, u_m increases with increasing α in Sato's [3] work, also holds good even in the rotating case until $T = 1$ and beyond that it decreases. However, when $T = 5$, the variation of u_m is almost the same for $\alpha = 2$ and 5.

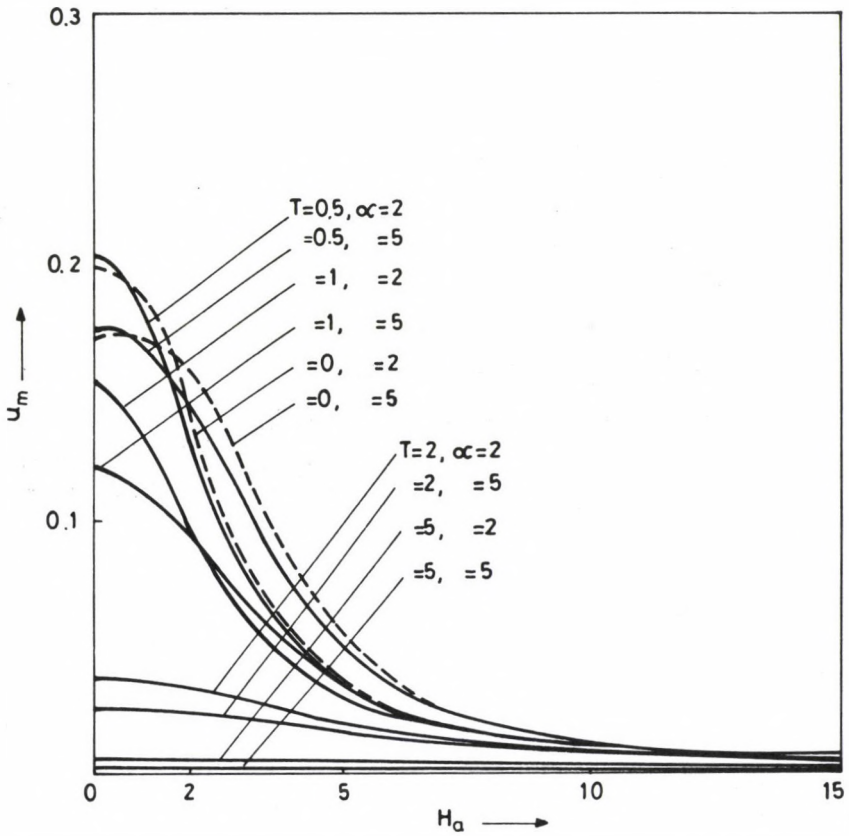

Fig. 10. Mean velocity u_m (conducting walls). $s = 1/2$. Broken line: Sato's calculation ($T = 0$)

When α is fixed u_m always decreases as H_a increases. This is true only when $T \leq 1$. When $T > 1$, its tendency is just the opposite. When $T = 5$ the secondary mean velocity w_m decreases with increasing α up to $H_a = 5$ and beyond this value of H_a, it always increases. This conclusion is valid for $T = 0.5$ and $H_a = 3.5$. As T increases further, w_m always increases. When $T = 5$, w_m is almost the same for $\alpha = 2$ and 5.

Figures 4 and 6 show the primary velocity distributions against y and for different values of T and H_a when $\alpha = 2$ and 5, respectively. It is concluded that

for fixed H_a the primary velocity u decreases at any point of the channel with increasing rotation. It is also concluded that for fixed $T < 2$, u decreases with increasing H_a at any point of the channel. Note that when $T = 2$ or 5, there are two points about the central line $y = 0$, at which u is maximum. For large rotation, the boundary layer thickness decreases as H_a increases. This is in agreement with the conclusion that the magnetic field causes thinning of the boundary layer.

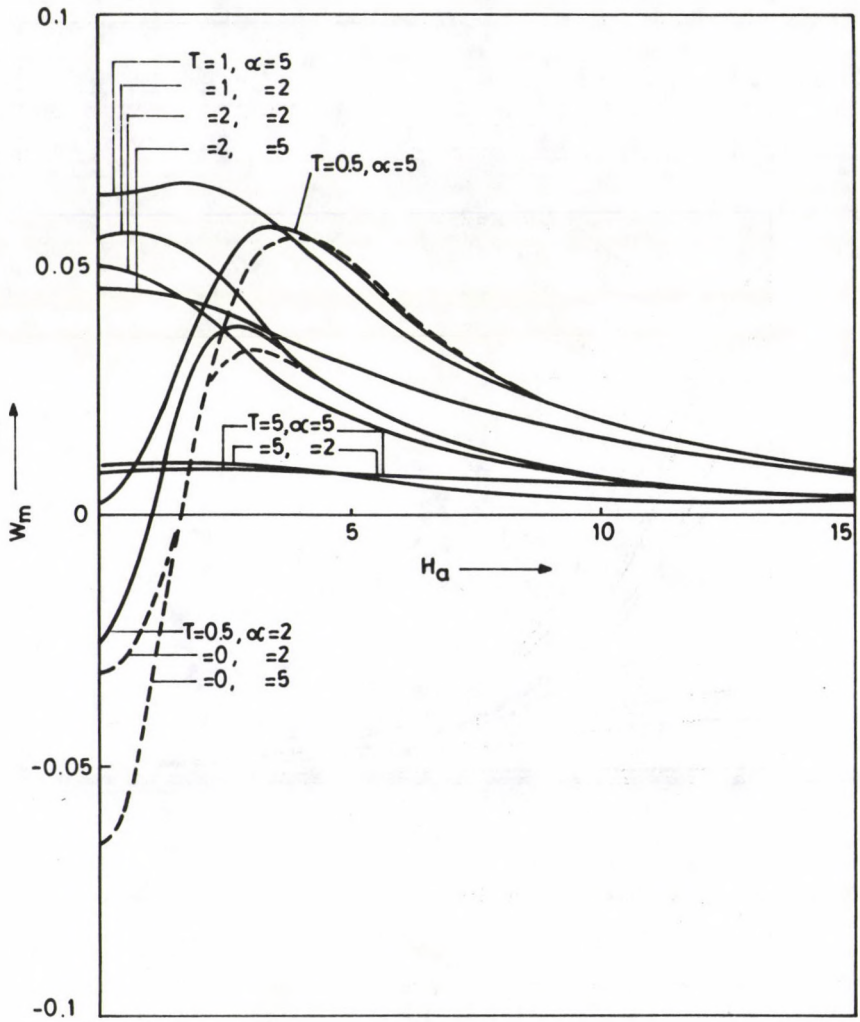

Fig. 11. Mean velocity w_m (conducting walls). $s = 1/2$. Broken line: Sato's calculation ($T = 0$)

Figures 5 and 7 show the secondary velocity distribution against y and for different T and H_a when $\alpha = 2$ and 5, respectively. For fixed H_a it is concluded that

as rotation increases, the secondary velocity w increases at any point of the channel till a value of T is reached and beyond which it decreases with further increasing values of rotation. For fixed $T(\leq 1)$, as H_a increases, w increases at any point of the channel and for $T > 1$, an opposite result holds good. For large T (approximately 5) the influence of the magnetic field is inappreciable. However, there are two points about the central line $y = 0$, at which this velocity is maximum.

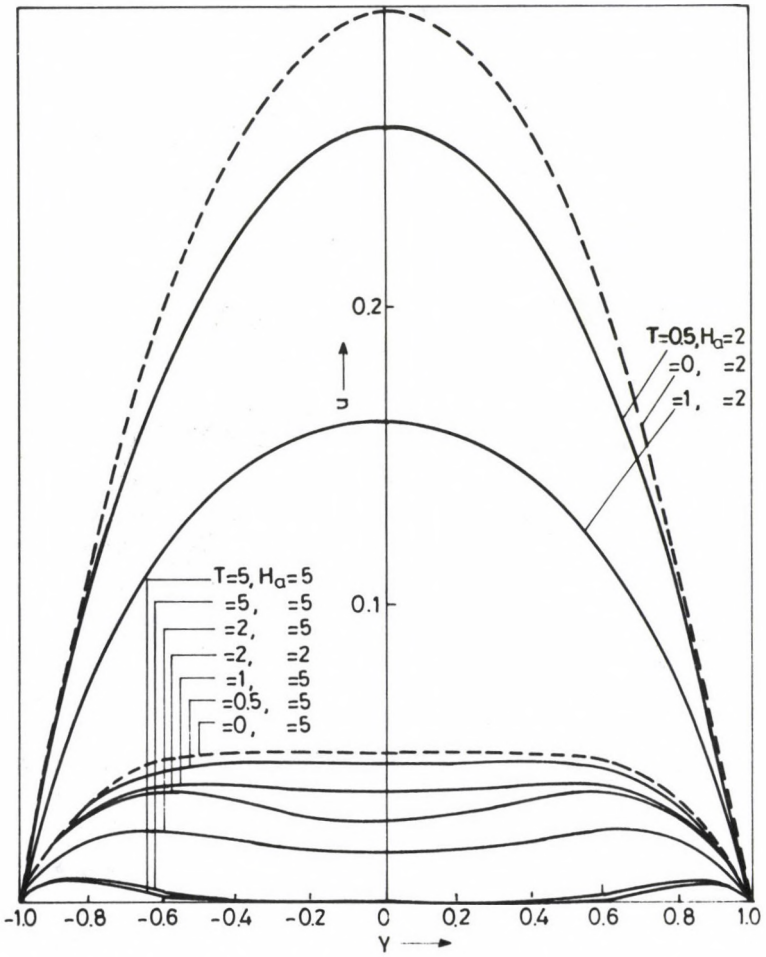

Fig. 12. Primary velocity distribution for $\alpha = 2$ (conducting walls). $s = 0$
Broken line: Sato's calculation ($T = 0$)

Conducting walls

Figures 8 and 10 show the primary mean velocity u_m for $s = 0$ and $\frac{1}{2}$, respectively. When $T = 0$, we recover the work of Sato [3] from these two Figures. In the

case of a weakly-ionized gas, it is found from Fig. 8, that the effect of increasing rotation is to reduce u_m for fixed values of α and H_a. Also for fixed T and H_a, u_m increases with an increase in α, when T and α are fixed, u_m decreases as H_a increases. For large rotations greater than or equal to 2, no noticeable variation in u_m is seen with increasing α. In this case for fixed T, the limiting value of u_m at $H = 0$ is the same for different α.

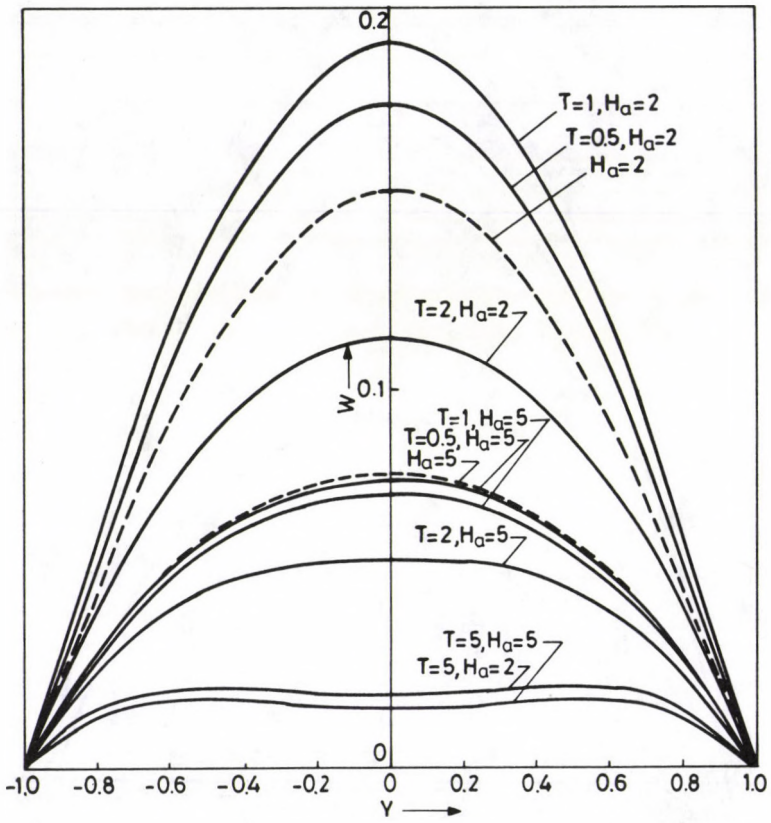

Fig. 13. Secondary velocity distribution for $\alpha = 2$ (conducting walls). $s = 0$
Broken line: Sato's calculation ($T = 0$)

From Fig. 10 corresponding to $s = \frac{1}{2}$, it is noted that for $T = 0$, u_m decreases within a range $0 \leq H_a < H_a^*$ (critical) and increases within the range $H_a^* \leq H_a < \infty$, as α increases. For $T = 0$, H_a^* is found to be about 1.5. This is true for all $T > 0$. For fixed α, as T increases within the interval $0 < T \leq 0.5$, u_m increases and decreases in the interval $0.5 < T \leq 5$, with increasing values of Hartmann number. These conclusions can be attributed to the fact that in this case the limiting value of u_m at $H_a = 0$ is not equal for various values of T and α. For both $s = 0$ and $\frac{1}{2}$, u_m always decreases as H_a increases when T and α are fixed.

Figures 9 and 11 show the secondary mean velocities w_m corresponding to $s = 0$ and $\frac{1}{2}$, respectively. It is found from Fig. 9, that for a weakly ionized and non-rotating gas, w_m decreases in the interval $0 < H_a < 2.5$ and increases in $2.5 \leq H_a \leq \infty$ with an increase in α. For $T \geq 1$ and fixed H_a, w_m increases with an increase in α. For fixed α, it is found that w_m increases in $0 \leq H_a < H_a^*$ and decreases in $H_a^* \leq H_a < \infty$, as T increases. In the limiting case at $H_a = 0$ and when T is fixed, w_m is same for different α (although not shown in Fig. 9).

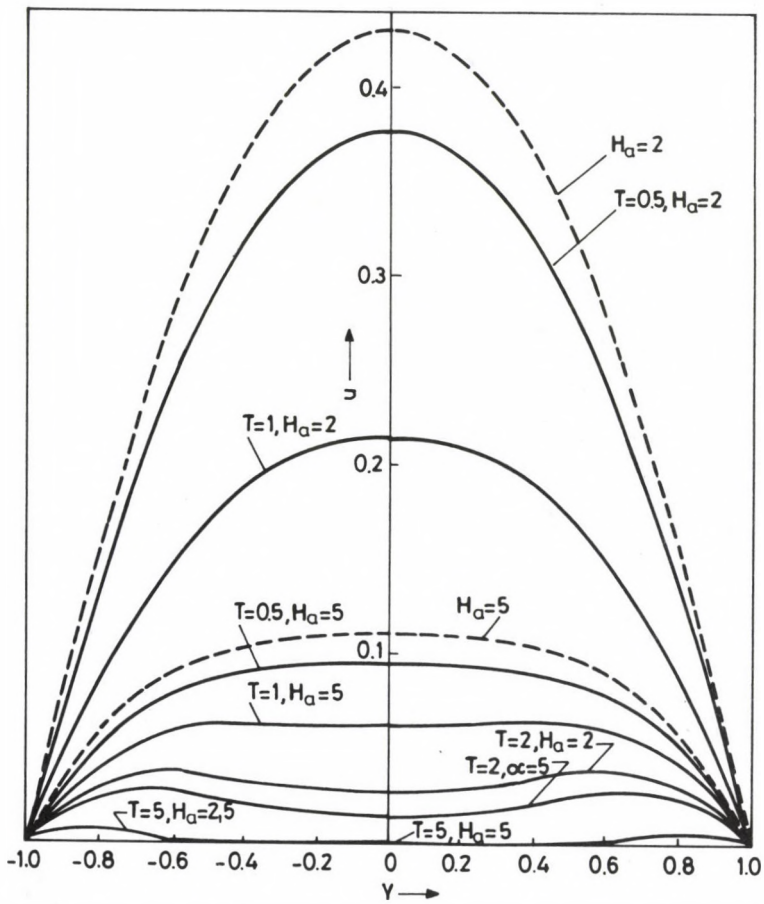

Fig. 14. Primary velocity distribution for $\alpha = 5$ (conducting walls). $s = 0$
Broken line: Sato's calculation ($T = 0$)

From Fig. 11, for a fully neutral-ionized plasma the secondary mean velocity w_m starts from a non-zero negative value and becomes positive at a certain Hartmann number. In particular, for $T = 0$, this H_a is found to be about 1.6. This is not only true when $T = 0$ (Sato's [3] work) but also for small values of Taylor

number say $T = 0.5$ and Hall parameter $\alpha = 2$. In the classical case ($T = 0$) w_m is found to increase as α increases for fixed H_a. For $\alpha = 2$ and fixed H_a, as T increases in $0 \leq T \leq 1$, w_m increases and decreases outside this range as T increases. For large α, say 5, there is a critical value of H_a so that for any H_a in $0 < H_a < H_a^*$, as T increases up to T^* (critical), w_m increases and for any H_a in $H_a^* < H_a < \infty$, w_m decreases and beyond T^*, it always decreases for any H_a.

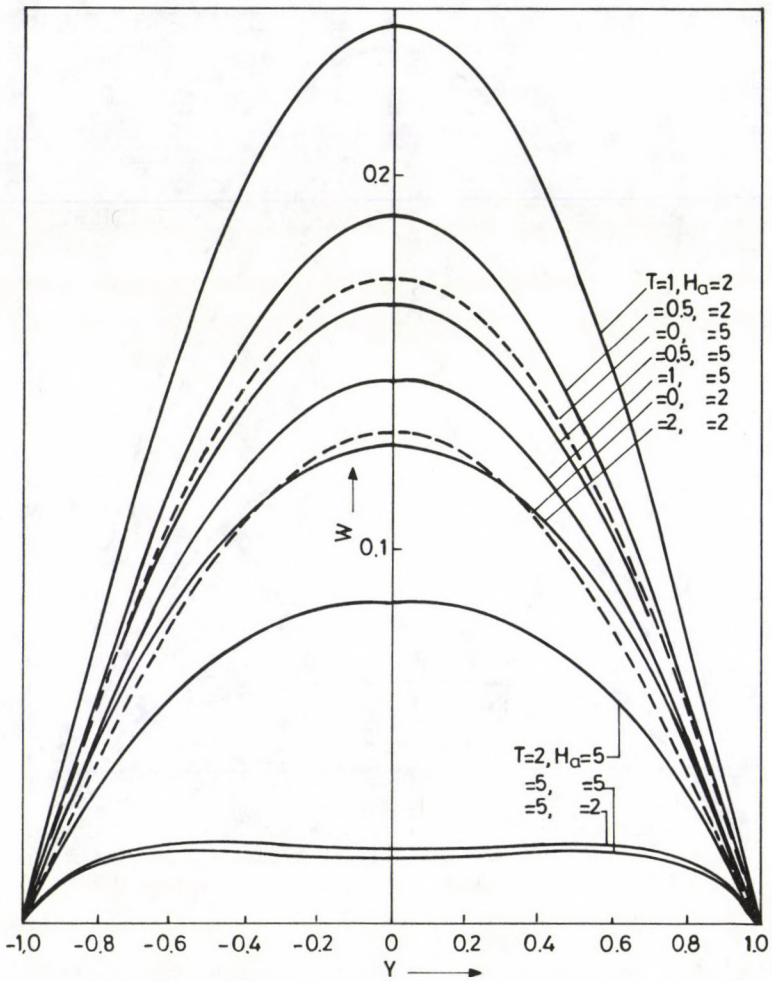

Fig. 15. Secondary velocity distribution for $\alpha = 5$ (conducting walls). $s = 0$
Broken line: Sato's calculation ($T = 0$)

Also it is concluded that as in the classical case and for small rotations say $T = T^* = 1$, w_m increases in the beginning and decreases afterwards as H_a increases.

But when $T^* > 1$, its tendency is such that it always decreases with an increase in H_a. This conclusion seems to hold good for $s = 0$ and for $T^* \leq 0.5$.

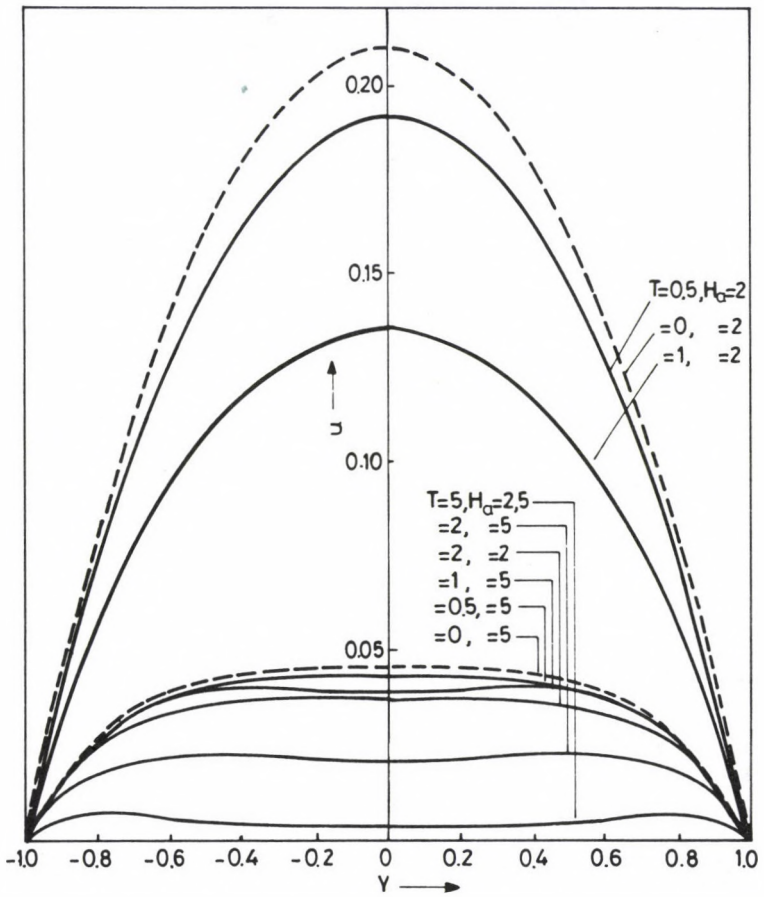

Fig. 16. Primary velocity distribution for $\alpha = 2$ (conducting walls). $s = 1/2$
Broken line: Sato's calculation ($T = 0$)

Figures 12 and 14 show the primary velocity distribution u in the case $s = 0$ and when $\alpha = 2$ and 5, respectively. When $s = 0$ and H_a is fixed, as rotation increases, u decreases at any point of the channel. When T is sufficiently large, there are two points symmetrically situated on either side of the axis of the channel, i.e., $y = 0$, at which this velocity becomes maximum. It is noted that when $\alpha = 2$ and for large T, say 5, the boundary layer thickness becomes thin as the Hartmann number increases. But when $\alpha = 5$ and large T, i.e., 5, u is almost the same for $H_a = 2$ and 5 at any point of the channel except that near $y = 0$, u becomes negative when $T = 5$.

Figures 13 and 15 show the secondary velocity distribution w in the case $s = 0$ and when $\alpha = 2$ and 5, respectively. It is concluded that as T increases in $(0, 1)$, w increases at any point of the channel for fixed values of α and $H_a = 2$. Outside this range as T increases, it decreases. When $H_a = 5$, as T increases the secondary velocity always decreases at any point of the channel for fixed values of α.

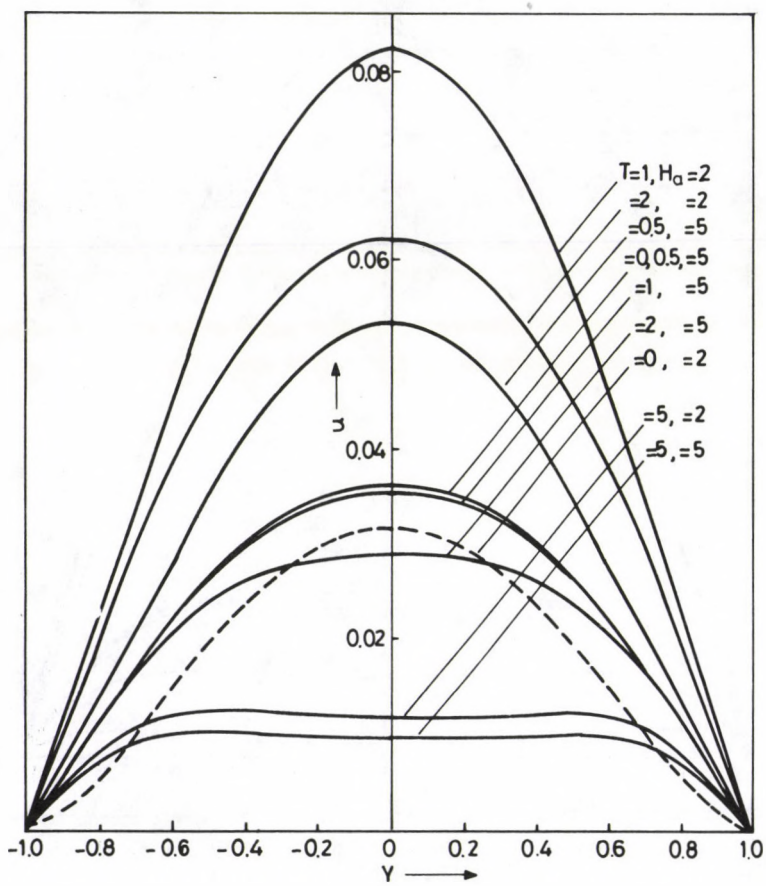

Fig. 17. Secondary velocity distribution for $\alpha = 2$ (conducting walls). $s = 1/2$
Broken line: Sato's calculation ($T = 0$)

In particular for $T = 5$, w is maximum at two points situated symmetrically about $y = 0$. This can be regarded as the effect of rotation.

Figures 16 and 18 show the primary velocity distribution in the case $s = \frac{1}{2}$ and when $\alpha = 2$ and 5, respectively. For fixed values of H_a and α, it is found that as T increases, the primary velocity at any point of the channel decreases. The two symmetrical points about $y = 0$, at which the velocity is maximum have been

observed in this case, too, for large rotation. And u is almost the same for fixed α at any point for large T, whatever H_a be.

Figures 17 and 19 show the secondary velocity distribution in the case $s = \frac{1}{2}$ when $\alpha = 2$ and 5, respectively. The discussion in this case remains the same as secondary velocity distribution corresponding to $s = 0$ as in Figs 13 and 15.

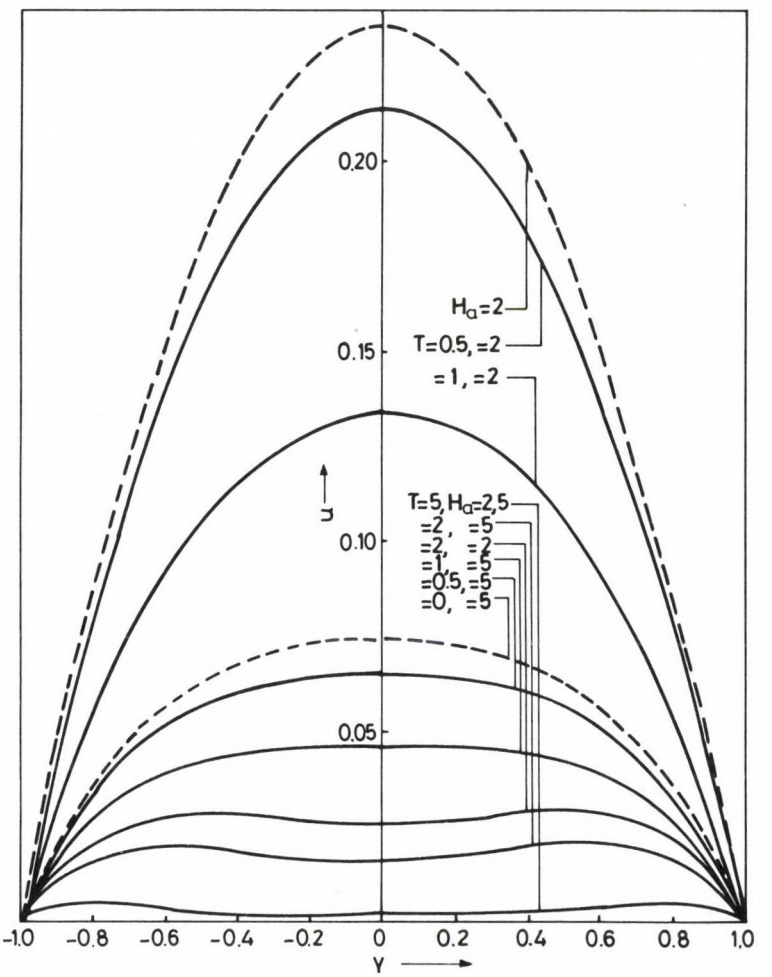

Fig. 18. Primary velocity distribution for $\alpha = 5$ (conducting walls). $s = 1/2$
Broken line: Sato's calculation ($T = 0$)

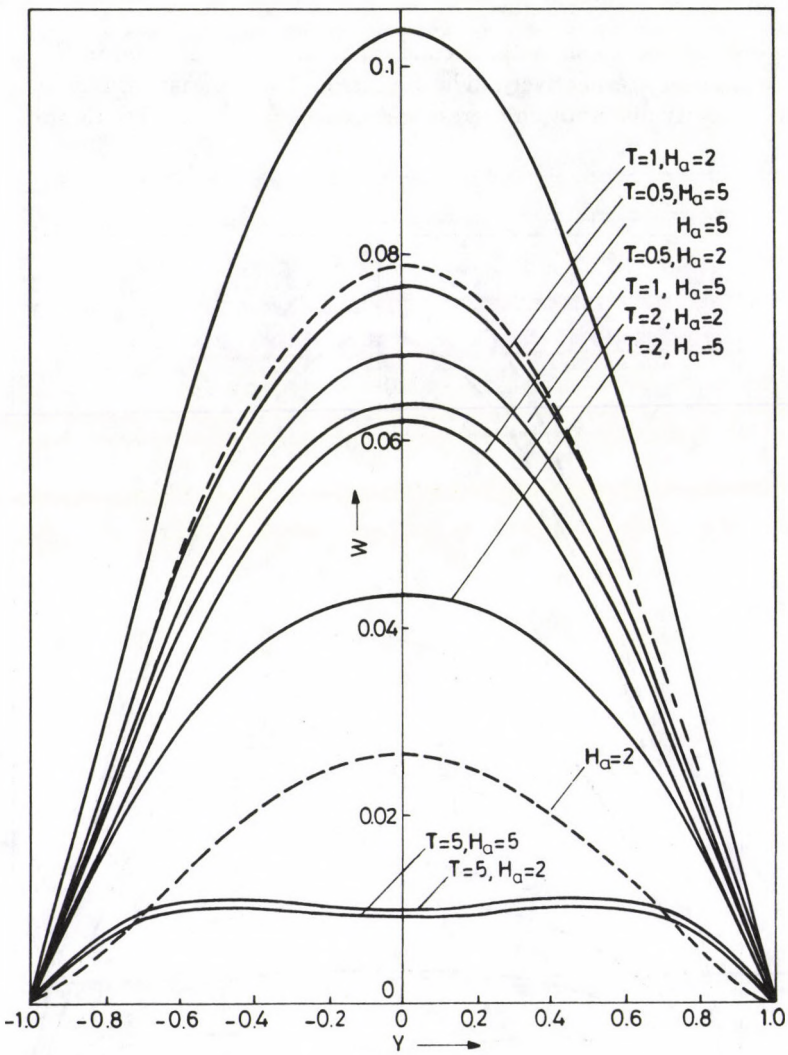

Fig. 19. Secondary velocity distribution for $\alpha = 5$ (conducting walls). $s = 1/2$
Broken line: Sato's calculation ($T = 0$)

References

1. I. Tani, J. Aero. Space Sci., *29*, 297, 1962.
2. L. J. F. Broer, L. A. Peletier and L. Van Wijugaarden, Appl. Sci. Res. Ser. B, *8*, 259, 1960.
3. H. Sato, J. Phys. Soc. Japan, *16*(7), 1427, 1961.
4. A. Sherman and G. W. Sutton, Magnetohydrodynamics, Evanston, Illinois, 1961, p. 173.

5. T. Yaminishi, J. Phys. Soc. Japan, *5*, 29, 1962.
6. M. Katagiri, J. Phys. Soc. Japan, *27*, 1051, 1069.
7. I. Pop, J. Math. Phys. Sci., *5*(4), 375, 1971.
8. A. S. Gupta, Acta Mechanica, *22*, 281, 1975.
9. N. Datta and R. N. Jana, J. Phys. Soc. Japan, *40*, 1469, 1976.
10. R. N. Jana and N. Datta, Acta Mechanica, *28*, 211, 1977.
11. R. N. Jana, N. Datta and B. S. Mazumder, J. Phys. Soc. Japan, *45*, 1034, 1977.
12. G. Krishnam Raju and V. V. Ramana Rao, Acta Phys. Hung., *44*, 363, 1978.
13. E. G. Sakhnovskii, Zh. Techon. Fsz., *33*, 631, 1963.
14. A. B. Vatazhin, Zh. Prikl. Mech. Techon. Fsz, *2*, 3, 1965.
15. L. Debnath, S. C. Ray and A. K. Chatterjee, ZAMM, *59*, 469, 1979.
16. L. Spitzer, Physics of Fully Ionized Gas, Intersci. Publ., New York, 1956.

Acta Physica Hungarica 72 (1), pp. 47–54 (1992)

MARTENSITIC FORMATION AND INTERNAL FRICTION

ALI DOGAN

Department of Physics, Faculty of Science and Arts, Firat University
23169 Elazig, Turkey

(Received 20 December 1991)

Coherent phonons which start martensitic formation are the solutions of the Duffing equation. By using this idea the frictional force was included in this undamped nonlinear equation. Numerical results were obtained for Au–Cu–Zn (30 at% Cu, 47 at% Zn) and In–Tl (21 at% Tl) single crystal. Dependence of vibrational amplitude of the phonons on frequency of driving force was researched for various temperatures in the austenitic range. It was found that damping effects change that strongly as the martensitic transformation temperature, M_s, is approached. The proposed model in this study can explain the jump phenomenon in the response curves more clearly and realistically when damping is included.

1. Introduction

Nonlinear differential equation systems have become increasingly important in metal physics. Martensitic transformation is associated with certain thermodynamical features relating to phonons: This transformation occurs with the velocity of sound, pre-transformation vibrational mode softening, etc. Therefore, in recent years several phonon models relevant to martensitic transformation have been presented [1]. Zhang has stated that the coherent phonons will be able to start martensitic transformation [2]. In his model the researcher has neglected the frictional effects which have a retarding role against leaving of interface from austenite. In this paper pre-martensitic internal friction effects, contrary to Zhang's investigation were included in the nonlinear differential equation of atomic motion. The main result of this study is that the damping parameter affects considerably the vibrational amplitude of the phonons during the martensitic transformation. The new model improved in this paper can explain the characteristics of the transformation and reverse transformation and describes rather well hysteresis phenomena associated with the transformation.

2. Forced oscillations

2.1 Undamped equation of atomic motion

According to the theory of coherent phonon starting martensitic transformation, a phenomenon starting transformation depends on cooperative atomic movement in a potential well of coherent phonon waves propagated in austenite phases.

Therefore, it is supposed that there are various regions including the lattice displacement waves above the martensitic starting temperature, M_s. The amplitude of the lattice displacement wave is enhanced enough to go beyond the critical amplitude atoms crowd through the energy barriers into the positions determined by the crystal lattice of the low-temperature equilibrium phase and these dynamical displacements are frozen out, resulting in the martensitic structure. The equation describing the motion of the atoms can be derived from a potential $\varphi(r)$ as martensitic transformation is characterized by cooperative atomic movements. By using the expression

$$F = -d\varphi(r)/dr \tag{1}$$

it is obtained as

$$m\ddot{r} + kr + \gamma r^3 = 0, \tag{2}$$

where

$$\varphi(r)/m = \mu r^2/2 + \beta r^4/4,$$

which is called coherent phonon potential, m is the total mass of atoms, k and γ are constants. The frequency of the soft-mode of the transformation is

$$w_0^2 = \mu = C_2(T - T_c) = k/m, \tag{3}$$

where T_c is martensitic start temperature and $\beta = \gamma/m$. Since the amplitude of atoms is enhanced by the coherent phonon waves the motion of atoms must also be under the influence of an external force $F_0 \cos wt$. This driving force represents the stress caused by the vibrating atoms driven by the pre-transformation lattice displacement waves which crowd into the space between the neighbouring atoms and cause the deformation of crystal lattice in the transformed region. By considering this force the equation describing the motion of atoms termed Duffing equation can be represented by

$$d^2r/dt^2 + \mu r + \beta r^3 = (F_0/m)\cos wt. \tag{4}$$

The solution of this equation is given [3]

$$\begin{aligned} r &= r_0 \cos wt, \\ w^2 &= w_0^2 + 3\beta r_0^2/4 - f/r_0, \end{aligned} \tag{5}$$

where $f = F_0/m$. Zhang used this equation to study the amplitude of atomic displacements during martensite transformation.

2.2 Damped equation of atomic motion

During the martensitic phase transformation it is known that the interface of austenite–martensite moves with the velocity of sound. When the interface is influenced from the austenite, this effect appears as frictional force. Therefore, the

frictional force which is proportional to the velocity of the interface should be added to the equation describing the motion of the atoms so that the potential used is much more reasonable. In this study this force acting on such a system executing small oscillations of phonons may be written $-\alpha\dot{r}$, where α is a positive coefficient and the minus sign indicates that the force acts in the direction opposite to that of the velocity. Adding this force on the right-hand side of the Eq. (4) we obtain

$$d^2r/dt^2 + 2\lambda dr/dt + \mu r + \beta r^3 = f\cos wt, \tag{6}$$

where $2\lambda = \alpha/m$. By using the Van der Pol method [4–6], the solution of this equation is found as

$$\begin{aligned} r &= r_0 \cos wt, \\ w^2 &= w_0^2 + 3\beta r_0^2/4 \pm [(f/r_0)^2 - (2w_0\lambda)^2]^{1/2} \end{aligned} \tag{7}$$

or

$$\nu^2 = \nu_0^2 + 3\beta r_0^2/16\pi^2 \pm [(F_0/4\pi^2 m r_0)^2 - (\nu_0\lambda/\pi)^2]^{1/2}.$$

The coefficient β which depends strikingly on the properties of the material was taken as a positive constant in the equations mentioned. Therefore, the solutions already obtained above were found for the hard spring case. In the soft spring case this constant is negative [7].

3. Results and discussion

It is interesting to compare the results obtained in this paper with those for the response curve which is suggested by Zhang. For this purpose the amplitude of oscillation displaying atomic displacements during the martensitic transformation is plotted against the frequency of the driving force for damping parameter, λ, and a given amplitude of that force. The values $C_2 = 48\times10^6\,\mathrm{jm^{-3}K^{-1}}$, $\beta = 6\times10^{11}\,\mathrm{jm^{-3}}$, $m = 95.1\times10^{-3}$ kg for a gram mole of the alloy Au-30 at% Cu-47 at% Zn and $C_2 = 2.5\times10^6\,\mathrm{jm^{-3}K^{-1}}$, $\beta = 1.04\times10^{12}\,\mathrm{jm^{-3}}$, $m = 133.6\times10^{-3}$ kg for a gram of the alloy In-21 at% Tl were used in computing amplitude-frequency response curves [8–10].

The effect of the damping parameter λ, which represents the friction of the interface between austenite and martensite, is shown in Fig. 1 when all other parameters are held constant. The peak amplitude of the response increases as λ decreases and its corresponding frequency decreases. But at $\nu = \nu_0$ (resonance), the amplitude of the response does not decrease appreciably as λ increases. The curves are nested and bent to the left (since $\beta < 0$).

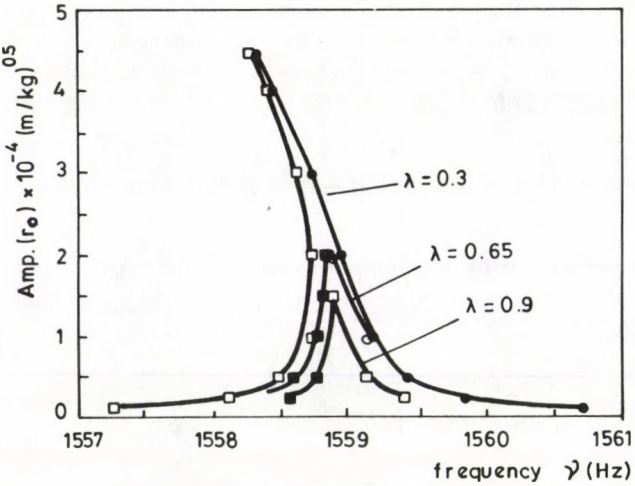

Fig. 1. Effect of the damping parameter λ on the response. Driving amplitude $F_0 = 0.25$, $T = 210$ K

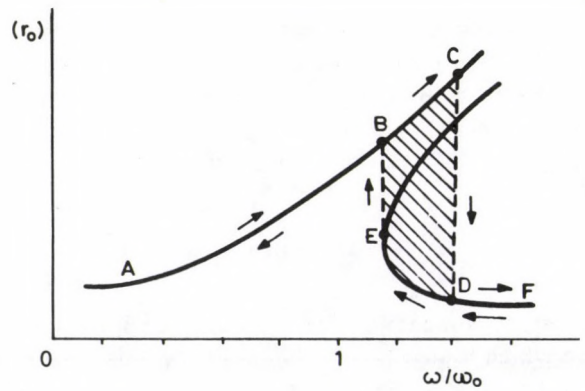

Fig. 2. The phase transformation jump phenomenon described by the Duffing equation. This curve was taken from reference [2]. Here $\lambda = 0$, $\beta > 0$

The response curve for $\lambda = 0$ was discussed by Zhang's paper (Fig. 2). From this Figure, it is not understood that the amplitude jumps definitely to which values of the driving frequency. But the response curves with damping have several fixed peak values.

Figure 3 shows the effect of the driving amplitude F_0 on the response. The amplitude of response increases as F_0 increases and the curves are spaced out in all regions of the driving frequency.

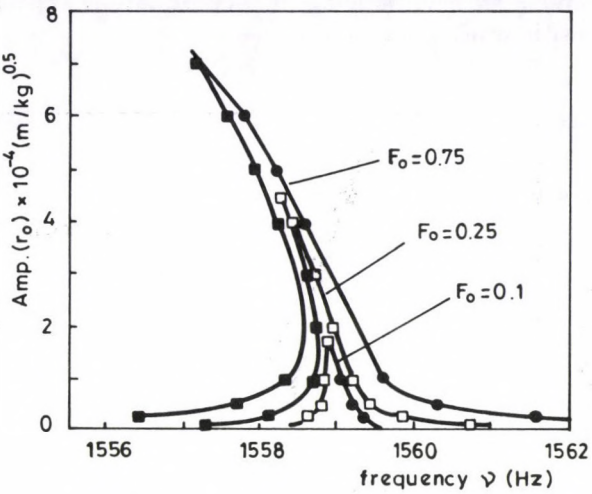

Fig. 3. Effect of driving amplitude F_0 on the response curve for $\lambda = 0.3$, $T = 210$ K

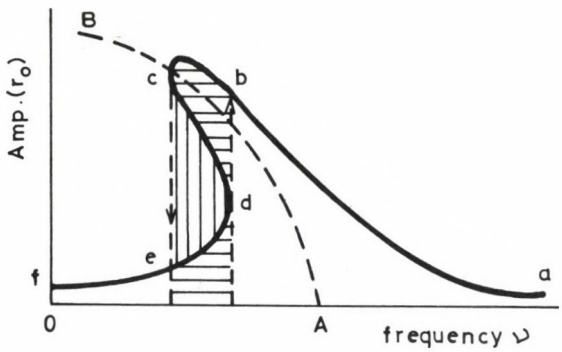

Fig. 4. Amplitude response curve in the case of a damped soft spring Duffing equation ($\beta < 0$)

The most characteristic feature in Eq. (7) is a jump in the response when the driving amplitude is held constant and the frequency is slowly varied through the response region. In the case of the soft spring system the amplitude response curve will be as shown in Fig. 4. The path *cd* is unstable and there is a sudden fall in the response from *c* to *e* when the frequency of the driving force is decreased whereas there is a corresponding jump in response from *d* to *b* on increasing the driving force. Consequently, the location of the peak response will depend upon direction when slowly sweeping the driving frequency, i.e. whether it is upward or

downward. The hatched region in Fig. 4 shows clearly the transformation hysteresis loop. Both reverse transformation and transformation hysteresis are striking features of martensitic transformation [11].

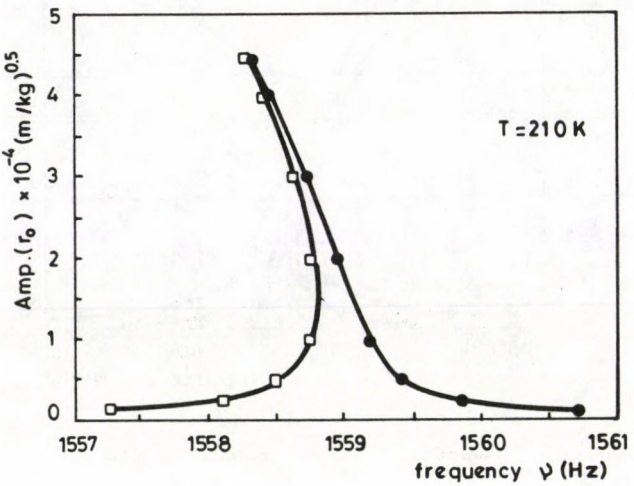

Fig. 5. Amplitude response curve of Au-30 at% Cu, 47 at% Zn alloy for $F_0 = 0.25$ and $\lambda = 0.3$

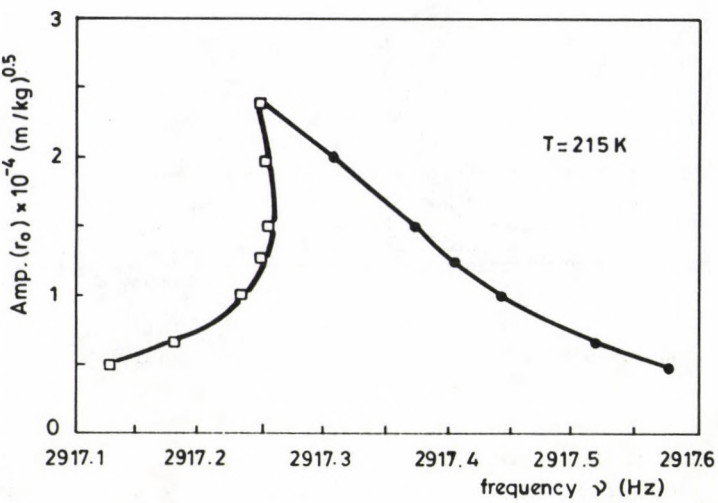

Fig. 6. Amplitude response curve of Au-30 at% Cu, 47 at% Zn alloy for $F_0 = 0.25$ and $\lambda = 0.3$

Figures 5 through 8 demonstrate the nonlinear character of the resonance curves of Au-30 at% Cu-47 at% Zn alloy ($M_s = 208$ K). It can be seen from these

Figures that the nonlinearity effects increase and the response character changes systematically as the martensitic transformation is approached.

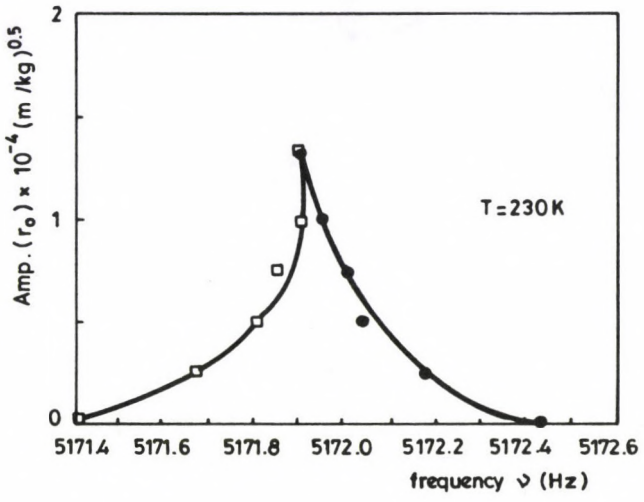

Fig. 7. Amplitude response curve of Au-30 at% Cu, 47 at% Zn alloy for $F_0 = 0.25$ and $\lambda = 0.3$

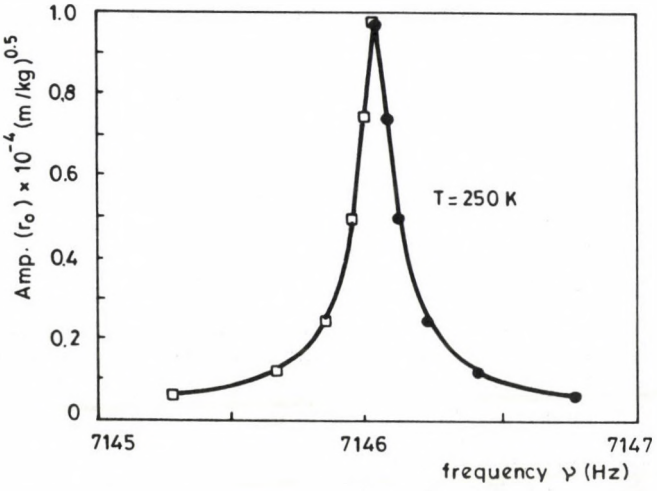

Fig. 8. Amplitude response curve of Au-30 at% Cu, 47 at% Zn alloy for $F_0 = 0.25$ and $\lambda = 0.3$

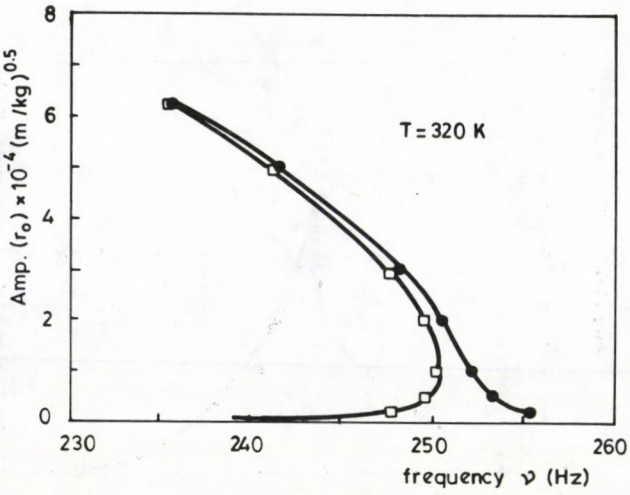

Fig. 9. Amplitude response curve of In-21 at% Tl alloy for $F_0 = 0.25$ and $\lambda = 0.3$

Figure 9 demonstrates the nonlinear character of the response curve for an In-21 at% Tl alloy ($M_s = 314$ K).

Consequently, the maximum amplitude of the resonance curve is governed by the value of the damping parameter and a similarity between the shape of the curves in this paper and those of reference [12] can be readily seen.

References

1. P. C. Clapp, Metall. Trans., *12A*, 589, 1981.
2. J. M. Zhang, J. Phys., F: Met. Phys., *14*, 769, 1984.
3. W. T. Thomson, Theory of Vibration with Applications. Prentice Hall, Englewood Cliffs, N. J., 1972, pp. 392–396.
4. J. K. Hale, Ordinary Differential Equations, John Wiley and Sons, New York, 1969, pp. 168–170, 195–202.
5. J. B. Hunt and J. C. Nissen, Journal of Sound and Vibration, *83*, 573, 1982.
6. A. H. Nayfeh, Introduction to Perturbation Techniques. Wiley–Interscience, New York, 1981.
7. E. L. M. Flerackers, H. J. Janssen and L. Beerden, Am. J. Phys., *53*, 574, 1985.
8. F. Falk, Z. Phys., *B51*, 169, 1983.
9. F. Falk, Z. Phys., *B54*, 177, 1983.
10. Y. Murakami, J. Phys. Soc. Japan, *38*, 404, 1974.
11. J. Ortin, A. Planes, Acta Met., *36*, 1873, 1988.
12. M. Wuttig, C. Lei and I. Hwang, J. de Physique, *46*, C 10–621, 1985.

Acta Physica Hungarica 72 (1), pp. 55–69 (1992)

ANALYTIC STUDY OF THE CLASSICAL EQUILIBRIUM OF HIGHLY ROTATING SPHEROIDAL POLYTROPES

J . P. SHARMA and R. B. YADAVA*

Department of Applied Sciences, M. M. M. Engineering College
Gorakhpur (U. P.) 273010 - India

(Received 21 January 1992)

We have considered some aspects of the structural features of the classical (Newtonian) equilibrium of a highly rotating spheroidal polytrope $n = 1$, governed by the equation of state: $P =$ constant ρ^{γ} (P denotes the pressure, ρ the density and γ the adiabatic constant). Approximate analytical solutions to the equilibrium equations suitable for use in very short computer programs or on small calculators have been given in (u_Θ, v_Θ), (u_p, v_p), (u_ρ, v_ρ) and (ξ_Θ, Θ) planes for $\gamma = 2$ following Padé (2,2) approximation technique. Under certain transformations, the equilibrium equation has been cast into first order differential equations in (u_Θ, v_Θ), (u_p, v_p), (u_ρ, v_ρ), (z_Θ, y_Θ), (z_p, y_p) and (z_ρ, y_ρ) planes. Transformations connecting solutions in these planes have been derived. Graphical material is included showing a comparative study of the runs of u_Θ with v_Θ (Fig. 1), u_p with v_p (Fig. 2), u_ρ with v_ρ (Fig. 3), Θ with ξ_Θ (Fig. 4) and ξ with Δw (Fig. 5) for rotating ($w = 0.05$ and $w = 0.15$) and non-rotating ($w = 0$) configurations. It has been found that the present method of approach is also more suitable for the study of both slowly and highly rotating configurations.

1. Introduction

The study of the properties of polytropes has been a fascinating subject of discussion to applied mathematicians in general and to astrophysicists in particular since long (10^2 yrs according to some estimates). The theory of polytropes is fundamental not only in precise investigations of stellar structure, star formation, galactic dynamics, etc. but also in the rough estimation of some processes in real stars. Most of the stars in the sky are adequately described by Newtonian physics, without taking into account general relativity. Such Newtonian stars deserve some attention here, both because they serve as limiting cases for the more exotic objects that interest general relativists, and also because they guide us in understanding the qualitative properties of these objects. The fundamental problem of the equilibrium of a configuration under its own gravitation with underlaying law

$$P = K\rho^{1+\frac{1}{n}} \tag{1}$$

is almost due to Ritter [1] (K is a disposable constant). The foregoing relation can represent a variety of different possible physical conditions. For example, $n = 0$

* Working as a Research Assistant supported by a grant from CST, U. P., Lucknow, India

represents a homogeneous liquid, $n = 1$, a not centrally condensed matter (which is quite reasonable approximation for neutron stars of one solar mass or greater; and planets like the Earth are better approximated by a polytrope with $n = 7/10$ (Allen [2]). White dwarfs and main-sequence stars are approximated by polytropes with $1.5 \leq n \leq 3$. An isothermal perfect gas is defined by $n \to \infty$. Mass distribution and velocity dispersion in the bulge halo subsystems correspond approximately to that of a polytrope of index 5 (Mark [3]). Knowledge of polytropic (or isothermal) configurations is useful in the study of gaseous filaments or of spiral arms and globular star clusters.

Considerable amount of work has already been done towards the study of the equilibrium of static, polytropic (or isothermal) configurations (for example, Emden [4]; Eddington [5]. Milne [6]; Chandrasekhar [7]; Ostriker [8]; Taff et al [9]; Lightman [10]; Srivastava [11]; Seidov and Sharma [12]; Sharma [13]; Sharma and Yadav [14]) and rotating configurations (Jeans [15]; Chandrasekhar [16]; Roberts [17]; James [18] Monaghan and Roxburgh [19]; Carl J. Hansen et al [20]; Cunningham [21]; Sharma and Yadav [14]) in classical (Newtonian) theory. Extensive studies have also been made towards the above mentioned configurations under special relativistic treatment (for example, Stoner [22]; Kothari [23]; Chandrasekhar [7], Schatzmann [24], Sharma [13, 25, 26]) and slowly or highly rotating configurations (neutron, supermassive and polytropic stars) under general relativistic treatment (for example, Hartle [27]; Hartle and Thorne [28]; Hartle et al [29]; Hartle and Munn [30]; Sharma [31]).

In most of the above works, particularly, in rotating cases, with which we are presently concerned, the following methods have generally been adopted to solve the equilibrium equations (i) a perturbation approach, (ii) the Roche approximation, (iii) variational principle, (iv) formation of self-consistent density and potential distributions, and (v) numerical methods.

The above mentioned methods are, however, lengthy, cumbersome, and involve considerable mathematical complexities. Hence, these may not be economical for computer programming. Further, one is faced with inherent analytical difficulties for the case of highly rotating polytropes (high angular velocity Ω or w as it needs developing in powers of Ω, expansions for the departures of the equilibria from Emden spheres). All this could be avoided by employing a much simpler method known as Padé (2,2) approximation technique, as used elsewhere (see for example, Seidov and Sharma [12], Seidov [32], Sharma [13], Sharma and Yadav [14]), to solve the equilibrium equation for rotating spheroidal polytrope of index unity ($n \leq 1$ are only physically admissible values to the present case). The main advantages of the present approach are: (i) it does not involve too much mathematical complexity related with computational work, (ii) it is less time consuming, (iii) it is computationally efficient and economical, and (iv) it is suitable for both cases of slowly and highly rotating polytropes.

First, in Section 2, we will present the structural equation in (ξ_Θ, Θ) plane. In Section 3, we will derive first-order differential equations in (u_Θ, v_Θ), (u_p, v_p), (u_ρ, v_ρ), (z_Θ, y_Θ), (z_p, y_p) and (z_ρ, y_ρ) planes. Section 4 deals with certain transformations connecting the solutions in these planes. Approximate analytical solutions

describing the physical structure of the configurations in (u_Θ, v_Θ), (u_p, v_p), (u_ρ, v_ρ) and (ξ_Θ, Θ) planes for $\gamma = 2$ have been given in Section 5. Section 6 throws some light on possible values of the critical angular velocity attainable by the configurations. Concluding remarks are given in Section 7. Results of our calculations are displayed in Figs 1–5. Stability considerations or bifurcation analysis could be another interesting aspect of the problem which we, however, intend to include in future work, as some light has already been thrown towards this aspect by some of the above mentioned authors following different methods than the present one.

2. Structure equation

Structure equation in the (ξ_Θ, Θ) *plane*

The fundamental equation of classical equilibrium of a highly rotating (spheroidal) mass of fluid obeying a polytropic equation of state (1) is given by

$$K(n+1)\frac{1}{r^2}\frac{d}{dr}\left(r^2\frac{d\rho^{1/n}}{dr}\right) = -\left[\frac{4\pi G}{e}(1-e^2)^{\frac{1}{2}}\sin^{-1}e\right]\rho + 2\Omega^2, \tag{2}$$

where G is the gravitational constant, e the eccentricity, and Ω the angular velocity.

To reduce the foregoing equation to a manageable, dimensionless form, we introduce the dimensionless variables Θ and ξ_Θ defined by

$$\rho = \lambda\Theta^n; \quad r = \left[\frac{e}{(1-e^2)^{\frac{1}{2}}\sin^{-1}e}\frac{(n+1)K}{4\pi G}\lambda^{\frac{1}{n}-1}\right]^{\frac{1}{2}}\xi_\Theta, \tag{3}$$

and w and v by

$$w = \frac{e}{(1-e^2)^{\frac{1}{2}}\sin^{-1}e}v, \quad v = \frac{\Omega^2}{2\pi G\lambda}. \tag{4}$$

Then, Eq. (2) in (ξ_Θ, Θ) plane is obtained in the form

$$\frac{1}{\xi_\Theta^2}\frac{d}{d\xi_\Theta}\left(\xi_\Theta^2\frac{d\Theta}{d\xi_\Theta}\right) = -\Theta^n + w, \tag{5}$$

which satisfies the initial boundary conditions

$$\Theta(0) = 1, \quad \frac{d\Theta(0)}{d\xi_\Theta} = 0 \quad \text{at} \quad \xi_\Theta = 0. \tag{6}$$

3. First-order differential equations in (u_Θ, v_Θ), (u_p, v_p), (u_ρ, v_ρ), (z_Θ, y_Θ),(z_p, y_p) and (z_ρ, y_ρ) planes

3.1 First-order differential equations in (u_Θ, v_Θ), (u_p, v_p) and (u_ρ, v_ρ) planes

Let the two independent functions u_Θ and v_Θ be related with the variables ξ_Θ and Θ by

$$u_\Theta = -\frac{\xi_\Theta(\Theta^n - w)}{\Theta'}, \quad v_\Theta = -\frac{\xi_\Theta \Theta'}{\Theta}. \tag{7}$$

Then, Eq. (5) reduces to its equivalent first-order differential equation:

$$\frac{du_\Theta}{dv_\Theta} = -\frac{u_\Theta}{v_\Theta}\left[\frac{u_\Theta + n\alpha_\Theta v_\Theta - 3}{u_\Theta + v_\Theta - 1}\right]; \quad \alpha_\Theta = \frac{\Theta^n}{\Theta^n - w}. \tag{8}$$

In (r, P) and (r, ρ) planes, Eq. (5) can be written as

$$\frac{1}{r^2}\frac{d}{dr}\left(\frac{r^2}{P^{\frac{n}{n+1}}} \cdot \frac{dP}{dr}\right) = -P^{\frac{n}{n+1}} + cw; \quad c = \lambda K^{\frac{n}{n+1}}, \tag{9}$$

$$\frac{1}{r^2}\frac{d}{dr}\left(\frac{r^2}{\rho^{\frac{n}{n+1}}} \cdot \frac{d\rho}{dr}\right) = -\rho + \lambda w, \tag{10}$$

where the dimensionless variables ξ_P and ξ_ρ are defined by

$$r \equiv \alpha_P \xi_P \equiv \left[(n+1)K^{\frac{n-1}{n+1}} \lambda^{\frac{1}{n}-1}\right]^{\frac{1}{2}} \xi_P \tag{11}$$

and

$$r \equiv \alpha_\rho \xi_\rho \equiv \left[n\lambda^{\frac{1}{n}-1}\right]^{\frac{1}{2}} \xi_\rho. \tag{12}$$

Further, if we define the four independent variables u_P and v_P, u_ρ and v_ρ by equations

$$u_P = -\frac{\gamma(P^{\frac{2n}{n+1}} - CP^{\frac{n}{n+1}} w)}{P'}, \quad v_P = -\frac{rP'}{P} \quad (P' = \frac{dP}{dr}), \tag{13}$$

$$u_\rho = -\frac{r(\rho^{2-\frac{1}{n}} - \lambda\rho^{1-\frac{1}{n}} w)}{\rho'}, \quad v_\rho = -\frac{r\rho'}{\rho} \quad (\rho' = \frac{d\rho}{dr}). \tag{14}$$

Then, we obtain from Eq. (5) the following first-order differential equations

$$\frac{du_P}{dv_P} = -\frac{u_P}{v_P}\left[\frac{u_P + \alpha_P v_P - 3}{u_P + \alpha'_P v_P - 1}\right]; \quad \alpha_P = \left(\frac{n}{n+1}\right)\frac{P^{\frac{n}{n+1}}}{P^{\frac{n}{n+1}} - Cw}, \quad \alpha'_P = \frac{1}{n+1} \tag{15}$$

and

$$\frac{du_\rho}{dv_\rho} = -\frac{u_\rho}{v_\rho}\left[\frac{u_\rho + \alpha_\rho v_\rho - 3}{u_\rho + \alpha'_\rho v_\rho - 1}\right]; \quad \alpha_\rho = \frac{\rho}{\rho - \lambda w}, \quad \alpha'_\rho = \frac{1}{n}. \tag{16}$$

3.2 First-order differential equations in (z_Θ, y_Θ), (z_P, y_P) and (z_ρ, y_ρ) planes

The relations between the variables (z_Θ, y_Θ) and (ξ_Θ, Θ) like those used in the discussion of static polytropic gas spheres are (Chandrasekhar [7])

$$z_\Theta = \log\{n(\Theta^n - w)\} + 2\log\xi_\Theta \tag{17}$$

and

$$y_\Theta = \frac{dz_\Theta}{dt_\Theta} = -\frac{n\Theta^{n-1}}{\Theta^n - w}\xi_\Theta \frac{d\Theta}{d\xi_\Theta} - 2, \tag{18}$$

respectively. In consequence of the foregoing Eqs (17) and (18), Eq. (5) reduces to the form of first order differential equation

$$\left[y_\Theta \frac{dy_\Theta}{dz_\Theta} - y - 2 - u(\Theta, y_\Theta)\right] v(\Theta) + e^{z_\Theta} = 0, \tag{19}$$

where

$$u(\Theta, y_\Theta) = \left\{\frac{(1-\frac{1}{n})(\Theta^n - w)}{\Theta^n} - 1\right\}(y+2)^2, \quad v(\Theta) = \frac{(\Theta^n - w)}{\Theta^{n-1}}.$$

If we further define

$$\begin{aligned} &\text{(i)}\ z_P = \xi_P^{-m} P, \quad m = -2, \\ &\text{(ii)}\ y_P = \frac{dz_P}{dt_P} = -\xi_P^{-m+1}\frac{dP}{d\xi_P} + m z_P, \quad \xi_P = e^{-t_P} \end{aligned} \tag{20}$$

and

$$\begin{aligned} &\text{(i)}\ z_\rho = \xi_\rho^{-m} \rho, \quad m = -2, \\ &\text{(ii)}\ y_\rho = \frac{dz_\rho}{dt_\rho} = -\xi_\rho^{-m+1}\frac{d\rho}{d\xi_\rho} + m z_\rho, \quad \xi_\rho = e^{-t_\rho}, \end{aligned} \tag{21}$$

then Eqs (9) and (10) get transformed into two similar first-order differential equations

$$\begin{aligned} y_P \frac{dy_P}{dz_P} - y_P + m z_P - \left(\frac{n}{n+1}\right) z_P^{-1} y_P^2 + \left(\frac{m}{n+1}\right)(m z_P - 2y_P) \\ + F_{1,P}(\xi_P, z_P) - C w F_{2,P}(\xi_P, z_P) = 0, \end{aligned} \tag{22}$$

where

$$F_{1,P}(\xi_P, z_P) = \xi_P^{\frac{2-m}{n+1}} z_P^{\frac{2n}{n+1}}$$

and

$$F_{2,P}(\xi_P, z_P) = \xi_P^{\frac{mn}{n+1}} z_P^{\frac{n}{n+1}},$$

$$y_\rho \frac{dy_\rho}{dz_\rho} - y_\rho + mz_\rho + \frac{1}{n}(m^2 z_\rho - 2my_\rho) - (1 - \frac{1}{n}) z_\rho^{-1} y_\rho^2 + F_{1,\rho}(\xi_\rho, z_\rho) + F_{2,\rho}(\xi_\rho z_\rho) = 0, \tag{23}$$

where

$$F_{1,\rho}(\xi_\rho, z_\rho) \equiv \xi_\rho^2 z_\rho (\xi_\rho^m z_\rho)^{1-\frac{1}{n}},$$

and

$$F_{2,\rho}(\xi_\rho, z_\rho) \equiv -\lambda w\, \xi_\rho^{2-m} (\xi_\rho^m z_\rho)^{1-\frac{1}{n}}.$$

4. Transformations connecting solutions of polytropic equations in (u_Θ, v_Θ), (u_P, v_P), (u_ρ, v_ρ) planes and (z_Θ, y_Θ), (z_P, y_P) and (z_ρ, y_ρ) planes

Dividing the first equation in (7) by the first equation in (13), and using relations in (3) and (11), we have

$$\frac{u_\Theta}{u_P} = \frac{(1-e^2)^{\frac{1}{2}} \sin^{-1} e \cdot 4\pi G}{e \cdot K^{\frac{2n}{n+1}}}, \tag{24}$$

since

$$P' = \frac{dP}{dr} = \frac{(n+1) K \lambda^{1+\frac{1}{n}} \Theta^n \cdot \Theta'}{\alpha_\Theta}, \quad (\Theta' = \frac{d\Theta}{d\xi_\Theta}) \tag{25}$$

$$\alpha_\Theta = \left[\frac{e(n+1)K}{(1-c^2)^{\frac{1}{2}} \sin^{-1} e\, 4\pi G} \lambda^{\frac{1}{n}-1} \right]^{\frac{1}{2}}.$$

We find from (24)

$$u_\Theta = c_1 u_P, \quad \text{where} \quad c_1 = \frac{(1-e^2)^{\frac{1}{2}} \sin^{-1} e \cdot 4\pi G}{e \cdot K^{\frac{2n}{n+1}}}. \tag{26}$$

Further dividing the first equation in (7) by the first equation in (14), and using relations in (3) and (12), we get

$$u_\Theta = c_2 u_\rho; \quad c_2 = \left(\frac{n}{n+1} \right) \left\{ \frac{(1-e^2)^{\frac{1}{2}} \sin^{-1} e}{e} \right\} \cdot \frac{4\pi G}{K}, \tag{27}$$

because

$$\rho' = \frac{d\rho}{dr} = \frac{n\lambda \Theta^{n-1} \cdot \Theta'}{\alpha_\Theta}.$$

Hence from Eqs (26) and (27), we can easily deduce that

$$\begin{aligned} v_\Theta &= \frac{1}{n+1} v_P, \\ v_\Theta &= \frac{1}{n} v_\rho, \\ v_P &= (1+\frac{1}{n}) v_\rho. \end{aligned} \tag{28}$$

Similarly, using Eqs (3), (11), (12), (17), (18) and (21), one may obtain the transformations connecting the solutions in (z_Θ, y_Θ), (z_P, y_P) and (z_ρ, y_ρ) planes.

From the viewpoint of astrophysical applications, we are more interested in obtaining approximate analytical solutions of some of the above first-order differential equations, say, Eqs (5), (8), (15) and (16), as given in the following Section 5.

5. Approximate analytical solutions of the structure equations for $\gamma = 2$

5.1. Approximate analytical solutions of Eq. (8)

We assume a series expansion of Eq. (8) of the form

$$u_\Theta = 3 + a^*_\Theta v_\Theta + b^*_\Theta v^2_\Theta + c^*_\Theta v^3_\Theta + d^*_\Theta v^4_\Theta, \tag{29}$$

which satisfies the initial conditions $u_\Theta \to 3$, $v_\Theta \to 0$ as $\xi_\Theta \to 0$. With the help of Eqs (8) and (29), we may determine the coefficients $a^*_\Theta, b^*_\Theta, c^*_\Theta, d^*_\Theta, \ldots$, successively by equating the coefficients of like powers of v_Θ. Thus, we have

$$\begin{aligned} a^*_\Theta &= -\frac{3}{5} n\alpha_\Theta, & b^*_\Theta &= -\frac{1}{7} a^*_\Theta (2a^*_\Theta + 1 + n\alpha_\Theta), \\ c^*_\Theta &= -\frac{1}{9} b^*_\Theta (5a^*_\Theta + 2 + n\alpha_\Theta), & d^*_\Theta &= -\frac{1}{11}\{3b^{*2}_\Theta + c^*_\Theta (6a^*_\Theta + 3 + n\alpha_\Theta)\}. \end{aligned} \tag{30}$$

Now, we may express the function u_Θ as Padé (2.2) approximant:

$$u_\Theta = 3 \cdot \frac{1 + A^*_\Theta v_\Theta + B^*_\Theta v^2_\Theta}{1 + C^*_\Theta v_\Theta + D^*_\Theta v^2_\Theta}, \tag{31}$$

where

$$\begin{aligned} A^*_\Theta &= \frac{1}{3} a^*_\Theta + C^*_\Theta, \quad B^*_\Theta = \frac{1}{3}(b^*_\Theta + a^*_\Theta C^*_\Theta) + D^*_\Theta, \\ C^*_\Theta &= \frac{a^*_\Theta d^*_\Theta - b^*_\Theta c^*_\Theta}{\Delta^*_\Theta}, \quad D = \frac{c^{*\,2}_\Theta - b^*_\Theta d^*_\Theta}{\Delta^*_\Theta}, \\ \Delta^*_\Theta &\equiv b^{*2}_\Theta - a^*_\Theta c^*_\Theta. \end{aligned} \tag{32}$$

Figure 1 shows run of u_Θ with v_Θ for highly rotating ($w = 0.05$ and 0.15) and non-rotating ($w = 0$) configurations.

5.2. Approximate analytical solutions of Eqs (15), (16) and (5)

The series expansion of Eq. (15), near the origin $\xi_P \to 0$, satisfying the initial conditions $u_P \to 3$, $v_P \to 0$, is given by

$$u_P = 3 + a_P v_P + b_P v_P^2 + c_P v_P^3 + d_P v_P^4 + \ldots . \tag{33}$$

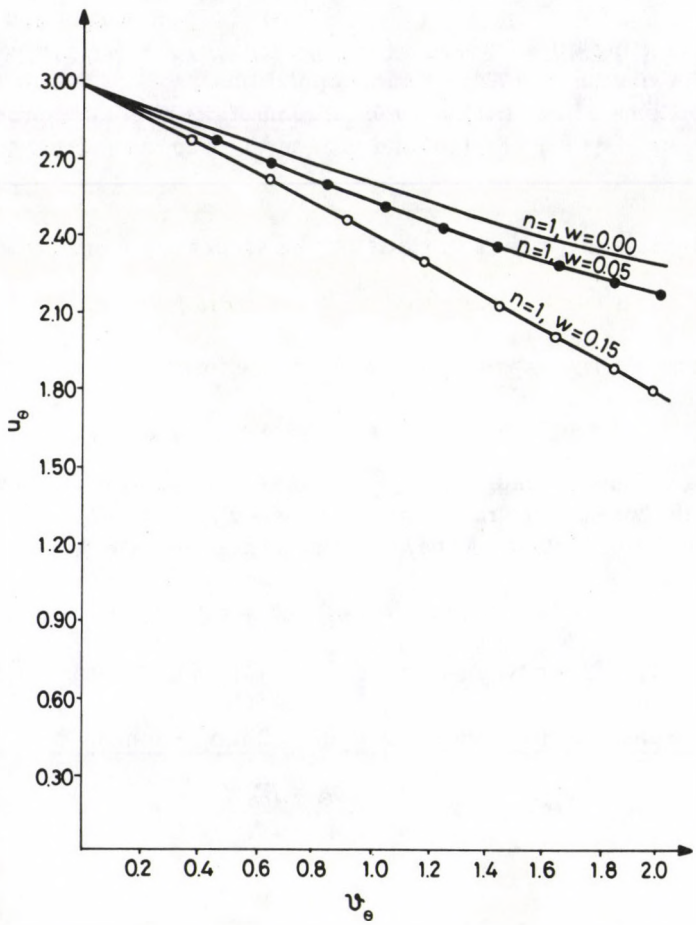

Fig. 1. Run of u_Θ with v_Θ for the rotating polytrope $n = 1$

With the initial conditions $u_\rho \to 3$, $v_\rho \to 0$, near the origin $\xi_\rho \to 0$, we obtain the series solution of Eq. (16):

$$u_\rho = 3 + a_\rho v_\rho + b_\rho v_\rho^2 + c_\rho v_\rho^3 + d_\rho v_\rho^4 + \ldots . \tag{34}$$

The series solution of Eq. (5), satisfying the initial conditions in (6), can be written as

$$\Theta = 1 + a_\Theta \xi_\Theta^2 + b_\Theta \xi_\Theta^4 + c_\Theta \xi_\Theta^6 + d_\Theta \xi_\Theta^8 + \ldots . \tag{35}$$

Corresponding to the above three series solutions u_P, u_ρ and Θ [Eqs (33), (34) and (35)], we obtain the following expressions for Padé (2.2) approximant:

$$u_P = 3 \cdot \frac{1 + A_P v_P + B_P v_P^2}{1 + C_P v_P + D_P v_P^2}, \tag{36}$$

$$u_\rho = 3 \cdot \frac{1 + A_\rho v_\rho + B_\rho v_\rho^2}{1 + C_\rho v_\rho + D_\rho v_\rho^2} \tag{37}$$

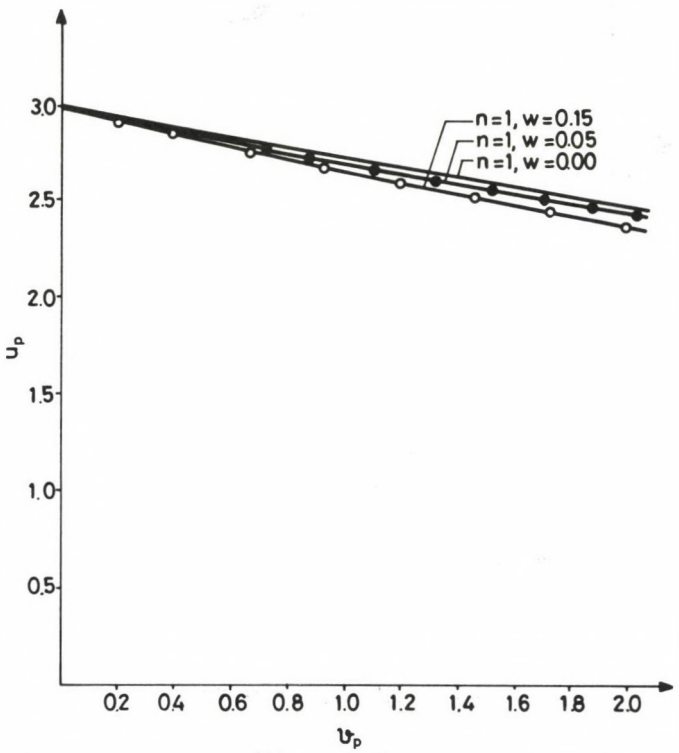

Fig. 2. Run of u_P with v_P for the rotating polytrope $n = 1$

and

$$\Theta = 3 \cdot \frac{1 + A_\Theta \xi_\Theta^2 + B_\Theta \xi_\Theta^4}{1 + C_\Theta \xi_\Theta^2 + D_\Theta \xi_\Theta^4}, \tag{38}$$

respectively.

Results of our calculations are displayed in Figs 2, 3 and 4, respectively, for two chosen values of angular velocity ($w = 0.05$ and 0.15). For comparison, the non-rotating case ($w = 0$) is shown by smooth curve (for values of A_P, B_P, C_P, D_P, a_P, b_P, c_P, d_P, A_ρ, B_ρ, C_ρ, D_ρ, etc. see Appendix 1).

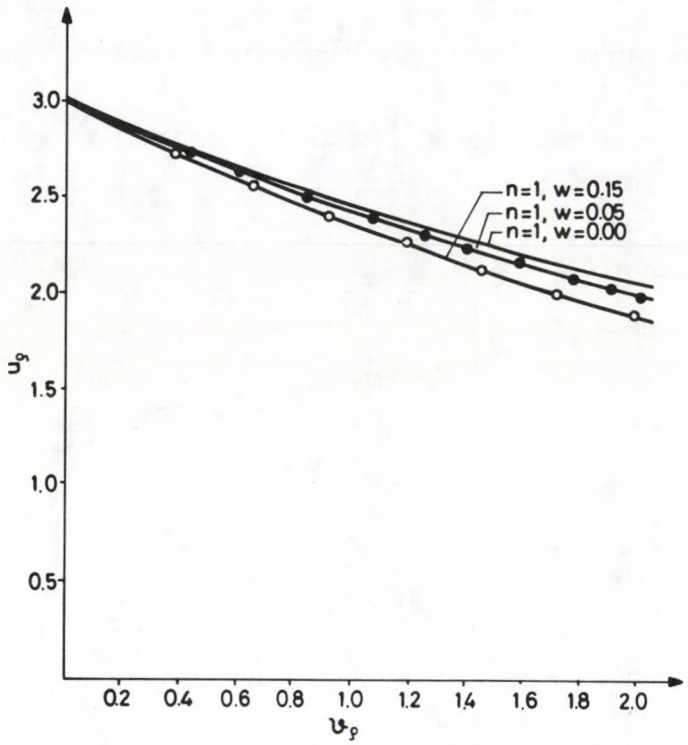

Fig. 3. Run of u_ρ with v_ρ for the rotating polytrope $n = 1$

6. Critical angular velocity

Spheroidal equilibria would bifurcate at $\Omega = \Omega_b$ (subindex 'b' means bifurcation). More explicitly, we may say that bifurcation (possibility of the two equilibria: the 'spheroidal' and 'ellipsoidal') would occur if $\Omega_b \leq \Omega_c$ or equivalently if $w_b \leq w_c$ (subindex 'c' denotes the critical value), and it does not if $w_b > w_c$. The equilibrium is broken at Ω_c. If the angular velocity Ω is increased more and more the matter would flunge away from the equator, and it would form a thin disk.

From our approximate analytical solution in Eq. (38) we may find that the value of the critical angular velocity w_c is $\simeq 0.18$ for $n = 1$ polytrope, for which $\Theta \to 0$ at $\xi = \xi_1 = 4.2976495$. This clearly suggests that due to rotation the

geometrical size ξ_1 is increased by 36.94 % over its spherical shape. This result is in good agreement with that of Roberts [17] as found by variational technique.

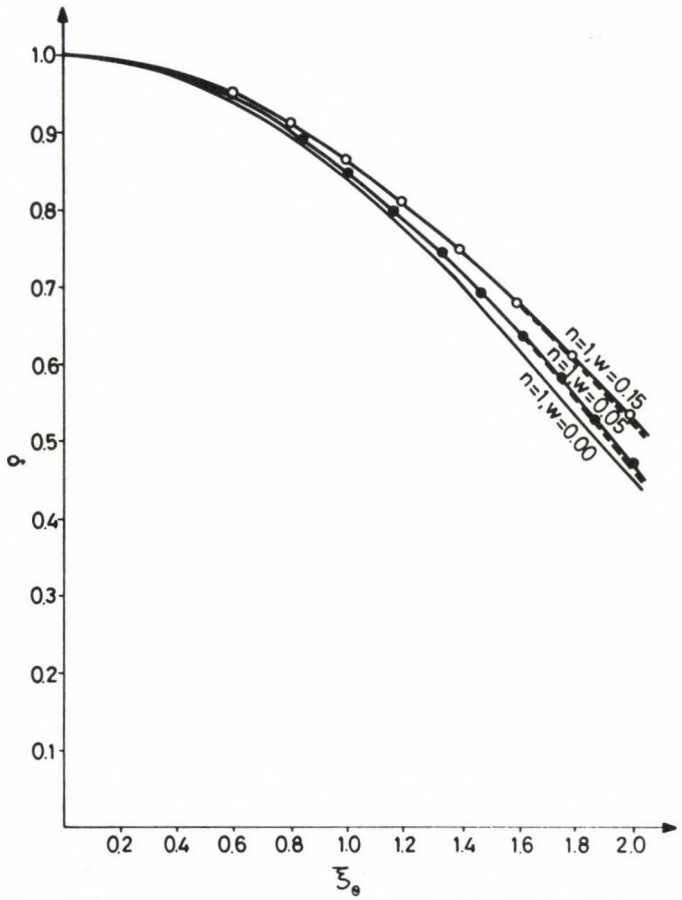

Fig. 4. Variation of density ρ, measured in units of central density λ, plotted as a function of equatorial radius ξ, for rotating polytrope $n = 1$. For comparison, cases of non-rotating and rotating polytropes ($n = 1$), respectively, are shown by solid (Chandrasekhar [7]) and dashed (Roberts [17]) curves

Further, our interest is to calculate small variation Δw $(= w_c - w_P)$ in angular velocity for $n = 1$ polytrope for two chosen values of $w_P = 0.05$ and 0.15 (subindex 'P' means particular) by employing the formula.

$$w_c = \alpha^{-n} w_P, \tag{39}$$

where α is the limiting value of Θ when ξ is small. In Fig. 5 Δw is plotted with ξ.

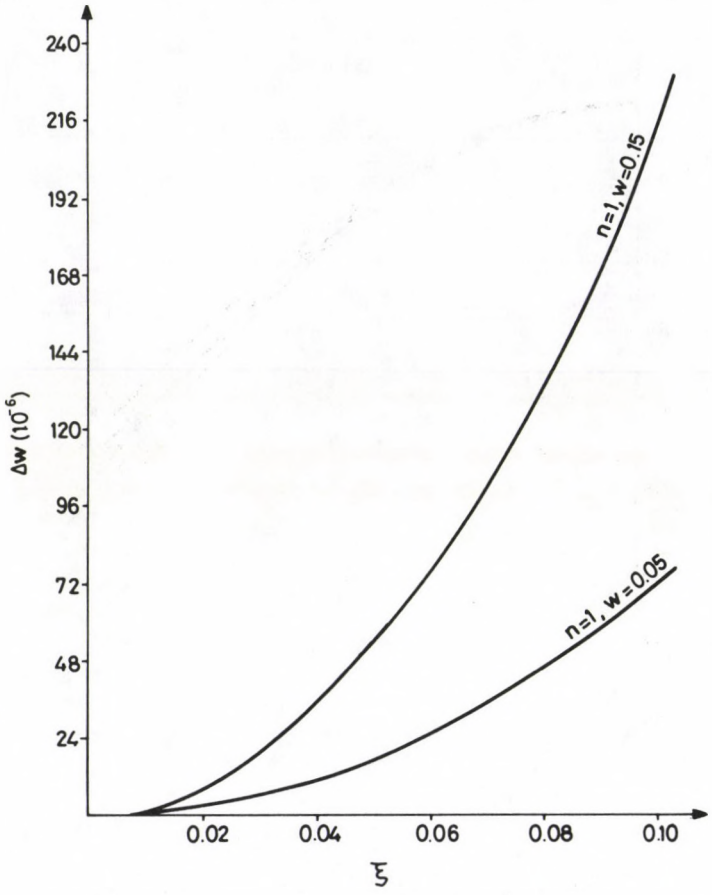

Fig. 5. Run of $\Delta w = (w_c - w_P)$ with ξ for rotating polytrope $n = 1$

7. Conclusions

The present formalism attempts to analyze analytically some structural features of the classical equilibrium of a highly rotating spheroidal $n = 1$ polytrope which obeys an equation of state: $P = K\rho^{\gamma}$. For this purpose, equation of equilibrium (2) has been transformed into first-order differential equations in (u_Θ, v_Θ), (u_P, v_P), (u_ρ, v_ρ), (z_Θ, y_Θ), (z_P, y_P) and (z_ρ, y_ρ) planes (Eqs (8), (15), (16), (19), (22), (23)). Since our previous methods, numerical, variational, perturbation analysis, etc.) would involve mathematical difficulty associated with computational work, we have derived here simple approximate analytical formulae (Eqs (31), (36), (37),

(38)) in concise form from which the desired value of the physical parameter can be obtained using even an electronic pocket calculator (without using computer programs). Evidently, therefore, the present method seems more economical on computer machine than the previous ones.

Results of our calculations are displayed in Figs 1–5, for two chosen values of angular velocities, $w_P = 0.05$ and 0.15. Monotonic falls in u_Θ with v_Θ, u_P with v_P, u_ρ with v_ρ, Θ with ξ_Θ and increasing trend in Δw with ξ have been noted. As pointed out in the main body of this paper (Section 6), our present approach, when applied to bifurcation analysis, leads to yielding the value of critical angular velocity $w_c \simeq 0.18$ which is quite a good approximation in view of the previous findings (Roberts [17]).

With the help of our analytical formulae in Eqs (31), (36), (37) and (38), one may also obtain very conveniently solutions for other values of n. Our present approach may find notable applications in the discussion of stability analysis which has, however, not been included in the present work.

Acknowledgements

The co-author, R. B. Yadava gratefully acknowledges the valuable guidance of Dr. J. P. Sharma, Asst. Professor of Mathematics, at several stages of this work. He is also thankful to CST, U. P., Lucknow, India, for Research Assistantship.

Appendix 1

Values of the coefficients in Eqs (36), (37) and (38):

$$A_P = \frac{1}{3}a_P + C_P, \qquad B_P = \frac{1}{3}(b_P + a_P C_P) + D_P,$$
$$C_P = \frac{a_P d_P - b_P c_P}{\Delta_P}, \qquad D_P = \frac{c_P^2 - b_P d_P}{\Delta_P},$$
$$\Delta_P \equiv b_P^2 - a_P c_P$$

$$a_P = -\frac{3}{5}\alpha_P, \qquad b_P = -\frac{1}{7}a_P(2a_P + \alpha_P + \alpha'_P),$$
$$c_P = -\frac{1}{9}b_P(5a_P + \alpha_P + 2\alpha'_P),$$
$$d_P = -\frac{1}{11}[3b_P^2 + c_P(6a_P + \alpha_P + 3\alpha'_P)],$$

$$A_\rho = \frac{1}{3}a_\rho + C_\rho, \qquad B_\rho = \frac{1}{3}(b_\rho + a_\rho C_\rho) + D_\rho,$$
$$C_\rho = \frac{a_\rho d_\rho - b_\rho c_\rho}{\Delta_\rho}, \qquad D_\rho = \frac{c_\rho^2 - b_\rho d_\rho}{\Delta_\rho},$$
$$\Delta_\rho \equiv b_\rho^2 - a_\rho c_\rho,$$

$$a_\rho = -\frac{3}{5}\alpha_\rho, \qquad b_\rho = -\frac{1}{7}a_\rho(2a_\rho + \alpha_\rho + \alpha'_\rho),$$
$$c_\rho = -\frac{1}{9}b_\rho(5a_\rho + \alpha_\rho + 2\alpha'_\rho),$$
$$d_\rho = -\frac{1}{11}[3b_\rho^2 + c_\rho(6a_\rho + \alpha_\rho + 3\alpha'_\rho)],$$

$$A_\Theta = a_\Theta + C_\Theta, \qquad B_\Theta = b_\Theta + a_\Theta C_\Theta + D_\Theta,$$
$$C_\Theta = \frac{a_\Theta d_\Theta - b_\Theta c_\Theta}{\Delta_\Theta}, \qquad D_\Theta = \frac{c_\Theta^2 - b_\Theta d_\Theta}{\Delta_\Theta},$$
$$\Delta_\Theta \equiv b_\Theta^2 - a_\Theta c_\Theta$$

$$a_\Theta = -\frac{1}{6}(1-w), \qquad b_\Theta = -\frac{A' a_\Theta}{20},$$
$$c_\Theta = -\frac{1}{42}(A' b_\Theta + a_\Theta^2 B'), \quad d_\Theta = -\frac{1}{72}(A' c_\Theta + 2a_\Theta b_\Theta B' + a_\Theta^3 C'),$$
$$A' = \frac{n}{1!}, \quad B' = \frac{n(n-1)}{2!}, \quad C' = \frac{n(n-1)(n-2)}{3!}.$$

References

1. A. Ritter, Wiedemann Annalen, *8*, 172, 1878–1879.
2. C. W. Allen, Astrophysical Quantities, Athlone Press, London, 1977.
3. James W-K. Mark, Ap. J. *206*, 418, 1976.
4. V. R. Emden, Gaskugeln, Teubner, Leipzig, 1907.
5. A. S. Eddington, The Internal Constitution of the Stars, Cambridge University Press, London, 1926.
6. E. A. Milne, Hdb. d. Ap., *3*, 65, 1930.
7. S. Chandrasekhar, An Introduction to the Study of Stellar Structure, Chicago University Press, Chicago, 1939.
8. J. Ostriker, Ap. J., *140*, 1056, 1964; J. Ostriker, Ap. J. Suppl., *11*, 167, 1964.
9. L. G. Taff, H. M. Van Horn, Carl J. Hansen and R. Randy Ross, Ap. J., *197*, 651, 1975.
10. A. P. Lightman, Ap. J., *215*, 914, 1977.
11. Gopalji Srivastava, Ph. D. Thesis, Theory of Polytropes, University of Agra, Agra (U. P.), India, 1977.
12. Z. F. Seidov and J. P. Sharma, DAN USSR, *35*, 5, 1979.
13. J. P. Sharma, D. Sc. Thesis, A Study of Some Problems of Stellar and Planetary Structures, University of Gorakhpur, Gorakhpur (U. P.), India, 1981.
14. J. P. Sharma and R. B. Yadav, 59th Annual Session, Natn. Acad. Sci., India, 1990; J. P. Sharma and R. B. Yadav, Jour. P.A.S. Jaunpur, *1*, 95, 1990.
15. J. Jeans, Astronomy and Cosmogony, Chicago University Press, Chicago, 1929.
16. S. Chandrasekhar, M. N. R. A. S., *33*, 391, 1933.
17. P. H. Roberts, Ap. J., *137*, 1129, 1963.
18. R. James, Ap.. J., *140*, 552, 1964.
19. J. Monaghan and Ian W. Roxburgh, M. N. R. A. S., *131*, 1965.
20. Carl J. Hansen, L. Morris, B. Aizenman and R. Randy Ross, Ap. J., *207*, 736, 1976.
21. C. T. Cunningham, Ap. J., *211*, 568, 1977.
22. E. C. Stoner, Phil. Mag., *7*, 63, 1930, ibid., *9*, 944, 1931.

23. D. S. Kothari, Phil. Mag., *12*, 665, 1931.
24. E. Schatzman, White Dwarfs, Interscience, New York, 1958.
25. J. P. Sharma, Annales de la Société Scientifique de Bruxelles, *91*, III, 131–144, 1977.
26. J. P. Sharma, Astrofizika USSR, *15*, 179, 1979.
27. J. B. Hartle, Ap. J. *150*, 1005, 1967; J. B. Hartle, Ap. J., *161*, 111, 1970; J. B Hartle, Ap. J., *195*, 203, 1975.
28. J. B. Hartle and K. S. Thorne, Ap. J., *153*, 807, 1968.
29. J. B. Hartle, K. S. Thorne and S. M. Chitre, Ap. J., *176*, 177, 1972.
30. J. B. Hartle and M. W. Munn, Ap. J., *198*, 467, 1975.
31. J. P. Sharma, Ap. J., *329*, 232, 1988.
32. Z. F. Seidov, Experientia, *36*, 813, 1980.

Acta Physica Hungarica 72 (1), pp. 71–88 (1992)

EQUATION FOR CATHODIC GLOW SHEATH

S. Holló and B. Nyíri

Light Source Development Department, TUNGSRAM Ltd
1340 Budapest, Hungary

(Received 17 March 1992)

The classical one dimensional approach of cathodic glow discharge is extended into a two dimensional time dependent model. A radial ion transport equation is derived on the basis of the space charge balance. Axial effects are accounted for in a nonlinear source term. It is shown that the radial transport of the ions caused by the radial electric field can be described as a diffusion process with a cathode fall dependent diffusion coefficient. The effect of the motion of sheath boundary and the displacement current are also incorporated.

The model exhibits all of the well-known macroscopic phenomena of glow discharges: subnormal, normal, anomal glow behaviour; pressure dependence of voltage current characteristics; (nearly) piecewise constant current density distributions; the effect of absorbing or reflecting walls; stability limits; subnormal glow oscillations; the lateral spread of glow discharge.

1. Introduction

Basic characteristics, namely subnormal, normal and anomal regions of glow discharge between two parallel disc electrodes, in a few millibars of electropositive gas, with DC supply have been discussed widely (Von Engel, Klyarfeld et al, Emeleus, Ingold and Vlasov et al [1–5]).

Extensive theoretical and experimental analysis has been done to understand the steady state behaviour of the cathode dark space and negative glow (Von Engel and Steenbeck, Emeleus [6–8]). Most of the theoretical works have studied the one dimensional situation assuming infinite parallel plane electrodes and laterally homogeneous discharge. The classical assumptions were: (i) the electric field is linear through the cathode dark space; (ii) in this space charged domain the electron density is negligible beside the ion density; (iii) all transport parameters and source densities (ionisation) in the continuum description depend on the local electric field. (Ward, Neuringer, Davies and Evans [9–12]). It has been shown experimentally that the linearity of the field is a good approximation (Lawler and Doughty, Doughty et al [13,14]). One dimensional calculations gave nearly linear field distribution in a time dependent case as well (Bayle and Perrin [15]).

It is accepted that the ion influx from the negative glow can be neglected in normal glow while in strongly anomalous glows it cannot (Emeleus [8, 16]).

Assumption (iii) on the transport parameters has been widely criticized pointing out that due to the high gradient of the electric field the transport and source terms cannot depend on the local electric field only. To get beyond the limits of

this assumption a more detailed set of transport equations for density, momentum and energy of the components, and also equations of electric field has to be used. The field dependent ionization function is replaced by functionals of distribution functions. Recently Bayle et al [17] have presented such a one dimensional time dependent model for CO_2 glow discharges. To obtain a more correct description of ionisation the Boltzmann equation and Monte-Carlo simulations are used (Tran Ngoc An et al, Boeuf and Marode, Segur et al, Sato and Tagashira, Carman, Paulick and Schoenbach et al [18–24]. With these methods macroscopic transport parameters have also been reexamined.

Regarding the radial coordinate the most exciting question is the normal glow behaviour, i.e. what mechanisms keep the current density and the cathode fall constant in a wide range of current. This question is sometimes put as how the active area on the cathode is stabilized. The first explanations were based on Steenbeck's minimum principle. There were attempts to solve this problem by using equivalent circuitry (Emeleus [16]). Another attempt was based on the focusing effect of radial field on the electron motion (Von Engel et al [25]). Several aspects of radial behaviour have been analyzed by studying the lateral spread of the glow discharge. Applying a voltage higher than the normal cathode fall the edge of the discharge front propagated on the cathode with constant velocity (Emeleus and Von Engel [26]). Clearly, the axial effects should be treated simultaneously with radial ones; normal glow behaviour is a two dimensional phenomenon. Recently Boeuf [27] has presented such a numerical model based on the usual balance equations, stressing the importance of the lateral electric field. The model showed some basic features of normal and anomalous glow.

We see that although the actual glow discharge is a 3D phenomenon, the results of 1D models and theories are able to predict many qualitative features of the glow. Processes in the axial and radial directions are, evidently, different, viz. both their spatial and time scales may differ. So it may be worthwhile to make use of this, applying different approximations in different directions, thus decreasing numerical requirements and, the more important, easing the physico-mathematical analysis.

2. The model

2.1. The charge balance

In order to concentrate on the evolution of the sheath itself we make use of the results of the classical one dimensional calculations and measurements. This, of course, will simplify the form of the balance equations.

First, on the basis of the general ion balance equation we derive a radial balance for the sheath charge density (Q). The general ion balance for a changing volume reads:

$$\frac{d}{dt}\int_V \rho_i dV + \oint_A (J_i - \rho_i v)\cdot dA - \int_V \sigma dV = 0. \tag{1}$$

Here ρ_i is the ion charge density, J_i is the ion current density, σ is the source density, and v is the velocity of the boundary A of the (moving) volume V.

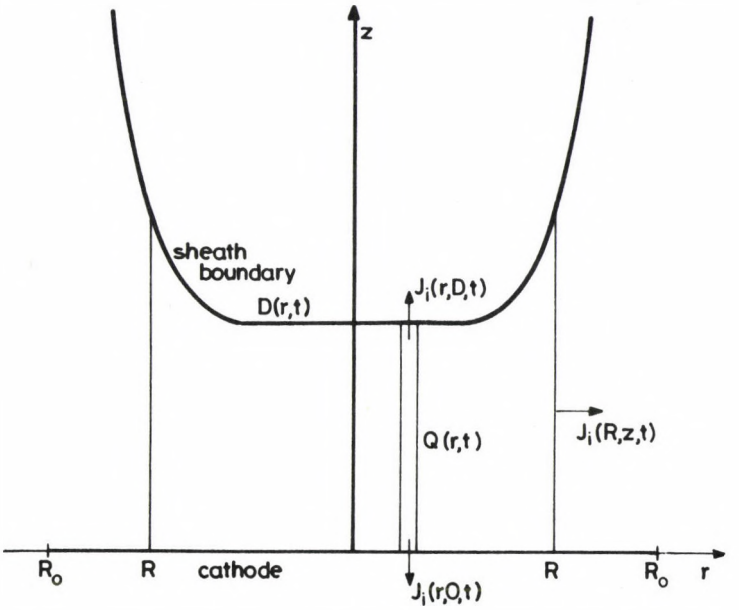

Fig. 1. Schematic representation of the system. The cathode is a disc with radius R_0 lying in the $r, 0$ plane of the cylindrical coordinate system. $D(r,t)$ is the (moving) boundary of the cathode fall sheath

The model situation is shown in Fig. 1, assuming cylindrical symmetry. The cathode surface is a disc of radius R_0. The boundary surface of the cathode fall region is described by its distance from the cathode as a function of radial position and time, $D(r,t)$. Applying Eq. (1) to the region with a radius $R \leq R_0$, and $0 \leq z \leq D(r,t)$, and transforming the surface integral using Gauss theorem, we get

$$\int_0^R 2\pi r \left[\frac{\partial}{\partial t} \int_0^D \rho_i(r,z)\, dz + J_{iz}(r,0) + J_{iz}(r,D) + \right. \tag{2}$$

$$\left. + \frac{1}{r} \frac{\partial}{\partial r} r \int_0^D J_{ir}(r,z)\, dz - \rho_i(r,D) \frac{\partial D}{\partial t} - \int_0^D \sigma dz \right] dr = 0.$$

We also made use of the fact that the velocity of cathode sheath boundary is $\frac{\partial D}{\partial t}$. Since Eq. (2) must hold for any R, the integrand with respect to r must vanish. To exploit this we define the quantity $Q(r,t)$ as

$$Q(r,t) = \int_0^D \rho_i\, dz. \tag{3}$$

This is the sheath charge per unit cathode area at radius r at the time t, provided that the electron density can be neglected. By these the balance equation reads

$$\frac{\partial Q}{\partial t} + J_{iz}(r,0) + J_{iz}(r,D) + \frac{1}{r}\frac{\partial}{\partial r} r \int_0^D J_{ir}(r,z)dz - \rho_i(r,D)\frac{\partial D}{\partial t} = \int_0^D \sigma dz. \tag{4}$$

2.2. The electric field

If we want to obtain an equation for the quantity Q without solving the two dimensional equations we need further assumptions. These we take from the results of the classical 1D approximation. As the electron density is neglected only ions contribute to the space charge. So an assumption on the potential distribution will have a direct consequence on the ion density distribution. As long as the axial electric field is accepted to depend linearly on the distance from the cathode the electric potential ϕ is

$$\phi(r,z,t) = \frac{U(t)}{D(r,t)}\left(2z - \frac{z^2}{D(r,t)}\right). \tag{5}$$

Clearly, the potential at the cathode ($z = 0$) is zero, while at the sheath boundary ($z = D$) it is the time dependent cathode fall $U(t)$ The axial and radial components of the electric field are

$$E_z = \frac{2U}{D}\left(\frac{z}{D} - 1\right); \qquad E_r = \frac{2U}{D^2}\left(z - \frac{z^2}{D}\right)\frac{\partial D}{\partial r}, \tag{6}$$

respectively. This z dependence of E_z is supported both by $2D$ calculations of Boeuf [28] and by experimental evidences cited above.

Integrating the corresponding charge density with respect to z we see that

$$\int_0^D \rho_i dz = \frac{2\varepsilon_0 U}{D}\left(1 + \frac{D}{6r}\cdot\frac{\partial D}{\partial r} + \frac{D}{6}\cdot\frac{\partial^2 D}{\partial r^2}\right), \tag{7}$$

where ε_0 is the permittivity of the vacuum. Let us neglect the terms containing the derivatives, and accept the consequence that our results become less accurate at rapidly changing D. Thus we get

$$Q = \frac{2\varepsilon_0 U}{D}. \tag{8}$$

Now, using Eqs (6), (8), we express all the terms in Eq. (4) with the new basic variables $Q(r,t)$ and $U(t)$.

2.3. Radial transport of ions

If the ion transport is mobility dominated the radial ion current density is $J_{ir} = \mu_i \rho_i E_r$, with ion mobility μ_i. Thus the total radial ion current reads

$$\int_0^D J_{ir}\,dz = \frac{2\varepsilon_0 \mu_i U^2}{3D^2} \cdot \frac{\partial D}{\partial r}\left(1 + \frac{D}{5r} \cdot \frac{\partial D}{\partial r} - \frac{1}{10}\left(\frac{\partial D}{\partial r}\right)^2 + \frac{D}{6} \cdot \frac{\partial D^2}{\partial r^2}\right). \tag{9}$$

Neglecting the higher order terms in the bracket, again:

$$\int_0^D J_{ir}\,dz = \frac{2\varepsilon_0 \mu_i U^2}{3D^2} \cdot \frac{\partial D}{\partial r}. \tag{10}$$

Substituting D from Eq. (8) it is seen that

$$\int_0^D J_{ir}\,dz = -\frac{\mu_i U}{3} \cdot \frac{\partial Q}{\partial r}. \tag{11}$$

2.4. Axial ion current densities

The ion current density at the cathode surface, using Eq. (6), reads

$$J_{iz}(r,0) = \mu_i \rho_i(r,0) E_z(r,0) = \frac{\mu_i}{2\varepsilon_0^2} \cdot \frac{Q^3}{U}. \tag{12}$$

We assume that the ion influx from the negative glow is negligible, i.e.

$$J_{iz}(r,D) = 0. \tag{13}$$

2.5. Ionisation

For the sake of simplicity we apply Townsend's formula and assume that the radial component of the electron current does not contribute to the ionisation. This is consistent with the neglection of higher order terms to get equations (8) and (10). So

$$\int_0^D \sigma\,dz = \int_0^D J_{ez}\alpha_T(E_z)\,dz. \tag{14}$$

Assuming stationarity the local balance for the electrons is

$$\frac{\partial J_{\Theta z}}{\partial z} = J_{ez}\alpha_T(E_z), \tag{15}$$

where $\alpha_T(E) = Ap\exp[-Bp/E]$ is Townsend's ionisation function; A, B are material constants, p is the pressure.

Integrating Eq. (15) and substituting into (14), it is seen that

$$\int_0^D \sigma dz = J_{e0}\left(\exp(\int_0^D \alpha_T(E_z)\,dz) - 1\right), \tag{16}$$

where J_{e0} is the electron current density at the cathode. If secondary emission is the only source of electron emission then

$$J_{e0} = \gamma J_{iz}(r,0) = \gamma\frac{\mu_i}{2\varepsilon_0^2}\cdot\frac{Q^3}{U}, \tag{17}$$

where γ is the secondary emission coefficient.

Substituting E_z from Eq. (6) and D from (8) into Eq. (16) we get the source term as a function of U, and Q

$$\int_0^D \sigma dz = J_{e0}\left(\exp\left(2\varepsilon_0^2 ABp^2\frac{U}{Q^2}\mathcal{A}rh\left(\frac{Q}{\varepsilon_0 Bp}\right)\right) - 1\right), \tag{18}$$

where the 'Arrhenius integral' $\mathcal{A}rh(x)$ is defined as

$$\mathcal{A}rh(x) \equiv \int_0^x \exp\left(-\frac{1}{y}\right)dy. \tag{19}$$

It should be noted that although the particular source term given by Eq. (18) is based on Townsend's local ionisation formula, it is generally a functional of the distribution functions. The distribution functions, however, are macroscopically determined by the macroscopic parameters J_{e0}, D and U. Thus, our approach is able to incorporate a considerable variety of ionisation theories.

2.6. Moving sheath boundary term

We have now only one term not discussed in Eq. (4), the last term on the left hand side corresponding to the motion of the sheath boundary. We set the value of $\rho_i(r,D)$ to the average ion charge density at r. Hence, by using Eq. (8) we get

$$\rho_i(r,D)\frac{\partial D}{\partial t} = \frac{Q}{U}\frac{dU}{dt} - \frac{\partial Q}{\partial t}. \tag{20}$$

2.7. The sheath equation

The final form of the radial balance equation (4) using Eqs (11), (12), (13), (18), (20) reads

$$2\frac{\partial Q}{\partial t} - \frac{Q}{U}\frac{dU}{dt} - \frac{\mu_i U}{3}\frac{1}{r}\frac{\partial}{\partial r}\left(r\frac{\partial Q}{\partial r}\right) =$$

$$= \frac{\mu_i}{2\varepsilon_0^2}\cdot\frac{Q^3}{U}\left(\gamma\exp\left(2\varepsilon_0^2 ABp^2\frac{U}{Q^2}\mathit{Arh}\left(\frac{Q}{\varepsilon_0 Bp}\right)\right) - (1+\gamma)\right). \qquad (21)$$

The terms in balance equation (21) are well interpretable. The first term is the usual rate of change of the sheath charge. The second is an unusual term related to the effect of the motion of the sheath boundary. The third term describes the radial transport of the sheath charge caused by the radial electric field which is formally a diffusion term with a diffusion coefficient depending on U. The source term at r.h.s. includes two processes (as it is clear from its derivation): ions are produced by volume ionisation caused by drifting electrons, and ions disappear from the space charge by the ion current flowing into the cathode.

2.8. Boundary and subsidiary conditions

The boundary conditions we chose for $Q(r,t)$ are very simple

$$\xi Q(R_0,t) + (1-\xi)\frac{\partial Q}{\partial r}\bigg|_{r=R_0} = 0 \quad \text{and} \quad \frac{\partial Q}{\partial r}\bigg|_{r=0} = 0. \qquad (22)$$

We use two values of parameter ξ. $\xi = 0$ corresponds to the totally reflecting wall while $\xi = 1$ to the totally absorbing wall.

In the time dependent case the displacement current should be taken into account as well. Since in our approximation the electric displacement vector $(\varepsilon_0 E)$ at the cathode surface is equal to Q, the current in the external network is given by

$$I = \int_0^{R_0}(1+\gamma)\frac{\mu_i}{2\varepsilon_0^2}\cdot\frac{Q^3}{U}2r\pi\,dr + \int_0^{R_0}\frac{\partial Q}{\partial t}2r\pi\,dr, \qquad (23)$$

which, in steady state, reduces to the surface integral of the ion and electron current density.

3. Results and discussion

3.1. Standard form of equations

In order to simplify the discussion, we regard two solutions essentially identical if one of them can be obtained from the other by a linear transformation of the

quantities Q, U, I, r, t, p. To reflect this we transform Eqs (21) and (23) to the (dimensionless) standard form

$$2\frac{\partial Q}{\partial t} - \frac{Q}{U}\frac{dU}{dt} - \frac{U}{6\alpha^2}\frac{1}{r}\frac{\partial}{\partial r}\left(r\frac{\partial Q}{\partial r}\right) = S(U,Q),$$

$$S(U,Q) = \frac{Q^3}{U}\left(\gamma \exp\left(\frac{U}{Q^2}\mathcal{A}rh\,(Q)\right) - (1+\gamma)\right), \tag{24}$$

$$I = \int_0^{\mathcal{R}} J\, 2r\pi\, dr + \int_0^{\mathcal{R}} \frac{\partial Q}{\partial t} 2r\pi\, dr$$

with

$$J(r,t) = (1+\gamma)\cdot\frac{Q^3}{U}. \tag{25}$$

The quantities in Eqs (24) and (25) are related to the real ones as follows:

$$\begin{aligned}
\mathcal{R} &= \frac{R_0}{L}, \\
p &= \frac{1}{AL}\alpha, \\
r_{\text{real}} &= Lr, \\
Q_{\text{real}} &= \frac{\varepsilon_0 B}{AL}\alpha Q, \\
U_{\text{real}} &= \frac{B}{2A}U, \\
I_{\text{real}} &= \epsilon_0\mu_0\frac{B^2}{A}\alpha^2 I, \\
t_{\text{real}} &= \frac{L}{\mu_0 B}\frac{1}{\alpha}t.
\end{aligned} \tag{26}$$

Here L is the unit of length, and μ_0 is the pressure independent factor in the simplest approximation of mobility, that is $\mu_i = \mu_0/p$. Note the definition of α: it is the dimensionless pressure for a given cathode. The secondary emission coefficient γ has not been transformed. From Eqs (24) and (25) it is clear that this system has two similarity parameters, the numbers α and γ. From now on we shall use the notation applied here in Eqs (24), (25) and (26). For the calculations $\mathcal{R} = 2$ was used.

The applied numerical procedure is a combination of Galerkin's method in space and a Runge–Kutta based time march. The Q distributions were represented by a polynomial of order 16. Non-obvious results were checked by order 32.

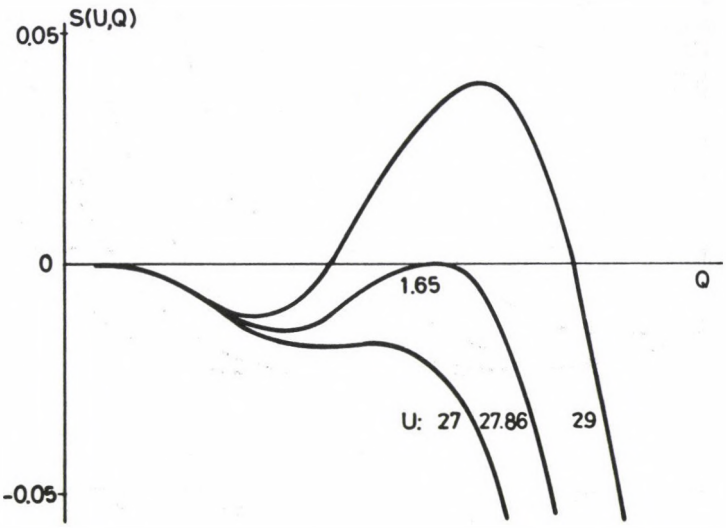

Fig. 2. Lines of the source function $S(U,Q)$ in Eq. (24) at different voltages U at $\gamma = 0.01$

3.2. The source function

The solution of Eq. (24) is highly influenced by the topology of the nonlinear source term $S(U,Q)$. Lines of this function with $\gamma = 0.01$ at different U are depicted in Fig. 2. The function always has the trivial root at $Q = 0$, which means that if there is no space charge, there are, evidently, no processes. If U is low then $S(U,Q) < 0$ for all $Q > 0$. There is a definite voltage $U_0 = 27.86$ when $S(U,Q)$ has one root at $Q = 1.65$. At higher voltages the function has two nontrivial roots. The lower root Q_L decreases while the higher one Q_H increases with rising U.

3.3. Steady state results

Steady state solutions have been obtained by prescribing the current. First we discuss results for the totally absorbing wall, i.e. $\xi = 1$ in Eq. (22).

In Fig. 3 a series of the steady state voltage–current characteristics is presented for $\gamma = 0.01$ at various pressures (α). The three different discharge states can easily be identified. The normal glow range increases with the pressure. The curves converge to a limit as α (pressure) moves to infinity. Since α is proportional to the pressure times cathode size (see Eqs (26)) this limit curve is identical to the pressure independent characteristics of the infinite cathode.

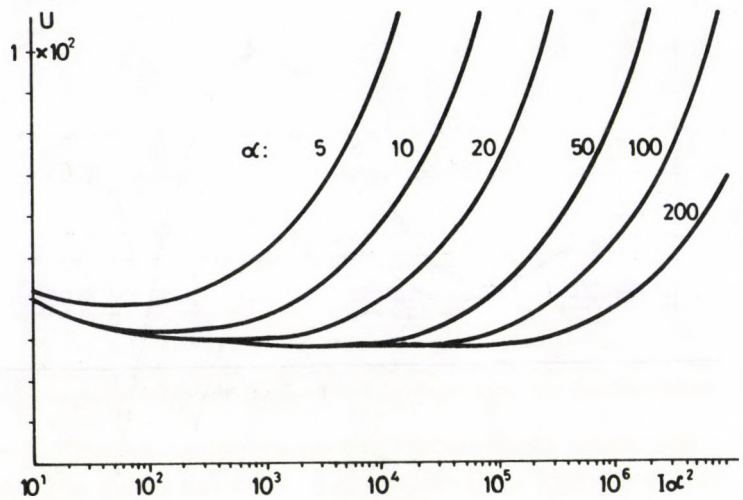

Fig. 3. Voltage–current characteristics at different pressures (times radii) α, with $\gamma = 0.01$

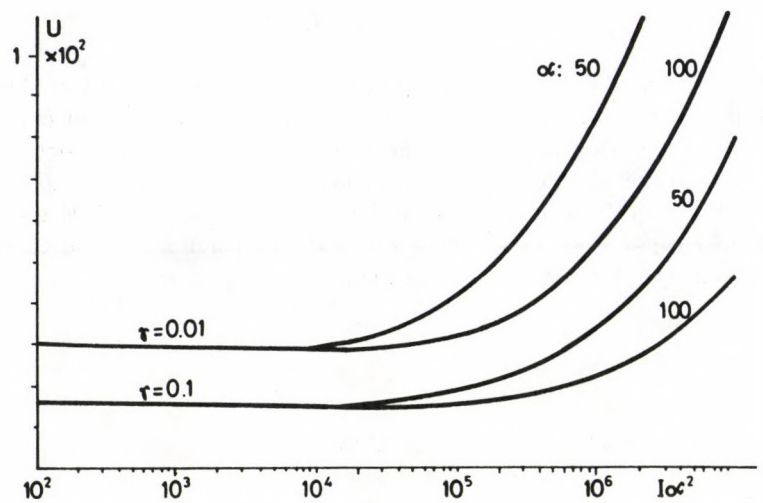

Fig. 4. Comparison of voltage–current characteristics belonging to $\gamma = 0.1$ and $\gamma = 0.01$ at $\alpha = 50$ and $\alpha = 100$

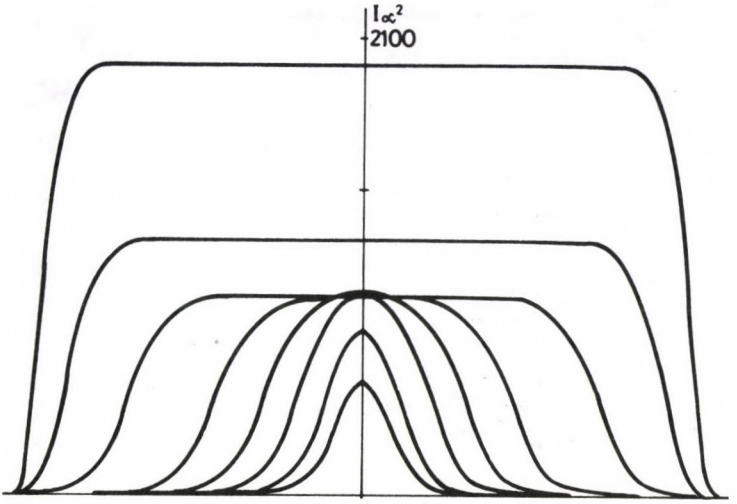

Fig. 5. Current density distributions over the cathode surface at different total currents, with $\alpha = 50$, i.e. "moderate pressure" and $\gamma = 0.01$. The currents corresponding to the curves from inside outwards are: $I \cdot \alpha^2 = 100, 200, 500, 1000, 2000, 5000, 10000, 20000$

Fig. 4 illustrates the influence of γ on the voltage–current characteristics. The normal glow voltage increases with decreasing γ, while the shape of the curves changes but slightly.

The stationary current density distributions belonging to $\alpha = 50$, i.e. to the third curve from the right in Fig. 3, are depicted in Fig. 5. Curves from the third to the sixth from inwards exhibit the typical distribution of normal glow while the corresponding current changes one order of magnitude. When the active area reaches the edge of the cathode the current density starts rising, as expected for the anomal glow.

Reducing the value of α (i.e. the pressure for a given cathode) a qualitatively different solution is obtained as shown in Fig. 6. The normal glow range is missing, consistently to the corresponding characteristics in Fig. 3.

The pressure (α) dependence of the characteristics and the Q distributions can be explained in the frame of the basic balance equation (24). At high pressure the diffusion term is small, so is the radial loss. At low pressure this term becomes significant and the radial transport causes the discharge to distribute smoother over the cathode surface. As the source term $S(U, Q)$ is α independent this increased radial loss can be compensated only by higher source density, i.e. higher voltage. As a result, for $\alpha < 50$, the typical normal glow range is missing.

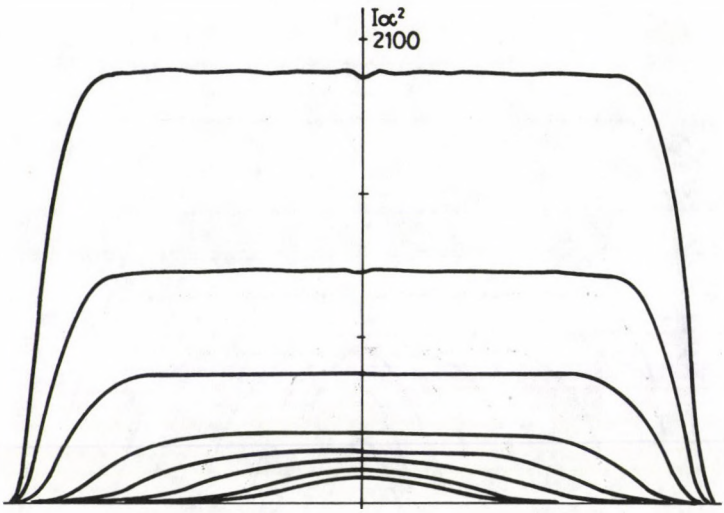

Fig. 6. Current density distributions over the cathode surface at different total currents, with $\alpha = 20$, i.e. "low pressure" and $\gamma = 0.01$. The currents corresponding to the curves from inside outwards are the same as in Fig. 5: $I \cdot \alpha^2 = 100, 200, 500, 1000, 2000, 5000, 10000, 20000$

Though the qualitative agreement of the results to experiments is apparent, we made a comparison to measurements of Klyarfeld et al for argon [2]. The curves in Fig. 7 are not a best fit. The parameter γ was determined by fitting the normal glow voltage, while the rest of the parameters and the ionisation function were taken from the literature (Ward [9]).

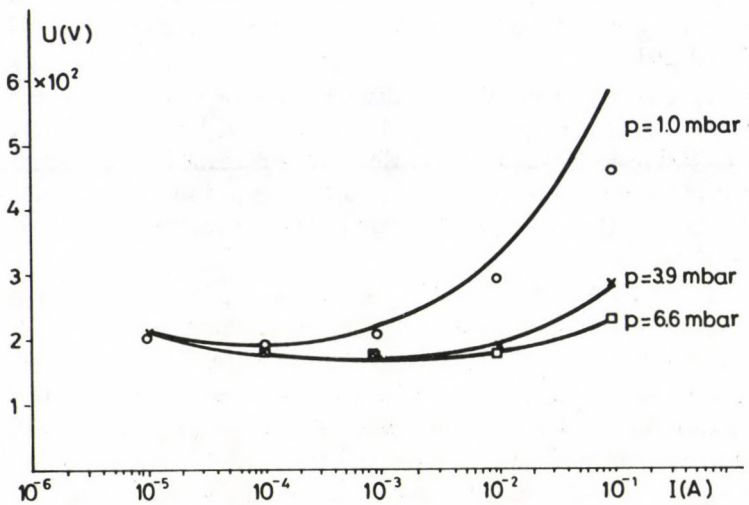

Fig. 7. Comparison of the theoretical curves to experimental results of Klyarfeld et al [2] for pressures of 6.6 mbar, 3.9 mbar and 1.0 mbar of argon. Parameters and formula for ionisation are taken from Ward [9]

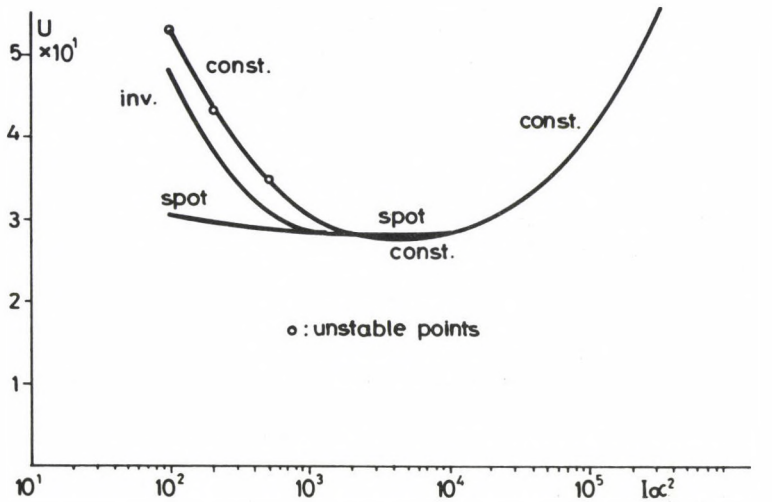

Fig. 8. Voltage–current characteristics with reflecting wall. The unstable parts of the subnormal glow branch of the constant distribution are marked with "o". Below this runs the subnormal branch of the inverse distribution, and that of the spot-like one (bistability). Where the inverse branch approaches the normal glow plateau we find tristability. At the end of the plateau of the spot the voltage of the constant distribution runs lower. In the anomal range only the constant distribution is stable. $\alpha = 50$, $\gamma = 0.01$

We examined the effect of the boundary conditions, viz. the totally reflecting wall ($\xi = 0$). It is evident that in this case there exists always a constant solution, namely the solution Q of the reduced equation $S(U, Q) = 0$. These solutions are necessarily identical to the classical 1D glow model [6,10]. The constant solutions are, however, not always stable. Fig. 8 presents the variety of voltage current characteristics belonging to this boundary condition. Starting from a spot-like distribution at a current $I \cdot \alpha^2 = 100$ we have solutions very similar to those of absorbing wall, and have the constant voltage plateau till approximately $I \cdot \alpha^2 = 10^4$. Here the spot-like solution loses its stability, and the constant current density dominates the full anomal glow range. Coming back from higher currents the voltage decreases below the previous plateau, and the constant distribution is maintained. Thus, here we see two stable solutions. Decreasing further the current we see the voltage rise high above the plateau, yet somewhere below $I \cdot \alpha^2 = 1000$ the stability of the constant solution is lost. Depending on the type of perturbation the system reaches either the original, spot-like state, or an 'inverse' distribution with the current density being the highest at the wall. In Fig. 8 the branch belonging to this inverse distribution runs between that of the unstable (thus non-existing) constant solution and the branch of the normal spot. In Fig. 9 the three charge density distributions of the *tristable*, $I \cdot \alpha^2 = 1000$ current state are presented.

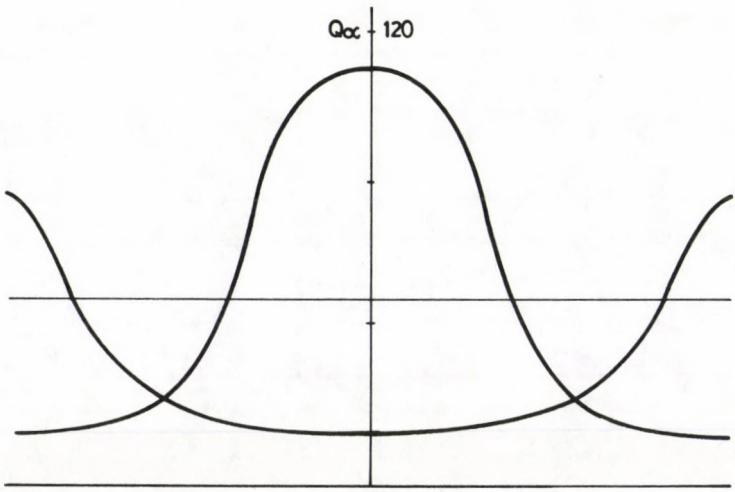

Fig. 9. The charge density distributions of the three stable states: the spot-like, the inverse, and the constant distribution taken at the current $I \cdot \alpha^2 = 1000$, $\alpha = 50$, $\gamma = 0.01$ (see also Fig. 8)

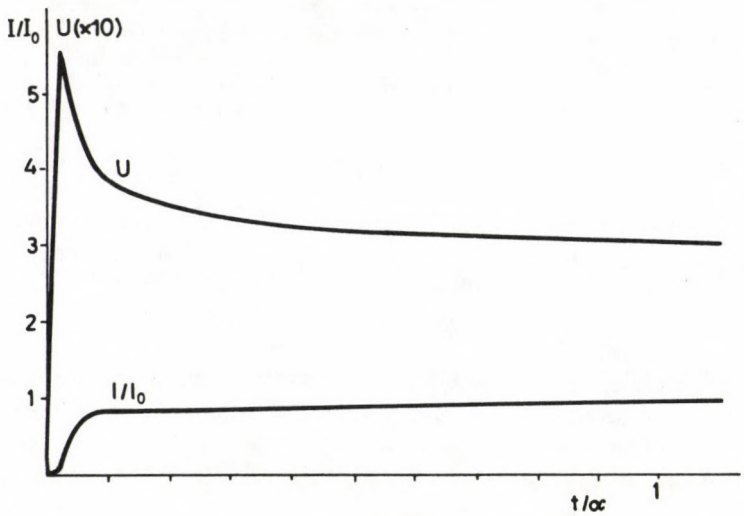

Fig. 10. The evolution of voltage and conductive current during an initial transient. $\alpha = 50$, $\gamma = 0.01$, $I_0 \cdot \alpha^2 = 1000$. The conductive current has been divided by total current I_0 on the plot

3.4. Initial transient

An evolution of the voltage and conductive current (not containing the displacement current) as the system approaches the steady state is shown in Fig. 10.

While the initial conductive current is low the external current generator charges the system that behaves now as a capacitor. The rising voltage is accompanied by steep increase in Q (see Fig. 11), which, in turn, later leads to a breakdown in the voltage. The abrupt change at the very beginning affects only the core of the charge distribution (where the source term is positive). Finally the drift spreads the distribution radially (see Fig. 11).

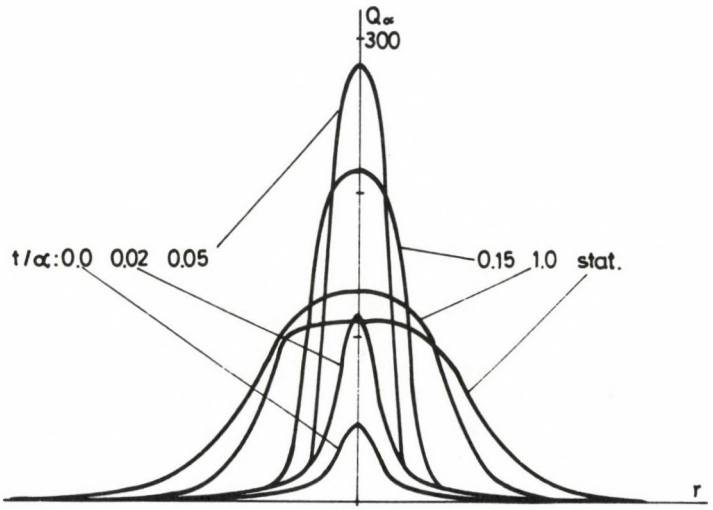

Fig. 11. Charge distributions during the transient shown in Fig. 10 taken at times 0, 0.02, 0.05, 0.15, 1.0, and infinity

3.5. The lateral spread of the discharge

Applying constant voltage the subnormal glow states showed to be unstable. The stability of the anomal glow, in turn, at constant voltage is due to the limiting effect of the wall. Thus on an infinite electrode with the voltage held constant the discharge spreads endlessly.

For simulation of the experimental situation summarized by Emeleus and von Engel [26] instead of the cylindrical geometry we used the simple one dimensional infinite electrode system with voltage generator

$$2\frac{\partial Q}{\partial t} - \frac{U}{6}\frac{\partial^2 Q}{\partial x^2} = S(U, Q). \tag{27}$$

Due to the infinity of the cathode α could be transformed out from the equation.

In Fig. 12 the evolution of the charge distribution Q is presented. The even propagation (constant velocity) of the discharge front can be clearly seen. The

velocity of the discharge front was roughly the half of the average ion drift velocity calculated at the edge of the curves. The propagation of the edge is a result of two processes, namely the radial ion drift and the axial effect consisting of ionisation and surface recombination, represented by the source term.

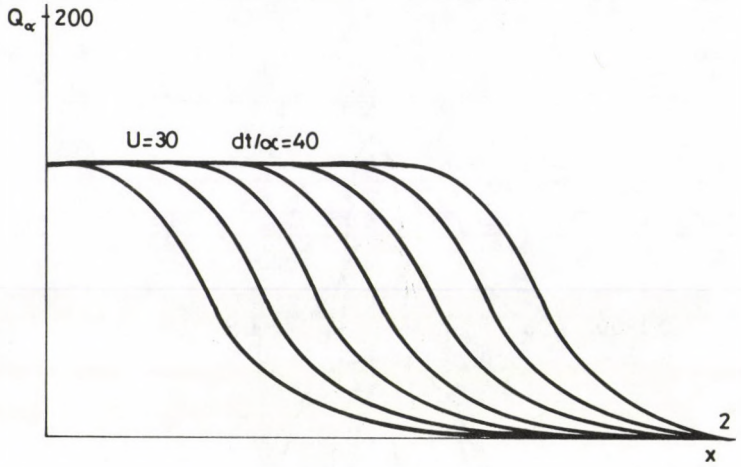

Fig. 12. The constant velocity spread of the discharge at voltage $U = 30$. The time elapsed between subsequent states $dt/\alpha = 40$, $\gamma = 0.01$

Seeking the solution of this equation in the form $Q = f(vt - x)$ it can be shown by simple calculation using also Eqs (26) that this phase velocity must be α, that is pressure independent. This is consistent with the experimental results. The voltage dependence of the spread velocity is shown in Fig. 13.

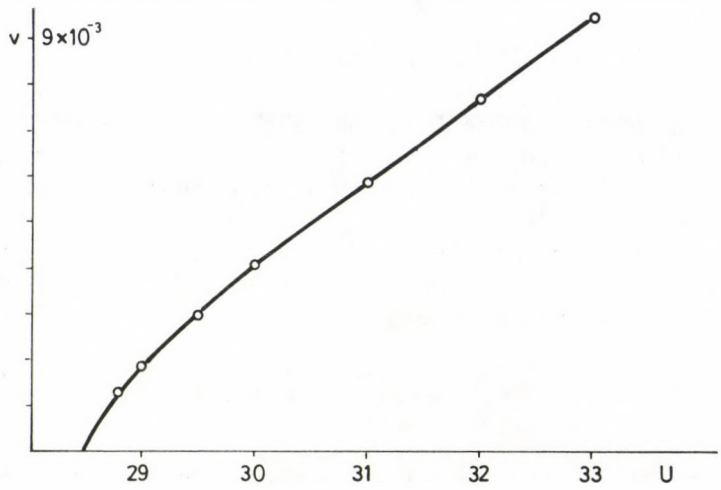

Fig. 13. The velocity of the spread as a function of the voltage, at $\gamma = 0.01$

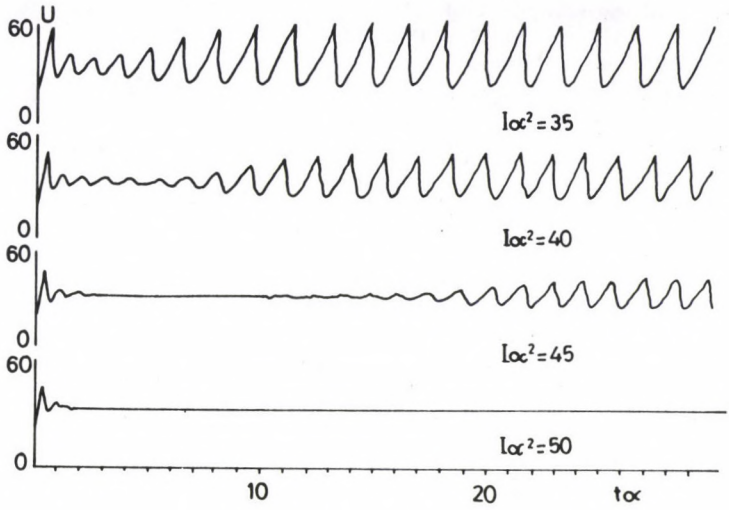

Fig. 14. Subnormal glow oscillation at different currents $I \cdot \alpha^2 = 35$, 40, 45 and 50, $\gamma = 0.01$

3.6. Subnormal glow oscillations

The model gives back this well-known peculiar phenomenon, too [2]. A series of voltage transients obtained at constant current, and absorbing wall is shown in Fig. 14. At very low currents the system reaches the periodical state after a few oscillations. At higher currents the oscillations first seem to damp or (on a low resolution plot) even to disappear, yet after a longer delay the non-damped oscillations reappear. At still higher currents these oscillations cease. The ceasing of the oscillation can be checked by the vanishing of the sign changes of dU/dt. In the frame of the model this self exciting oscillation is a two dimensional phenomenon as the checked one dimensional time dependent system gave only strongly damped quasi oscillations.

References

1. A. von Engel, Ionized Gases, Oxford U. P., New York, 1965.
2. B. N. Klyarfeld, L. G. Guseva and A. S. Pokroskava-Soboleva, Soviet Phys. – Techn. Phys., *11*, 520, 1966.
3. K. G. Emeleus, Z. Physik, *268*, 175, 1974.
4. J. H. Ingold, in: Gaseous Electronics, M. N. Hirsch and H. J. Oskam (eds), Academic Press, New York, 1978.
5. V. V. Vlasov, L. G. Guseva and B. N. Klyarfeld, 10th International Conference on Ionized Gases, Oxford, Contributed papers 98, 1971.

6. A. von Engel and M. Steenbeck, Elektrische Gasentladungen, Springer, Berlin, 1934.
7. K. G. Emeleus, Int. J. Electronics, *36*, 1, 1974.
8. K. G. Emeleus, J. Phys. D., *14*, 2179, 1981.
9. A. J. Ward, J. Appl. Phys., *33*, 2789, 1962.
10. A. J. Ward, IEEE Trans. Electron. Dev., *ED-10*, 255, 1963.
11. J. L. Neuringer, J. Appl. Phys., *49*, 590, 1978.
12. A. J. Davies and J. G. Evans, J. Phys. D., *13*, 161, 1980.
13. J. E. Lawler and D. A. Doughty, Symposium on Physics of Ionized Gases, Yugoslavia, Invited papers 293, 1986.
14. D. K. Doughty, E. A. Den Hartoy and J. E. Lawler, Appl. Phys. Lett., *45*, 611, 1984.
15. P. Bayle and A. Perrin, International Conference on Phenomena in Ionized Gases, Belgrade, Contributed Papers 1004, 1989.
16. K. G. Emeleus, Int. J. Electronics, *51*, 269, 1981.
17. P. Bayle, J. Vacquié and M. Bayle, Phys. Rev., *A 34*, 360, 1986.
18. Tran Ngoc An, E. Marode and P. C. Johnson, J. Phys. D., *10*, 2317, 1977.
19. J. P. Boeuf and E. Marode, J. Phys. D., *15*, 2169, 1982.
20. P. Segur, M. Yousfi, J. B. Boeuf, E. Marode, A. J. Davies and J. G. Evans, in: Electrical Breakdown and Discharges in Gases, Part A, E. E. Kunhardt and L. H. Leussen, (eds), Plenum, New York, 1983.
21. N. Sato and H. Tagashira, J. Phys. D., *18*, 2451, 1985.
22. R. J. Carman, J. Phys. D., *22*, 55, 1989.
23. T. C. Paulick, J. Appl. Phys., *67*, 2775, 1990.
24. K. H. Schoenbach, Hao Chen and G. Schaefer, J. Appl. Phys., *67*, 154, 1990.
25. A. von Engel, K. J. Emeleus and M. Kennedy, Phys. Lett., *42A*, 191, 1972.
26. K. G. Emeleus and A. von Engel, J. Phys. D., *12*, 555, 1979.
27. J. P. Boeuf, J. Appl. Phys., *63*, 1342, 1988.
28. J. P. Boeuf, ICPIG XVIII. Contributed Papers, *4*, 748, 1987.

Acta Physica Hungarica 72 (1), pp. 89–100 (1992)

IDENTIFICATION OF THE SOURCE OF DEFICIENT FUNCTIONING IN LOC LASER HETEROSTRUCTURES

A. MALAG*, J. PFEIFER, L. CSONTOS, Z. LÁBADI and GY. HOFFMANN

Research Institute for Technical Physics of the Hungarian Academy of Sciences
1325 Budapest, Hungary
**Institute of Electron Technology*
02-668 Warsaw, Poland

(Received in revised form: 30 April 1992)

In this paper we determine the parameters of LOC type AlGaAs laser heterostructures in order to find the reasons of their deficient functioning. The methods of characterization are as follows:

- broad-area laser test;
- scanning electron microscopy of selective etched sample;
- contact resistance profiling;
- optical microscopy of an angle-lapped, anodized sample;
- electrochemical C–V profiling.

Reasons for relatively high threshold current densities found by the broad-area laser test are suggested.

Comparison of results, as well as some advantages and disadvantages of the foregoing methods are discussed.

In our case the optical microscopy identifies most clearly the origin of the deficient functioning, the other techniques seem to be inadequate. This result shows the importance of this simple tool for a quick analysis of the LPE grown laser structures.

1. Introduction

Finding the connection between the parameters and functioning — sometimes deficient functioning — of semiconductor laser structures is an important factor in their continuous quality improvement. In particular, the most significant parameters are the structure of the device, the composition and doping of the layers, and the resultant electrical characteristics.

There are a number of reasons of interest in the separate confinement heterostructures (SCH) for the construction of laser diodes (LDs) as an alternative to the conventional double heterostructure (DH). For a low threshold current LD very thin active layer is needed. For the active layer thickness below 0.1 μm, however, the light guiding becomes weak in the DH (i.e. the confinement factor Γ decreases) and the threshold current steeply increases [1]. In SCH, in turn, a very thin active layer is placed "inside" the light-guiding layer (Fig. 2a). Thus, the composite waveguide consists of three layers numbered in Fig. 2a by 3, 4, 5 (including the active layer (4)). For a low-threshold LD this waveguiding "triple layer" is designed to reach the maximum Γ-value and is typically 0.3–0.4 μm [1,2] or even less in some cases

[3,4]. Also the Al-contents of all layers has to be carefully controlled to reach the desired Γ-value.

A version of the SCH is the large optical cavity (LOC) heterostructure, in which the waveguiding triple layer is thick, in the order of 1 μm [5–7]. For such thickness the Γ-factor is smaller leading to the higher threshold current densities. Simultaneously, however, this appears in the elevation of the catastrophic mirror damage level, whereby the LOC heterostructures are primarily intended for high optical power LD-s.

The results presented in this paper concern two exemplary AlGaAs heterostructures of separate confinement type, grown by LPE.

In the course of our work relatively high threshold currents have been found by broad-area laser test.

Efforts have been intended to find out this deficient functioning by the measurement of structural, doping and electrical parameters of the foregoing laser structures using the following methods:

- scanning electron microscopy of selective etched sample;
- contact resistance profiling;
- optical microscopy of an angle-lapped, anodized sample;
- electrochemical C–V profiling.

2. Experimental

The heterostructures presented here are of LOC type. They were grown by LPE process with compulsory squeezing out of melts [8]. The starting temperature of the growth was 715 °C with a cooling rate of 0.6 °C/min, such that the active layer was grown in the temperature range of 676–675.75 °C.

Two exemplary LOC heterostructures (referred to further as "H1" and "H2") have been subjected to some characterization processes, which are convenient for the quick evaluation of the heterostructure quality. The characterization methods are described and the results are discussed in the following.

2.1. Broad-area laser test

This is a key test for rejection or acceptance of a heterostructure to further technological process.

The broad-area test lasers are prepared on a small part of the heterostructure slice. After thinning it, the p-contact metallization (Ag–Cd alloy) is evaporated through a metallic mask to obtain stripes of about 60 μm width and spaced 500 μm to each other. Then AuGeNi alloy is evaporated onto the whole n-side surface and both contacts are alloyed. Finally bars of such broad-area test lasers are formed by cleaving. Bars are not divided into chips because of the large distance between adjacent stripes (lasers). Therefore, this method ensures that a current provided

by a pin-like probe is confined only to the given stripe in the bar and the current spreading below contact is negligible.

Light-current pulse (200 ns, 10^4 kpps) characteristics of the broad area contact lasers (made from H1 and H2) are show in Fig. 1. As it is clear from the Figure, J_{th} values of about $2 \div 3$ kAcm^{-2} are rather high (e.g. too high for CW operation).

2.2. SEM characterization of the selectivity etched samples

This characterization allows the measurement of heterostructure layer thicknesses and the rough evaluation of their Al-content. Some additional information can be obtained at this occasion, which is usually accessible with the help of more expensive methods.

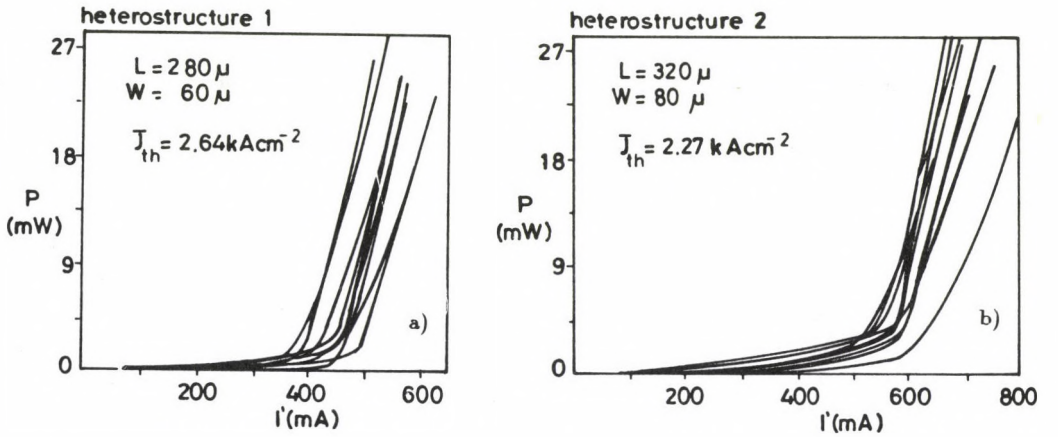

Fig. 1. Light–current characteristics of broad-area lasers made from H1 (a) and H2 (b) samples a) resonator length $L = 280$ μm and width $W = 60$ μm, threshold current density $J = 2.6$ kAcm^{-2}; b) $L = 320$ μm, $W = 80$ μm, $J = 2.27$ kAcm^{-2}

Results of such characterization are shown in Figs 2b–g. For sample preparation, two parallel bars (freshly cleaved from each heterostructure slice) were etched, one in the I2 solution (100 g H_2O, 113 g KJ, 65 g J_2 [9]) for 30 s and another one in boiled HCl for 45 s. Both of these etchants selectively etch AlGaAs without spoiling GaAs, resulting in the selective lateral underetching of cleaved walls. This was followed by the perpendicular cleaving of bars into chips. Corners of the chips are analysed using SEM photographs. There is a difference in "threshold composition" (x_{th}) of AlGaAs above which the etchants start to etch. For I2 solution x_{th} is about 0.20 [10], while for HCl it is 0.42 [11]. Then the comparison of the results of etching with both etchants enables one to evaluate x to lie in one of three ranges, i.e. $x < 0.25$, $x \in (0.25, 0.42)$, and $x > 0.42$, which is often sufficient to reject or accept a heterostructure to further technological processes.

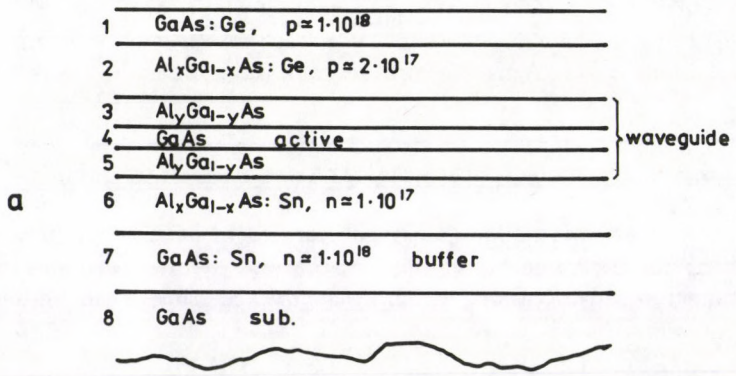

Fig. 2. a) The configuration SCH (LOC) laser heterostructure (sample H1, H2)

In this way precise layer thicknesses can be obtained, e.g. for H1 they are 0.6 μm for the cap layer, 1.7 and 1.8 μm for p and n claddings, respectively, and 1 μm for the waveguide triple layer. The reversal slopes of etched walls of H1 and H2 are caused by preparation of bars in perpendicular directions.

2.3. Contact Resistance Profiling (CRP)

The CRP [12,13] was carried out on mechanically bevelled samples of heterostructures. On the bevelled surface of the sample there is a stripe of silver paste with a gold wire dipped in it. Constant potential (U_{ps} = 1.5 V) is maintained between the probe and the stripe. The tip of probe traces along the surface of the sample parallel with the stripe contact. Simultaneously, the current flowing between the probe and stripe is monitored by a log-operational amplifier. Its output voltage is converted by IBM PC/AT into resistance-depth (or current-depth) dependence of the heterostructure sample. This dependence is the contact resistance profiling (CRP) record.

The CRP records of samples H1, H2 are shown in Figs 3a,b. To determine the position of p–n junction two CRP records were plotted for each sample at both the positive and the negative polarity of U_{ps}. They are marked as "+" and "–", respectively.

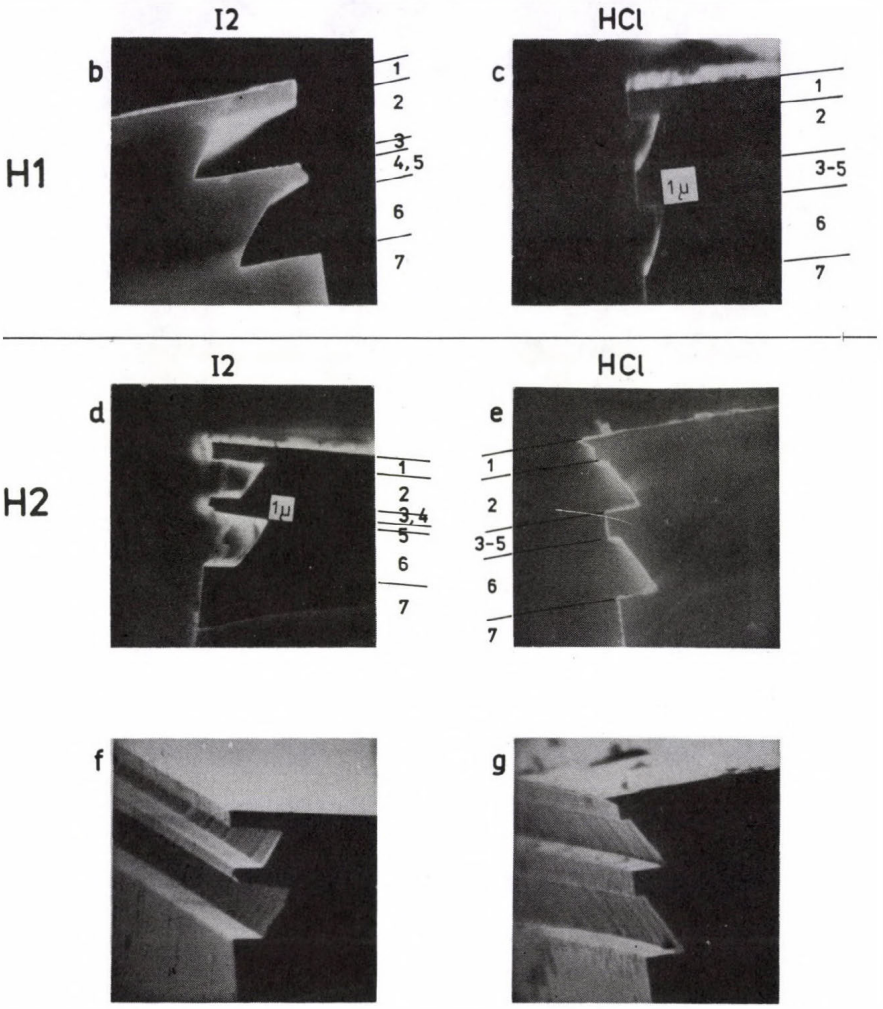

Fig. 2. b–g) SEM photos of selectively etched samples H1, H2. The etchants for b, d, f and c, e, g were I2 and HCl, respectively

CRP is a semi-microscopic method, because the width of the probe trace is of some microns, while this trace crosses the layers of "magnified" thickness.

The "geometric" thickness resolution of CRP can be defined as the least layer thickness for which the tip of the probe can be found only in this layer. Easy to prove that the geometric thickness resolution is

$$D_0 = b\cos\alpha + r(1 - \cos\alpha), \tag{1}$$

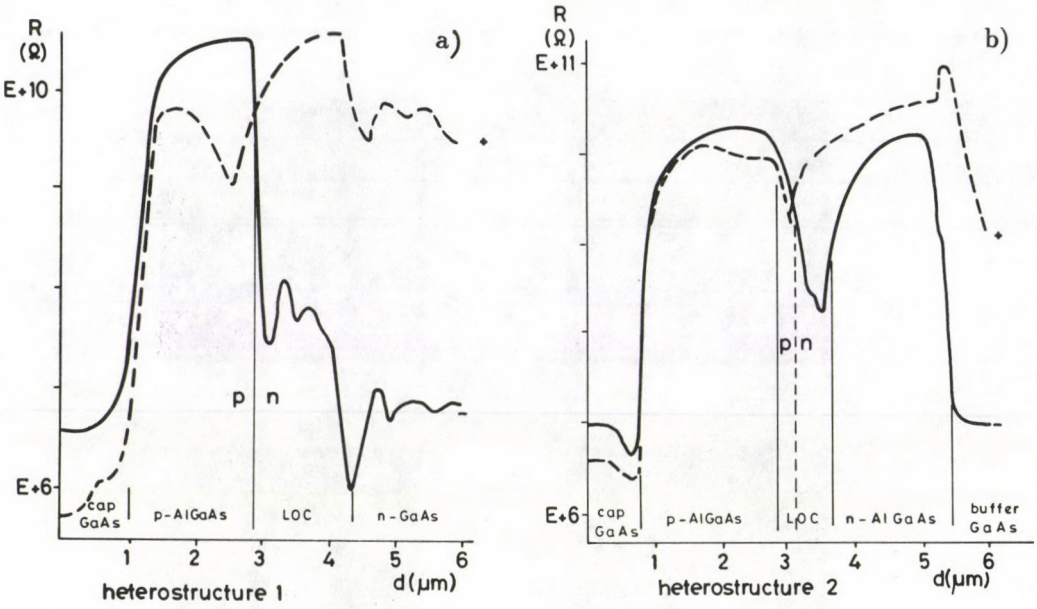

Fig. 3. Contact resistance versus depth into the sample. a–b) CRP for samples H1 and H2, respectively

where $b = r - (r^2 - d^2/4)^{1/2}$ is the depth of the probe's trace, r is the radius of the probe tip, d' is the width of the probe trace, and α is the bevelling angle.

In our measurements, for $r = 10$ μm, $d' = 5$ μm, $\alpha = 1.5$ deg we have $b = 0.317$. Substituting this into (1) we obtain $D_0 = 0.32$ μm.

The contact resistance is given by

$$R = U_{ps}/I, \tag{2}$$

where $I = c_1 \exp(2.303 * c_2 * U_{op})$ is the current between the probe and the silver stripe, c_1 and c_2 being constants of calibration of the log-operational amplifier ($c_1 = 1.95 * 10^{-12}$, $c_2 = 0.889$), U_{op} is the output voltage of this amplifier.

The relative precision dR/R of our apparatus is given as

$$dR/R = 2.047 \times dU_{op}. \tag{3}$$

The inaccuracy of the measurement of U_{op} (standard deviation) is $dU_{op} = 0.1 - 0.15$ V (such that $dU_{op}/U_{op} = 0.01 - 0.05$), therefore, from (3) we have $dR/R = 0.2 - 0.3$.

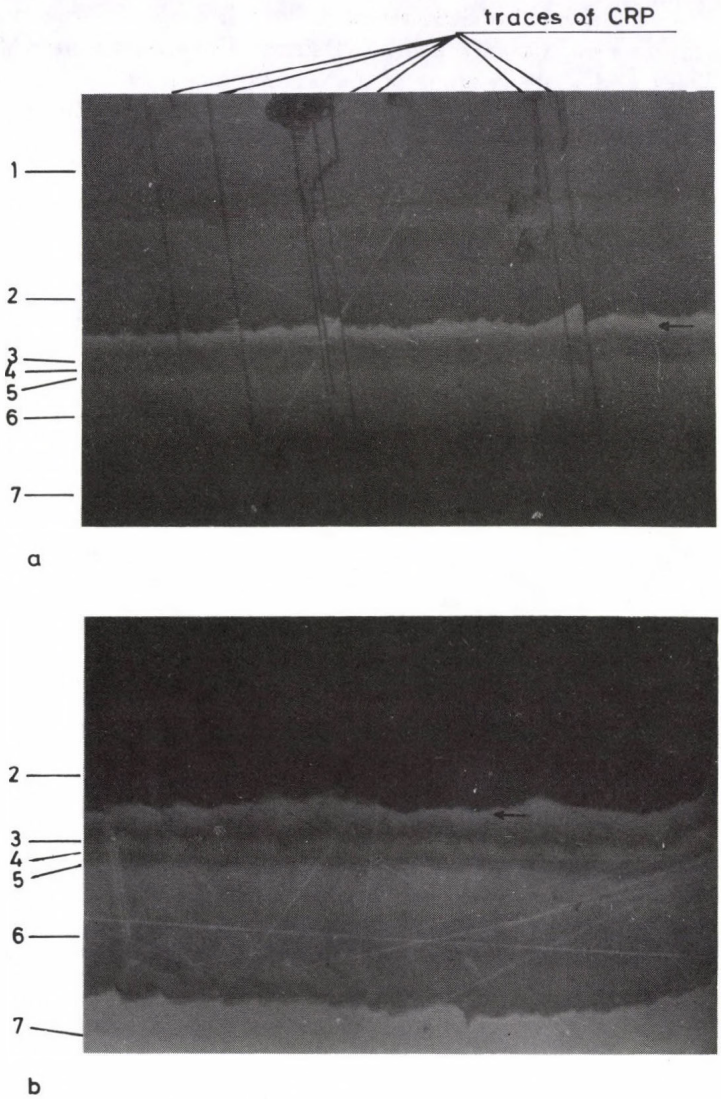

Fig. 4. Photos of angle-lapped, anodized surfaces of samples H1 (a) and H2 (b). Magnification is about 50

2.4. Optical Microscopy of Angle-Lapped, Anodized Surface of Samples (OMALA)

After CRP recording the angle-lapped samples have been anodized in the common solution ((5 % water solution of citric acid + NH_4OH; pH=6) + ethylene

glycol = 1 : 3); ($U = 50$ V, $t = 15$ s). Depending on the thickness and composition of anodic oxides, the layers have been revealed by their proper interference colours. The coloured layers were examined using a "Reichert Universal Camera Microscope MeF". The black and white versions of the originally coloured photos of H1 and H2 samples are shown in Figs 4a,b with a magnification of about 50. This method can be also considered as semimicroscopic.

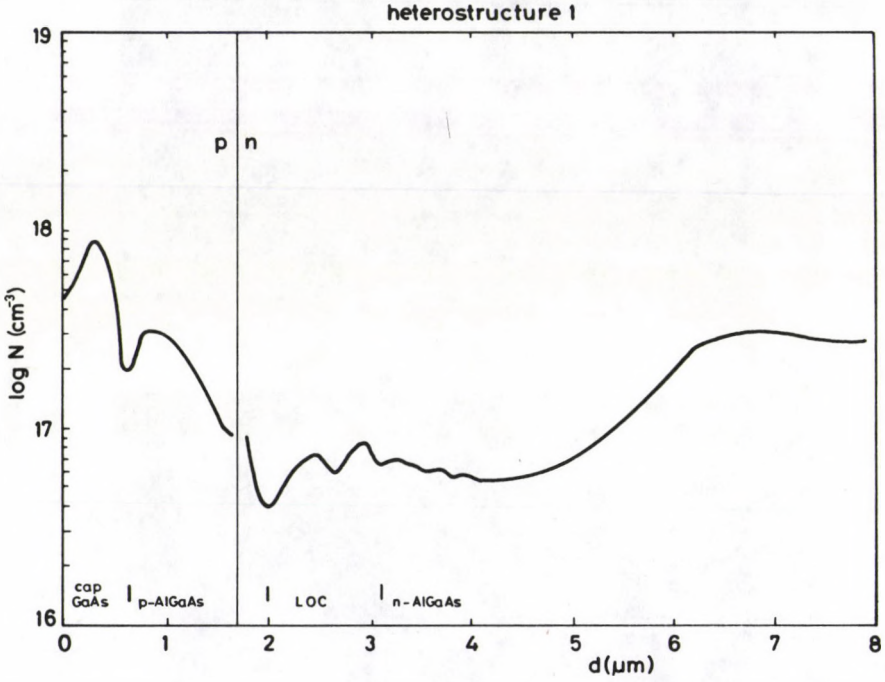

Fig. 5. Carrier concentration versus depth into the sample H1 measured by electrochemical C–V profiling

2.5. Electrochemical C–V Profiling (ECVP)

The ECPV method is a fast but destructive method of simultaneous carrier concentration and layer thickness determination in a multilayer structure. This technique is based on the formation of a Schottky barrier between the semiconductor sample and a sufficiently concentrated electrolyte. The concentration of the electrically active charge carriers at the interface can be evaluated from the measured capacitance–voltage characteristic of the reverse biased junction. The profiling of the sample is possible by step-by-step anodic dissolution of the material under proper circumstances (illumination or forward bias in the case of an n and

p type semiconductor, respectively), and by calculation of the anodically removed thickness on the basis of Faraday's law [14].

In spite of its simplicity and fastness this method has a few disadvantages. In order to ensure the precise measurement of the wetted surface it should be in the range of 10 mm^2 so the measured concentration profile always represents only an average value of a macroscopic spot and its usefulness strongly depends on the lateral homogeneity of the substrate. A measured graded concentration profile at the side of a layer may either be the consequence of the roughness of the interface or the real diffusion profile of the dopants. A further possible theoretical limit of depth resolution of an ECPV profile is the presence of depletion layers in the sample (at heterojunctions or p–n junctions) because near to these regions the measured capacitance is a superposition of two capacitances and the cc. curve evaluated on the basis of the simple Schottky equation gives only indirect information.

In Fig. 5 we present the free carrier concentration vs depth curve of the H1 sample. We observed a p-type region on the top of the sample which contains two layers with a concentration step. After dissolving 1.7 μm thick material the phase angle of the impedance changed its sign indicating the p–n junction. The region under the junction contains at least three different n-type layers within a 1.3 μm thick region so we identified these layers as LOC region, and the p–n junction is situated at the upper side of the waveguiding structure.

3. Discussion

The measured results presented in Section 2 allow us some conclusions on the quality of the heterostructures under consideration.

SEM photos in Fig. 2 show results of selective chemical etching using I2 and hot HCl etchants in the left and right column, respectively. Two upper photos (b,c) and other photos (d–g) concern H1 and H2, respectively. As for H1, it is seen that the composition of both outer claddings (layers 2, 6) are slightly above 0.42, and the composition of p-type cladding $x(2)$ is somewhat higher than $x(6)$. The waveguide triple layer (3–5) thickness is 1 μm but the waveguide is asymmetric. The bevelled remainder of the "lower" inner cladding (5) indicates (see photo b), that its composition $y(5)$ approaches 0.20, while $y(3)$ is clearly lower. This asymmetry can somewhat reduce the Γ-factor value. A small-angle bevel between layers 2 and 3 indicates the presence of the thin sublayer, which can be a consequence of melt mixing during squeezing out. Of course, hot HCl does not attack the waveguide triple layer, so photos b and c show their equal thicknesses. On the contrary, in H2 (photos d, e) the difference of 0.13 μm is seen in waveguide thicknesses inferred from I2 and hot HCl etching. This difference is presumably caused by a thin sublayer of $x \in (0.20, 0.42)$ present at the interface of layers 5 and 6. This arises from the comparison of thicknesses of n and p outer claddings in photos d and e. Then the waveguide in H2 is also asymmetric. The step indicating layer 5 (of slightly higher Al-contents) on photo d corroborates it.

In turn, photos f, g of the same corners show flatness of interfaces and uniformity of layers (smoothness of the etched walls) in H2. This also concerns H1 (photos are not shown), in general, however, it is not a rule in heterostructures made by LPE [10].

The layers are also clearly represented on CRP records (Figs 3a,b), because their thicknesses are above or close to the "geometric" resolution of the method ($D_0 = 0.3$ μm, see Part 2.2). Thicknesses of the 3–5 components of the waveguiding triple layer are comparable with D_0, so they are only qualitatively resolved. The main part of the waveguiding structure in both H1 and H2 is on the n-side of the p–n junction, which is found as the cross-point of the "+" and "−" CRP records.

All the layers as well as traces of CRP probe are shown on the OMALA photos of H1 and H2 samples in Figs 3a and b, respectively. *Nonuniformities of layer thicknesses, wavy-like and sawtooth-shaped perturbations of interfaces are revealed by these photos.*

The doping concentration profile given by ECVP for H1 (Fig. 4) is in general in agreement with the previous design. The boundaries between layers are not sharp in this profile (the reasons are discussed in Part 2.4). On the contrary, abrupt changes at the layer boundaries are seen in the CRP records. Moreover, the tendencies of these changes disagree with those of electromechanical C–V profiles (see Figs 3 and 5). Presumably, this is due to differences in the nature of the measurements. The C–V method is mainly sensitive to the doping concentration, while in CRP the resultant resistance depends on concentration, Al-content, carrier mobility and properties of the contact metal probe with p- and n-type semiconductor.

The actual distance from the surface is inferred in the electrochemical profiler from the etching time (based on Faraday's law) and in CRP from the angle of the mechanical bevel. So some discrepancies can be expected in the evaluation of the layer thickness using both these methods and the SEM measurements described above. In the CRP method some error can be caused by a rounding of the bevel at the surface of the sample: i.e. just in the region of heterostructure layers. The discrepancies can be seen by comparison of Figs 2 and 5: some underestimation in electrochemical C–V profiles and overestimation in CRP records are seen in comparison to SEM measurement results.

In general, however, the CRP and electrochemical C–V profiling results are convergent. For H1 for example, a wavy-like segment indicating LOC area and a small distance between p–n junction and LOC edge are seen similarly in both profiles (Figs 3,5).

Concerning the reasons for the relatively high J_{th}-value obtained in the broad-area laser test, there are four possible reasons of the deficient functioning which are potentially observable by our simple methods. We discuss them as entries a–d in the following.

a) The first reason can be the rather high thickness of the triple-layer waveguide, which can reduce the Γ-value. The thickness of such LOC triple layer is far from the optimum value for minimizing J_{th} [2–4], however, even in high power lasers with LOC heterostructure of similar waveguide thickness, the J_{th} value can be maintained on the level of 1–1.5 kAcm^{-2} [6,7].

b) The next possible reason for J_{th} increase is the compositional asymmetry observed in SEM photos of Figs 1b–g, however, this cannot sufficiently explain such high J_{th} either.

c) One of the most important factors influencing the J_{th} is the active layer thickness. Unfortunately, the actual thickness of the active layer is very difficult to be defined using the present simple methods. This is caused by difficulties with the extraction of the active layer from the waveguide triple layer, unless the Al-contents in the inner cladding layers are above 0.25.

d) *The last and most considerable reason for the observed high J_{th} can be the terrace-like structure of interfaces (and surface) and the resulting diffraction loss* [15]. The terraces are related to a substrate misorientation and the LPE growth conditions. *The presence of terraces is clearly seen on the OMALA photos as wavy-like (Fig. 4a) or sawtooth-shaped (Fig. 4b) perturbations of interfaces.* Taking into account the magnitude of these perturbations (especially in some parts of both heterostructures) *they can be considered as an important reason for so high values of J_{th}.*

4. Conclusion

As it is clear from the discussion we applied relatively simple and quick methods for the qualification of the LOC heterostructures, but these techniques were applicable for the detection of the simplest and most important sources of the high J_{th} value. We found the source of the deficient functioning of the devices in the poor interface qualities of the heterostructures. It is important to note that these defects were observable only by the OMALA technique. Neither the SEM nor the CRP and ECVP methods are adequate to identify the interface perturbations in the case of our samples.

However, this problem does not concern only the LOC structures, but is common for all LPE heterostructures, and not sufficiently good substrate orientations. Our results show the importance of the OMALA technique as a quick reference method of the LPE structures.

5. Summary

Broad-area laser test has indicated high threshold current density (J_{th} values) of examined LOC laser structures. A set of characterisation methods have been used to determine parameters of these heterostructures to find reasons for the mentioned deficient functioning.

The thickness of layers, estimated Al-contents, contact resistance profiles, position of p–n junction, doping concentration profile seem to fill the requirements.

The microscopic photos of the surface of the angle-lapped and then anodized heterostructure samples revealed nonuniformities of layer thicknesses and perturbation of interfaces. These faults have been introduced to the heterostructure by

epitaxial growth. The high threshold current density of our LOC laser structures is caused by just the foregoing faults.

Only the optical microscopy of the angle-lapped, anodized samples was able to identify the source of the deficient functioning.

Acknowledgements

The authors express their thanks to Dr. K. Franc for heterostructure growth, to Dr. F. Koltai for useful discussions, I. Juhász for the preparation of the evaluation program of CRP, J. Ratajczak for SEM documentation, F. Abrasits and P. Gulyás for their help in sample preparation.

References

1. H. C. Casey and M. B. Panish, Heterostructure Lasers, Part A, Academic Press, New York, 1978.
2. T. Sanada, M. Kuno and O. Wada, Jap. J. Appl. Phys., *25*, 1443, 1986.
3. S. Mukai, Y. Tsunekawa, Y. Takabe and H. Yojuna, J. Appl. Phys., *58*, 1052, 1985.
4. O. Wada, Materials from Intl. Symp. on GaAs and Related Compounds, Kuruizawa, Japan, Instr. Phys. Conf. Ser. No. 79, Chapter 12, 1985.
5. M. B. Chang and E. Garmire, Appl. Optics, *19*, 2370, 1980.
6. R. W. Glew, B. Garrett, J. E. A. Whiteaway and E. J. Thrush, J. Cryst. Growth, *77*, 613, 1986.
7. B. Garrett, IEE Proc., *133*, 319, 1986.
8. Zh. I. Alferov, V. M. Andreev, S. G. Konnikov, V. R. Larionov, B. V. Pushny, Kristall und Technik, *11*, 1013, 1976.
9. B. F. Levine, R. A. Logan, W. T. Tsang, C. G. Bethea and F. R. Merritt, Appl. Phys. Lett., *42*, 339, 1983.
10. A. Malag, ITE Reports, *7*, 92, 1986.
11. Zh. I. Alferov, V. M. Andreev, D. Z. Garbuzov, N. Y. Davidyuk, V. R. Larionov, V. D. Rumyancev, FTP, *9*, 1265, 1975.
12. L. Csontos and Gy. Hoffmann, Proc. of 2nd Conf. Tech. GaAs and Other III–V Semiconductors, Trans. Tech. Publ., 257, 1987.
13. L. Csontos and Gy. Hoffmann, Acta Phys. Hung., *61*, 145, 1987.
14. P. Blood, Semic. Sci. Techn., *1*, 17, 1986.
15. G. H. B. Thompson, IEEE J. Quantum Electron., *QE–11*, 481, 1975.

Acta Physica Hungarica 72 (1), pp. 101–105 (1992)

TEMPERATURE DEPENDENCE OF GAMMA RAY INDUCED LUMINESCENCE IN TOLUENE BASED LIQUID SCINTILLATOR BETWEEN 220 AND 290 K

FAIZAN-UL-HAQ, M. Z. BUTT and S. H. ZAIDI

Centre for Advanced Studies in Physics, Government College Lahore–54000, Pakistan

(Received 26 May 1992)

The fluorescence of toulene based liquid scintillator (toulene + 6 g/l butyl-PBD + 0.1 g/l POPOP) has been studied as a function of temperature in the range 220 to 290 K. It has been observed that under gamma excitation the light output increases with decrease in temperature by a factor of 1.43. The data are well encompassed by an Arrhenius relation, in which the activation energy of rate process (0.21 eV) is compatible with thermally-activated diffusion mechanism.

1. Introduction

The organic scintillation counter has proved to be an extremely versatile and useful instrument for the detection and study of nuclear radiations. A lot of work has been done to explore the influence of various factors, e.g. solvent–solute composition, oxygen dissolved in the solution, addition of wavelength shifter, magnetic field and temperature, etc. on the luminescence properties of organic scintillators under excitation by radiations of different wavelengths [1–13]. However, literature survey shows that data pertaining to the effect of temperature on the fluorescence efficiency of organic liquid scintillators are very scanty. Furst et al [1] investigated the effects of temperature above ambient (300–550 K) on energy transfer from the bulk material (solvent) to the emitting substance (solute) in a number of organic solutions under gamma rays and ultraviolet excitation. They found that, in general, fluorescence reduces with a rise in temperature by a factor which ranges from 1.3 to 20, depending on the nature of both the organic solution and radiation causing excitation. For low temperatures Seliger and Ziegler [2,3] reported an increase by a factor of 1.20 in the scintillation pulse height of two efficient de-oxygenated liquid scintillators (8 g/l PBD + 2 g/l POPOP in xylene and 3.2 g/l alpha NPO in xylene) on reducing the temperature from 303 to 243 K. Later, Laustrait and Coche [4,5] studied the temperature dependence of the scintillation pulse height of three scintillation solutions (3 g/l PPO, 5 g/l PBD or 3 g/l alpha NPO in toluene) with and without dissolved oxygen, from 313 to 243 K. However, the temperature effects observed by them were much less than those reported by Seliger and Ziegler [3]. Recently, Faizan-Ul-Haq et al [6] have reported that the scintillation response of liquid scintillator NE 213 (purified xylene + naphthalene + POPOP) increases by a factor

of 1.34 on cooling from 300 to 225 K. The primary concern of this communication is to report (i) the effect of low temperature on the fluorescence efficiency of toluene based liquid scintillator containing 6 g/l butyl – PBD and 0.1 g/l POPOP, and (ii) the mechanism responsible for quenching of the luminescence when temperature increases from 220 to 290 K.

2. Materials and measurements

To study the effect of low temperature on the fluorescence response of the liquid scintillator referred to, a vacuum-flask type cylindrical chamber of copper was constructed in order to keep the liquid scintillator at a desired temperature below ambient. It had four coaxial walls having space between them. A vacuum of the order of 10^{-3} mmHg ($\approx 10^{-2}$ Pa) was maintained between the two outer walls, whereas the space between the two inner walls contained liquid nitrogen. This copper cylinder was housed in a light tight hardboard chamber along with an EMI photomultiplier tube 6255 and a long light guide, the latter being covered with aluminium foil.

Argon was passed through the liquid scintillator to eliminate and bubble out the dissolved oxygen, if any. A small pyrex glass bottle, covered with aluminium foil excluding its base, and containing liquid scintillator as well as thermocouple of digital thermometer, was first dipped in liquid nitrogen for some time to attain a temperature of about 220 K. Then it was taken out and placed at the centre of the copper cylinder along its axis. By this arrangement the temperature of the liquid scintillator went on increasing very slowly, and for a particular reading, i.e. counts per minute (regarded as index of light output) under gamma excitation, it remained constant for a few minutes. The purpose of interposing a long light guide between the base of the liquid scintillator bottle and the photomultiplier was to eliminate any cooling effect on the latter.

For inducing luminescence in the liquid scintillator gamma rays from Ra^{226} source were used, while the integral counting circuit comprised a quartz photomultiplier tube (EMI 6255), preamplifiers, linear amplifier, discriminator of energy analyser, stabilised power supply and a digital scalar (all ORTEC design). Measurements of light output (counts/minute) were made by keeping the gain of amplifier, operating voltage of photomultiplier, and discriminator bias of energy analyser constant while temperature was increased from 220 to 290 K.

3. Results and discussion

The points in Fig. 1 represent the measured values of the light of deoxygenated toluene based liquid scintillator under gamma excitation as a function of temperature T in the range 220 to 290 K. It is evident that scintillation response increases 1.43 times when temperature falls by a factor of 0.76. Figure 2 refers to

the fluorescence data given in Fig. 1 as a function of T^{-1} in log-linear coordinates; it is well encompassed by the relation

$$I_{low} - I = I_0 \exp(-E/kT), \tag{1}$$

where I is the count rate (index of light output) at temperature T, I_{low} is the saturation value equal to 1200 counts/minute, I_0 is the pre-exponential factor equal to 2×10^6 counts/minute, k is the Boltzmann constant and E is the activation energy of the rate process. The latter parameter is evaluated from the slope $d\ln(I_{low} - I)/d(1/T)$ of the straight line drawn through the data points in Fig. 2, using the expression $E = kd\ln(I_{low} - I)/d(1/T)$ which is readily derivable from Eq. (1), and is found to be equal to 0.21 eV.

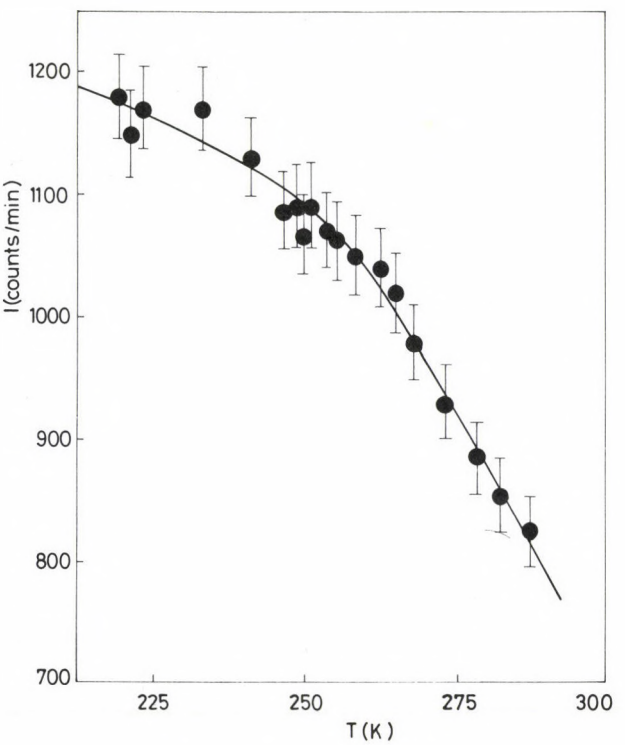

Fig. 1. Temperature dependence of the light output I for liquid scintillator: toluene + 6 g/l butyl - PBD + 0.1 g/l POPOP under gamma excitation. The error bars represent statistical error $\pm\sqrt{I}$

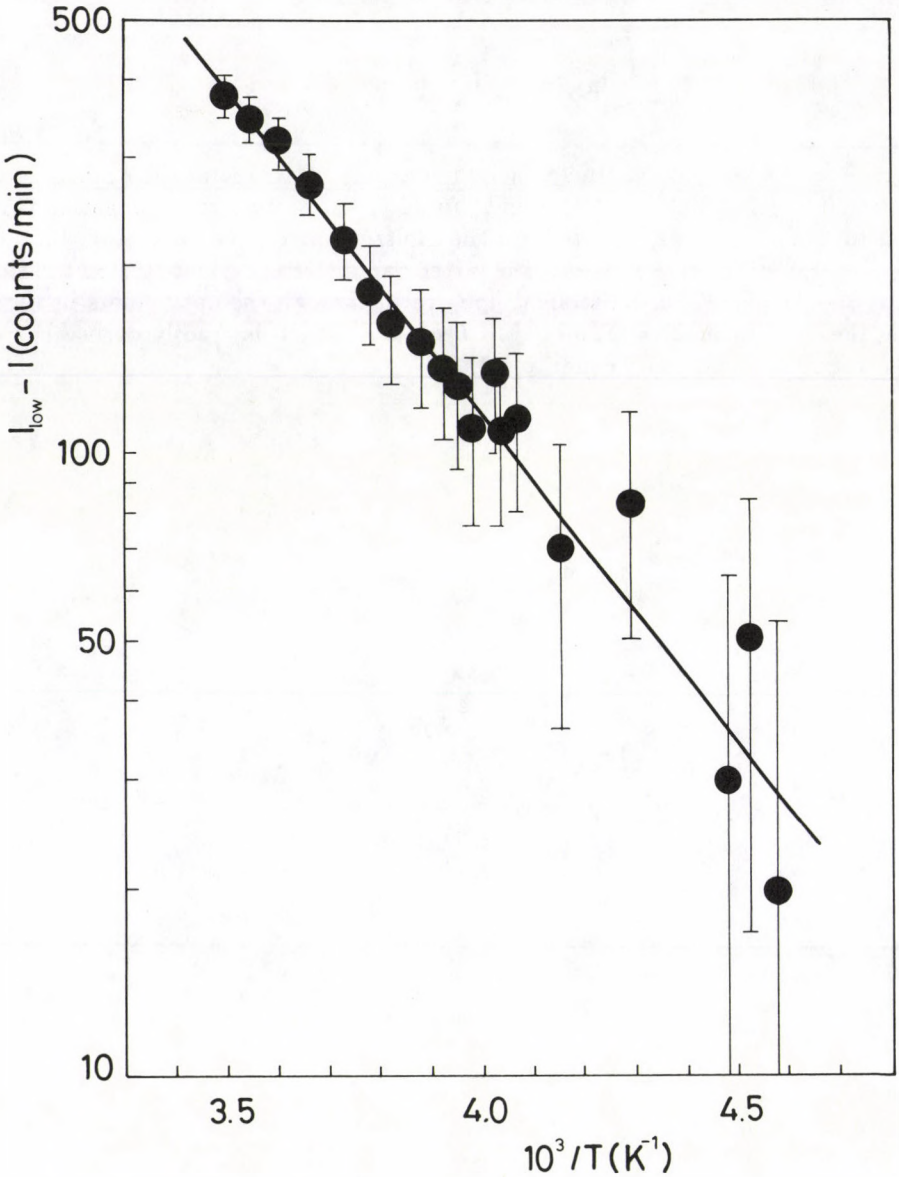

Fig. 2. Arrhenius plot of the light output parameter $I_{low} - I$ versus $1/T$, where $I_{low} = 1200$ counts/minute and values of I have been taken from Fig. 1

The decrease in the light output of liquid scintillator consisting of toluene + 6 g/l butyl - PBD + 0.1 g/l POPOP with increase in temperature from 220

to 290 K under gamma excitation can be attributed to the change in the mean free path of a gamma ray excited ion or electron with temperature; thermally-activated diffusion seems to cause quenching of the luminescence, as in the case of xylene based liquid scintillator NE 213 [6]. The value of the activation energy ($E = 0.21$ eV) obtained from the data given in Fig. 2 and compatible with Eq. (1), is typical for a diffusion controlled process in the temperature range investigated, and strongly supports this view. However, this may not be the unique interpretation of the observations referred to above. One may also seek the origin of the observed effects in intramolecular quenching due to internal conversion and/or inter-system crossing.

References

1. M. Furst, H. Kallmann and E. Levin, Molecular Crystals, *4*, 213, 1968.
2. H. H. Seliger and C. A. Ziegler, Nucleonics, *14*, 49, 1956.
3. H. H. Seliger and C. A. Ziegler, J. Res. Nat. Bur. Stand., *58*, 125, 1957.
4. G. Laustrait and A. Coche, J. Phys. Radium, *19*, 927, 1958.
5. G. Laustrait and A. Coche, J. Phys. Radium, *21*, 487, 1960.
6. F. Ul-Haq, M. Z. Butt, W. Ali, S. Jamil and F. A. Durrani, Radiation Effects and Defects in Solids, *115*, 135, 1990.
7. T. B. Elkareh and H. C. Wolf, Molecular Crystals, *4*, 195, 1968.
8. H. H. Seliger, C. A. Zieĝler and I. Jaffe, Phys. Rev., *101*, 998, 1956.
9. E. Jeenicke, P. Liaud, B. Vignon and R. Wilson, Nuclear Instruments and Methods, *126*, 459, 1975.
10. E. Bodenstedt, L. Ley, H. O. Schlen and U. Wohman, Nucl. Phys., *A 137*, 33, 1969.
11. C. Swenberg and N. E. Geacinitor, in Organic Molecules Photophysics, J. B. Birks, (ed.), J. Wiley and Sons, New York, 1973. Vol. I.
12. R. Siddique, F. Ul-Haq, M. Z. Butt and F. A. Durrani, J. Nat. Sci. Maths., *27*, 131, 1987.
13. F. Ul-Haq, M. Z. Butt, G. Ali, S. Q. M. Zaidi and R. Siddique, Acta Phys. Hung. *71*, 35, 1992.

Acta Physica Hungarica 72 (1), pp. 107–113 (1992)

SPECTROMETER CORRECTIONS FOR A RETARDING FIELD ANALYSER USED FOR ELASTIC PEAK ELECTRON SPECTROSCOPY AND AUGER ELECTRON SPECTROSCOPY[1]

A. SULYOK, G. GERGELY and B. GRUZZA*

Research Institute for Technical Physics, Hungarian Academy of Sciences
1325 Budapest, Hungary
**Laboratoire de Physique des Milieux Condensés, CNRS 796*
Université Blaise Pascal Clermont-Ferrand II
6317 Aubière CEDEX-France

(Received 7 July 1992)

Elastic peak electron spectroscopy using a retarding field analyser (RFA) proved to be an efficient tool for several applications. The advantage of RFA lies in its simultaneous LEED-AES application, in its large aperture averaging angular effects and in the possibility of surface analysis with the elastic peak. The difficulty of the RFA is its poor energy resolution integrating also the background adjacent to the peak observed (elastic or Auger peak) and producing peak distortion. Spectrometer correction was made by determining the spectral distribution function of the RFA energy window, using an approach of sum of Gaussians. Parameters of the Gaussian functions have been determined by decomposition of elastic peak spectra measured with an RFA Riber OPR-304 on Ag. Ag and Au elastic peaks at 1 and 2 keV energy were compared with highly resolved spectra obtained with a hemispherical analyser. Calculated elastic peak spectra exhibited reasonable agreement with experimental data obtained with the RFA spectrometer.

Introduction and the problem

Elastic peak electron spectroscopy [1] (EPES) proved to be an efficient auxiliary method of AES and EELS (electron energy loss spectroscopy). EPES was applied using a retarding field (RFA) 4 grids analyser [2] for determining:

- the elastic reflection coefficient $r_e(E)$ of solids [2];
- the inelastic mean free path of electrons [3];
- surface composition [4] of InP;
- In island formation [5] on InP;
- evaluation of EELS [6] on Si;
- evaluation of appearance potential spectroscopy [7].

The advantages of the RFA are:

- high luminosity;
- averaging the elastic scattering of electrons within large angular aperture;

[1] The paper is dedicated to Professor Imre Tarján on the occasion of his 80th birthday

- suitability for EPES surface analysis based on characteristic maxima of elastic reflection [2,4];
- simultaneous structural (low energy electron diffraction) and surface analysis (AES).

The quantitative evaluation of EPES measurements needs the amount of elastically backscattered electrons collected by the analyser. The measured elastic peak ($N_m(E)$), however, is affected by the analyser, in mathematical description:

$$N_m(E) = \int R(E' - E, E_p) N(E') dE', \tag{1}$$

where $N(E')$ is the original energy distribution of electrons and $R(E, E_p)$ is the transmission function (known, too, as response function) at primary energy E_p. Usually, electron spectrometers are characterized [9] by the transmission function ($T(E)$) and ΔE_s which are the response function integrated over E and the full width at half maximum (FWHM) at a given E_p, respectively. This simplified description is suitable when the shape of $R(E, E_p)$ is close to Gaussian. Little attention has been paid to the "line shape", i.e. real distribution of $R(E, E_p)$. For CMA [10] (cylindrical mirror analyser), the apparent broadening and possible enhancement of the elastic peak height were calculated.

The problem of RFA is its poor energy resolution resulting in wide instrumental response function [8]. The whole response function is needed to describe the results of measurement by RFA analyser. Beside the real elastic peak, the adjacent part of continuous background $N_b(E)$ is integrated resulting in $N_m(E)$. The transmission function with highly non-Gaussian shape may cause distortion or artificial shoulder of the peak detected. Unfortunately, the background has energy, angular and material dependencies.

The same effects arise from the wide transmission function in case of Auger peaks resulting in the distorted Auger peaks detected.

The goal of this work was to reconstruct the elastic and Auger peaks by means of $R(E, E_p)$.

Experimental method

An RFA analyser Riber OPR-304 (covering the $\alpha = 3 - 55°$ range) was operated in derivative mode, with small modulation (0.1 V). With the detection of the first derivative producing $N(E)$, the spectral distribution of backscattered electrons was recorded at energies at and close to the elastic peak.

The undistorted elastic peak $N(E_p)$ of Au and Ag have been measured with a hemispherical analyser [10] (HSA) of $\Delta E_s = 100$ MeV energy resolution. The FWHM of the elastic peak is determined by the Boersch width of the primary electron gun [1]. The elastic peak spectra of Ag and Au have been measured with the RFA in the $E_p = 100 - 2000$ eV range. Measurements were carried out in UHV on clean surfaces, produced by Ar^+ ion bombardment, and checked by AES.

The ΔE_s of the RFA was determined from the measured FWHM of elastic peak. RFA experimental spectra of Ag are displayed in Fig. 1.

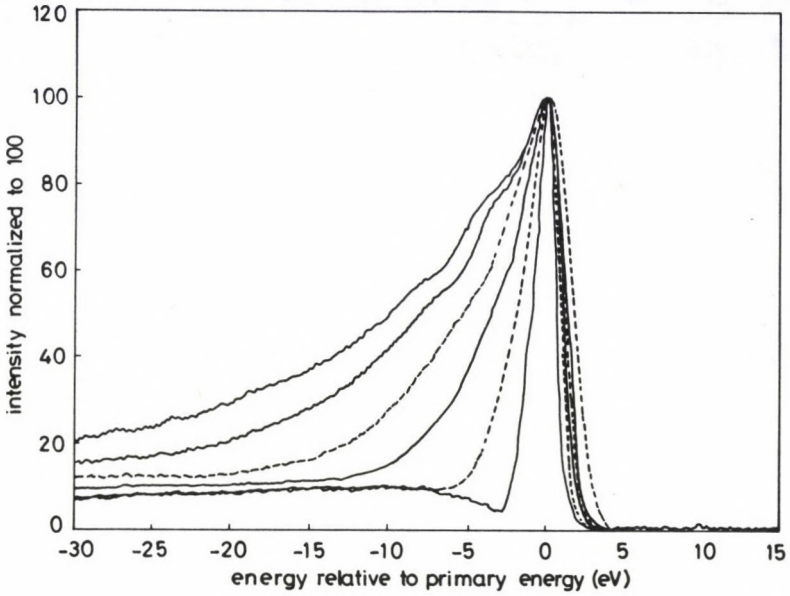

Fig. 1. Normalized elastic peaks of Ag measured by RFA with primary energies 200 eV, 500 eV, 1000 eV, 1400 eV, 2000 eV and 2500 eV

Evaluation of experiments

In our previous works $R(E, E_p)$ for a CMA Riber OPC 103 was determined using Gaussian–Lorentzian approach [10,11]. Calculated and measured elastic peaks on RFA were compared. The difference of inelastic tail is explained by the different arrangement of the two measurements (HSA has high incident angle electron beam while RFA is operated under normal incidence).

Decomposition of elastic peak measured on RFA was carried out to produce a synthetic elastic peak which can be applied to any energy for the previous tasks. $R(E, E_p)$ of our RFA was deduced from measured elastic peak by

step 1: inelastic background subtraction;

step 2: deconvolution to the energy distribution of primary electron beam with 1.2 eV FWHM;

step 3: normalizing its integral value to 1.

It turns out that the response function does not fit to a single Gaussian peak at energy measured higher than 200 eV (Fig. 2). This is due to the imperfections of the 4 grid system, observed also by Taylor [12,13].

Table I

The separated components of an elastic peak measured on Ag; height is normalized to the highest component; width and position are given in % of the primary energy

Component	Height	Width	Position
1	100	0.14	0
2	64	0.17	−0.15
3	37	0.22	−0.32
4	21	0.30	−0.52
5	10	0.58	−0.80

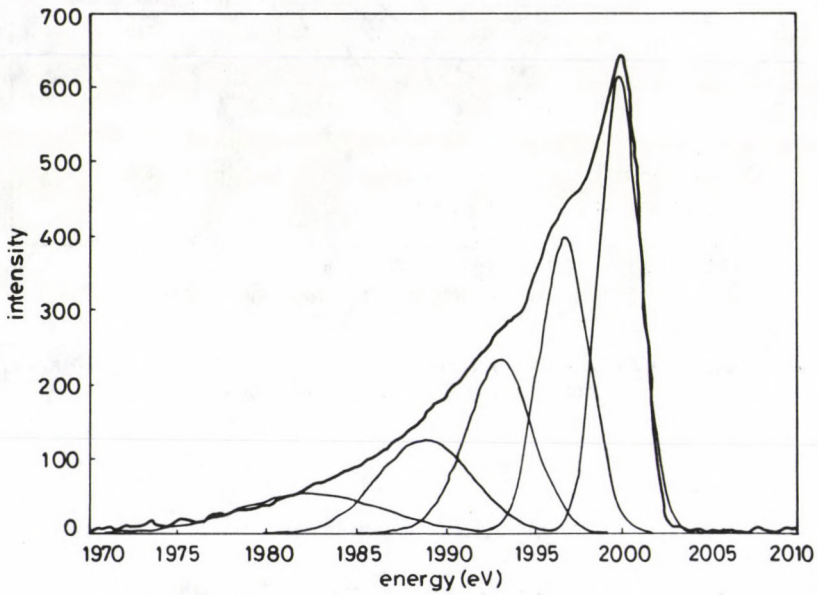

Fig. 2. Ag elastic peak at 2 keV (heavy line) and its Gaussian components (the 5 peaks in thin line) after decomposition

At 1–2 keV, a sum of 5 Gaussians proved to be adequate.

$$R(E, E_p) = \sum_{i=1}^{5} \text{Gauss}\,(A_i, B_i, C_i), \tag{2}$$

where the parameters appearing in the parentheses are the amplitude factor (A_i), the FWHM of a Gaussian peak (B_i) and the displacement relative to the primary energy (C_i). The observed values of these constants for our RFA were determined by averaging the results of 1 keV, 1.4 keV and 2 keV and they are shown in Table I. The accuracy is better than 3% regarding the smallest (which is the widest) component.

Below 800 eV, the $R(E, E_p)$ shape is smoothed by the original distribution of electron beam enabling us to separate only 4, 3 or 2 components. Finally, below 200 eV, one cannot discover more than one component part of the elastic peak detected. However, the sum of 5 Gaussians defined here is also applicable to fit the elastic peak measured by RFA at low energies.

The measured elastic peak $N_m(E_p)$ is determined by the original energy distribution of the backscattered electrons $N_0(E_p, E)$ and response function according to (1). The results of a calculation are shown in Fig. 3 and Fig. 4 for Ag and Au, respectively. The heavy distortion of spectra is obvious. The calculated spectra are compared with the real spectra measured by RFA.

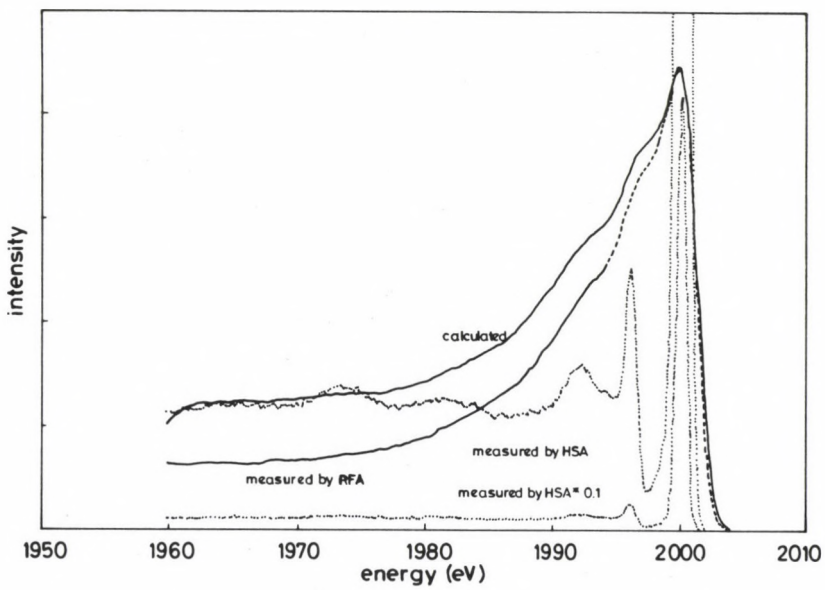

Fig. 3. Ag elastic peak at 2 keV measured by HSA and calculated to RFA. The experimental RFA spectrum is shown for comparison

The agreement between the calculated and measured spectra is reasonable. The difference in the background is due to the different arrangement used in the experiments. Primary electron beam incident on the sample surface at 70 degrees in the measurement with HSA is contrary to the normal incidence applied in RFA (see [14]).

The evaluation of EPES measurements is based on the peak height, affected by the background adjacent to the elastic peak. Spectrometer correction is needed. It is affected by $N_b(E)$ and material dependent. The correction factors determined by Eq. (2) are applied to experimental results.

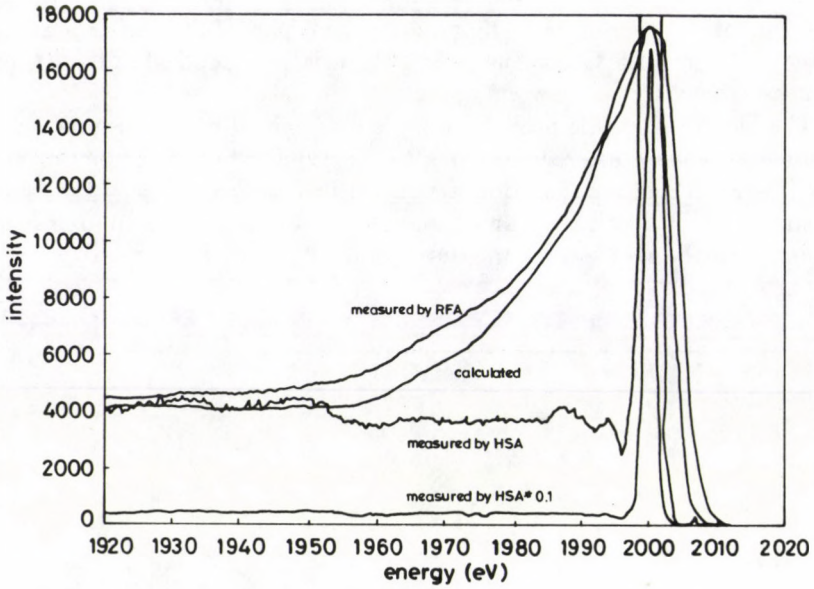

Fig. 4. Au elastic peak at 2 keV measured by HSA and calculated to RFA. The experimental RFA spectrum is shown for comparison

Conclusions

Spectrometer correction of the measured elastic peak is based on the shape of response function $R(E, E_p)$ of the RFA electron spectrometer. $R(E, E_p)$ fits to the sum of five Gaussians. They are determined from the elastic peak of Ag measured by RFA and by deconvolution of experimental elastic peak spectra. The response function is energy-dependent but its parameters proportional to primary energy. The parameters of Gaussian components (A_i amplitude, B_i FWHM, C_i displacement) were calculated for our RFA and shown here. It makes possible to build the response function valid to energies between 100 eV and 2500 eV. The process is applicable to any RFA.

Based on the response function, spectrum calculations were carried out to RFA. A reasonable agreement was found between calculated and measured elastic peak spectra on Ag.

Acknowledgement

The authors express their thanks to Z. Zsoldos for valuable contribution in HSA experiment.

References

1. G. Gergely, Surf. Interface Anal., *3*, 201, 1981; Scanning, *8*, 203, 1986.
2. R. Schmid, K. H. Gaukler and H. Seiler, Scanning Electron Microscopy, *2*, 501, 1983; SEM Inc. AMF. O'Hare, p. 501.
3. W. Dolinski, H. Nowicki and S. Mróz, Surf. Interface Anal., *11*, 229, 1988.
4. B. Gruzza, B. Achard and C. Pariset, Surface Sci., *162*, 202, 1985.
5. B. Gruzza and C. Pariset, Surface Sci., *247*, 408, 1991.
6. Ch. Kleint and S. M. Abd. El Halim, Surface Sci., *247*, 375, 1991.
7. L. Eckertova and Ch. Kleint, Surface Sci., *231*, 168, 1990.
8. M. P. Seah, Surf. Interface Anal., *9*, 85, 1986.
9. J. Osterwalder, M. Sagurton, P. J. Orders, S. S. Fadley, B. D. Hersmeier and D. J. Friedman, J. Electron Spectrosc. Relat. Phenom., *48*, 55, 1989.
10. G. Gergely, L. Guczi, A. Jablonski, B. Lesiak, A. Sulyok and Z. Zsoldos, Proc. 12 ICXOM 1989, Cracow, eds S. Josienska and L. J. Maksymowicz, Academy of Mining an Metallurgy, Cracow, Poland, *2*, p. 506.
11. P. M. A. Sherwood, in Practical Surface Analysis, D. Briggs and M. P. Seah (eds), J. Wiley, New York, 1983, p. 459.
12. N. J. Taylor, Rev. Sci. Instrum., *40*, 792, 1969.
13. Y. Ballu, in Adv. Electronics and Electron Phys. Suppl., *13B*, 257, 1980.
14. H. J. Fitting and R. Technow, Phys. Stat. Sol., *A76*, K151, 1983.

Acta Physica Hungarica 72 (1), pp. 115-119 (1992)

SHORT COMMUNICATION

ROLE OF DISPERSION IN THE LATTICE THERMAL CONDUCTIVITY OF Ge

A. H. AWAD

Department of Physics, College of Education, University of Basrah
Basrah, Iraq

(Received 25 February 1992)

One of the difficult problems in the relaxation time approach to the lattice thermal conductivity is the evaluation of the three phonon scattering relaxation times [1,2] which have a complicated dependence on phonon frequency and temperature due to the complicated structure of the phonon branch and of the dispersion in the phonon spectrum. Consequently, the approximated expressions may only have validity for a limited phonon frequency and temperature range.

By assuming a Debye phonon spectrum ($k = \omega/v$) and making several assumptions, Callaway [3] derived an expression for the lattice thermal conductivity of solids. The success of this model lies in the fact that the Debye approximation is valid at low temperatures. Using this model, the phonon conductivity of several materials was calculated [4–7], and good fitting was obtained between the calculated and the experimental findings at low temperatures. The Callaway model was modified by Holland [8] taking account of the phonon dispersion. However, he also used the Debye approximation in this theory, and divided the Brillouin zone into two regions $0 - \frac{1}{2}k_{\max}$ and $\frac{1}{2}k_{\max} - k_{\max}$. He used two different velocities of the transverse phonons, while for longitudinal phonons he suggested only one velocity value. Verma [9] and his co-workers proposed a modification of the Holland model (known as SDV model) utilizing Guthrie [10] classification of phonon scattering events. Considering the same classification and including the contribution of normal and umklapp processes, Dubey [11] proposed an expression for the three phonon scattering relaxation rate (Dubey model). This model was incorporated successfully by the present author [12–14] to explain the experimental data of different samples at high as well as at low temperatures. Instead of using the acoustic approximation ($k = \omega/v$), which is valid only at low temperatures, Verma et al [15] assumed an empirical expression for the phonon wave vector as a function of the phonon frequency in order to calculate the phonon phase and group velocities as a function of the phonon frequency.

The aim of the present work is to test the validity of the Verma dispersion relation in the temperature range 4–1000 K. The effect of the phonon dispersion on the lattice thermal conductivity of Ge has been studied by evaluating the percentage change in the lattice thermal conductivity. This percentage change has also been studied separately for the transverse as well as for longitudinal phonons. The lattice

thermal conductivity has been studied in the frame of the Holland model [8], SDV model [9], and Dubey model [11] of three phonon scattering rates.

Considering the role of the three phonon normal processes, Callaway [3] expressed the lattice thermal conductivity as

$$K_i = \frac{N}{2} \int_0^{Q_i/T} \tau_{c,i} F(x)(v_{g,i}/v_{p,i}^2) dx, \tag{1}$$

where $F(x) = x^4 e^x (e^x - 1)^{-2}$, $x = \hbar\omega/K_B T$, $N = (K_B/3\pi^2)(K_B T/\hbar)^3$, Q_i is the temperature corresponding to a frequency at the zone boundary of the crystal, v_g and v_p are the group and phase velocities of the phonon, the subscript i refers to T and L for the transverse and longitudinal phonons, respectively, $\tau_{c,i}$ is the combined scattering relaxation time, and ω is the phonon frequency.

In order to calculate v_g/v_p^2 for the conductivity integral in Eq. (1), Verma [15] suggested a quadratic dispersion relation in the form

$$k = (\omega/v)(1 + r\omega^2), \tag{2}$$

where k is the phonon wave vector, v is the phonon velocity and r is the dispersion constant which depends on the crystal structure. The effect of the dispersion on the lattice thermal conductivity is expressed as percentage change

$$K(R) = \frac{K(R) - K}{K(R)} \times 100, \tag{3}$$

where K is the lattice thermal conductivity for $r = 0$.

The constants and parameters used in the present study are taken from the earlier reports of Holland [8], Verma et al [9] and Dubey [11] (therefore not reported here). With the help of these constants and using the conductivity integrals $K(R)$ has been calculated for Ge in the temperature range 4–1000 K. The results are given in Table I. Separate percentage changes in the lattice thermal conductivity of the transverse and longitudinal phonons are calculated and listed in Table II. With the help of these Tables, one can conclude the following:

1. The percentage change in the lattice thermal conductivity increases with increasing temperature (30–1000 K). It can be said that the effect of the phonon dispersion on the lattice thermal conductivity increases with increasing temperature. This is mainly due to the fact that at high temperatures the phonons of high frequency are more dispersive. However, there are some discrepancies at the low temperatures, so a deviation of the dispersion relation, as suggested by Verma, from Debye phonon spectra has been found at low temperatures (4–20 K). As a result, one can conclude that the assumed dispersion relation is not valid for low frequency phonons.

2. At any particular temperature (above 20 K), the percentage change in the lattice thermal conductivity in the frame of the SDV model is smaller than those obtained in the frame of other models. This comes from the fact that the SDV model

Table I
Percentage change in the lattice thermal conductivity of Ge in the temperature range 4–1000 K in the frame of the Holland, SDV and Dubey models

T(K)	Holland model	SDV model	Dubey model
4	−1.023	−0.960	−0.961
5	−1.305	−1.147	−1.226
8	−1.996	−1.785	−1.876
10	−2.354	−2.196	−2.201
20	−3.104	−2.675	−2.529
30	−2.174	−2.191	−2.099
40	−0.349	−1.965	−1.253
50	1.561	−1.855	−0.138
60	3.238	−1.673	0.879
70	4.621	−1.295	1.611
80	5.751	−1.000	2.324
90	6.688	−0.750	2.880
100	7.483	−0.537	3.353
200	12.046	0.362	5.441
300	14.071	0.607	5.988
400	15.020	0.726	6.209
500	15.507	0.796	6.320
600	15.781	0.844	6.384
700	15.952	0.875	6.419
800	16.064	0.901	6.442
900	16.140	0.921	6.456
1000	16.193	0.937	6.462

only includes the effect of the three phonon umklapp processes in the range $0 - k_{\max}$ for both the transverse and longitudinal phonons. At the same time the Holland model does not consider the contribution of the three phonon umklapp processes in the range $0 - \frac{1}{2}k_{\max}$ for the transverse phonons, and in the range $0 - k_{\max}$ for the longitudinal phonons. In other words, the contribution of the three phonon unklapp processes is one of the factors which are responsible for minimizing the effect of dispersion on the lattice thermal conductivity, so it is more realistic to use the SDV model of the three phonon scattering relaxation rate. The reverse nature is true at low temperatures (4–20 K). The original cause of such kind of variation can be explained by considering the role of the three phonon umklapp processes which seldom happen in the low frequency region ($\omega < \omega_1$). We must state here that the Dubey model includes both three phonon normal and umklapp processes in the same expression.

3. For longitudinal phonons, the percentage changes ($\%K_L(R)$) in the frame of the Holland model are zero. Similar results have also been obtained for other models at low temperature (below 30 K). This can be attributed to the value of the dispersion constant for the longitudinal phonons in the range $0 - \frac{1}{2}k_{\max}$ ($r = 0$) (For more details see [8,9 and 11]).

4. The studied sample, Germanium has a very dispersive transverse acoustic phonon spectrum, which is similar to the findings of previous reports [16,17]. But

Table II
Percentage change in the lattice thermal conductivity of transverse and longitudinal phonons of Ge in the temperature range 4–1000 K in the frame of Holland, SDV and Dubey models

T(K)	% $K_T(R)$*			% $K_L(R)$*		
	Holland model	SDV model	Dubey model	Holland model	SDV model	Dubey model
4	−1.32	−1.31	−1.31	0	0	0
5	−1.67	−1.57	−1.57	0	0	0
8	−2.57	−2.25	−2.22	0	0	0
10	−3.06	−3.01	−3.00	0	0	0
20	−4.49	−4.92	−3.89	0	0	0
30	−3.72	−4.77	−2.86	0	0	0
40	−0.68	−4.03	−1.44	0	0.04	0.15
50	3.28	−3.36	0.18	0	0.18	0.71
60	9.92	−2.81	0.86	0	0.48	0.11
70	11.73	−2.38	1.72	0	0.78	1.32
80	13.69	−2.03	2.42	0	1.17	1.64
90	13.02	−1.74	2.99	0	1.60	1.04
100	13.92	−1.51	3.47	0	2.00	2.44
200	16.09	−0.47	5.52	0	3.88	2.19
300	16.31	−0.15	6.06	0	4.32	4.52
400	16.37	0.01	6.28	0	4.49	4.62
500	16.40	0.10	6.38	0	4.57	4.72
600	16.41	0.16	6.45	0	4.62	4.73
700	16.41	0.20	6.50	0	4.66	4.74
800	16.42	0.24	6.53	0	4.66	4.76
900	16.43	0.27	6.53	0	4.67	4.78
1000	16.43	0.28	6.54	0	4.67	4.83

* % $K_i = \frac{K_i(R) - K_i}{K_i(R)} \times 100$

from Table II it can be seen that the transverse phonons of the SDV model are exceptions, due to the presence of umklapp processes in both class I and class II events for longitudinal phonons, which reduce the effect of dispersion.

5. Germanium has been chosen in this analysis because of its very dispersive phonon spectra [8].

References

1. P. Carruthers, Rev. Mod. Phys., *33*, 92, 1961.
2. P. G. Klemens, Proc. Roy. Soc. (London), *A208*, 108, 1951.
3. J. Callaway, Phys. Rev., *113*, 1046, 1959.
4. R. O. Pohl, Phys. Rev., *118*, 1499, 1960.
5. J. Callaway and H. C. von Baeyer, Phys. Rev., *120*, 1149, 1960.
6. A. M. Toxen, Phys. Rev., *122*, 787, 1961.
7. J. Callaway, Phys. Rev., *122*, 787, 1961.
8. M. G. Holland, Phys. Rev., *132*, 2461, 1963.

9. P. C. Sharma, K. S. Dubey and G. S. Verma, Phys. Rev., *B4*, 1306, 1971.
10. G. L. Guthrie, Phys. Rev., *152*, 801, 1966.
11. K. S. Dubey, J. Thermal Anal., *19*, 263, 1980.
12. A. H. Awad, Acta Phys. Hung., *63*, 331, 1988.
13. A. H. Awad, Iraqi J. of Science, *32*, 22, 1991.
14. A. H. Awad and K. S. Dubey, J. Thermal Anal., *24*, 233, 1982.
15. Y. P. Joshi and G. S. Verma, Phys. Rev., *B1*, 750, 1970.
16. B. N. Brockhouse and P. K. Iyengar, Phys. Rev., *11*, 747, 1958.
17. B. N. Brockhouse, Phys. Rev. Letters, *2*, 256, 1959.

Acta Physica Hungarica 72 (1), pp. 121-122 (1992)

BOOK REVIEWS

Interaction of Charged Particles with Solids and Surfaces
A. Gras-Martí, H. M. Urbassek, N. R. Arista and F. Flores (eds)
Proceedings of a NATO Advanced Study Institute on Interaction of Charged Particles with Solids and Surfaces (Alacant, Spain, 1990), NATO ASI Series B: Physics, Vol. 271, Plenum Press, New York and London, 1991, pp. 716

This is the first book on the subject which has been aimed at offering a tutorial introduction of comprehensive level into the topic of interaction of charged particles with solids and surfaces. The concepts, theoretical tools, and experimental techniques and results presented in these Proceedings are of interest to a vast interdisciplinary community of scientists and engineers. For example, researchers involved in surface physics, material sciences, ion implantations and so on will find in this Volume of NATO ASI Series a sound introduction to the field of charged particle–surface interaction.

This book covers theory, experiments, and applications of the stopping of charged particles (ions and electrons) in matter. The lectures have been classified into three categories: main stream lectures, invited lectures and contributed papers. Within each category the topic has been divided into the following main chapters: stopping of ions, stopping of electrons, low energy phenomena, and applications. Main stream lectures include: dynamical interaction of charges with condensed matter (F. Flores); density functional theory of stopping power (P. M. Echenique and M. E. Uranga); statistics of charged-particle penetration (P. Sigmund); accelerators and stopping power experiments (H. H. Andersen); electron spectra in solids (R. R. Ritchie, R. N. Hamm, J. C. Ashley and P. M. Echenique); low energy ion penetration and collision cascades in solids (H. M. Urbassek); interaction of low-energy ions, atoms and molecules with surfaces (W. Heiland); desorption induced by electronic transitions (R. A. Baragiola and T. E. Madey).

The volume is recommended to advanced researchers as well as beginners who are working in solid state and surface pysics.

B. Apagyi

P. N. BUTCHER and D. COTTER: *The Elements of Nonlinear Optics*
Cambridge Studies in Modern Optics 9
Cambridge University Press, Cambridge 1991, £ 16.95, US$ 29.95

This book is the newest volume of the series "Cambridge Studies in Modern Optics" which series deals with various fields and subjects of today's optics, all of them having a large amount of interest. In this way since nonlinear optics is also a basic part of recent research and practical applications it has a good place in this series. Regarding the large number of lasers and nonlinear elements used in science and technology, the need for a basic knowledge in the field is becoming more and more important. The book has the aim of presenting basic, mainly theoretical knowledge in the field of nonlinear optics starting from the basic principles and this aim is well reached by the authors.

The first chapter starts with the origin of optical nonlinearity, This is presented in a simple straightforward way thus giving a firm base to build further the more complicated theoretical descriptions. This is followed in the second chapter by the necessary fundamental properties related to electromagnetic waves while the third chapter gives the basic concepts of the quantum mechanics used. The semi-classical description is used in the book by the authors in which the electromagnetic field is treated in a classical manner, while the material properties are treated in a quantum mechanical way. The fourth and fifth chapters give detailed knowledge on the susceptibility tensors and symmetry properties which are both important for the understanding of nonlinear optics. Chapter six describes resonant nonlinearities, the last three chapters deal with wave propagation in nonlinear media, dynamic optical nonlinearities in semiconductors and optical properties of artificial materials.

Usually, it is difficult to write a theoretically oriented book for non-specialist readers. The authors have succeeded, however, to explain all basic physics in a clear way without losing the base showing the origin of results and the way they are obtained. The chapters dealing with semiconductors and artificial materials, the latter including quantum wells, give the book a real modern character.

Although the book is well written, well organized and its content is easy to follow in itself it does not give a complete survey of all aspects of the very broad subject of nonlinear optics and applications. This was not the authors' aim, however, and they admit that the book is really useful as a theoretical base for other published books including experimental and practical aspects of the field. The book is recommended for graduate students of physics and electrical engineering and also for scientists and engineers working in this field. For research workers in the field the book is considered to be a basic reference for fundamental formulas and explanation of basic physics leading to these.

To summarize the book is an enjoyable and useful reading and is particularly useful when it is in hand together with other reviews including the more practical sides of the field.

M. Jánossy

Physics

Spacetime without Reference Frames

by
T. MATOLCSI

In the concept of this book spacetime is the fundamental notion; the points of spacetime are structured with the assumption of absolute time and absolute velocity of light resulting in the non-relativistic and special relativistic case, respectively. This gives the possibility of developing both the non-relativistic and the special relativistic chapters along the same notions: world line, observer, splitting of spacetime to space and time, reference frames, splitting of classical fields to spacelike and timelike components, the symmetry groups of spacetime (the Galilean and the Poincaré group).
The book contains lots of examples with detailed calculations through which the reader can clearly understand the connection between the traditional way of thinking and the new way of handling the problems presented in the book; the well-known special relativistic paradoxes are treated in detail. In the general relativistic case, only the basic thoughts are expressed.
The mathematics involved is rather simple and it is summarized in the second part of the book.

Readership: lecturers in physics, mathematics, undergraduate students

In English. 1992. Approx. 400 pages. Numerous figures. 17 x 25 cm. Hardbound.
Approx. $ 50.00

Akadémiai Kiadó, Budapest

Manuscript received by Akadémiai Kiadó:
18 July 1992
Manuscript received by TYPOTEX Ltd for TEX typesetting:
31 July 1992
Date of publication: 30 November 1992
PRINTED IN HUNGARY
Akadémiai Kiadó és Nyomda Vállalat
Budapest

NOTES TO CONTRIBUTORS

I. PAPERS will be considered for publication in Acta Physica Hungarica only if they have not previously been published or submitted for publication elsewhere. They may be written in English, French, German or Russian.

Papers should be submitted to

Prof. I. Kovács, Editor
Department of Atomic Physics, Technical University
1521 Budapest, Budafoki út 8, Hungary

Papers may be either articles with abstracts or short communications. Both should be as concise as possible, articles in general not exceeding 25 typed pages, short communications 8 typed pages.

II. MANUSCRIPTS

1. Papers should be submitted in three copies.
2. The text of papers must be of high stylistic standard, requiring minor corrections only.
3. Manuscripts should be typed in double spacing on good quality paper, with generous margins.
4. The name of the author(s) and of the institutes where the work was carried out should appear on the first page of the manuscript.
5. Particular care should be taken with mathematical expressions. The following should be clearly distinguished, e.g. by underlining in different colours: special founts (italics, script, bold type, Greek, Gothic, etc.); capital and small letters; subscripts and superscripts, e.g. x^2, x_3; small *l* and l; zero and capital O; in expressions written by hand: *e* and *l*, *n* and *u*, *v* and v, etc.

A List of Symbols on a separate sheet should be attached to each paper.

6. References should be numbered serially and listed at the end of the paper in the following form: J. Ise and W. D. Fretter, Phys. Rev., *76,* 933, 1949.

For books, please give the initials and family name of the author(s), title, name of publisher, place and year of publication, e.g.: J. C. Slater, Quantum Theory of Atomic Structures, I. McGraw-Hill Book Company, Inc., New York, 1960.

References should be given in the text in the following forms: Heisenberg [5] or [5].

7. Captions to illustrations should be listed on a separate sheet, not inserted in the text.
8. In papers submitted to Acta Physica all measures should be expressed in SI units.

III. ILLUSTRATIONS AND TABLES

1. Each paper should be accompanied by three sets of illustrations, one of which must be ready for the blockmaker. The other sets attached to the copies of the manuscript may be rough drawings in pencil or photocopies.
2. Illustrations must not be inserted in the text.
3. All illustrations should be identified in blue pencil by the author's name, abbreviated title of the paper and figure number.
4. Tables should be typed on separate pages and have captions describing their content. Clear wording of column heads is advisable. Tables should be numbered in Roman numerals (I, II, III, etc.).

IV. RETURN OF MATERIAL

Owing to high postage costs, the Editorial Office cannot undertake to return *all* material not accepted for any reason for publication. Of papers to be revised (for not being in conformity with the above Notes or other reasons) only *one* copy will be returned. Material rejected for lack of space or on account of the Referees' opinion will not be returned to authors outside Europe.

Index: 26.022

Acta Physica Hungarica

VOLUME 72 · NUMBERS 2–4, 1992

Akadémiai Kiadó, Budapest

ACTA PHYS. HUNG. APAHAQ 72 (2–4) 123-306 (1992) HU ISSN 0231–4428

ACTA PHYSICA HUNGARICA

A JOURNAL OF THE HUNGARIAN ACADEMY OF SCIENCES

EDITED BY
I. KOVÁCS

Acta Physica publishes original papers on subjects in physics. Papers are accepted in English, French, German and Russian.

Acta Physica is published in two yearly volumes (4 issues each) by

AKADÉMIAI KIADÓ
Publishing House of the Hungarian Academy of Sciences
H–1117 Budapest, Prielle Kornélia u. 19–35.

Subscription information

Orders should be addressed to

AKADÉMIAI KIADÓ
H–1519 Budapest, P.O. Box 245

Acta Physica Hungarica is abstracted/indexed in Chemical Abstracts, Mathematical Reviews, Science Abstracts, Physics Briefs, Risk Abstracts, Engineering Information, Inc. EI Page One Database

CONTENTS

Acta Physica Hungarica 72 (2-4), pp. 123-132 (1992)

THE CORRECTION TERM IN A DISLOCATION CONTAINING LATTICE

A. H. AWAD

Department of Physics, College of Education, University of Basrah
Basrah, Iraq

(Received 23 January 1992)

The correction term of a sample having dislocation (strain field as well as core) has been studied at low temperatures on the basis of the Callaway integral as well as in the frame of the generalized Callaway integral. Assuming four types of the scattering mechanisms, viz. boundary, dislocation, point defect and three phonon, analytical expressions for the correction term are given under two different conditions. The expressions derived give results in agreement with the findings of previous works.

1. Introduction

Callaway [1] was the first who distinguished the three phonon normal processes from the three umklapp processes. He derived an expression for the lattice thermal conductivity of an insulator as a sum of two parts. The first one is attributed to the combined scattering relaxation rates, whereas the second part is very complicated known as the correction term (ΔK) due to the three phonon normal processes.

Kosarev et al [2] and Parrot [3] have published a generalization of Callaway's approach to thermal conductivity when different polarizations are taken into account. Later on, the generalized expression was modified by Dubey [4] introducing the dispersion of phonons.

The lattice thermal conductivity due to the correction term has been studied in the frame of the Callaway integral as well as in the frame of the generalized Callaway integral [5–11], and it is usually found that the contribution to the lattice thermal conductivity arising from the correction term is negligibly small. (Exceptions are solid He [9], LiF [10] and solid HD [11]). These studies are confined to samples of perfect structures only. In none of them was an analytical expression obtained for the correction term in a lattice having dislocations (strain field and core). Recently, the present author [12,13] studied the contribution of the correction term for a sample containing core dislocation in the frame of the Callaway integral as well as the generalized Callaway integral. It was found that analytical expressions are very necessary to avoid the complicated integrals of the correction term.

The aim of the present investigation is to obtain a simple analytical expression for the correction term on the basis of the Callaway integral and also the generalized Callaway integral at very low temperatures.

2. Analytical expression for ΔK in the frame of the Callaway integral

According to Callaway [1], the lattice thermal conductivity of an insulator can be written as

$$K = c_0 L_1 + \Delta K, \tag{1}$$

where

$$\Delta K = c_0 L_2^2 / L_3, \tag{2}$$

$$L_1 = \int_0^{\Theta_D/T} (\tau_N^{-1} + \tau_R^{-1})^{-1} F(x) dx, \tag{3}$$

$$L_2 = \int_0^{\Theta_D/T} \tau_N^{-1} (\tau_N^{-1} + \tau_R^{-1})^{-1} F(x) dx, \tag{4}$$

$$L_3 = \int_0^{\Theta_D/T} \tau_R^{-1} \tau_N^{-1} (\tau_N^{-1} + \tau_R^{-1})^{-1} F(x) dx. \tag{5}$$

$c_0 = (K_B/2\pi^2 v)(K_B T/\hbar)^3$, $F(x) = x^4 e^x (e^x - 1)^{-2}$, $x = \hbar\omega/K_B T$, ω is the phonon frequency, Θ_D is the Debye temperature of the sample, v is the velocity of the phonon, τ_N^{-1} is the three phonon normal processes scattering relaxation rate and τ_R^{-1} is the total scattering relaxation rate due to all momentum nonconserving processes. The expressions used for the scattering relaxation rate can be derived as

$$\tau_R^{-1} = \tau_B^{-1} + \tau_{pt}^{-1} + \tau_{ds}^{-1} + \tau_{dc}^{-1} + \tau_U^{-1}, \tag{6}$$

$$\tau_{pt}^{-1} = A\omega^4 = Dx^4, \tag{7}$$

$$\tau_{ds}^{-1} = a'\omega = a_1 x, \tag{8}$$

$$\tau_{dc}^{-1} = d\omega^3 = cx^3, \tag{9}$$

$$\tau_N^{-1} = B\omega^2 T^3 = b_1 x^2, \tag{10}$$

$$\tau_U^{-1} = B'\omega^2 T^3 = b_2 x^2, \tag{11}$$

$$E = b_1 + b_2, \tag{12}$$

where τ_B^{-1}, τ_{pt}^{-1}, τ_{ds}^{-1}, τ_{dc}^{-1} and τ_U^{-1} are the scattering relaxation rates ascribed to boundary [13], point defect [15], strain field dislocation [15], core dislocation [15] and three phonon umklapp processes [1], respectively. A, a', d, B and B' are scattering strengths of the respective processes.

The analytical expressions have been obtained in the low temperature approximation under two different conditions, i.e. $\tau_{ds}^{-1} \gg (\tau_B^{-1} + \tau_{dc}^{-1})$ and $\tau_B^{-1} \gg (\tau_{dc}^{-1} + \tau_{ds}^{-1})$.

(A) $\tau_{ds}^{-1} \gg (\tau_B^{-1} + \tau_{dc}^{-1})$

For this case, the simplified forms of L_2 and L_3 can be written as

$$L_2 = \frac{b_1 I_5}{a_1}\left[1 - G_1 F_5^4 - G_3 F_5^8 - G_2 F_5^6 - G_4 F_5^7\right], \tag{13}$$

$$\begin{aligned} L_3 = b_1 I_6 \Big[1 &- \frac{PG_2}{1+P} F_6^7 - G_4^2 F_6^{10} - 2G_1 G_4 F_6^7 - 2G_3 G_4 F_6^{11} - \frac{(2+P)}{(1+P)} G_2 G_4 F_6^9 \\ &- G_1^2 F_6^4 - 2G_1 G_3 F_6^8 - G_1 G_2 \frac{(2+P)}{(1+P)} - G_3^2 F_6^{12} - \frac{(2+p)}{(1+P)} G_2 G_3 F_6^{10} \\ &- \frac{G_2^2}{(1+P)} F_6^8 \Big], \end{aligned} \tag{14}$$

where $G_1 = \tau_B^{-1}/a_1$, $G_2 = E/a_1$, $G_3 = D/a_1$, $G_4 = c/a_1$, $P = b_1/b_2$, $F_n^m = I_m/I_n$, m and $n = 1, 2, 3, \ldots$, etc. and the I's are integrals which can be expressed as

$$I_r = \int_0^{\Theta_D/T} x^r e^x (e^x - 1)^{-2} dx,$$

where $r = 2, 3, 4, \ldots$, etc. At very low temperatures, the upper limit of the integrals can be taken as infinity. Thus I_r can be evaluated as

$$I_r = \int_0^{\infty} x^r e^x (e^x - 1)^{-2} dx = r! \sum_{j=1}^{\infty} \frac{1}{j^r}. \tag{15}$$

It is observed that the contribution of the three phonon umklapp processes scattering relaxation rate is very small compared to τ_R^{-1} and it can be ignored. A further approximation can be made by neglecting the lower order term and then the expression for ΔK is given by

$$\Delta K = \frac{c_0 b_1 I_5 F_6^5}{a_1^2}\left[1 - 2G_1 F_5^4 - 2G_3 F_5^8 - 2G_2 F_5^6 + G_2 F_6^7 - 2G_4 F_5^7\right], \tag{16}$$

(B) $\tau_B^{-1} \gg (\tau_{dc}^{-1} + \tau_{ds}^{-1})$

Applying this condition and evaluating (4) and (5), we get

$$L_2 = b_1 \tau_B I_6 \left[1 - c\tau_B F_6^9 - a_1 \tau_B F_6^7 - D\tau_B F_6^{10} - E\tau_B F_6^8\right], \tag{17}$$

$$\begin{aligned} L_3 = b_1 I_6 \Big[1 &- b_1 \tau_B F_6^8 - c^2 \tau_B^2 F_6^{12} - 2a_1 c \tau_B^2 F_6^{10} - 2Dc\tau_B^2 F_6^{12} - a_1^2 \tau_B^2 F_6^8 \\ &- (E + b_2) c \tau_B^2 F_6^{11} - 2a_1 D \tau_B^2 F_6^{11} - (E + b_2) a_1 \tau_B^2 F_6^9 - D^2 \tau_B^2 F_6^{14} \\ &- (E + b_2) D \tau_B^2 F_6^{12} - E b_2 \tau_B^2 F_6^{10}\Big]. \end{aligned} \tag{18}$$

Using these equations, ΔK is expressed as

$$\Delta K = c_0 b_1 \tau_B^2 I_6 \left[1 - 2c\tau_B F_6^9 - 2a_1 \tau_B F_6^7 - 2D\tau_B F_6^{10} - b_1 \tau_B F_6^8\right]. \tag{19}$$

With the help of Eq. (15), one can get an expression for ΔK as follows:

$$\Delta K = 720 c_0 b_1 \tau^2 \left[1 - 1008c\tau_B - 14a_1\tau_B - 10080D\tau_B + 56b_1\tau_B\right]. \tag{20}$$

In the absence of strain field dislocation, ΔK reduces to

$$\Delta K = c_0 b_1 \tau_B^2 I_6 \left[1 - 2c\tau_B F_6^9 - 2D\tau_B F_6^{10} - b_1 \tau_B F_6^8\right], \tag{21}$$

which is similar to that obtained by Awad [12] for a sample having core dislocation in the frame of the Callaway integral.

The expression for ΔK will be

$$\Delta K = c_0 b_1 \tau_B^2 I_6 \left[1 - 2D\tau_B^2 F_6^{10} - b_1 \tau_B^2 F_6^8\right] \tag{22}$$

for a sample without dislocation, which is the same as that obtained by Dubey [8].

3. Analytical expression for ΔK in the frame of the generalized Callaway integral

The generalized form of the Callaway integral of the lattice thermal conductivity can be given as

$$K = c_1 \left[\sum_s (1/v_s) \int_0^{\Theta_s/T} (\tau_{N,s}^{-1} + \tau_{R,s}^{-1})^{-1} (1 + R_s x^2)^2 (1 + 3R_s x^2)^{-1} F(x) dx + \Delta K\right], \tag{23}$$

where $c_1 = K_B/6\pi^2 v_s)(K_B T/\hbar)^3$, R is a constant depending on the dispersion curve of the sample, suffix s represents the mode of phonon and all other terms have their meaning as in Section 2.

According to Dubey [4], ΔK can be written as

$$\Delta K = c_1 \left[2(T_1 + T_2) + (L_1 + L_2)\right]^2 / \left[2(T_3 + T_4) + (L_3 + L_4)\right]. \tag{24}$$

It was found that the contributions of T_2, T_4, L_2 and L_4 are very small in comparison to the contributions of T_1, T_3, L_1 and L_3 due to their integration limit. Thus ΔK becomes:

$$\Delta K = c_1 \left[(2T_1 + L_1)^2/(2T_3 + L_3)\right], \tag{25}$$

where

$$T_1 = (1/v_{T_1}^3) \int_0^{\Theta_1/T} \tau_{N,T}^{-1}(\tau_{N,T}^{-1} + \tau_{R,T}^{-1})^{-1}(1 + R_1x^2)^3 F(x)dx, \tag{26}$$

$$T_3 = (1/v_{T_1}^5) \int_0^{\Theta_1/T} \tau_{N,T}^{-1}\tau_{R,T}^{-1}(\tau_{N,T}^{-1} + \tau_{R,T}^{-1})^{-1}(1 + R_1x^2)^4(1 + 3R_1x^2)^4 F(x)dx, \tag{27}$$

$$L_1 = (1/v_{L_1}^3) \int_0^{\Theta_3/T} \tau_{N,L}^{-1}(\tau_{N,L}^{-1} + \tau_{R,L}^{-1})^{-1}(1 + R_3x^2)^3 F(x)dx, \tag{28}$$

$$L_3 = (1/v_{L_1}^5) \int_0^{\Theta_3/T} \tau_{N,L}^{-1}\tau_{R,L}^{-1}(\tau_{N,L}^{-1} + \tau_{R,L}^{-1})^{-1}(1 + R_3x^2)^4(1 + 3R_3x^2)^4 F(x)dx. \tag{29}$$

Θ's are the characteristic temperatures, suffixes T and L represent transverse and longitudinal phonons, respectively. The expressions used for the above stated scattering relaxation rate can be expressed as

$$\tau_{N,L}^{-1} = B_1\omega^2T^3 = b_3x^2, \tag{30}$$

$$\tau_{U,L}^{-1} = B_2\omega^2T^3e^{-\Theta D/\alpha T} = b_4x^2, \tag{31}$$

$$\tau_{N,T}^{-1} = B_3\omega T^4 = b_5x, \tag{32}$$

$$\tau_{U,T}^{-1} = B_4\omega T^4e^{-\Theta_D/\alpha T} = b_6x, \tag{33}$$

where B_1 and B_2 are the three phonon normal and umklapp processes scattering strengths, respectively, for longitudinal phonons, B_3 and B_4 are the same for the transverse phonons, α is a constant [15] and other terms have been defined in Section 2.

As stated earlier, our interests are confined to low temperature only, therefore our study is limited to two approximations.

(A) $\tau_B^{-1} \gg (\tau_{cd}^{-1} + \tau_{sd}^{-1})$

In the framework of the above approximation, the integrals T_1, L_1, T_3 and L_3 can be given

$$T_1 = \frac{b_5\tau_B I_5}{v_{T_1}^3}\left[X_5^7(R) - H_1F_5^8X_8^{10}(R_1) - H_2F_5^9X_9^{11}(R_1) - (H_3 + H_5)F_5^6X_6^8(R_1)\right], \tag{34}$$

$$L_1 = \frac{b_3\tau_B I_6}{v_{L_1}^3}\left[X_6^8(R_3) - H_1F_6^9X_9^{11}(R_3) - H_2F_6^{10}X_{10}^{12}(R_3) - H_4F_6^8X_8^{10}(R_3) - H_5F_6^7X_7^9(R_3)\right], \tag{35}$$

$$T_3 = \frac{b_5 I_5}{v_{T_1}^5}\Big[Y_5^7(R_1) - \frac{P'H_3}{(1+p')}F_5^6Y_6^8(R_1) - H_1^2F_5^{11}Y_{11}^{13}(R_1) - 2H_1H_5F_5^9Y_9^{11}(R_1)$$
$$- 2H_1H_2F_5^{12}Y_{12}^{14}(R_1) - \frac{(2+P')}{(1+P')}H_1H_3F_5^9Y_9^{11}(R_1) - H_5^2F_5^7Y_7^9(R_1)$$
$$- 2H_2H_5F_5^{10}Y_{10}^{12}(R_1) - \frac{(2+P')}{(1+P')}H_3H_5F_5^7Y_7^9(R_1) - H_2^2F_5^{13}Y_{13}^{15}(R_1)$$
$$- \frac{(2+P')}{(1+P')}H_2H_3F_5^{10}Y_{10}^{12}(R_1) - \frac{H_3^2}{(1+P')}F_5^7Y_7^9(R_1)\Big], \tag{36}$$

$$L_3 = \frac{b_3 I_6}{v_{L_1}^5}\,[\,Y_6^8(R_3) - \frac{P_1}{(1+P_1)}H_4F_6^8Y_8^{10}(R_3) - H_1^2F_6^{12}Y_{12}^{14}(R_3)$$
$$- 2H_1H_5F_6^{10}Y_{10}^{12}(R_3) - 2H_1H_2F_6^{13}Y_{13}^{15}(R_3) - \frac{(2+P_1)}{(1+P_1)}H_1H_4F_6^{11}Y_{11}^{13}(R_3)$$
$$- H_5^2F_6^8Y_8^{10}(R_3) - H_5^2F_6^8Y_8^{10}(R_3) - H_2H_5F_6^{11}Y_{11}^{13}(R_3)$$
$$- \frac{(2+P_1)}{(1+P_1)}H_4H_5F_6^9Y_9^{11}(R_3) - H_2^2F_6^{14}Y_{14}^{16}(R_3) - \frac{(2+P_1)}{(1+P_1)}H_2H_4F_6^{12}Y_{12}^{14}(R_3)$$
$$- \frac{H_4^2}{(1+P_1)}F_6^{10}Y_{10}^{12}(R_3)\Big], \tag{37}$$

where

$$X_m^n(R_i) = 1 + 3R_iF_m^n + 3R_i^2F_m^{n+2} + R_i^3F_m^{n+4},$$
$$Y_m^n = 1 + 7R_iF_m^n + 18R_i^2F_m^{n+2} + 22R_i^3F_m^{n+4} + 7R_i^4F_m^{n+5} + 3R_i^5F_m^{n+8},$$
$$H_1 = c\tau_B, \quad H_2 = D\tau_B, \quad H_3 = (b_5 + b_6)\tau_B, \quad H_4 = b_3\tau_B,$$
$$H_5 = a_1\tau_B, \quad P' = \frac{b_5}{b_6} \quad \text{and} \quad P_1 = \frac{b_3}{b_4}.$$

At low temperatures, the contribution of the three phonon umklapp process scattering relaxation rate is very small to the combined scattering relaxation rate and it can be ignored in the calculation of ΔK. Neglecting τ_U^{-1} as well as other lower terms, ΔK can be approximated to

$$\Delta K = 3c_1b_5\tau_B^2(Z_1 + Z_2)/(1 + a/2)v_sZ_3, \tag{38}$$

where

$$Z_1 = N_1 \left[N_1 - 2H_1F_5^8(1+\frac{qa^3}{2}F_8^9) - 2H_5F_5^6(1+\frac{qa^3}{2}F_6^7) - 2H_2F_5^9(1+\frac{qa^3}{2}F_9^{10}) \right.$$
$$\left. -2b_5\tau_B F_5^6(1+\frac{q^2a^3}{2}F_6^8) \right], \tag{39}$$

$$Z_2 = 6R_1F_5^7 \left[(1+\frac{qa^3}{2}F_5^6 + \frac{qa^3}{2}c'F_7^8 + \frac{q^2a^6}{2}c'F_7^8F_5^6) - H_1F_7^{10}\left\{1+F_{10}^7F_5^8 \right.\right.$$
$$+\frac{qa^3}{2}F_5^6(1+F_{10}^7F_6^9) + \frac{qa^3}{2}c'F_{10}^{11}(1+F_5^8F_{11}^8) + \frac{q^2a^6}{4}c'F_5^6F_{10}^{11}(1+F_6^8F_{11}^9)\Big\}$$
$$- H_5F_7^8\left\{1+F_8^7F_5^6 + \frac{qa^3}{2}F_5^6(1+F_8^7F_6^7) + \frac{qa^3}{2}c'F_8^9(1+F_5^6F_9^8)\right.$$
$$\left.+\frac{q^2a^6}{4}c'F_5^6F_8^9(1+F_6^7F_9^8)\right\} - H_2F_7^{11}\left\{1+F_{11}^7F_5^9 + \frac{qa^3}{2}F_5^6\right.$$
$$(1+F_{11}^7F_6^{10}) + \frac{qa^3}{2}c'F_{11}^{12}(1+F_5^9F_{12}^8) + \frac{q^2a^6}{4}c'F_5^6F_{11}^{12}(1+F_6^8F_{12}^{10})\Big\} - b_1\tau_BF_7^8$$
$$\left\{1+F_8^7F_5^6 + \frac{qa^3}{2}F_5^6(1+c') + \frac{q^2a^3}{2}F_5^7(1+c'F_7^5F_8^{10})\right.$$
$$\left.+\frac{q^2a^6}{4}c'F_5^8(1+F_8^6F_8^{10})\right\}\Big], \tag{40}$$

$$Z_3 = N_2 - b_5\tau_BF_5^6(1+\frac{q^2a^5}{2}F_6^8 + 7R_1F_5^7\left\{(1+\frac{qa^5}{2}c'F_7^8) - b_5\tau_BF_7^8\right.$$
$$\left.(1+\frac{q^2a^5}{2}c'F_8^{10})\right\}. \tag{41}$$

$N_1 = 1+\frac{qa^3}{2}F_5^6$, $N_2 = 1+\frac{qa^5}{2}F_5^6$, $c' = \frac{R_1}{R_3}$, $a = \frac{v_{T_1}}{v_{L_1}}$ and $q = \frac{b_3}{b_5}$. With the help of Eq. (15) and neglecting the dispersion of phonons, Eq. (38) reduces to

$$\Delta K = 960c_1b_5v_s^{-1}\tau_B^2[1-924c\tau_B - 13.3a_1\tau_B - 9072D\tau_B - 130.5b_5\tau_B]. \tag{42}$$

In the absence of the strain field dislocation, we get

$$\Delta K = 960c_1b_5v_s^{-1}\tau_B^2[1-924c\tau_B - 9072D\tau_B - 130.5b_5\tau_B]. \tag{43}$$

A similar expression was obtained by Awad [13] for a crystal having core dislocations. The expression for ΔK reduces to

$$\Delta K = 960c_1b_5v_s^{-1}\tau_B^2[1-9072D\tau_B - 130.5b_5\tau_B] \tag{44}$$

for a sample having perfect structure, which is similar as the one obtained by Dubey [11].

(B) $\tau_{sd}^{-1} \gg (\tau_B^{-1} + \tau_{cd}^{-1})$

The terms T_1, L_1, T_3 and L_3 can also be approximated as

$$T_1 = \frac{b_5 I_4}{a_1 v_{T_1}^3} \left[X_4^6(R_1) - G_1 F_4^3 X_3^5(R_1) - G_6 X_4^6(R_1) - G_3 F_4^7 X_7^9(R_1) - G_4 F_4^6 X_6^8(R_1)\right], \tag{45}$$

$$L_1 = \frac{b_3 I_5}{a_1 v_{L_1}^3} \left[X_5^7(R_3) - G_1 F_5^4 X_4^6(R_3) - G_3 F_5^8 X_8^{10}(R_3) - G_4 F_5^7 X_7^9(R_3) - G_5 F_5^6 X_6^8(R_3)\right], \tag{46}$$

$$\begin{aligned} T_3 = \frac{b_5 I_5}{v_{T_1}^5} \Bigg[& (1 - \frac{P'}{(1+P')} G_6 Y_5^7(R_1) - G_1^2 F_5^3 Y_3^5(R_1) - 2G_1 G_4 F_5^6 Y_6^8(R_1) \\ & - 2G_1 G_3 F_5^7 Y_7^9(R_1) - \frac{(2+P')}{(1+P')} G_1 G_6 F_5^4 Y_4^6(R_1) - G_4^2 F_5^9 Y_9^{11}(R_1) \\ & - 2G_3 G_4 F_5^{10} Y_{10}^{12}(R_1) - \frac{(2+P')}{(1+P')} G_6 G_4 F_5^7 Y_7^9(R_1) - G_3^2 F_5^{11} Y_{11}^{13}(R_1) \\ & - \frac{(2+P')}{(1+P')} G_6 G_3 F_5^8 Y_8^{10}(R_1) - \frac{G_6^2}{(1+P')} Y_5^7(R_1) \Bigg], \end{aligned} \tag{47}$$

$$\begin{aligned} L_3 = \frac{b_3 I_6}{v_{L_1}^5} \Bigg[& Y_6^8(R_3) - \frac{P_1}{(1+P_1)} G_5 F_6^7 Y_7^9(R_3) - G_1^2 F_6^4 Y_4^6(R_3) - 2G_1 G_4 F_6^7 Y_7^9(R_3) \\ & - 2G_1 G_3 F_6^8 Y_8^{10}(R_3) - \frac{(2+P_1)}{(1+P_1)} G_1 G_5 Y_6^8(R_3) - G_4^2 F_6^{10} Y_{10}^{12}(R_3) \\ & - 2G_3 G_4 F_6^{11} Y_{11}^{13}(R_3) - \frac{(2+P_1)}{(1+P_1)} G_4 G_5 F_6^9 Y_9^{11}(R_3) - G_3^2 F_6^{12} Y_{12}^{14}(R_3) \\ & - \frac{(2+P_1)}{(1+P_1)} G_3 G_5 F_6^{10} Y_{10}^{12}(R_3) - \frac{G_5^2}{(1+P_1)} F_6^8 Y_8^{10}(R_3) \Bigg], \end{aligned} \tag{48}$$

where $G_5 = (b_3 + b_4)/a_1$ and $G_6 = (b_5 + b_6)/a_1$. Neglecting the lower value terms, the expression for ΔK can be simplified as

$$\Delta K = \left[\frac{3c_1 b_5 I_4 F_5^4}{a_1^2 v_s (1 + a/2)}\right] \left[\frac{S_1 + S_2}{S_3}\right], \tag{49}$$

where

$$S_1 = N_3 \left[N_3 - 2G_1 F_4^3 (1 + \frac{qa^3}{2} F_3^4) - 2G_3 F_4^7 (1 + \frac{qa^3}{2} F_7^8) - 2G_4 F_4^6 (1 - \frac{qa^3}{2} F_6^7)\right.$$

$$-2G_7(1+\frac{q^2a^3}{2}F_4^6)\Big], \tag{50}$$

$$S_2 = 6R_1F_4^6\Big[1+\frac{qa^3}{2}F_4^5+\frac{qa^3}{2}c'F_6^7+\frac{q^2a^6}{4}c'F_4^5F_6^7-G_1F_5^6\{1+F_5^6F_4^3$$
$$+\frac{qa^3}{2}F_4^5(1+F_5^6F_5^4)+\frac{qa^3}{2}c'F_5^6(1+F_4^3F_6^7)+\frac{q^2a^6}{4}c'F_4^6(1+F_4^3F_6^7)\Big\}$$
$$-G_3F_6^9\{1+F_9^6F_4^7+\frac{qa^3}{2}F_4^5(1+F_9^6F_5^8)+\frac{qa^3}{2}c'F_9^{10}(1+F_4^7F_{10}^7)$$
$$+\frac{q^2a^6}{4}c'F_4^5F_9^{10}(1+F_5^8F_{10}^7)\Big\}-G_4F_6^8\Big\{1+F_8^6F_4^6+\frac{qa^3}{2}F_4^5(1+F_8^6F_5^7)$$
$$+\frac{qa^3}{2}c'F_8^9(1+F_4^6F_9^7)+\frac{q^2a^6}{4}c'\ F_4^5F_8^9(1+F_5^7F_9^7)\}-G_7\Big\{2+\frac{qa^3}{2}F_4^5$$
$$\cdot(1+c'F_5^4F_6^7)+\frac{q^2a^3}{2}F_4^6(1+c'F_6^4F_6^8)+\frac{q^2a^6}{4}c'F_4^7(1+F_7^5F_6^8)\Big\}\Big], \tag{51}$$

$$S_3 = N_2-G_6(1+\frac{q^2a^5}{2}F_5^7)+7R_1F_5^7\Big\{1+\frac{qa^5}{2}c'F_7^8-G_7(1+\frac{q^2a^5}{2}c'F_7^9)\Big\}, \tag{52}$$

$$N_3 = 1+\frac{qa^3}{2}F_4^5 \quad \text{and} \quad G_7 = b_5/a_1.$$

Neglecting the dispersion and with some mathematical manipulation, Eq. (49) can be expressed as

$$\Delta K = 31.86c_1b_5v_s^{-1}a_1^{-2}\left[1-0.45\tau_B^{-1}/a_1-76.7c/a_1-572.5D/a_1-3.42b_5/a_1\right]. \tag{53}$$

In the absence of core dislocations, ΔK will be:

$$\Delta K = 31.86c_1b_5v_s^{-1}a_1^{-2}\left[1-0.45\tau_B^{-1}/a_1-572.5D/a_1-3.42b_5/a_1\right]. \tag{54}$$

This is similar to an expression obtained by Saleh et al [16].

4. Discussion

In the frame of the Callaway integral as well as the generalized Callaway integral and assuming the additive nature of scattering relaxation rates, analytical expressions for the correction term are rederived for a lattice having dislocation for two different approximations. These expressions are very simple and easily computable in comparison with the complicated phenomenological expressions given by Callaway.

With the help of Eqs (16), (20), (42) and (53), it is obvious that the expression of ΔK is mainly governed by the three phonon normal scattering process. At the same time, with the help of Eqs (20) and (42), it is clear that for $\tau_B^{-1} \gg (\tau_{cd}^{-1} + \tau_{sd}^{-1})$, the correction term shows a $b_N \tau_B^2$ dependence. By examining Eqs (16) and (53) it can be seen that for $\tau_{sd}^{-1} \gg (\tau_B^{-1} + \tau_{cd}^{-1})$, $\Delta K \propto b_N / a_1^2$, which suggests that the correction term is mainly governed by the three phonon normal process and strain field dislocation scattering relaxation rate. These results obtained show similarity with the previous findings of earlier workers for the correction term [4–6, 11–13, 16].

References

1. J. Callaway, Phys. Rev., *113*, 1046, 1959.
2. V. V. Kosarev, P. V. Tamarin and S. S. Shalyt, Phys. Stat. Sol., (b)*44*, 525, 1971.
3. J. E. Parrot, Phys. Stat. Sol., (b)*48*, K159, 1971.
4. K. S. Dubey, Phys. Stat. Sol., (b)*63*, K35, 1974.
5. Y. P. Joshi, M. D. Tiwari and G. S. Verma, Physica, *47*, 231, 1970.
6. K. S. Dubey, Indian J. Pure and Appl. Phys., *11*, 265, 1973.
7. K. S. Dubey, J. de Physique, *37*, 267, 1976.
8. K. S. Dubey, Phys. Stat. Sol., (b)*81*, K83, 1977.
9. B. K. Agrawal and G. S. Verma, Phys. Rev., *128*, 603, 1962.
10. J. Callaway and M. C. V. Bayer, Phys. Rev., *120*, 1149, 1960.
11. K. S. Dubey, Solid State Commun., *23*, 963, 1977.
12. A. H. Awad, Acta Phys. Hung., *67*, 211, 1990.
13. A. H. Awad and J. S. Saif, Phys. Stat. Sol., (b)*151*, 495, 1989.
14. H. B. G. Casimir, Physica, *5*, 595, 1938.
15. P. G. Klemens, Solid State Physics, *7*, 1, 1958.
16. A. F. Saleh, R. H. Misho and K. S. Dubey, Acta Phys. Hung., *47*, 325, 1979.

Acta Physica Hungarica 72 (2-4), pp. 133–140 (1992)

PHONONS AND ELASTIC CONSTANTS FOR SCANDIUM, ZIRCONIUM AND MAGNESIUM

A. SINGH, R. P. S. RATHORE and R. M. AGRAWAL*

Department of Physics, R. B. S. College
Agra-2, India
* *Department of Physics, D. E. I. (Deemed University)*
Dayalbagh, Agra-5, India

(Received 5 May 1992)

The generalised exponential potential and the Born–Mayer potential are employed to describe the paired and the unpaired interactions in the hexagonally closed pack (hcp) metals. These forces are found to explain simultaneously the phonon dispersion and the elastic behaviours of the metals like Scandium (Sc), Zirconium (Zr) and Magnesium (Mg). The input data for lattice constants inverse compressibility and cohesive energy give rise to such results on the said behaviour of the metals which compare satisfactorily with the experimental values.

1. Introduction

Various phenomena such as electron density dependence [1] of the central pairwise forces, charge transfer [2] mechanism during lattice excitations, multiple scattering [3] of electrons by ions, the existence of Cauchy's discrepancy in elastic constants of various orders, the disagreement of experimental findings from Warren [4] sum rule and the substantial concentration [5] of electrons along the bonding directions suggest the important role played by unpaired forces in determining the various properties of the hexagonally closed pack (hcp) metals. The third order perturbative studies [6–8] dealing with these forces held out clearly the message of enormous computational efforts, cost and time and suggest the real space analysis of these forces. For the correct ordering of dispersion mode, the dynamical matrix element $[D_{12}(q, 11)]$ should not vanish. This constraint is violated by the Keating's forces [9] which are used [10] to explain the behaviour of the unpaired forces. The studies due to Sharma and Sinha [11] also suffer with the deficiency of using a large number of parameters possessing the least bearings on the physical nature of the forces.

The pseudopotential studies [12] invariably involve the attractive pairwise forces to explore the lattice dynamical behaviour of the hcp metals. The phenomenological models [13] employ a large number of input data to evaluate the parameters. These studies either ignore the consideration of lattice stability or observe it extraneously.

We have developed a model, which accounts for the paired forces through a generalised potential [14] comprising the attractive as well as the repulsive interactions. The exponent to this potential modifies the potential for the exchange and correlation effects of the electrons. The unpaired interactions are expressed through the Born–Mayer potential [15]. The procedure adopted to evaluate the defining parameters incorporates the basic criterion of the lattice equilibrium. These interactions, requiring only four input data for their definition, are deployed to predict simultaneously the phonon energy and the elastic constants of various orders in the hcp metals scandium (Sc), zirconium (Zr) and magnesium (Mg). It is credible to note that the theory based on the present lines has displayed its efficacy in explaining the elastic and lattice dynamical behaviour of cubic metals [16–20]. The present investigation therefore, rightly attempts to explore the prospect of a unified theory, which could rope in the said behaviours of hcp metals, too.

2. Formulation and computations — the paired potential

The generalised form of the exponential potential [14] comprising the attractive and the repulsive components finds the form

$$\Phi^2(r_j) = D[2(m-1)]^{-1} \sum_j [\beta^m \exp(-m\alpha r_j) - m\beta \exp(-\alpha r_j)], \tag{1}$$

where

$$\beta = \exp(\alpha r_0), \tag{2}$$

and α, D and r_0 are the defining parameters of the potential. This pairwise potential extends to seven nearest neighbours of the hcp metals and requires the input data of the lattice constants, the inverse compressibility and the cohesive energy for its complete definition. Table I shows the input data along with the computed defining parameters for the said metals.

2.1. The unpaired potential

The Born–Mayer potential [15], i.e.

$$\Phi^3(R) = -b \exp(-\frac{\mathbf{R} \cdot \hat{n}}{\varrho}) \tag{3}$$

is employed to couple the atoms lying in the meridian plane of the hcp metals. The parameters b and ϱ of the potential are evaluated by the knowledge of the total volume and the Cauchy's discrepancy in the second order elastic constants.

Table I
Input data and computed defining parameters for Sc, Zr and Mg

Metals	Input data	Computed defining parameters
Sc	$C = 5.27 \times 10^{-10}$ m	$\alpha = 0.3574 \times 10^{10}$ m^{-1}
	$a = 3.31 \times 10^{-10}$ m	$r_0 = 4.9045 \times 10^{-10}$ m
	$K = 0.435 \times 10^{11}$ N/m^2	$D = 2.7796 \times 10^{-20}$ J
	$B = 6.2478 \times 10^{-19}$ J	
Zr	$C = 5.15 \times 10^{-10}$ m	$\alpha = 0.3845 \times 10^{10}$ m^{-1}
	$a = 3.23 \times 10^{-10}$ m	$r_0 = 4.7539 \times 10^{-10}$ m
	$K = 0.833 \times 10^{11}$ N/m^2	$D = 4.5105 \times 10^{-20}$ J
	$B = 10.0125 \times 10^{-19}$ J	
Mg	$C = 5.21 \times 10^{-10}$ m	$\alpha = 0.4898 \times 10^{10}$ m^{-1}
	$a = 3.21 \times 10^{-10}$ m	$r_0 = 4.6084 \times 10^{-10}$ m
	$K = 0.354 \times 10^{12}$ N/m^2	$D = 1.196 \times 10^{-20}$ J
	$B = 2.416 \times 10^{-19}$ J	

2.2. The lattice equilibrium and the phonon dispersion

For the sustenance of lattice stability the first derivatives of both potentials (Eqs 1 and 3) are made to vanish simultaneously. The second derivatives β_1, β_2, β_3, β_4, β_5, β_6 and β_7 of the paired potential and γ of the unpaired potential (Table II) are fed to the usual secular determinant to obtain the phonon dispersion along the directions [0001] and [01$\bar{1}$0], which are shown in Figs 1, 2 and 3 for Sc, Zr and Mg, respectively. The details for arriving at the elements of the dynamical matrix and subsequently the phonon frequencies are taken from our earlier study [21]. The experimental findings due to Wakabayashi et al [22], Bezdek et al [23] and Kohn and Sham [24] are represented by the markings ($\triangle, \bigcirc, \square, \blacktriangle, \bullet, \blacksquare,$).

Table II
Computed force constants for Sc, Zr and Mg

Force constants N/m	Sc	Zr	Mg
β_1	3.028	6.177	4.036
β_2	2.889	5.987	3.962
β_3	0.845	1.626	0.755
β_4	0.427	0.782	0.245
β_5	0.243	0.431	0.110
β_6	0.233	0.411	0.107
β_7	0.099	0.154	−0.015
γ	56.300	49.139	30.290

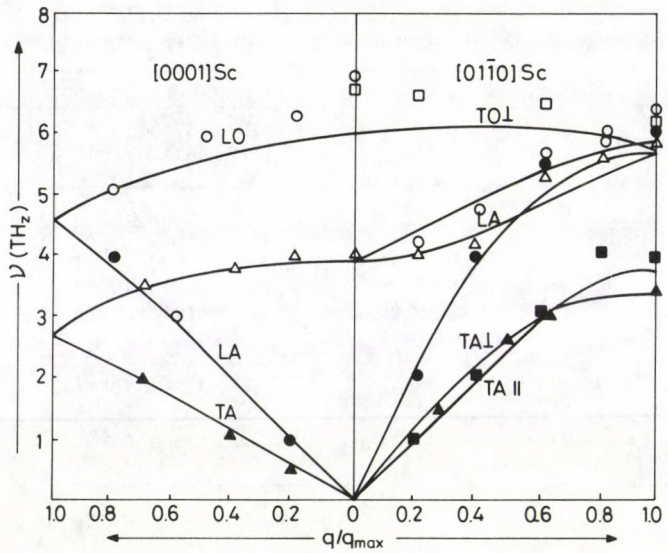

Fig. 1. Dispersion relation for Sc along the directions [0001] and [01$\bar{1}$0]. (△, ○, □, ▲, •, ■) represent the experimental findings due to Wakabayashi et al [22], Bezdek et al [23] and Kohn and Sham [24]

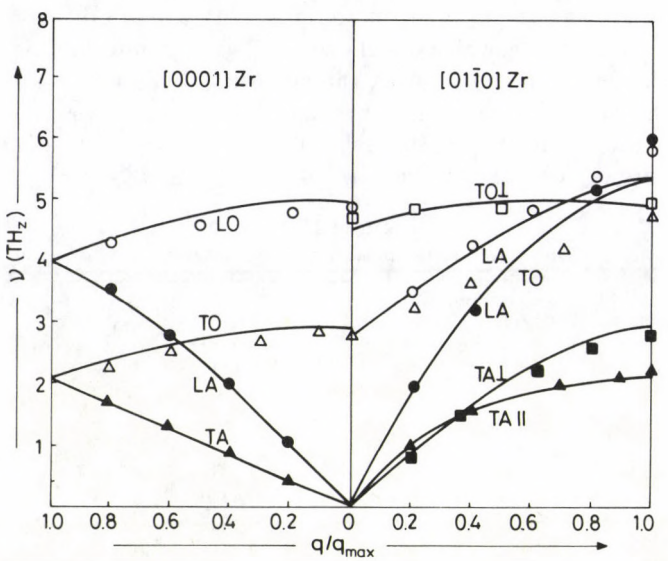

Fig. 2. Dispersion relation for Zr along the directions [0001] and [01$\bar{1}$0]. For markings see the caption of Fig. 1

2.3. The elastic constants

The second, third and the fourth derivative of the paired energy density with respect to infinitesimal strain tensors are determined to predict the second, third and fourth order elastic constants in the metals under investigation. The method given by Naiman et al [25] is followed to compute the TOEC and FOEC of the hcp metals. The computed values along with the available observed data and data revealed by other available theoretical studies for the metals are listed in Table III.

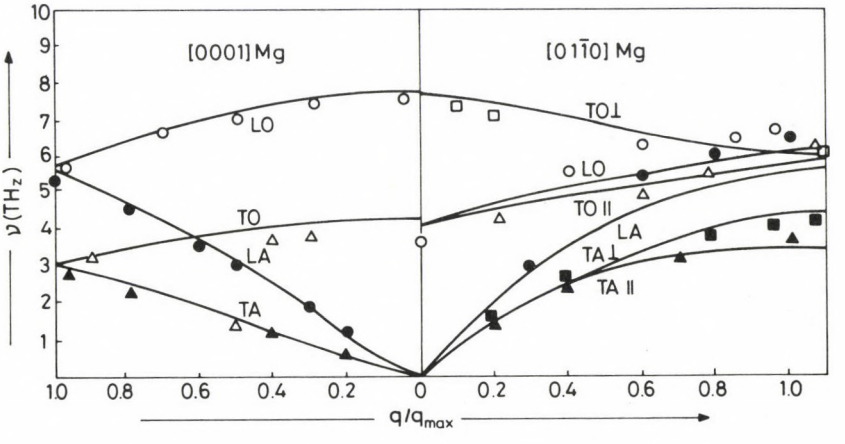

Fig. 3. Dispersion relation for Mg along the directions [0001] and [01$\bar{1}$0]. For markings see the caption of Fig. 1

3. Conclusion

The present study reveals that the good agreement with the measured data in respect of the phonon dispersion in Sc, Zr and Mg is attained by putting $m = 1.1$. The relative standard errors creeping into the dispersion calculations of Sc, Zr and Mg amount to 0.301, 0.129 and 0.213, respectively. The computed predictions of second order elastic constants show good qualitative agreement with those computed by the other investigators [29–31]. Our predictions for these constants fairly agree with the measured data [26–28] also. The computed results on third order elastic constants for Mg follow the trend revealed by the experimental values [32]. These results show good agreement with those computed by other workers [30, 33, 34]. The fourth order elastic constant revealed by the present study could not be compared because of the lack of similar data.

Table III

Computed elastic constants for Sc, Zr and Mg (10^{11} N/m^2)

Elastic constants	Computed values of present study			Measured values			Computed values of other studies		
	Sc	Zr	Mg	Sc	Zr	Mg	Sc	Zr	Mg
1	2	3	4	5	6	7	8	9	10
C_{11}	0.919	1.422	0.669	0.993	1.43	0.5918	0.993	1.43	0.624
C_{12}	0.479	0.711	0.283	0.457	0.73	0.2568	0.457	0.73	0.235
C_{13}	0.277	0.341	0.204	0.294	0.658	–	0.294	0.659	0.217
C_{33}	0.7498	1.59	0.581	1.069	1.65	0.6147	0.865	1.790	0.634
C_{44}	0.277	0.341	0.204	0.277	0.32	0.1634	0.310	0.317	0.160
C_{66}	0.479	0.711	0.283	0.268	0.352	0.1675	0.268	0.352	–
				Ref. [19]	Ref. [20]	Ref. [21]	Ref. [22]	Ref. [23]	Ref. [24]
C_{111}	−7.430	−7.674	−6.198	–	–	−6.63	−8.96	−9.37	−6.43
C_{112}	−3.89	−6.97	−1.63	–	–	−1.78	−3.15	−7.90	−1.79
C_{113}	−0.320	−0.959	0.328	–	–	0.30	−0.45	−0.93	−0.63
C_{123}	−0.526	0.372	−0.448	–	–	−0.76	−0.72	0.26	−0.47
C_{133}	−0.261	−2.706	−0.806	–	–	−0.86	−2.35	−2.13	−1.71
C_{222}	−13.69	−14.50	−7.041	–	–	−8.64	−10.95	−14.70	−7.37
C_{333}	−12.26	−21.54	−6.017	–	–	−7.26	9.40	−20.05	−6.32
C_{334}	−2.41	−2.706	−1.870	–	–	−1.93	−2.35	−2.13	−1.71
C_{144}	−0.526	0.372	0.448	–	–	0.30	−0.59	−1.54	−0.45
C_{155}	−2.61	−2.706	−0.806	–	–	−0.58	−0.59	0.95	−0.65
						Ref. [25]	Ref. [26]	Ref. [23]	Ref. [27]
C_{1111}	298.183	379.946	182.379	–	–	–	–	–	–
C_{1112}	43.378	48.175	21.351	–	–	–	–	–	–
C_{1113}	15.213	19.213	8.263	–	–	–	–	–	–
C_{1122}	25.573	31.679	14.456	–	–	–	–	–	–
C_{1123}	3.244	4.064	1.810	–	–	–	–	–	–
C_{1133}	3.249	4.354	2.021	–	–	–	–	–	–
C_{4455}	0.720	2.236	0.898	–	–	–	–	–	–
C_{1222}	42.151	57.839	28.189	–	–	–	–	–	–
C_{1244}	2.908	3.695	1.547	–	–	–	–	–	–
C_{1333}	1.124	4.309	1.786	–	–	–	–	–	–
C_{2222}	291.235	351.017	163.328	–	–	–	–	–	–
C_{3333}	4.105	10.492	6.781	–	–	–	–	–	–
C_{4444}	11.725	17.163	7.688	–	–	–	–	–	–

The computations lead to the following Cauchy relations in various orders of elastic constants.

$$C_{12} = C_{66}, \quad C_{13} = C_{14}, \tag{4}$$

$$C_{123} = C_{144}, \quad C_{133} = C_{155}, \tag{5}$$

$$C_{1222} = C_{1155}, \quad C_{1255} = C_{1266} = C_{6666} = C_{1122},$$
$$C_{1133} = C_{5555} = C_{1233}. \tag{6}$$

It may be concluded that the present theory beside being fairly successful in explaining the phonon dispersion and elastic constants of the hcp metals (Sc, Zr, Mg) establishes the credential of a unified theory for the cubic and hcp metals both.

References

1. S. H. Taole and H. R. Glyde, Can. J. Phys., *57*, 1870, 1979.
2. S. O. Lundqvist, Ark. Fys., *9*, 435, 1955; *12*, 263, 1957.
3. G. Gilat, C. Rizzi and G. G. Cubiotti, Phys. Rev., *185*, 971, 1969.
4. J. L. Warren, Rev. Mod. Phys., *40*, 38, 1968.
5. G. H. Wannier, C. Misner and G. Shay, Jr., Phys. Rev., *185*, 983, 1965.
6. E. G. Brovman, Yu. Kagan and A. Kholas, Sov. Phys. Solid State, *11*, 733, 1969; JETP, *30*, 394, 1972.
7. C. M. Bertoni, O. Bisi, C. Calandra and F. Nizzoli, J. Phys. *F-5*, 419, 1975; *F-4*, 19, 1974.
8. P. Lloyd and C. A. Sholl, J. Phys. *C-1*, 1620, 1968.
9. P. N. Keating, Phys. Rev., *145*, 637, 1966; *149*, 674, 1968.
10. R. Ramji Rao and R. Srinivasan, Phys. Stat. Solidi, *29*, 865, 1968.
    R. Ramji Rao and S. Ramanand, Acta Cryst., *A23*, 146, 1977; J. Phys. Chem. Solids, *38*, 831, 1977; J. Low Temp. Phys., *27*, 837, 1977;
    R. Srinivasan and R. Ramji Rao, J. Phys. Chem. Solids, *32*, 1761, 1969.
    C. S. Menon and R. Ramji Rao, J. Phys. Chem. Solids, *33*, 2129, 1972.
11. A. K. Sharma and H. P. Sinha, Ind. J. Pure and Appld. Phys., *19*, 526, 1981; Ind. J. Theor. Phys., *28*, 57, 1980.
12. A. P. Roy and G. Venkateraman, Phys. Rev., *156*, 769, 1967.
    R. W. Shaw, Jr., Phys. Rev., *174*, 769, 1968.
    M. F. King and P. H. Cutler, Phys. Rev. *B-2*, 1733, 1964; J. Phys. Chem. Solids, *32*, 761, 1971.
    B. A. Oli, J. Phys. *F-4*, 2007, 1981.
    M. V. H. Ambikaprasad, H. C. Gupta and B. B. Tripathi, Can. J. Phys., *62*, 845, 1984.
    J. C. Upadhyaya, Phys. Rev., *26*, 743, 1982.
13. J. C. Upadhyaya and M. P. Verma, Phys. Rev., *B-8*, 593, 1974.
    D. B. Vibhute and M. P. Verma, Phys. Rev., *B12*, 4302, 1975.
    J. C. Upadhyaya and H. P. Sinha, J. Phys. Chem. Solids, *36*, 975, 1975.
    S. P. Singh and S. S. Kushwaha, Nuovo Cimento, *D-5*, 365, 1985.
14. F. Milstein, J. Appld. Phys., *44*, 3825, 1973.
15. M. Born and J. E. Mayer, Z. Phys., *75*, 1, 1932.
16. R. M. Agrawal, Km. Amita and R. P. S. Rathore, Ind. J. Pure and Appld. Phys., *29*, 741, 1991.
17. M. K. Mishra and R. P. S. Rathore, Acta Physica Pol., *A-75*, 525, 1989.
18. R. M. Agrawal, Km. Aradhana and R. P. S. Rathore, Ind. J. Pure and Appld. Phys., *29*, 517, 1991.

19. Km. Aradhana and R. P. S. Rathore, Phys. Stat. Solidi (b), *156*, 77, 1989.
20. Km. Aradhana and R. P. S. Rathore, Czech. J. Phys., *B-40*, 689, 1990.
21. R. P. S. Rathore, A. Singh and R. M. Agrawal, Phys. Stat. Solidi (b), *165*, 95, 1991.
22. N. Wakabayashi, R. H. Schern and H. G. Smith, Phys. Rev., *B-25*, 5122, 1982.
23. H. F. Bezdek, R. E. Schumunk and L. Fine Gold, Phys. Stat. Solidi (b), *42*, 275, 1970.
24. W. Kohn and L. J. Sham, Phys. Rev., *B-140*, 133, 1970.
25. E. R. Naiman, T. Suzuki and A. V. Granto, Phys. Rev., *B-4*, 4297, 1971.
26. E. S. Fisher and O. Dever, Proc. 7th Rare Earth Res., Conf. *1*, 237, 1968.
27. E. S. Fisher, M. H. Manghanana and T. J. Sokolowski, J. Appld. Phys., *41*, 2991, 1970.
28. H. B. Huntington, Solid State Phys., *7*, 132, 1958.
29. R. Ramji Rao and C. S. Menon, Solid State Comm., *12*, 527, 1973.
30. C. S. Menon and R. Ramji Rao, J. Phys. Chem. Solids, *33*, 1325, 1972.
31. B. Dutta, S. K. Sarkar and D. Roy, Phys. Stat. Solidi (b), *132*, 345, 1985.
32. E. R. Naiman, Phys. Rev., *B-4*, 4291, 1971.
33. R. Ramji Rao and A. Ramanand, Phys. Stat. Solidi (b), *87*, 751, 1978.
34. R. Srinivasan and R. Ramji Rao, J. Phys. Chem. Solids, *32*, 1769, 1971.

Acta Physica Hungarica 72 (2-4), pp. 141–145 (1992)

NEW PIEZO-MIRROR TRANSLATOR FOR FREQUENCY STABILISATION OF LASER OSCILLATORS

H. EL-KASHEF and G. E. HASSAN

Physics Department, Faculty of Science, Tanta University
Tanta, Egypt

(Received in revised form 19 May 1992)

For frequency stabilisation and tuning of active and passive laser oscillators, a new construction of piezo-mirror translator has been developed. It has compact size, high mechanical stability, high voltage tensile strength, high adjustable speed and low cost. If it is driven by an appropriate control electronics, it allows to suppress efficiently the frequency changes of laser cavities.

Introduction

The frequency stability of lasers depends upon the stability of the optical length of resonators. Firstly, the geometrical length L of resonators can be changed by different causes which are practically present due to changes in the ambient conditions around the laser resonators. Examples are: the mechanical vibrations, the change of the refractive index of air in the resonators with temperature, air pressure fluctuations, turbulences and acoustic waves. These changes lead to frequency fluctuation in the range of a few 10 MHz. Secondly, the frequency changes due to changes of the optical characteristics of the active medium in active resonators. Examples are: in dye lasers the refractive index of the dye stream depends on its temperature which changes due to the absorption of a part of pumping laser power and the power running in the dye laser resonator. This causes variation of the refractive index with time, i.e. stable surface and thickness of dye stream do not exist. On the other hand, small dirt particles and air bubbles which pass through the focus will change the thickness and refractive index of dye stream for a short time. This affects directly the laser frequency. For improving the frequency stability of the laser resonator, the deviation of laser frequency from the desired frequency must be regulated through changing the optical length $n \cdot L$ of the resonator ($n =$ refractive index of the medium in the resonator). The regulation system must be placed so that the frequency changes are controlled. For changing the geometrical length, there exist different methods which depend on mechanical or electrical operations. The mechanical changes can be achieved by using Brewster plate on micrometer displacement table or galvokipper. The electrical one often uses piezoceramic elements. The latter method has the advantage that changes with relative high frequencies up to 1 MHz are achieved [1, 2]. Most of the commercial products of lasers and other optical elements such as air-spaced etalons, spectrum analysers

(Fabry–Perot interferometers) and others, use a piezo driver for frequency tuning and stabilisation [3, 4 and others]. This paper reports about a new construction of a compact and low cost piezo-ceramic mirror translator used efficiently for axial drive applications.

Practical construction

The mirror translator works according to the phenomena of piezo-ceramic material "piezoelectricity". When voltage is applied to such crystalline material a proportional deflection will result. The direction of both electrical and mechanical axes depends on the direction of the original d. c. voltages applied to the electrodes of the piezo element.

For an optical resonator with fixed mirror spacing, i.e. discrete resonance frequencies, it is necessary for the resonance frequency to be tuned through changing the mirror spacing. According to the practical need of the optical resonator, it must be calculated how many free spectral ranges (FSR) are necessary for the tuning process, i.e. how long the piezo translator is. The active length (6 mm in Fig. 1a) of the present translator is selected to be used for frequency tuning and stabilisation of the Mach–Zehnder interferometer [5] and 2 GHz spectrum analyzer [6]. For changing the resonance frequency about 1 FSR = 2 GHz, the necessary change of length is calculated as follows:

$$\Delta L = \lambda/2 = 0.6/2 = 0.3\,\mu\text{m}, \quad \lambda = 600\,\text{nm},$$

i.e. a piezo change of length of about 1.05 μm = 3.5 FSR is required. This change can be achieved by applying a voltage of about 500 V on the piezo. The dimensions of the plates can be estimated using the formula [7]: $L = \Delta L \cdot d/v \cdot C$, where ΔL is the change of length, C is the piezo material constant, L the active length of the piezo plate, d the thickness of the piezo plate and v the applied voltage.

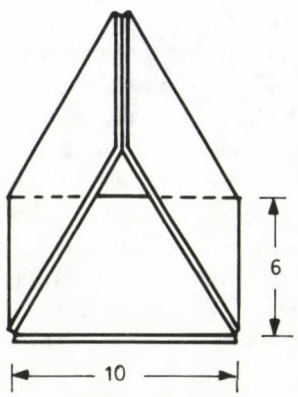

Fig. 1a. Triangle tube piezo driver

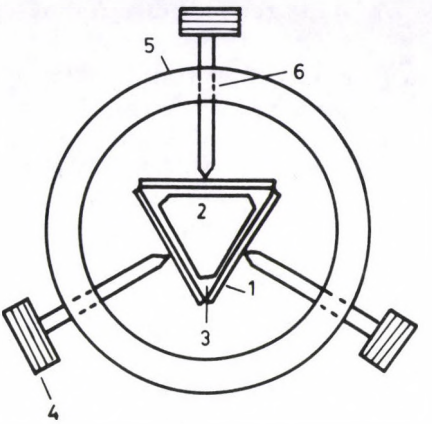

Fig. 1b. Model for construction. 1 – piezo plate, 2 – middle guide block, 3 – air space, 4 – screw, 5 – adjusting vessel, 6 – thread-in vessel

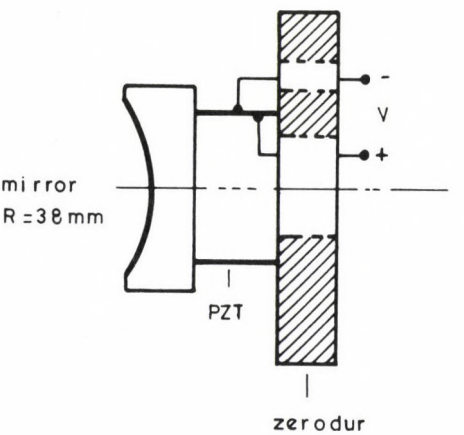

Fig. 1c. Piezo-mirror head

The mirror translator is made from piezo material type PXE-5 from Firma Valvo, Germany. Piezo rectangular plates of dimensions $12 \times 6 \times 0.3$ mm are used. The length of 12 mm is shortened using laboratory cutting and polishing method to 10 mm to be suitable for the use in [5, 6] and constructed to make a triangle tube as in Fig. 1a. Using the plastic model as shown in Fig. 1b, the plates are fixed together by epoxy material [8]. The fixing must be regular which requires high skill. The inner and outer wall surfaces are connected together using conductive epoxy. The testing process for the piezo-translator is achieved by connecting two fine isolated wires to the positive and negative electrodes and used as voltage driving cables. Fig. 1c shows the piezo mirror head used in [5, 6].

Advantages and discussion

This type of piezo PXE-5 changes relatively highly in length where $C = -175 \times 10^{-12}$ m/v. These plates have a thickness of 0.3 mm. This means that the piezo sensitivity is high (for an active length of 6 mm, the sensitivity is 3.5 μm/kv). The nonlinearity of piezo expansion at high voltage can be avoided and the translator can efficiently be used in the linear range using voltages up to 500 V. The electrical sensitivity $\Delta v/\Delta\nu = 0.071$ V/MHz.

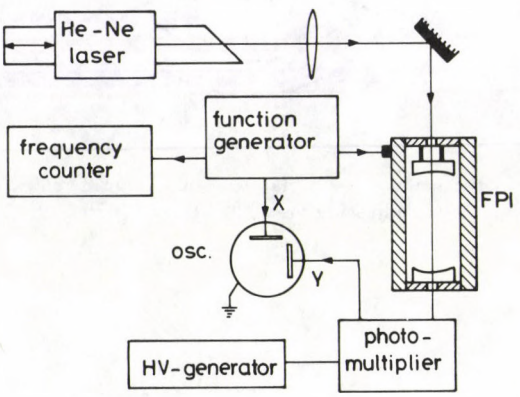

Fig. 2. Measuring system of the response characteristics

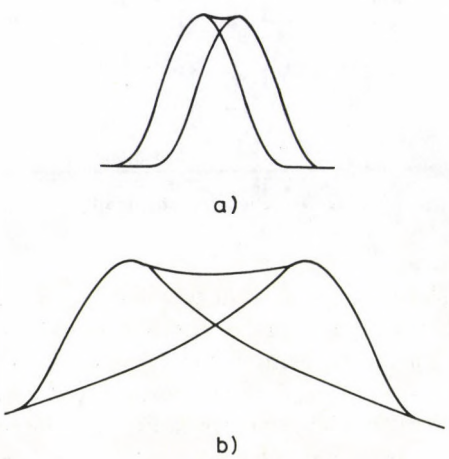

Fig. 3. Oscilloscope photo a) by frequency tuning;
b) at the resonance positions

The first test during the construction of the piezo triangle tube against high voltage must be measured using an ohm-meter, the resistance showed infinity by the 20 MΩ range. This guarantees that no current flow between the poles as a result of construction leaks. The second test is made by using a regulated limited current high voltage generator. A resistance of 1 MΩ and 0.25 W is used for insurance and current limiting. A micro-ampere meter (μA-meter) can be used for observing small current flows by applying high voltage up to 1000 volts on the piezo. By good constructive isolation the μA-meter showed no current flow.

Figure 2 shows the measuring system for the response characteristics of the mirror translator. The free running He–Ne laser beam is computerized mode matched [9] to be incident on the spherical mirror spectrum analyser. One can observe the resonance of the analyser on the oscilloscope separated by a distance of 2 GHz. An a.c. voltage of ca 20 V with the desired frequency is taken from the function generator in order to be applied on the piezo translator. By slightly tuning the frequency we observe Fig. 3a on the oscilloscope. The expansion of this motion is a measure for the amplitude of the mirror translator as a function of the frequency of the applied voltage. At the resonance positions, the mirror translator shows qualitative circa Fig. 3b on the oscilloscope. The results showed that the first and second main resonances lie by 13 and 39 KHz, respectively. In comparison with other earlier standard piezo transducers, the present translator has the following characteristics: (i) with the used thickness (= 0.3 mm), the desired change of the mirror separations of the interferometer is accomplished by the available high voltage apparatus. (ii) It can be made in compact and different forms and sizes according to the required number of the FSR and of low cost. (iii) It is stable and can be used efficiently in all high precision laser frequency control, tuning and many other axial drive applications. This construction of mirror translator is used efficiently for frequency selection and tuning of a new construction of Mach–Zehnder interferometer [5] and spectrum analyser [6]. If a piezo driver (high electrical sensitivity) is needed from this type, the transversal mechanical vibrations can drastically be reduced by tungsten filled rubber which is epoxied to it to be used as an absorber for ultrasonic test equipment.

References

1. W. Jitschin and G. Meisel, Appl. Phys., *19*, 181, 1979.
2. W. Lackner, Thesis, University of Bonn, 1982.
3. Instruction and Service Manual, copyright Jodon Engineering Associates, Inc., Michigan, 1971.
4. Spectra Physics, Model 380D, Frequency Stabilized Ring Dye Laser, Instruction Manual.
5. H. El-Kashef and G. E. Hassan, J. Mod. Opt., *39*, 43, 1992.
6. H. El-Kashef, accepted in Acta Physica Slovaca, 1992.
7. J. Koch, Piezooxide Wandler (Grundlagen, Anwendungen und Schaltungen), Valvo GmbH Hamburg, Germany, 1973.
8. W. Mai and K. J. Müller, Versuchsprotokoll, Klebemittel/Adhäsion, Bonn University, 1981.
9. H. El-Kashef and G. E. Hassan, Bulg. J. Phys. *18*, No. 4, 1991.

Acta Physica Hungarica 72 (2-4), pp. 147–159 (1992)

INFLUENCE OF CROSS-FIELD CONFIGURATION ON THE EINSTEIN RELATION IN QUANTUM WIRES OF TETRAGONAL SEMICONDUCTORS

K. P. GHATAK

Department of Electronics and Telecommunication Engineering
Faculty of Engineering and Technology, Jadavpur University
Calcutta 700032, India

(Received in revised form 9 June 1992)

An attempt is made to study the Einstein relation for the diffusivity–mobility ratio of the electrons in quantum wires of tetragonal semiconductors in the presence of crossed electric and magnetic fields on the basis of a newly derived electron energy spectrum considering all types of anisotropies in the band parameters. It is found taking n-Cd_3As_2 as an example that the same ratio increases with electron concentration in an oscillatory way. Besides, it decreases with increasing thickness and the crystal field splitting influences significantly the ratio in the whole range of the variables considered. We have also suggested an experimental method of determining the Einstein relation in degenerate materials having arbitrary dispersion laws. The results for quantum wires of parabolic semiconductors have been also obtained from our generalized expressions in the absence of cross-field configuration under certain limiting conditions.

1. Introduction

With the advent of fine lithographical methods [1], molecular beam epitaxy [2], organometallic vapor-phase epitaxy [3] and other experimental techniques, low-dimensional structures [4] having quantum-confinement in two and three dimensions such as quantum-well wires and quantum-well boxes have in the last few years attracted much attention not only for their potential in uncovering new phenomena in solid state science but also for their interesting device applications [5]. Extremely high mobility in quantum wires [6], high performance of quantum wire lasers [7] and modulators [8] have been realised. In quantum wires, the electron gas is quantized in two transverse directions and the charge carriers are free to move only in the longitudinal direction [9].

The potential use of the quantum well wires (hereafter referred to as QWW) for high speed devices under different physical conditions makes the knowledge of their appropriate band structure desirable. It appears from the literature that the Einstein relation for the diffusivity-to-mobility ratio of the electrons in QWW's in the presence of crossed electric and magnetic fields has yet to be investigated even for parabolic energy bands. We wish to note in this context that the investigations of electrons in semiconducting materials in the presence of crossed electric and magnetic fields offer interesting physical possibilities, both experimental and theoretical [10]. The cross-field configuration is fundamental for studying the classical

and quantum transport phenomena in degenerate materials [10]. Optical investigations of bulk semiconductors began with the theoretical work of Hansel and Peter [11], who indicated that an influence of electric field on the Landau levels should lead to observable effects in cyclotron resonance transition in solids [11]. Aronov [12] pointed out that the electric field effects should be visible in the interband magneto-optical transitions. It is observed that [13] the low values of E_0/B (E_0 is the electric field along x axis and B is the magnetic field along z axis) leads to oscillatory effects whereas at large values of the E_0/B ratio one deals with the non-oscillatory effects and we essentially arrive at the Keldysh–Franz effect in a quantizing magnetic field. In degenerate materials, the creation of a large electric field is not possible and hence the E_0/B ratio is small [14]. It appears that the non-parabolic semiconductors are degenerate [14]. We have used tetragonal semiconductors which are being extensively investigated as non-linear optical materials [15] and light emitting diodes [16]. In the present communication we shall study the diffusivity–mobility ratio in QWW of tetragonal semiconductors under cross-field configuration.

It is well known that the diffusivity–mobility ratio is a very useful relation since this is more accurate than any of the individual expressions for the diffusivity or the mobility, which are considered to be the two most widely used parameters of carrier transport in solid state devices. The performance of the devices at the device terminals and the speed of operation of modern switching semiconductor devices are significantly influenced by the degree of carrier degeneracy present in these devices [17, 18]. The simplest method of analysing the compound semiconductor devices taking into account the degeneracy of the bands is to use the Einstein relation to express the performance at the device terminals and the switching speed in terms of carrier concentration. In recent years, the connection of the Einstein relation with the velocity auto correlation function [19], its relation with the screening length [20] and the different modifications of the diffusivity–mobility ratio (hereafter referred to as DMR) under various physical conditions have extensively been investigated [21–30]. It appears from the literature that the DMR in QWW of even parabolic semiconductors under cross electric and magnetic fields has yet to be derived.

As stated above, we have used the tetragonal semiconductors, having non-parabolic and non-standard energy bands, as an example of small-gap semiconductors. We shall work out the problem for the more interesting case which occurs from the presence of various types of anisotropies in the energy spectrum. This will make our analysis a generalized one since we can obtain the DMR in QWW's of even parabolic semiconductors in the absence of cross-field configuration. Rowe and Shay [31] have demonstrated that the quasicubic model [32] can be used to explain the observed splitting and symmetry properties of the conduction and valence bands at the zone centre of tetragonal semiconductors. The s-like conduction band is single degenerate and p-like valence bands are triply degenerate. The latter splits into 3 subbands because of spin–orbit and crystal field interactions. The largest contribution to the crystal field splitting of the valence band occurs from the non-cubic potential [33]. The experimental results have produced strong evidence that the conduction band in the same semiconductor corresponds to a single ellipsoid

of revolution at the zone centre in **k** space. Incorporating the anisotropic crystal potential to the Hamiltonian, Kildal [34, 35] proposed an $E - \mathbf{k}$ dispersion relation for the conduction electrons in the same semiconductors based on the assumptions of isotropic spin–orbit splitting parameters of the valence band and isotropic inter-band momentum-matrix elements, respectively, though the anisotropies in the two aforementioned band parameters are significant physical features of tetragonal semiconductors [36].

In what follows, in Section 2.1 we shall derive the DMR in QWW of tetragonal materials under cross-field configuration by using the generalized dispersion relation of the conduction electrons incorporating the above mentioned anisotropies as derived elsewhere [37]. In Section 2.2 we shall derive the limiting cases of the three-band Kane model, the two-band Kane model and that of parabolic energy bands in QWW's in the absence of electric field and magnetic field. In Section 2.3 we shall suggest an experimental method of determining the Einstein relation in degenerate semiconductors having arbitrary dispersion relation. We shall study the concentration and thickness dependence of the DMR in quantum well wires of tetragonal semiconductors in the present case field taking n-Cd_3As_2 as an example which finds extensive applications in Hall pick-ups and thermal detectors.

2. Theoretical background

2.1. Formulation of DMR in QWW of tetragonal semiconductors in the presence of crossed electric and magnetic field

The generalized dispersion relation of the conduction electrons, incorporating the aforementioned anisotropies of the band parameters, in bulk specimens of tetragonal semiconductors can be expressed [37] as

$$p_s^2/2M_\perp + p_z^2 V(E)/2M_\parallel = U(E), \tag{1}$$

where $\mathbf{p}_s = \hbar\mathbf{k}_s$, $\hbar = h/2\pi$, h is the Planck's constant, $k_s^2 \equiv k_x^2 + k_y^2$, $M_{\parallel,\perp} \equiv m^*_{\parallel,\perp}(E_g + \frac{2}{3}\Delta_{\parallel,\perp})\cdot(E_g + \Delta_{\parallel,\perp})^{-1}$, $m^*_\parallel$ is the longitudinal effective mass at the edge of the conduction band along k_z axis, $m^*_\perp$ is the transverse effective mass at the edge of the conduction band in the k_xk_y plane, E_g is the band gap, $\Delta_\parallel$ is the spin–orbit splitting parameter along the C-axis, $\Delta_\perp$ is the spin–orbit splitting parameter in a plane perpendicular to the C-axis,

$$V(E) \equiv \frac{[(E+E_g)(E+E_g+\frac{2}{3}\Delta_\parallel)]}{[(E+E_g)(E+E_g+\frac{2}{3}\Delta_\parallel)+\delta(E+E_g+\frac{1}{3}\Delta_\parallel)+\frac{1}{9}(\Delta_\parallel^2-\Delta_\perp^2)]},$$

E is the total electron energy as measured from the edge of the conduction band in

the vertically upward direction in the absence of any quantization,

$$U(E) \equiv E(1+\alpha E)[(E+E_g)(E+E_g+\Delta_\parallel)+\delta(E+E_g+\frac{2}{3}\Delta_\parallel)+\frac{2}{9}(\Delta_\parallel^2-\Delta_\parallel^2)]$$
$$[(E+E_g)(E+E_g+\frac{2}{3}\Delta_\parallel)+\delta(E+E_g+\frac{1}{3}\Delta_\parallel)+\frac{1}{9}(\Delta_\parallel^2-\Delta_\perp^2)]^{-1}$$

and

$$\alpha \equiv 1/E_g.$$

Following Zawadzki [38,39], the modified electron energy spectrum in QWW of the same material in the presence of crossed electric field E_0 along the x-axis and magnetic field B along the z-axis can be written as

$$f+\frac{1}{2}q^2\sin^{-1}(\Psi)=e\pi B\hbar l, \tag{2a}$$

where

$$f \equiv [[b-eBd_1]\cdot 2^{-1}[q^2-(b+eBd_1)^2]^{1/2}-2^{-1}\cdot(b+eBd_1)\cdot[q^2-(b-eBd_1)^2]^{1/2}],$$
$$b \equiv (eB)^{-1}[2M_\perp\rho(E)eE_0+\pi\hbar leBd_2^{-1}],$$
$$q^2 \equiv [2M_\perp U(E)-M_\perp p_z^2a^{-1}(E)-\pi^2\hbar^2t^2(4d_2^2)^{-1}+b^2],$$
$$\Psi \equiv [\zeta_+(1-\zeta_-^2)^{1/2}-\zeta_-(1-\zeta_+^2)^{1/2}],$$
$$\zeta_\pm \equiv (b\pm eBd_1)/2.$$

$2d_1$ and $2d_2$ are the widths along z and y directions, respectively, $t=1,2,3$, $l=1,2,3,\ldots,$

$$\rho(E) \equiv U(E)\cdot\{(1+2\alpha E)[E(1+\alpha E)]^{-1}-J(E)[I(E)]^{-1}+(E+E_g+\Delta_\parallel)^{-1}$$
$$-(E+E_g+\frac{2}{3}\Delta_\parallel)^{-1}\},$$
$$J(E) \equiv [I(E)\{C(E)\cdot[1+A(E)]^{-1}-H(E)\cdot[1+G(E)]^{-1}\}],$$
$$I(E) \equiv [1+A(E)][1+G(E)]^{-1},$$
$$A(E) \equiv [(E+E_g+\Delta_\parallel)(E+E_g)]^{-1}\cdot[\delta(E+E_g+\frac{1}{3}\Delta_\parallel)+\frac{1}{9}(\Delta_\parallel^2-\Delta_\perp^2)],$$
$$G(E) \equiv [E+E_g)(E+E_g+\frac{2}{3}\Delta_\parallel)]^{-1}\cdot[\frac{1}{9}(\Delta_\parallel^2-\Delta_\perp^2)+\delta(E+E_g+\frac{1}{3}\Delta_\parallel)],$$
$$C(E) \equiv A(E)\cdot\{[\delta(E+E_g+\frac{2}{3}\Delta_\parallel)+\frac{2}{9}(\Delta_\parallel^2-\Delta_\perp^2)]^{-1}\cdot\delta-(2E+2E_g+\Delta_\parallel)$$
$$\cdot[(E+E_g)(E+E_g+\Delta_\parallel)]^{-1}\}.$$
$$H(E) \equiv G(E)\cdot\left\{\left[\delta(E+E_g+\frac{1}{3}\Delta_\parallel)+\frac{1}{9}(\Delta_\parallel^2-\Delta_\perp^2)\right]^{-1}\cdot\delta\right.$$
$$\left.-(2E+2E_g+\frac{2}{3}\Delta_\parallel)[(E+E_g)(E+E_g+\frac{2}{3}\Delta_\parallel)]^{-1}\right\}$$

and

$$a(E) \equiv M_{\|}^{*}/V(E).$$

The electron concentration per unit length can be expressed as

$$n_0 = (2/\pi)\sum_{l,t}(\alpha_1 + \alpha_2), \tag{3}$$

where $\alpha_1 \equiv k_z(E_F)$, E_F is the Fermi energy in the present case $\alpha_2 \equiv I[\alpha_1]$, $I \equiv 2(k_BT)^{2r} \cdot (1 - 2^{1-2r}) \cdot \zeta(2r)\frac{d^{2r}}{dE_F^{2r}}$. k_B is the Boltzmann constant, T is temperature, r is the set of real positive integer and $\zeta(2r)$ is the zeta function of order $2r$. Since the DMR can, in general, be expressed [14] as

$$\frac{D}{\mu} = (n_0/e)/\frac{dn_0}{dE_F}. \tag{4}$$

We can combine Eqs (3) and (4) to get the expression of DMR in the present case as

$$\frac{D}{\mu} = e^{-1}\left[\sum_{l,t}(\alpha_1 + \alpha_2)\right] \cdot \left[\sum_{l,t}(\alpha_1' + \alpha_2')\right]^{-1}, \tag{5}$$

where the primes denote the differentiation with respect to E_F.

2.2. Special cases

2.2.1. Under the substitutions $\delta = 0$, $\Delta_{\|} = \Delta_{\perp} = \Delta$ (the isotropic spin–orbit splitting parameter), $m_{\|}^{*} = m_{\perp}^{*} = m^{*}$ (the isotropic effective electron mass at the edge of the conduction band), Eq. (1) takes form

$$\frac{\hbar^2 k^2}{2m^*} = \gamma(E), \quad \gamma(E) \equiv \frac{E(E+E_g)(E+E_g+\Delta)(E_g+\frac{2}{3}\Delta)}{E_g(E_g+\Delta)(E+E_g+\frac{2}{3}\Delta)}, \tag{6}$$

which is the well-known three-band Kane model [40]. Thus, under the above substitutions, the electron energy spectrum can be expressed through the equation

$$F_1 + \frac{1}{2}Q_1^2 \sin^{-1}(\Theta_1) = eB\pi\hbar_l, \tag{7}$$

where

$$F_1 \equiv \frac{1}{2}[\Theta_+(Q_1^2 - \Theta_+^2)^{1/2} - \Theta_-(Q_1^2 - \Theta_-^2)^{1/2}],$$
$$\Theta_\pm \equiv [\hbar t \cdot \pi(2d_2)^{-1} + m^* E_0 \psi(E) B^{-1} \pm eBd_1],$$
$$\psi(E) \equiv [\gamma(E)\{E(1+\alpha E)\}^{-1}[1 + 2\alpha E + E(1+\alpha E) \cdot \{(E + E_g + \Delta)^{-1} - (E + E_g + \frac{2}{3}\Delta)^{-1}\}]],$$
$$\alpha \equiv 1/E_g,$$
$$\Theta_1^2 \equiv [2m^* \gamma(E)[(k_z(E))^2 \hbar^2] + m^{*2} E_0^2 \psi^2(E) B^{-2} + m^* E_0 \psi(E) t\pi\hbar(Bd_2)^{-1}],$$
$$\Theta_1 \equiv [\zeta_{1,+}\sqrt{1 - \zeta_{1,-}^2} - \zeta_{1,-}\sqrt{1 - \zeta_{1,+}^2}]$$

and

$$\zeta_{1,\pm} \equiv \Theta_{,\pm}/Q_1.$$

Thus the basic forms of n_0 and DMR for the generalized case as given by Eqs (3) and (5), will not be altered for the three-band Kane model where α_1 has to be determined from Eq. (7).

2.2.2. Under the conditons $\Delta \gg E_g$ or $\Delta \ll E_g$, Eq. (6) takes the form

$$E(1 + \alpha E) = \frac{\hbar^2 k^2}{2m^*}, \tag{8}$$

which is the well-known two-band Kane model [41]. Thus under the above substitutions the basic form of Eq. (7) remains the same where $\gamma(E) \equiv E(1 + \alpha E)$ and $\psi(E) \equiv (1 + 2\alpha E)$.

2.2.3. Under the condition $E_g \to \infty$, Eq. (8) assumes the form

$$E = \hbar^2 k^2 / 2m^*, \tag{9}$$

which is the well-known expression of the dispersion relation for parabolic energy bands. Thus, under the condition $\alpha \to 0$, the basic forms of Eqs (7) will not be altered where $\gamma(E) \equiv E$ and $\Psi(E) \equiv 1$.

2.2.4. Under the condition $E_0 \to 0$, the electron energy spectrum in QWW of tetragonal semiconductors in the presence of a magnetic field along the direction of free motion is given by

$$\overline{x} + \sin^{-1}(\beta) = 2eB\hbar\pi l, \tag{10}$$

where

$$\overline{x} \equiv [r_+^2(C_1^2 - r_+^2]^{1/2} - r_-^2(C_1^2 - r_-^2)^{1/2}],$$
$$r_\pm \equiv [t\pi\hbar(2d_2)^{-1} \pm eBd_1],$$
$$C_1^2 \equiv (2M_\perp U(E) - M_\perp a^{-1}(E) p_z^2)$$

and

$$\beta \equiv (r_+)\sqrt{C_1^2 - r_-^2} - (r_-)\sqrt{C_1^2 - r_+^2}.$$

Thus, the basic forms of n_0 and DMR as given by Eqs (3) and (5) will not change where α_1 has to be determined from Eq. (10).

2.2.5. For the three-band Kane model, the basic forms of the Eqs (10), (3) and (5) remain the same where

$$C_1^2 \equiv 2m^*\gamma(E) - p_z^2.$$

2.2.6. For the two-band Kane model, the basic forms of Eqs (10), (3) and (5) will not be changed, where

$$C_1^2 = 2m^* E(1 + \alpha E) - p_z^2.$$

2.2.7. For parabolic energy bands

$$C_1^2 = 2m^* E - p_z^2.$$

2.2.8. In the absence of magnetic field, Eq. (10) assumes the form

$$U(E) = \frac{\hbar^2}{2M_\perp}\left[\left(\frac{t\pi}{2d_1}\right)^2 + \left(\frac{l\pi}{2d_2}\right)^2\right] + \frac{p_z^2 V(E)}{2M_{11}}, \tag{11}$$

which is the well-known dispersion relation for QWW of tetragonal semiconductors as given elsewhere [9].

The basic forms of n_0 and DMR as given by Eqs (3) and (5) will not alter in the present case where

$$\alpha_1 \equiv [2M_{11}/V(E_F)\hbar^2]^{1/2} \cdot \left[U(E_F) - \left(\frac{\hbar^2}{2M_\perp}\right)\left\{\left(\frac{t\pi}{2d_1}\right)^2 + \left(\frac{l\pi}{2d_2}\right)^2\right\}\right]^{1/2}.$$

2.2.9. For the three-band Kane model, the electron energy spectrum in QWW assumes the form

$$\gamma(E) = (\hbar^2\pi^2/2m^*)[(t/2d_1)^2 + (l/2d_2)^2] + (\hbar^2 k_z^2/2m^*). \tag{12}$$

The basic forms of n_0 and DMR as given by Eqs (3) and (5) will be unaltered where

$$\alpha_1 \equiv (2m^*/\hbar^2)^{1/2}[\gamma(E_F) - (\hbar^2\pi^2/2m^*)[(t/2d_1)^2 + (l/2d_2)^2]]^{1/2}.$$

2.2.10. For the two-band Kane model, the electron energy spectrum in QWW in the absence of cross-field configuration assumes the form

$$E(1 + \alpha E) = (\hbar^2\pi^2/2m^*)[(t/2d_1)^2 + (l/2d_2)^2] + (\hbar^2 k_z^2/2m^*). \tag{13}$$

The basic forms of Eqs (3) and (5) will not change either in this case, where

$$\alpha_1 \equiv (2m^*)/\hbar^2)^{1/2}[E_F(1+\alpha E_F) - (\hbar^2\pi^2/2m^*)\{(t/2d_1)^2 + (l/2d_2)^2\}]^{1/2}$$

2.2.11. The expressions of n_0 and DMR in QWWs of wide gap materials can be written under the condition $\alpha \to 0$ as

$$n_0 = \frac{2 \cdot (2\pi m^* k_B T)^{1/2}}{h} \sum_{l,t} F_{-\frac{1}{2}}(\eta) \tag{14}$$

and

$$\frac{D}{\mu} = (k_B T/e) \left[\sum_{l,t} F_{-\frac{1}{2}}(\eta)\right] \left[\sum_{l,t} F_{-\frac{3}{2}}(\eta)\right]^{-1}, \tag{15}$$

where $\eta \equiv (k_B T)^{-1}[E_F - \frac{\hbar^2\pi^2}{2m^*}[(t/2d_1)^2 + (l/2d_2)^2]]$ and $F_j(\eta)$ is the one parameter Fermi–Dirac integral of order j which can be written as [42]

$$F_j(\eta) \equiv (\Gamma(j+1))^{-1} \int_0^\infty y^j [1+\exp(y-\eta)]^{-1} dy \text{ for } j > -1;$$

or for all y, analytically continued as a complex integral around the negative axis,

$$F_j(\eta) = (\overline{\Theta}_j) \cdot \int_{(-\infty)}^{(0+)} y^j [1+\exp(-y-\eta)]^{-1} dy,$$

where $\overline{\Theta}_j \equiv [i/(\sin(\pi j)(\Gamma(j+1)))] = \Gamma(-j)/2\pi\sqrt{-1}$.

2.3. Experimental suggestion of determining the DMR

The thermoelectric power of the electrons in the present case is given by [43–44]

$$G_0 = H_0/en_0, \tag{16}$$

where H_0 is the corresponding entropy per unit length.

Following Tsidilkovskii [44] we get

$$G_0 = (\pi^2 k_B^2 T/3en_0)\left(\frac{dn_0}{dE_F}\right). \tag{17}$$

Thus, using Eqs (4) and (17) we get

$$\frac{D}{\mu} = \pi^2 k_B^2 T/3G_0 e^2. \tag{18}$$

Thus, by knowing G_0 we can determine D/μ for degenerate semiconductors having arbitrary dispersion relations.

3. Results and discussion

Using the appropriate equations together with the [36] parameters $m_{\perp}^{*} = 0.04m_0$, $m_{\parallel}^{*} = 0.03\, m_0$, $\delta = 0.085$ eV, $E_g = 0.095$ eV, $\Delta_{\parallel} = 0.24$ eV, $\Delta_{\perp} = 0.29$ eV, $T = 4.2$ K, $E_0 = 10^2$ V/m, $B = 2T$, $2d_1 = 40$ nm and $2d_2 = 50$ nm, we have plotted the normalized D/μ ratio as a function of electron concentration as shown in the plot of Fig. 1, in which the same dependence is also plotted by taking the crystal field parameter as zero for comparison (plot e). In addition, in Fig. 1, plot b corresponds to the degenerate three-band Kane model of n-Cd_3As_2 (taking $\Delta = 0.27$ eV and $m^{*} = 0.035\, m_0$ for the purpose of numerical computations). We have also plotted the DMR in accordance with the two-band Kane model and that of parabolic energy bands. Using the same parameters as used in obtaining Fig. 1 we have presented the DMR as a function of film thickness as shown in Fig. 2 in which the various simplified limiting cases have further been considered.

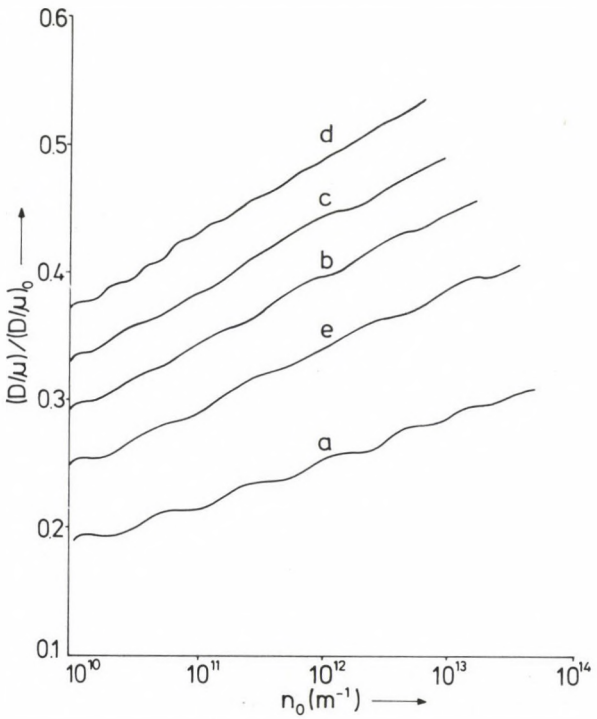

Fig. 1. Plot of the normalized diffusivity–mobility ratio in quantum well wires of n-Cd_3As_2 under cross field configuration as a function of n_0 in accordance with (a) our proposed dispersion law, (b) the three-band Kane model, (c) the two-band Kane model, (d) parabolic energy bands, (e) δ (crystal field splitting parameter) = 0.

It appears from Fig. 1 that the DMR increases with increasing electron concentration in an oscillatory way at a rate lower than that of when $\delta = 0$. Moreover,

for relatively low values of electron concentration, the effect of crystal field splitting decreases whereas the same parameter affects significantly the DMR for relatively large values of the carrier degeneracy. The crystal field splitting parameter lowers the value of the DMR in QWW of degenerate tetragonal semiconductors as compared with that corresponding to $\delta = 0$ at a given value of electron concentration in the whole range of concentrations considered. The influence of the energy band models on the DMR is also apparent from the two Figures. It is again noted that the variations of the DMR with n_0 and $2d_1$ are completely band-structure dependent for all models of QWW of degenerate tetragonal semiconductors. It appears that the DMR increases with decreasing thickness in an oscillatory way as apparent from Fig. 2.

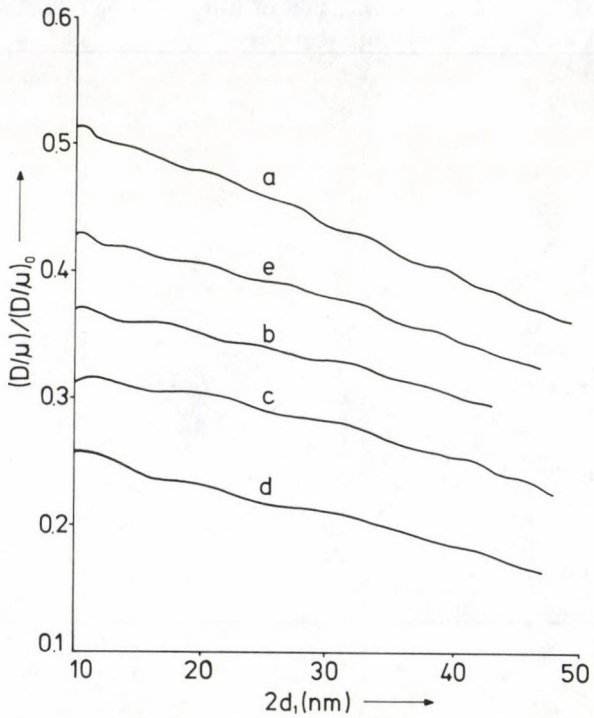

Fig. 2. Plot of the normalized diffusivity–mobility ratio in quantum well wires of n–Cd_3As_2 under cross field configuration as a function of film thickness for the above mentioned cases. ($n_0 = 10^{10}$/m, $2d_2 = 40$ nm).

It may be remarked that the D/μ ratio is connected with $\frac{dn_0}{dE_F}$, as given by Eq. (4). Our experimental suggestion for the determination of DMR for semiconductors having arbitrary dispersion laws given by Eq. (18) does not contain any band parameter. For constant temperature $(D/\mu) \propto (G)^{-1}$. Only the experimental values of G for any semiconductor as a function of electron concentration will

give the experimental values of the D/μ ratio for that range of n_0 for that very semiconductor. Since the experimental data of thermoelectric power in the present case is not available in the literature to the best of our knowledge, we cannot compare our theoretical formulation with the proposed experiment. The results are theoretical curves evaluated for parameters referring to real systems and the theoretical analysis as given here would be useful in analysing the experimental data when they appear. Since the above power decreases with increasing electron concentration, from Eq. (18) we can conclude that the DMR will increase with increasing electron concentration which is also evident from Fig. 1. The experimental result of G_0 in the present case will provide an experimental check on the D/μ ratio and also a technique for probing the band structure in degenerate materials.

We wish to note that in formulating the basic dispersion relation we have considered the crystal field splitting parameter, the anisotropies in the momentum matrix elements and the spin–orbit splitting parameters, respectively, since these are significant physical features of tetragonal semiconductors [36]. In the absence of crystal field splitting, together with the assumptions of isotropic effective mass and isotropic spin–orbit splitting parameter, Eq. (1) converts into the well-known form of the three-band Kane model (Eq. (6)). The three-band Kane model is the most valid model for III–V compound semiconductors, ternary and quaternary materials and they find extensive applications in the field of solid state science and technology. It is worth noting that the full three-band Kane model must be used as such for studying the electronic properties of n-InAs where the spin–orbit splitting parameter (Δ) is of the order of band-gap (E_g). However, for many important semiconductors $\Delta \gg E_g$ (e.g. InSb, etc.). Under this condition Eq. (6) gets simplified into the form $\frac{\hbar^2 k^2}{2m^*} = E(1 + \alpha E)$ which is our Eq. (8). This is the well-known two-band Kane model [41]. Also, under the condition $E_g \to \infty$ as for parabolic semiconductors, the above equation transforms into the well-known form $\frac{\hbar^2 k^2}{2m^*} = E$. The basic form of Eq. (2a) remains unaltered for our proposed dispersion relation, the three-band Kane model, the two-band Kane model and that of parabolic energy bands in QWW of semiconductors under cross-field configuration. The functions of Eq. (2a) are band structure dependent quantities. The above statement is also true in the presence of magnetic field only. This peculiarity of the transcendental nature of our present problem which is even valid for parabolic energy bands is not at all true in the bulk case. From the expressions of DMR and electron concentration as given by Eqs (5) and (3) we can get the corresponding expressions for QWW's of even parabolic semiconductors in the absence of cross-field configuration. It is worth remarking that the quantization of the energy in transverse plane of the direction of application of the magnetic field as valid for 3D electron gases in a cross-field configuration is not at all valid for QWW under the same physical conditions. Besides, the subband energies can be calculated from Eq. (2a) whose importance is well known in semiconductor science.

In recent years, the mobility of the electrons in QWW has been studied extensively but the diffusion constant (a very important device parameter which cannot be easily experimentally determined) of such materials has relatively been less investigated. Thus the theoretical results of this work will be useful in determining

the diffusion constant both in the presence and absence of cross-field configuration even for parabolic semiconductors. We note that the basic dispersion relation as given by Eq. (2a) covers various semiconductors under different physical conditions. Besides, the study of the transport phenomena and the formulation of the electronic properties of semiconductors are based on the dispersion relations in such materials. Finally, it may be remarked that the basic purpose of our present paper is not only to investigate the DMR in QWW of non-parabolic semiconductors under cross-field configuration but also to suggest an experimental method of determining the DMR in degenerate materials having arbitrary dispersion laws.

References

1. J. Cibert, P. M. Petroff, G. J. Dolan, S. J. Pearson, A. C. Gossard and J. H. English, Appl. Phys. Letts., *49*, 1275, 1986.
2. J. M. Gaines, P. M. Petroff, H. Kroemer, R. J. Simes, R. S. Geels and J. H. English, J. Vac. Sci. Tech., *6B*, 1378, 1988.
3. T. Fukui and H. Saito, Appl. Phys. Letts., *50*, 824, 1987.
4. H. Sakaki, Jap. J. Appl. Phys., *19*, 94, 1980; P. M. Petroff, A. C. Gossard, R. A. Logan and W. Weigmann, Appl. Phys. Letts. *41*, 635, 1982.
5. M. Isuchiya, J. M. Gaines, R. H. Yan, R. J. Simes, P. O. Holtz, L. A. Coldren and P. M. Petroff, Phys. Rev. Letts., *62*, 466, 1989.
6. H. Temkin, G. J. Dolan, M. B. Panish and S. N. G. Chu, Appl. Phys. Letts., *50*, 413, 1988.
7. Y. Arakawa and H. Sakaki, Appl. Phys. Letts., *40*, 939, 1982.
8. I. Swemune and L. A. Coldren, IEEE J. QE, *24*, 1178, 1988.
9. M. Mondal, S. Banik and K. P. Ghatak, J. Low Temp. Phys., *74*, 423, 1989.
10. W. Zawadzki, Surf. Sci., *37*, 218, 1973.
11. J. C. Hansel and M. Peter, Phys. Rev., *114*, 411, 1959.
12. A. G. Aronov, Sov. Phys. Solid State, *5*, 402, 1963.
13. Q. H. F. Verlen and B. Lax, Phys. Rev. Letts., *12*, 471, 1964.
14. B. R. Nag, Electron Transport in Compound Semiconductors, Springer-Verlag, Berlin, Heidelberg, New York, 1980.
15. G. D. Boyd, E. Buchler and F. G. Storz, Appl. Phys. Letts., *18*, 301, 1971.
16. J. L. Shay, K. J. Backman, E. Buchler and J. H. Wernick, Appl. Phys. Letts., *23*, 226, 1973.
17. T. I. Kamin and R. S. Muller, Solid State Electronics, *10*, 423, 1967.
18. G. D. Hatchell and A. E. Ruchli, IEEE Trans. Electron Devices, *15*, 437, 1968.
19. G. G. Emch, J. Math. Phys., *14*, 1775, 1973.
20. R. Kubo, J. Phys. Soc. Japan, *12*, 537, 1957.
21. H. Kroemer, IEEE Trans. *ED25*, 850, 1978.
22. M. Mondal and K. P. Ghatak, J. Phys. C (Solid State), *20*, 1671, 1987.
23. K. G. Ghatak and M. Mondal, Thin Solid Films, *148*, 219, 1987.
24. M. Mondal and K. P. Ghatak, Phys. Stat. Sol. (b), *133*, K67, 1986.
25. P. N. Butcher, A. N. Chakravarti and S. Swaminathan, Phys. Stat. Sol. (a), *25*, K47, 1974.
26. B. Mitra and K. P. Ghatak, Solid State Electronics, *32*, 810, 1989.
27. M. Mondal and K. P. Ghatak, J. Mag. and Mag. Materials, *26*, 115, 1986.
28. M. Mondal and K. P. Ghatak, Annalen der Physik, *46*, 502, 1989.
29. B. Mitra and K. P. Ghatak, Phys. Stat. Sol. (b), *164*, K13, 1991.
30. S. N. Biswas and K. P. Ghatak, Int. J. Electronics, *70*, 125, 1991.
31. J. W. Rowe and J. L. Shay, Phys. Rev., *83*, 451, 1971.
32. J. J. Hopfield, J. Phys. Chem. Solids, *15*, 97, 1960.
33. A. Shilika, Surface Science, *37*, 703, 1973.

34. H. Kildal, Phys. Rev., *10*, 5082, 1974.
35. J. L. Shay and H. Wernick, Ternary Chalcopyrite Semiconductors: Growth, Electronic Properties and Applications, Pergamon Press, London, 1975.
36. S. I. Radaustan, E. A. Arushanov, E. A. Nateprov and G. P. Chuiko, Cadmium Arsenide and Phosphide, Nauka Press, USSR, 1986.
37. M. Mondal, N. Chattopadhyay and K. P. Ghatak, J. Low Temp. Phys., *66*, 131, 1987.
38. W. Zawadzki, Phys. Rev. Letts., *16*, 1001, 1966.
39. W. Zawadzki, in: Springer Series in Solid State Science, Vol. 53, 2D Systems, Heterostructures and Superlattices, G. G. Bauer, F. Kachar and H. Heinrich (eds), Springer, Berlin, 1984, p. 1.
40. V. A. Viltkoskii, D. S. Domanevskii, R. A. Kakanokov and V. V. Krasovaskii, Sov. Phys. Semicond., *13*, 553, 1979.
41. A. N. Chakravarti and B. R. Nag, Phys. Stat. Sol. (a), *22*, K153, 1974.
42. K. P. Ghatak and B. Mitra, Internat. J. Electronics, *72*, 541, 1992.
43. K. P. Ghatak and A. Ghoshal, Phys. Stat. Sol. (b), *170*, K27, 1992.
44. I. M. Tsidilkovskii, Band Structure of Semiconductors, Pergamon Press, Oxford, 1982.

Acta Physica Hungarica 72 (2-4), pp. 161–168 (1992)

A LATTICE GAS MODEL FOR ENZYME KINETICS WITH NEXT-NEAREST NEIGHBOUR INTERACTIONS

R. MEJDANI, A. GASHI and M. IFTI

Department of Physics, University of Tirana
Tirana, Albania

(Received 16 June 1992)

We have shown that, by using a one-dimensional lattice gas model with the next-nearest neighbour interactions and calculating the thermodynamic potential of the system by means of the transfer matrix method, we can find numerically for enzyme kinetics some new diagrams of saturation curve. These diagrams in the limit of no interactions between sites reduce to the classical Michaelis–Henri diagrams and in the limit of the nearest neighbour interactions to some other diagrams which we have obtained before by using a correlated walks theory. These new diagrams of saturation curve can be useful for the experimental investigation.

1. Introduction

The Ising and related models like lattice gas have been applied with some success to a number of biological systems [1]. The number of articles using these models to derive enzyme kinetics equations is numerous and diverse. However, in [2] we have studied a lattice gas model with nearest neighbour interaction to find an equation for enzyme kinetics by using a correlated walks theory or variational procedures.

In the present paper, to study the saturation curves in the enzyme kinetics, we have used a one-dimensional lattice gas with the nearest-neighbour interaction and the next-neighbour interaction. The grand canonical partition function is calculated by means of the transfer matrix method. But the variations of the number density (or the average fraction of occupied sites) versus the fugacity, i.e. the saturation curves, are obtained numerically for different values of temperature and interactions constants.

2. The model and the Hamiltonian of the system

We consider an enzyme with N sites for substrate. We number the sites by an index $i = 1, 2, \ldots, N$ and associate with each site a parameter σ_i, which takes two values: $+1$, if the i-th site is occupied by substrate and 0, if the i-th site is unoccupied by substrate. So, a configuration of the molecule is specified by the values of $\sigma_1, \sigma_2, \ldots, \sigma_N$ and we can interpret it as a lattice gas model. For the

next-nearest-neighbour interactions, following [3], we assume that the energy J_{ij} of interaction between particles situated at the sites i and j in the system is given by:

$$J_{ij} = \begin{cases} \infty & \text{(if } i,j \text{ are on the same sites)}, \\ -J_1 & \text{(if } i,j \text{ are on the nearest neighbouring sites)}, \\ -J_2 & \text{(if } i,j \text{ are on second nearest neighbouring sites)}, \\ 0 & \text{(otherwise)}. \end{cases}$$

To each site i, as we have mentioned before, we assign a variable σ_i, defined by:

$$\sigma_i = \begin{cases} 1 & \text{(if site } i \text{ is occupied)}, \\ 0 & \text{(if site } i \text{ is unoccupied)}, \end{cases}$$

and assume the periodic boundary condition that $\sigma_{i+N} = \sigma_i$ for $i = 1, 2, \ldots, N$.

The Hamiltonian H in a given configuration $\{\sigma\} = \{\sigma_1, \sigma_2, \ldots, \sigma_N\}$ is given by:

$$H = (1/2)\sum_{i,j} J_{ij}\sigma_i\sigma_j = -J_1\sum_{i=1}^{N}\sigma_i\sigma_{i+1} - J_2\sum_{i=1}^{N}\sigma_i\sigma_{i+2} \tag{2.1}$$

and the grand canonical partition function of this system is given by:

$$Z(T,N,\mu) = \sum_{\{\sigma\}} \exp\{(\sum_{i=1}^{N}\mu\sigma_i - H)/kT\}, \tag{2.2}$$

where μ is the chemical potential, k the Boltzmann constant and T the absolute temperature. The sum $\{\sigma\}$ is taken over all the configurations.

3. The transfer matrix method

The grand canonical partition function of the system is calculated by means of the transfer matrix method ([3]–[5]). By using this method, we have:

$$Z(T,N,\alpha) = Tr(\overrightarrow{\overrightarrow{T}}^N), \tag{3.1}$$

where

$$\overrightarrow{\overrightarrow{T}} = \begin{Bmatrix} 1 & 1 & 0 & 0 \\ 0 & 0 & 1 & x^{1/2} \\ \alpha & \alpha y & 0 & 0 \\ 0 & 0 & \alpha x^{1/2} & \alpha xy \end{Bmatrix} \tag{3.2}$$

is the transfer matrix of this system with:

$$\begin{cases} x = \exp(J_1/kT), \\ y = \exp(J_2/kT), \\ \alpha = \exp(\mu/kT). \end{cases} \tag{3.3}$$

The eigenvalues of the transfer matrix (3.2) are determined as the roots of the following quartic equation for $\cap$:

$$\cap^4 - (1+\alpha xy)\cap^3 + \alpha(x-1)y\cap^2 + \alpha(y-1)(1+\alpha xy)\cap - \alpha^2(y-1)^2 x = 0. \quad (3.4)$$

Denoting:

$$t = kT/J_1 \ (J_1 > 0), \ x = K = \exp(1/t)$$
$$\text{and} \qquad (3.5)$$
$$y = \exp(J_2/kT) = \exp(\epsilon/t) = K^\epsilon, \ (\epsilon = J_2/J_1),$$

the equation (3.4) can be written:

$$\cap^4 + a\cap^3 + b\cap^2 + c\cap + d = 0, \quad (3.6)$$

where

$$\begin{cases} a = -(1+\alpha K^{1+\epsilon}), \\ b = \alpha(K-1)K^\epsilon, \\ c = \alpha(K^\epsilon - 1)(1+\alpha K^{1+\epsilon}), \\ d = -\alpha^2(K^\epsilon - 1)^2 K. \end{cases} \quad (3.7)$$

Since the maximum eigenvalue $\cap_1 = \cap_{\max}$ is equal to the grand partition function per site in the thermodynamic limit, the equations of state are derived as:

$$\begin{cases} p = kT \ln \cap_{\max}, \\ \varrho = \alpha(\partial/\partial\alpha)(\beta p) = \alpha(\partial/\partial\alpha)(\ln \cap_{\max}) \end{cases}, \quad (3.8)$$

where $\beta = 1/kT$, p denotes the pressure and ϱ is the number density or the average fraction of occupied sites.

4. The ϱ–α diagrams

In general, it is very complicated to solve analytically the equation (3.6). For the special case $\epsilon = 0$ ($J_2 = 0$) or $y = 1$ this equation can be solved analytically and we find for the density:

$$\varrho = \alpha \frac{KD_1 + [KD_2 + 2(1-K)]}{D_1(D_1 + D_2)}, \quad (4.1)$$

where $D_1 = [4\alpha + (1-K)^2]^{1/2}$ and $D_2 = 1 + K\alpha$. We have found the same equation (4.1) for enzyme kinetics by using a correlated walks theory [1] or the model of partition points [6]. So, it seems reasonable to interpret the second equation of (3.8), for the average fraction of occupied sites, as an equation for enzyme kinetics if α is interpreted as a measure of the concentration of substrate [1].

For the other cases ($\epsilon \neq 0$) we have found numerically the maximum eigenvalue $\cap_{max}$ of (3.6) and $\ln \cap_{max}$. By a special differentiation program, we have calculated $(\partial/\partial\alpha)(\ln \cap_{max})$ and then the density $\varrho = \alpha(\partial/\partial\alpha)(\ln \cap_{max})$ [7]. For the program calibration we have used the case $\epsilon = 0$ ($J_2 = 0$) which is analytically known by us ([1], [6]).

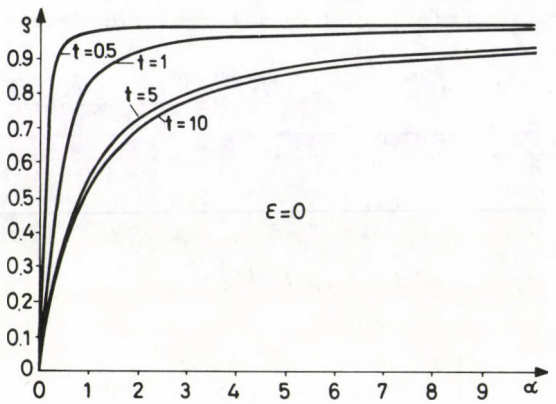

Fig. 1a. Variation of the saturation curve at some fixed reduced temperatures t in the $\varrho-\alpha$ diagram for the case $\epsilon = 0$ ($J_2 = 0$)

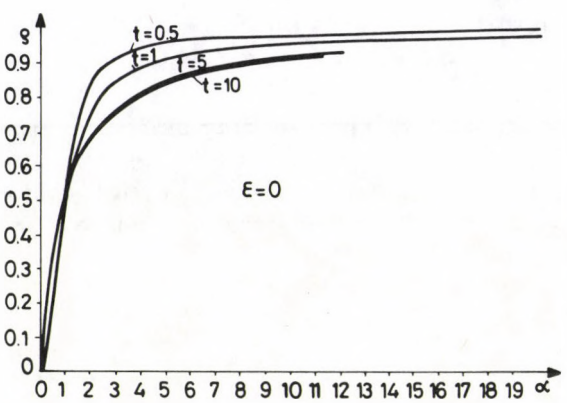

Fig. 1b. Fig. 1a plotted on a scale so that half-saturation always occurs at concentration unity

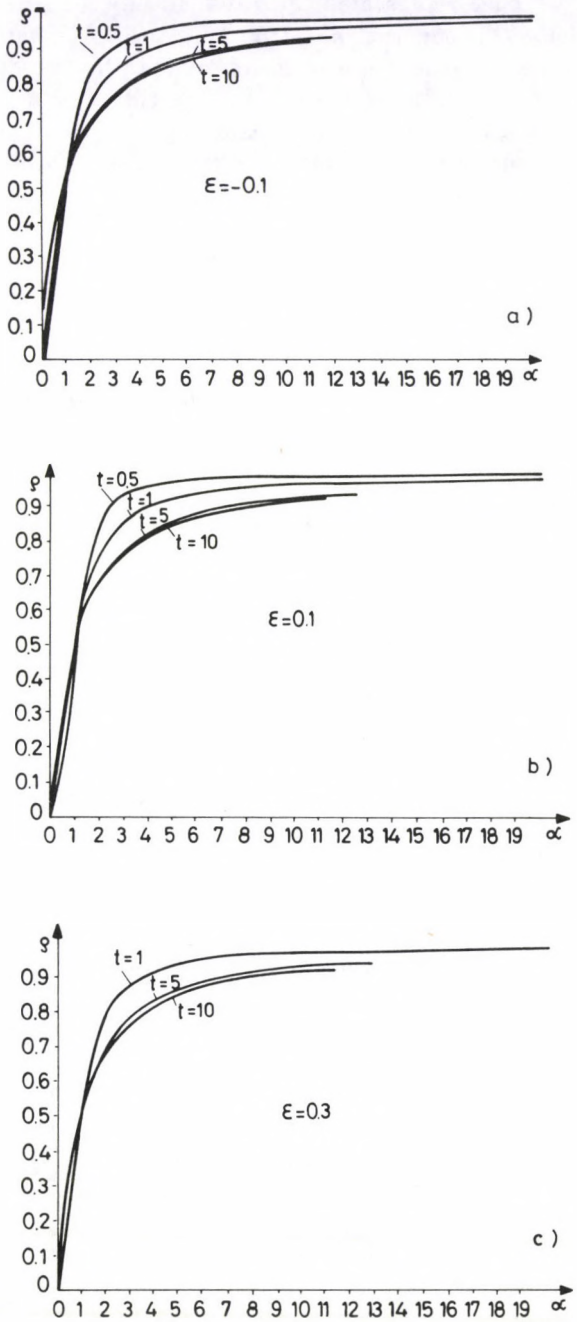

Fig.2. Variation of some rescaled saturation curves at some reduced temperatures t in the ϱ–α diagram (the half-saturation occurs at concentration unity). a) $\epsilon = -0.1$; b) $\epsilon = 0.1$; c) $\epsilon = 0.3$.

In Fig. 1a we have represented diagrammatically, for the case $\epsilon = 0$, the numerical variation of the function $\varrho = f(\alpha)$ (the saturation curve) at some fixed reduced temperatures t in the $\varrho - \alpha$ diagram. It is to be noted that in the limit $K = \exp(1/t) \to 1$ ($J_1 \to 0$ or $T \to \infty$) these curves reduce to the classical Michaelis–Henri saturation curve with the equation $f(\alpha) = \alpha/(1+\alpha)$, which fits to the myoglobin saturation curve and the initial reaction rate curve for classical enzymes extremely well. In this last equation the "units" are chosen so that half-saturation occurs at concentration unity. In Fig. 1b are replotted, for $\epsilon = 0$, the rescaled curves $\varrho = f(\alpha)$ on the concentration scale chosen so that half-saturation always occurs at concentration unity.

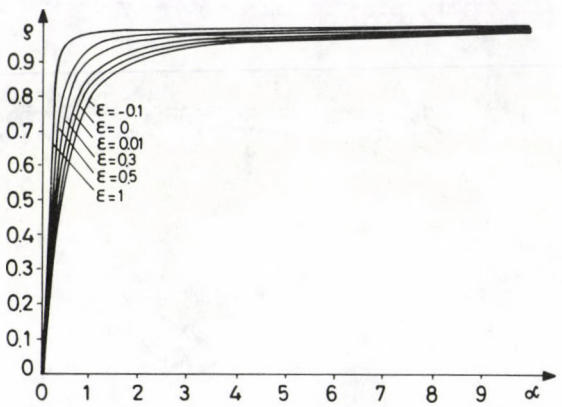

Fig. 3. Some of the non-rescaled saturation curves at a chosen reduced temperature $t = 1$ for different values of the interaction parameter ϵ

In Fig. 2a, b, c are replotted, following the same procedure, the rescaled curves $\varrho = f(\alpha)$ for $\epsilon = -0.1$ ($J_2 < 0$ i.e. the next-nearest-neighbour interaction is repulsive), $\epsilon = 0.1$ and $\epsilon = 0.3$, respectively. To represent diagrammatically the variation of the saturation curve from the values ϵ of the interaction constants in Fig. 3 are plotted in the $\varrho - \alpha$ diagram some of the non-rescaled functions $\varrho = f(\alpha)$ at a chosen reduced temperature ($t = 1$). It is clearly visible from this Figure that, in the case of repulsive next-nearest-neighbour interactions ($\epsilon < 0$), the saturation is "slower" than in the case of attractive next-nearest-neighbour interactions ($\epsilon > 0$). In all these cases the nearest neighbour interactions are attractive ($J_1 > 0$). By fitting these theoretical curves to experimental ones, it is possible to determine the "adjustable" parameters K and ϵ (i.e. the interaction constants J_1 and J_2).

In the particular case, when we confine ourselves to hard-core nearest-neighbour interaction ($J_1 = -\infty$ or $x = 0$), Eq. (3.4) is reduced to the cubic equation:

$$\cap^3 - \cap^2 - \alpha y \cap + \alpha(y-1) = 0. \tag{4.2}$$

Denoting $t_2 = kT/J_2$ ($J_2 > 0$), and following the same numerical procedure, we can find non-rescaled saturation curves at some fixed reduced temperatures t_2 (Fig. 4). It is clearly visible from this Figure that, for a hard-core nearest-neighbour interaction, the saturation value in the $\varrho - \alpha$ diagram is 0.5.

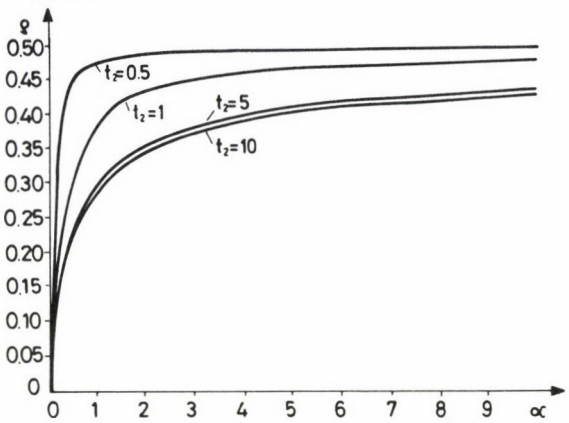

Fig. 4. Variation of the saturation curve at some fixed reduced temperatures t_2 in the $\varrho-\alpha$ diagram for the case $J_1 = \infty$ and $J_2 > 0$

5. Conclusion

In this paper, by using a one-dimensional lattice gas model with the next-nearest-neighbour interactions, we have demonstrated the influence of this interaction in the process of the saturation for the enzyme kinetics curves. It is obtained numerically and represented diagrammatically how slower is the saturation in the case of repulsive next-nearest-neighbour interactions in comparison with the case of attractive ones. Also we have shown that the saturation curves in the limit of the only nearest-neighbour interactions ($J_2 = 0$) reduce to some other diagrams which we have found before by using a correlated Walks theory, while in the limit of no interactions ($J_1 = 0, J_2 = 0$) between sites to the classical Michaelis–Henri diagrams. These new diagrams of saturation curve can be useful for the experimental investigation and by their fitting to experimental diagrams, it is possible to value the interaction constants.

References

1. C. J. Thompson, Mathematical Statistical Mechanics, Princeton University Press, New Jersey, 1979.
2. R. Mejdani, Il Nuovo Cimento, *D13*, 2, 131, 1991.

3. K. Nisizima, Prog. Theor. Phys., *85*, 39, 1991.
4. K. Tanaka, T. Morita and K. Hiroike, Prog. Theor. Phys., *77*, 68, 1987.
5. C. J. Thompson, Classical Equilibrium Statistical Mechanics, Clarendon Press, Oxford, 1988.
6. R. Mejdani, IC/91/143, IR, ICTP, Trieste, Italy.
7. R. Mejdani, A. Gashi and M. Ifti, Int. Rep., KFT FSHN/UT–AL. 7/1991.

Acta Physica Hungarica 72 (2–4), pp. 169–181 (1992)

НЕЙТРИННОЕ ИЗЛУЧЕНИЕ МАЛЫМИ ЧЕРНЫМИ ДЫРАМИ

А. П. Трофименко и В. С. Гурин

Астрономическая секция Минского отделения Астрономо-геодезического общества Минск–12, Белоруссия

(Поступило 7 июля 1992)

Производится расчет интенсивности и спектра излучения за счет эффекта Хокинга для безмассовых и массивных нейтрино малыми черными дырами с массами 10^8–10^{16} г, которые могут локализоваться внутри компактных небесных тел, в частности, в Земле. Основными особенностями нейтринного излучения от таких черных дыр, по которым оно в принципе может быть зарегистрировано нейтринными детекторами, являются высокие энергии частиц, тепловой энергетических спектр, кратковременность либо выраженная тенденция к повышению интенсивности и энергии частиц, а также направленный характер, связанный с расположением источника в недрах Земли, например вблизи вулканов или в области центра Земли.

1. Введение

Черные дыры (ЧД) считаются традиционно объектами изучения астрофизики звезд и галактик, а также их скоплений, где могут реализоваться теоретические конструкции связанных с ними моделей. Хотя сами по себе решения уравнений общей теории относительности (ОТО) не накладывают явных ограничений на массу ЧД, но при рассмотрении астрофизических моделей возникает величина массы, выше которой может происходить необратимый гравитационный коллапс под горизонт событий, приводящий к формированию ЧД. Это так называемый предел Чандрасекара, составляющий $2-5M_\odot$ [1]. Образование таких массивных объектов, как известно, хорошо вписывается в теорию звездной эволюции [1] и кроме того вполне вероятно и для более массивных тел типа ядер галактик, центров шаровых скоплений, квазаров и др. [2–4].

Гипотезы о возможной реальности ЧД малой массы высказывались, начиная с 1966 года, отводя им, в основном, космологическое происхождение [5,6], поскольку непонятны механизмы, которые могли бы привести к необходимой для коллапса малых масс концентрации материи. В ряде работ [7,8] обосновываются идеи о возможности присутствия малых ЧД внутри значительно менее массивных, нежели звезды, космических объектов: в планетах Солнечной системы [7–9] и, в частности, в Земле [7, 8,

10–12]. Несмотря на свою необычность, такие предположения не противоречат наблюдаемым фактам и даже могут помочь объяснить некоторые непонятные явления, связанные с различными телами Солнечной системы [8–10]. Весьма существенным при этом является тот факт, что ЧД малой массы ($10^8 - 10^{15}$ г) имеют размеры меньше атомарных и, по-видимому, весьма слабо взаимодействуют с веществом тех тел, в которых находятся [13, 14]. Поэтому возможно их длительное существование внутри подобных тел без явных проявлений.

Гипотеза о наличии микро-ЧД внутри планет и их спутников наиболее разумно увязывается с процессами зародышеобразования [7, 8] при их участии, которые эффективно могли привести к конденсации вещества и образования этих небесных тел. Однако, связанная с космогонией задача заслуживает отдельного рассмотрения, и в данной работе мы будем допускать возможное наличие малых ЧД в Земле, не касаясь вопроса об их происхождении.

Одним из характерных свойств малых ЧД, в том числе отличающее их от ЧД звездной массы, является хокинговское излучение. Эффект Хокинга может быть заметен для ЧД с массой не более $10^{20} - 10^{25}$ г и заключается в излучении целого набора элементарных частиц, причем чем меньше масса дыры, тем больше вероятность излучения массивных частиц и частиц с высоким значением спина [15]. Но основная доля излучаемых квантов приходится на безмассовые частицы, и поток излучения резко спадает для фотонов и гравитонов. Поскольку неизвестны безмассовые скалярные частицы, то следует ожидать, что нейтрино как раз и будут занимать основную долю в излучении малых ЧД с массами $10^{12} - 10^{18}$ г, которые наиболее вероятны внутри планетных тел типа Земли. Излучение нейтрино за счет эффекта Хокинга может оказаться одним из наблюдательных проявлений и удобным средством поиска малых ЧД [8, 10]. При высокой проникающей способности, известной для нейтрино, и хорошо изученном нейтринным излучением космического происхождения обнаружение повышенного потока нейтрино из недр Земли было бы весомым свидетельством в пользу наличия ЧД в нашей планете. Такое превышение потока нейтрино над фоновым следует ожидать, например, вблизи действующих вулканов, и в работах [8, 10] уже выполнены некоторые оценки энергетики микро-ЧД в сравнении с таковой для объяснения энергетики вулканов.

2. Поток нейтрино от невращающейся ЧД

В связи с принципиальной возможностью экспериментальной регистрации излучения частиц высоких энергий, в том числе нейтрино, от земных ЧД мы проведем более точные расчеты характеристик излучения нейтринного потока и сосредоточим внимание на излучении от невращающейся ЧД, так как интегральные характеристики излучения мало зави-

сят от факта вращения. Кроме того, быстро вращающаяся и тем более заряженная ЧД внутри плотных небесных тел будет быстро сбрасывать момент вращения и заряд из-за взаимодействия с окружающим веществом.

Общие формулы для излучения безмассовных частиц с определенными квантовыми числами от ЧД получены в работе [15], согласно которым уменьшение массы ЧД за счет излучения огного вида частиц с квантовыми числами l, m, p происходит по закону

$$\left(\frac{dm}{dt}\right) = -\frac{1}{2}\pi \sum_{l,m,p} \int \Gamma_{\omega lmp} \{\exp(8\pi M\omega) + 1\}^{-1} \omega d\omega, \tag{1}$$

где M – масса ЧД в данный момент, ω – энергия частиц (использованы геометризованные единицы $G = c = 1$). Учитывая доминирующий вклад от мод с $l = s = 1/2$ для безмассового нейтрино

$$\Gamma_{\omega lmp} = M^2\omega^2, \tag{2}$$

а для массивных частиц с массой покоя μ и спином $1/2$

$$\Gamma_{\omega lmp} = \frac{2\pi(\omega + \mu)M^3\omega^3[1 + (1 - \mu^2/\omega^2)]}{1 - \exp\{-2\pi M\omega[1 + (1 - \mu^2/\omega^2)](1 - \mu^2/\omega^2)^{-1/2}\}}. \tag{3}$$

Спектр излучения $dN/dtd\omega$ задается подинтегральным выражением (1) с соответствующей подстановкой (2) или (3):

$$dN/dtd\omega = \Gamma_{\omega lmp}/(\exp(8\pi M\omega) + 1). \tag{4}$$

Ниже мы представим результаты расчетов для параметров ЧД, которые предположительно могли бы находиться в недрах Земли.

Спектр излучения безмассового нейтрино шварцшильдовской ЧД представляет собой почти симметричную колоколообразную кривую, положение максимума которой определяется массой ЧД. Для ЧД различных масс спектры приведены на рис. 1. Можно видеть, что энергетика излученных частиц весьма существенно зависит от этого единственного здесь параметра ЧД: так, если основная доля нейтрино, излучаемая дырой с $M > 10^{16}$ г попадает в область энергий менее 10 МэВ, то переход к ЧД с $M < 10^{12}$ г дает основной вклад от нейтрино с энергиями более 1 ГэВ, а для ЧД с $M < 10^{10}$ г – излучаются нейтрино с энергиями более 1 ТэВ. Это обстоятельство важно для анализа проблемы регистрации нейтрино, возникающих при квантовом испарении микро-ЧД, так как в отличие от солнечных, когда энергии не превышают 15 МэВ, в случае ЧД указанного диапазона масс следует ожидать значительно (на 3–4 порядка) более энергетических частиц, которые могут быть и легче зарегистрированы из-за большего сечения поглощения в веществе (см. ниже).

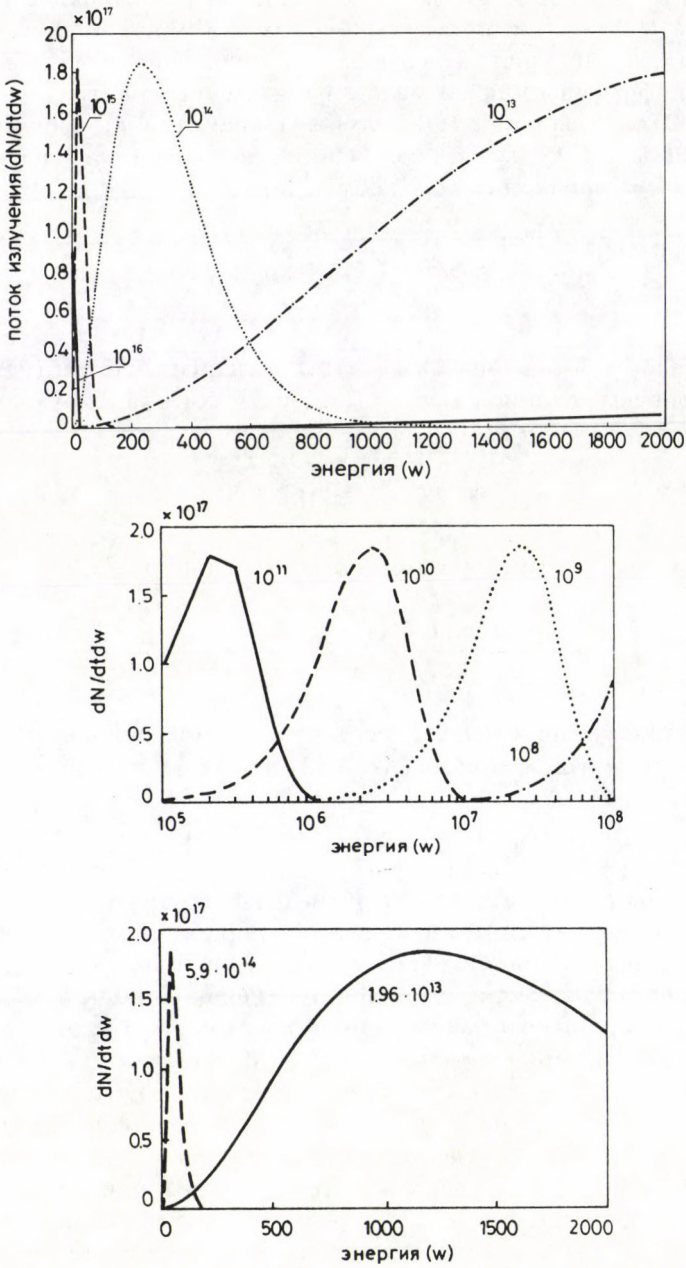

Рис. 1. Скорость излучения безмассовых нейтрино ЧД различных масс (числа около кривых, в г. $dN/dtd\omega$, частиц/сек·МэВ)

Положение максимума на спектре определяет область энергий нейтрино, которые следует ожидать от соответсвующих ЧД, и может быть определено из трансцендентного уравнения $\ln(x-2) = -x$, где $x = 8\pi M\omega_{\max}$, что дает (в геометризованных единицах)

$$\omega_{\max} = 1,8414/8\pi M.$$

Польный поток излучаемой энергии за счет рассматриваемого процесса в виде нейтрино (или поток частиц) по всему спектру либо по некоторому спектральному интервалу получается при интегрировании выражений для $dN/d\omega dt$ и также сильно возрастает с уменьшением массы ЧД.

Если допускать возможность массы покоя у нейтрино, что вполне вероятно по современным данным: $m(\nu_e) < 17$ эВ; $m(\nu_\mu) < 0,27$ МэВ; $m(\nu_\tau) < 35$ МэВ [15, 16], то представляет интерес проанализировать характер излучения этих частиц за счет эффекта Хокинга, т.е. частиц с теми же квантовыми числами, но обладающих ненулевой массой покоя по формуле (2). На рис. 2а показано влияние этой ненулевой массы покоя на спектр излучения, которое проявляется только для относительно массивных ЧД с $M > 10^{14}$ г для масс покоя в указанных пределах. Для нейтрино четвертого поколения [17], для которого оценка массы значительно больше: $m(\nu_4) \sim 45$ ГэВ, спектр излучения может существенно измениться, но испускание ν_4 тогда будет происходить наряду с другими тяжелыми частицами спина $1/2$ протонами, нейтронами, мюонами и др. Все значительно меньшие массы для ν_e и ν_μ для $M_{\text{ЧД}}$ менее $10^{14} - 10^{15}$ г практически не изменяют спектр и общий поток излучаемых нейтрино. В целом, характер спектра сходен с таковым для безмассовых частиц, а значения для полного потока и положение максимума спектра $dN/dtd\omega$ отличаются несущественно (рис. 2б). Вид спектров $dM/dtd\omega$ подобен таковым для числа частиц, и его интегрирование дает скорость потери масси ЧД, dM/dt, которая оказывается обратно пропорциональной M^2. В обычных единицах для потока безмассовых нейтрино получается

$$dN/dt = 7,275 \cdot 10^{33}/\text{м сек}^{-1},$$

а для массивных с массой покоя 10 МэВ

$$dN/dt = 1,133 \cdot 10^{34}/\text{м сек}^{-1},$$

а с массой покоя, соответствующей верхней оценке для ν_τ,

$$dN/dt = 1.151 \cdot 10^{34}/\text{м сек}^{-1}.$$

Для решения вопроса о регистрации нейтринного потока от ЧД, находящихся предположительно внутри планет, рассмотрим оценки для сечений поглощения нейтрино, например ν_e, за счет взаимодействий с электронами в невырожденном электронном газе (взаимодействия с нуклонами

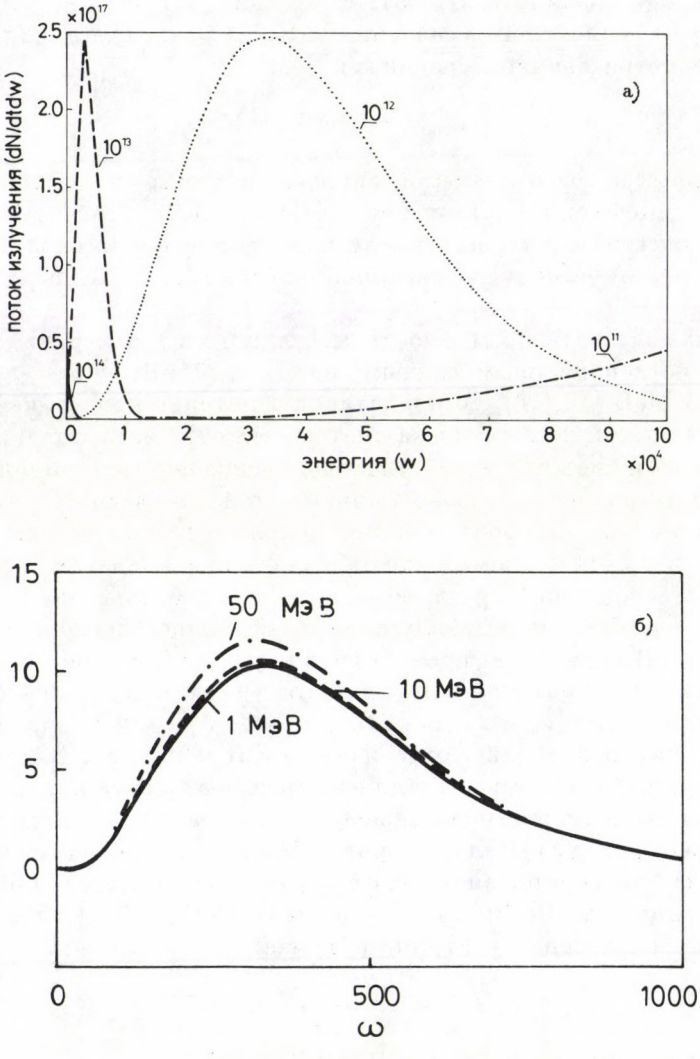

Рис. 2. Скорость излучения массивных ($m = 10$ МэВ) нейтрино ЧД различной массы (а) и влияние массы покоя нейтрино на вид энергетического спектра для ЧД с $M = 10^{14}$ г (в относительных единицах) – (б)

имеют меньшие сечения), которые могут иметь место при его детектировании. Величина сечения в сильной степени зависит от энергетики и определяется согласно следующим формулам [18]:

$$\sigma \approx 1,7 \cdot 10^{-44}(E_\nu/mc^2)^2, \quad E_\nu \ll mc^2, \tag{5}$$

$$\sigma \approx 0,85 \cdot 10^{-44}(E_\nu/mc^2), \quad E_\nu \gg mc^2, \tag{6}$$

где m – масса электрона.

Можно заметить, что в обоих случаях более вероятно детектирование частиц с более высокой энергией, доля которых велика для ЧД меньшей массы. В отличие от энергий солнечных нейтрино земные ЧД могут излучать нейтрино с энергиями более 10^3 МэВ, что на 2–3 порядка повышает сечение поглощения. Следовательно, при помещении детектора нейтрино на близком расстоянии от предполагаемого места локализации (выхода на поверхность) ЧД детекторы уже существующих конструкций должны фиксировать резкое превышение потока частиц по сравнению с фоновым и солнечным, причем направленность этого высокого потока будет свидетельствовать о возможном расположении его источника – ЧД. Одним из предполагаемых мест на Земле являются действующие вулканы [8, 10], однако существующие нейтринные детекторы располагаются безотносительно к геологической активности, в связи с чем ими и не могли быть зарегистрированы аномально высокие потоки от локализованных источников, так как они быстро убывают при удалении от источника.

Приведенные выше формулы отражают вклад в излучение от одного из видов частиц спина 1/2, а в действительности ЧД будет излучать и другие частицы [14, 19]. Для учета излучения нейтрино и антинейтрино трех поколений в случае их безмассовости вычисленные значения потока следует умножить на 6. Если же нейтрино имеют ненулевую массу покоя, то вклад каждого будет незначительно различаться, и для проблемы регистрации необходимо каждый тип нейтрино рассматривать в отдельности. Поскольку четвертый возможный тип нейтрино, по-видимому, если и существует, то обладает намного большей массой покоя, нежели остальные (≥ 45 ГэВ) [17], то его вклад в излучение ЧД будет проявляться уже после нуклонов и гиперонов для ЧД с $M \ll 10^{10}$ г.

3. Взрывы микро-ЧД и всплески нейтрино

Как можно убедиться, для ЧД с массами, наиболее интересными с точки зрения обсуждаемой модели ЧД в Земле, общий поток излучаемых частиц и, в частности нейтрино, столь значителен, что их масса может довольно быстро убывать, так что в течение некоторого времени ЧД полностью "сгорит" (конечное состояние при этом – это специальный вопрос [20]), излучая на последнем этапе очень энергетичные частицы. При этом в области рассматриваемого интервала масс еще остается справедливым подход без квантования гравитации и квазистационарное приближение, использованное при выборе результата о хокинговском излучении (хотя скорость излучения значительно возрастает), так как характерное время

жизни ЧД еще на много порядков больше характерных времен квантово-гравитационных эффектов – $t_{pl} \sim 10^{-44}$ с, и времени нахождения квантов на масшабах ЧД – r_g/c.

В связи с тем, что ЧД излучает не только нейтрино, точно определить темп потери массы за счет такого излучения и время жизни ЧД довольно трудно, но можно использовать оценки [21] на основании включения в состав излучающихся — частиц модели электрослабого взаимодействия [22], в которой фермионы со спином 1/2 составляют 90 видов частиц из 104. Это позволяет считать общий поток излучения приблизительно в 10^2 раз больше, чем за счет испускания нейтрино только одного типа. Тогда для времени существования ЧД получается $\tau = M^3/3\alpha$, где величина $\alpha \approx 10^{-3}$. Для ЧД из рассматриваемого диапазона масс, видимо, использование такой модели допустимо, так как "эффекты" Великого объединения будут давать вклад при энергиях около 10^{15} ГэВ. Для ЧД с $M = 10^8$ г и менее для α следует использовать большие значения. Время существования ЧД с массами $10^8 - 10^9$ г оказывается $0,001 - 1$ сек (не только за счет излучения ν), и такой ЧД соответсвует излучение ν с энергиями более 10^6 МэВ, что будет выглядеть как довольно кратковременный всплеск при его детектировании, а не какой-либо стационарный поток, который обычно регистрируется в экспериментах с нейтрино внеземного происхождения и нейтринными пучками, производящимися на ускорителях. Поэтому "сигнал" о нейтринном потоке от ЧД малой массы можно легко выделить на фоне малоизменяющегося космического. Но, очевидно, что это обстоятельство предъявляет специальные требования к регисрирующей аппаратуре и условиям постановки эксперимента.

ЧД с массой 10^{12} г, существующие десятки лет, можно считать предвзрывными, так как в течение ближайших лет наблюдений за потоком излучения от них будет фиксироваться рост энергии и интенсивности, все более резкий, и затем — всплеск (рис. 3). Уже для ЧД с $M \approx 10^{11}$ г τ окажется не более нескольких суток. Такое время может оказаться малым, чтобы однозначно зафиксировать микро-ЧД в том или ином месте и для изучения свойств нейтринного излучения.

Таким образом, несмотря на приближенный характер оценок, можно предложить наиболее вероятный диапазон масс ЧД ($10^{11} - 10^{12}$ г), и рассмотренные особенности их излучения, которое подтвердило бы обсуждаемую гипотезу.

При высокой интенсивности квантового излучения от микро-ЧД таких масс, находящихся предположительно внутри Земли, значительная часть будет переходить в тепловую энергию в результате взаимодействия частиц с веществом, но не будет сказываться на общем тепловом потоке из земных недр, так как для выхода тепловой волны на поверхность требуется более значительное время. Если в области центра нашей планеты имеются ЧД с предвзрывной массой, то можно вести эксперимент по исследованию последних этапов их испарения, причем нейтринные детекторы могут находиться в любой точке земной поверхности, а не только в геологиче-

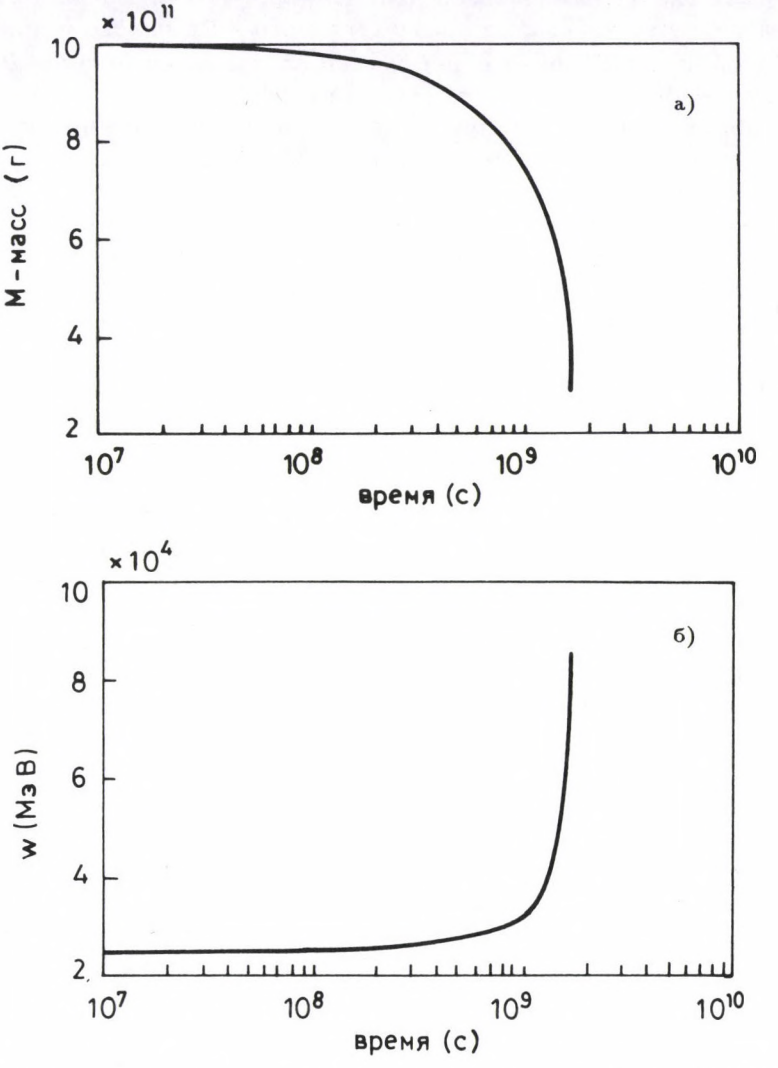

Рис. 3. Изменение массы ЧД с начальной массой 10^{12} г (а) и энергии, соответсвующей ω_{max} (б) со временем. Значения полного потока пропорциональны ω_{max}: $dN/dt = 2{,}9407 \cdot 10^{17} \cdot \omega_{max}$ (частиц/сек).

ски активных областях, так как особенности нестационарного излучения будут выделять излучение от таких объектов на общем фоне. Причем следует заметить, что область ядра Земли оказывается выделенной как наиболее древняя потенциальная яма, собирающая наиболее старые ЧД — менее массивные и короткоживущие; и концентрация таких ЧД в области

ядра может оказаться максимальной, что следует учитывать при выборе направления детектирования предполагаемого нейтринного потока.

Одной из характерных особенностей излучения от микро-ЧД из недр Земли может быть одиночность события взрыва ее на последних стадиях излучения, так как по мере приближения к конечной фазе влияние различия в массах ЧД на спектр излучения будет сказываться все острее, и чтобы ЧД взрывались одновременно, их массы должны оказаться практически равными, что маловероятно даже при их максимальном числе в Земле до $10^8 - 10^9$, ограниченным массой самой планеты и ее энергетикой. Распределены же ЧД по начальным массам могут быть весьма широко — от 10^{13} г до 10^{27} г [8]. Поэтому от взрывов совокупности ЧД следует ожидать некоррелированные одиночные всплески нейтринного излучения, существенно превышающие фоновый уровень, причем всплеску должно предшествовать более плавное возрастание как интенсивности так и энергии излучаемых частиц. Уровень фона может быть образован дополнительно к космическому и излучением ЧД с $M > 10^{12}$ г.

Проблема квантового излучения от малых ЧД, в том числе и нейтринного [23] в свое время вызывала значительный интерес, при допущении происхождения ЧД вследствие Большого взрыва, но, как показали расчеты [23–25], вклад ЧД в космический фон оказывается довольно малым, а определение верхнего наблюдательного предела на вспышки излучения в оптическом, радио- и гамма-диапазонах не дало оснований для утверждения такой гипотезы. Другими словами, микро-ЧД искали не там, где их можно зарегистрировать имеющимися средствами на Земле и в ближайшем космосе, поскольку наиболее характерное проявление таких объектов следует ожидать на малых расстояниях, что возможно для космических ЧД только при их самом ближайшем расположении от Земли. Необходимо отметить, что гипотеза о ЧД в недрах Земли совершенно не исключает и возможности образования ЧД космологического происхождения, в том числе и таких, которые могли и попасть внутри Земли и других небесных тел. Ожидать присутсвие ЧД в конденсированных телах более вероятно, нежели одиночных и изолированных, так как за длительное время их существования вполне реален гравитационный захват, а это обстоятельство в отношении Земли дает возможность постановки эксперимента по их регистрации. Следует отметить некоторую аналогию нейтринного проявления микро-ЧД с другим гипотетическим объектом — максимонами — частицами планковской массы (около 10^{-5} г), которые также должны иметь высокую проникающую способность в веществе Земли и могут служить источниками высокоэнергетичного излучения, нейтринная компонента которого может быть зарегистрирована [26]. Однако, в отличие от ЧД принципиальная возможность существования максимонов (планкеонов) остается открытой.

Кроме того, сопоставление теоретических и наблюдаемых характеристик излучения микро-ЧД при их регистрации может оказаться весьма полезным для уточнения теоретических положений относительно вза-

имодействий при сверхвысоких энергиях, т.е. ЧД могут оказаться полезной "лабораторией" для физики высоких энергий, теорий Великого объединения и единых теорий, и нейтринный эксперимент с излучением от ЧД может позволить продвинуться в область энергий, чем с нейтринными пучками, получаемыми на ускорителях [27]. При этом средства регистрации высокоэнергетичных нейтринных пучков [28], видимо, должны оказаться полезными и для излучения от микро-ЧД, так как поток излучения от ЧД, как можно видеть из данной работы, по энергетике оказывается довольно близким к получаемому искусственно. В частности, весьма популярные многомерные объединенные теории типа Калуцы – Клейна [29] без возможности непосредственной экспериментальной верификации приводят к значительному разнообразию схем и подходов к построению той или иной модели, а рассмотрение особенностей излучения ЧД в их многомерной трактовке [30–32], направленное на поиск экспериментально проверяемых фактов, может послужить средством выбора определенной теоретической схемы с дополнительными измерениями пространства-времени.

4. Заключение

Наиболее характерными свойствами потока нейтринного излучения от микро-ЧД, предположительно находящихся в недрах Земли, можно считать следующие:

1. энергии нейтрино должны превышать энергии солнечных нейтрино на 2–3 порядка и более, причем по мере расходования массы ЧД должно иметь место смещение в область более высоких энергий нейтрино;

2. излучение должно иметь тепловой энергетический спектр, максимум которого зависит от значения массы ЧД (и других ее параметров);

3. при малых массах ЧД — кратковременный характер излучения, возрастающий в течение нескольких суток с высокоэнергетичным всплеском в конце;

4. выраженная направленность излучения и резкое убывание интенсивности в зависимости от расстояния до предполагаемого источника.

По этим характеристикам ЧД в недрах Земли могут быть зарегистрированы нейтринными детекторами, в том числе и существующими, при соответствующем анализе экспериментальных данных и выборе условий для регистрации указанных особенностей.

На основании полученных данных можно предложить использование нейтринных детекторов (например, Камиоканде, IMB) для регистрации направленного из недр Земли потока частиц в области энергий 10 – 100 МэВ, а также поиск кратковременных или заметно меняющихся со временем потоков нейтрино сверхвысоких энергий 100 ГэВ – 1 ТэВ и более) в проектах Думанд и Байкальском [33, 34].

Таблица 1

Интервал энергетического спектра нейтринного излучения, и время существования микро-ЧД различных масс

M (г)	$\Delta\omega$ (МэВ)	$\tau = M^3 \cdot 1{,}74 \cdot 10^{30}/\alpha$ (сек)
10^9	$10^7 - 10^8$	$0{,}1 - 1$
10^{10}	$10^6 - 10^7$	$300 - 1000$
10^{11}	$10^5 - 10^6$	$2 \cdot 10^6$ (20 сут)
10^{12}	$10^4 - 10^5$	$2 \cdot 10^9$ (55 лет)
$1{,}96 \cdot 10^{13}$	$10^3 - 5 \cdot 10^3$	$\sim 10^{14}(4 \cdot 10^6$ лет)
$5{,}9 \cdot 10^{14}$	$50 - 500$	$\sim 10^{18}(3 \cdot 10^{10}$ лет)
10^{16}	$1 - 10$	$\sim 5 \cdot 10^{21}(1{,}5 \cdot 10^{14}$ лет)

Литература

1. S. L. Shapiro, S. A. Teukolsky, Black Holes, White Dwarfs and Neutron Stars, A Wiley-Interscience Publ., John Wiley & Sons, New York, 1983.
2. R. D. Blandford and K. S. Thorne, in: General Relativity: An Einstein Centenary Survey, Cambridge Univ. Press, Cambridge, 1979. Ch. 3.
3. M. S. Longair, High Energy Astrophysics, Cambridge Univ. Press, Cambridge, 1981.
4. Active Galactic Nuclei: Proc. 132th Symp. Int. Astron. Union. Santa Cruz, 1989, ed. D. E. Osterbrock, Dordrecht, etc. Kluwer Acad. Publ., 1989.
5. Я. Б. Зельдович, И. Д. Новиков, Астрон. журн., *43*, 758, 1966.
6. S. W. Hawking, Mon. Not. Roy. Astron. Soc., *152*, 75, 1971.
7. А. П. Трофименко, Принцип развития в астрофизике, Депонировано в ИНИОН АН СССР, 2027, 1978.
8. A. P. Trofimenko, Astrophys. Space Sci., *168*, 277, 1990.
9. J. Gribbin, New Scientist, No. 1732, 25, 1990.
10. A. P. Trofimenko, Bulg. Geophys. J., *15*, 80, 1990.
11. A. P. Trofimenko, Fizika (Yugoslavia), *22*, 545, 1990.
12. А. П. Трофименко, Белые и черные дыры во Вселенной, Университетское, Минск, 1991.
13. G. Greenstein and J. O. Burns, Amer. J. Phys., *52*, 531, 1984.
14. D. N. Page, Phys. Rev., *D13*, 198, 1976.
15. F. Boehm and P. Vogel, Physics of Massive Neutrinos, Cambridge Univ. Press, Cambridge, 1987.
16. Particle Data Group, Phys. Lett., *B259*, 1990.
17. C. T. Hill and E. A. Paschos, Phys. Lett., *B241*, 96, 1991.
18. K. R. Lang, Astrophysical Formulas, Springer Verlag, Berlin, 1974.
19. Black Holes: The Membrane Paradigm, ed. K. Thorne et al, Yale Univ. Press, New Haven and London, 1986.
20. N. D. Birrel and P. C. W. Dawies, Quantum Fields in Curved Space-Time, Cambridge Univ. Press, Cambridge, 1982.
21. J. Oliensis and C. T. Hill, Phys. Lett., *B143*, 92, 1984.
22. K. Gottfried and V. F. Weiskopf, Concepts of Particle Physics, Clarendon Press, Oxford, 1989.
23. Б. В. Вайнер, Астрофизика, *14*, 325, 1978.
24. J. V. Jelley, G. A. Baird and E. O'Mongain, Nature, *267*, 499, 1977.
25. N. A. Porter and T. C. Weekes, Astrophys. J., 212, 224, 1977; Nature, *267*, 500, 1977.
26. М. А. Марков, Журн. экспер. и теор. физики, *51*, 878, 1966.

27. L. M. Lederman, Rev. Mod. Phys., *61*, 547, 1989.
28. J. Steinberger, Rev. Mod. Phys., *61*, 533, 1989.
29. Ю. С. Владимиров, Размерность физического пространства-времени и объединение взаимодействий, МГУ, Москва, 1987.
30. V. S. Gurin and A. P. Trofimenko, Phys. Lett., *B241*, 328, 1990.
31. V. S. Gurin and A. P. Trofimenko, Hadronic J., *13*, 57, 1990.
32. V. S. Gurin and A. P. Trofimenko, Acta Phys. Hung., *67*, 275, 1990.
33. P. Kakas and D. Kiss, Acta Phys. Hung., *64*, 199, 1988.
34. A. M. Bakich, Space Sci. Rev., *49*, 259, 1989.

Acta Physica Hungarica 72 (2-4), pp. 183–192 (1992)

DIELECTRIC SCREENINGS AND ELASTIC AND THERMODYNAMIC PROPERTIES OF METALLIC GLASSES

P. C. AGARWAL, K. A. AZEZ* and C. M. KACHHAVA

Department of Physics, University of Rajasthan
Jaipur-302004, India
**Department of Physics, Jordan University of Science and Technology*
Irbid, Jordan

(Received 31 July 1992)

The elastic and thermodynamic properties of metallic glasses ($Ca_{70}Mg_{30}$, $Mg_{70}Zn_{30}$, $Cu_{57}Zr_{43}$ and $Pd_{77.5}Si_{16.5}Cu_6$) are obtained from dispersion relations in the low momentum region derived by us for various dielectric screenings, adopting a simple model given by Bhatia and Singh. This model assumes a central force, effective between nearest neighbours and a volume dependent force. For elastic properties, elastic constants C_{11} and C_{44} are obtained from slopes of longitudinal and transverse dispersion relations, respectively, whereas C_{12} is found by the requirement that elastic anisotropy for disordered systems, like metallic glass, is to be zero. For thermodynamic properties, Debye temperature is calculated for the glasses for various dielectric screenings.

1. Introduction

The advent of metallic glasses [1] has been one of the most exciting events in the fields of the material science and engineering. In recent years, metallic glasses have exhibited a remarkable and widespread development and a broad spectrum of applications [2–5]. This has motivated us to study the elastic and thermodynamic properties of binary ($Ca_{70}Mg_{30}$, $Mg_{70}Zn_{30}$ and $Cu_{57}Zr_{43}$) and ternary ($Pd_{77.5}Si_{16.5}Cu_6$) metallic glasses for various dielectric screenings due to conduction electrons through one of their dynamical properties, viz. the dispersion relation.

Theoretically, dispersion relations for the glass $Ca_{70}Mg_{30}$ have been derived by Hafner [6] taking $S(q,\omega)$, by Bhatia and Singh [7] using a model approach. In this approach a central force, effective between the nearest neighbours, and a volume dependent force is assumed. Saxena et al [8] derived them by choosing an interatomic potential and employing the method as proposed by Hubbard and Beeby [9]. Suck et al [10] derived them experimentally by taking neutron inelastic scattering data on $S(q,\omega)$. The dynamical properties of the glass $Mg_{70}Zn_{30}$ have been studied theoretically by von Heimendahl [11] using the equation of motion method, by Tomanek [12] using a model calculation, by Saxena et al [13] using the interatomic potential and employing the method proposed by Takeno and Goda [14], by Agarwal and Kachhava [15] using the model approach. Experimentally, the dispersion relation of longitudinal phonon frequencies for $Mg_{70}Zn_{30}$ glass was

determined by Suck et al [16] for a few momentum transfers near q_p ($= 2.61 \times 10^{10}$ m^{-1}, at which the first peak is found in static structure factor calculation) for the first time. Theoretically the vibrational dynamics of the glass $Cu_{57}Zr_{43}$ has been studied by Kobayashi and Takeuchi [17] using recursion method and by us [18] using the model approach; while no experimental data are available for the glass. The phonon dispersion relations for the glass $Pd_{77.5}Si_{16.5}Cu_6$ were derived by Agarwal and Kachhava [19] for the first time using the model approach, while no experimental data are available. We have experimental data for $Ca_{70}Mg_{30}$ only for lower wavelengths and for $Mg_{70}Zn_{30}$ only for a few momentum transfers around q_p. However, no experimental data are available for higher wavelengths, where the first peak is observed in the above theories. Moreover, the screening due to conduction electrons in this region contributes quite significantly to the phonon frequencies. In other words, in this region the $\omega - q$ relations are sensitive to the dielectric screening due to conduction electrons. For the other regions, the $\omega - q$ relations given by Bhatia and Singh [7] for $Ca_{70}Mg_{30}$ glass and by Agarwal and Kachhava [15] for $Mg_{70}Zn_{30}$ glass are in good agreement with the available experimental data. Dispersion relations of metallic glasses for various dielectric screenings due to conduction electrons in the region of higher wavelength are derived [20] following the model given by Bhatia and Singh [7]. To evaluate the elastic moduli of metallic glasses as Young's modulus (E), Bulk modulus (B) and Shear modulus (G) for various screenings, elastic constant C_{11} is obtained by taking the slope of corresponding longitudinal dispersion relation, C_{44} is obtained by taking the slope of transverse dispersion relation, whereas C_{12} is obtained by the requirement that elastic anisotropy, for disordered systems, like metallic glasses, is to be zero. Corresponding sound velocities are used to calculate Debye temperature for various dielectric screenings.

2. Theory

Consider a metallic glass having the coordination number N, the nearest neighbour distance a and mean atomic density $\rho = n_i M$, in which n_i is the ion density and $M = \sum_i C_i M_i$ is the mean atomic mass. M_i is the atomic mass of the i-th component of metallic glass with concentration C_i. n_e is the electron number density so that $n_e = n_i z$ and $z = \sum_i C_i z_i$ is the mean valence of glassy system. $k_F = (3\pi^2 n_e)^{1/3}$ is the Fermi wave number.

One of the simplest methods of evaluating the phonon frequencies is the force constant model in which the force constants β and δ are derived from the interatomic potential $W(r)$, as

$$\beta = (\rho a^2/(2M))[(1/r)(dW(r)/dr)]_{r=a}, \tag{1}$$

$$\delta = (\rho a^3/(2M))[d/dr[(1/r)(dW(r)/dr)]]_{r=a}. \tag{2}$$

The contribution of the conduction electrons to the phonon frequencies is explicitly represented by force constant κ_e which can be written on the basis of the Thomas–

Fermi model as

$$\kappa_e = 4\pi n_i^2 z^2 e^2 / K_{\mathrm{TF}}^2. \tag{3}$$

Here e is the charge of electron and $K_{\mathrm{TF}}^2 = 4k_{\mathrm{F}}/(n\alpha_0)$ is the Thomas–Fermi screening length, in which α_0 is the Bohr radius.

The expressions for the longitudinal (ω_L) and transverse phonon frequencies (ω_T) given by Bhatia and Singh [7] can be written as

$$\omega_L^2 = C[\beta I_0 + \delta I_2] + \kappa_e K_{\mathrm{TF}}^2 [G(qr_s)]^2/(\rho\epsilon(q)) \tag{4}$$

and

$$\omega_T^2 = C[(\beta + \delta/2)I_0 - \delta I_2/2], \tag{5}$$

with $C = 2N/(\rho a^2)$. Here

$$I_n = \int_0^{\pi} \sin\Theta \cos^n\Theta \left[\sin^2\left(\frac{1}{2} qa\cos\Theta\right)\right] d\Theta, \tag{6}$$

where q is the momentum wave vector and Θ is the angle between the unit vector along the displacement of the wave and the vector joining the atom at origin to one of its nearest neighbours.

The cancellation effects of kinetic and potential energies inside the core of ions making the effective potential weak in core gives a shape factor, $[G(qr_s)]^2$, as in Eq. (4), and is of the form [21]

$$[G(qr_s)]^2 = [3(\sin(qr_s) - (qr_s)\cos(qr_s))/(qr_s)^3]^2, \tag{7}$$

where $r_s = [3/(4\pi n_i)]^{1/3}$ is the radius of Wigner–Seitz sphere.

In Eq. (4), $\epsilon(q)$ is the dielectric screening function. To know the dielectric screening dependence of the phonon dispersion curve for longitudinal mode of vibrations we consider the screening functions [22, 23] due to Hartree (H), Hubbard (HB), Geldart and Vosko (GV) and Self-Consistent Screening due to Shaw [24] (SCS) and Overhauser (OH). Representing the Hartree function by $\epsilon_{\mathrm{H}}(q)$ and

$$\epsilon_{\mathrm{H}}(q) = 1 + Q_0(q), \tag{8}$$

where

$$Q_0(q) = (K_{\mathrm{TF}}^2/q^2) f(x) \quad \text{with} \quad x = q/k_{\mathrm{F}} \tag{9}$$

and

$$f(x) = 0.5 + ((4 - x^2)/(8x)) \ln\left|\frac{2+x}{2-x}\right|. \tag{10}$$

The HB, GV, SCS and OH screening functions are given by

$$\epsilon(q) = 1 + Q_0(q)/(1 - f(q)Q_0(q)), \tag{11}$$

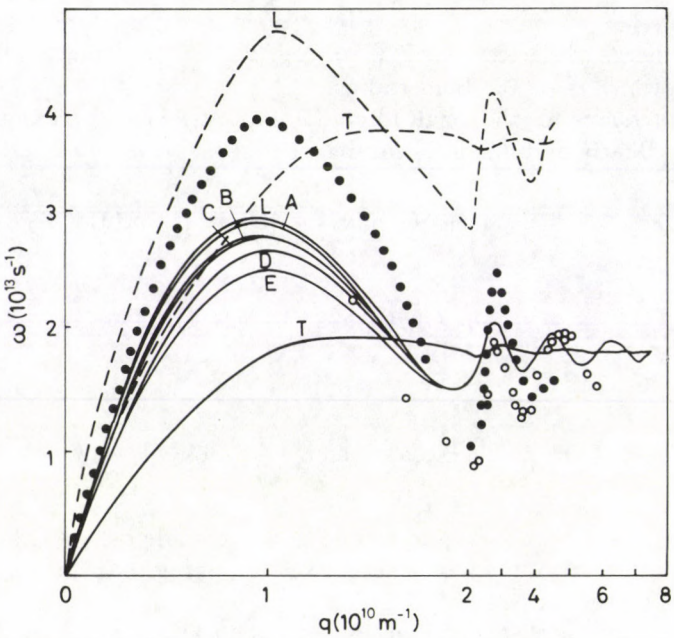

Fig. 1. Dispersion relations for $Ca_{70}Mg_{30}$. ω_L (—) and ω_T (—) on the basis of Eqs (4) and (5) derived by Bhatia and Singh (Ref. [7]); ω_L (- - -) and ω_T (- - -) by Saxena et al (Ref. [8]); •, those due to Hafner (Ref. [6]) from calculations of $S(q,\omega)$; ○ experimental points from neutron scattering (Ref. [10])

where

$$f_{\mathrm{HB}}(q) = 0.5q^2/(q^2 + k_{\mathrm{F}}^2 + K_{\mathrm{TF}}^2), \tag{12}$$

$$f_{\mathrm{GV}}(q) = 0.5q^2/(q^2 + \nu k_{\mathrm{F}}^2) \quad \text{with} \quad \nu = 2/(1 + .153\,(K_{\mathrm{TF}}^2/4k_{\mathrm{F}}^2)), \tag{13}$$

$$f_{\mathrm{SCS}}(q) = A[1 - \exp(-B(q/k_{\mathrm{F}})^2)] \quad \text{with} \quad A = 1 \quad \text{and} \quad B = 0.535 \tag{14}$$

and

$$f_{\mathrm{OH}}(q) = 0.275\,(q/k_{\mathrm{F}})^2/[1 + 2.5\,(q/k_{\mathrm{F}})^2 + .09375\,(q/k_{\mathrm{F}})^4]^{1/2}. \tag{15}$$

For the limiting case $q \to 0$ (low momentum region) Eqs (4) and (5) provide longitudinal and transverse sound velocities, respectively, as $V_L(0) = \omega_L/q$ and $V_T(0) = \omega_T/q$ as

$$\rho V_L^2(0) = N\left(\frac{1}{3}\beta + \frac{1}{5}\delta\right) + \kappa_e, \tag{16}$$

$$\rho V_T^2(0) = N\left(\frac{1}{3}\beta + \frac{1}{15}\delta\right). \tag{17}$$

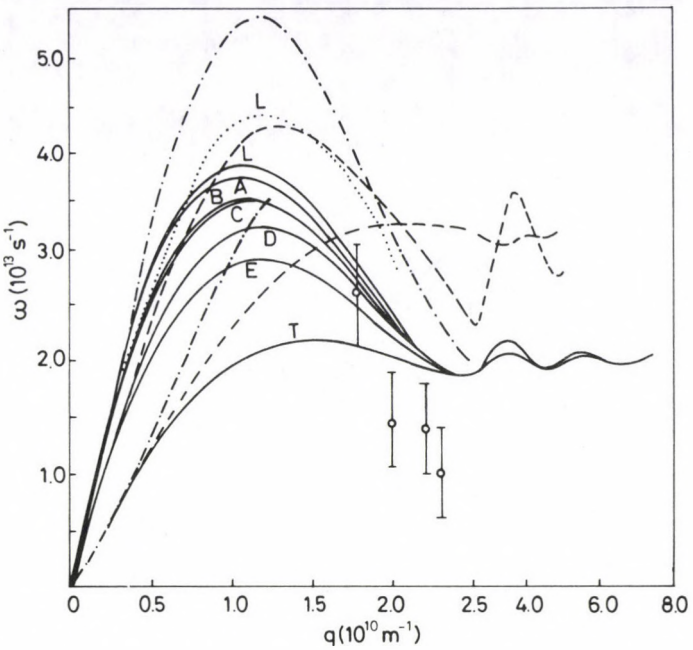

Fig. 2. Dispersion relations for $Mg_{70}Zn_{30}$. ω_L (—) and ω_T (—) on the basis of Eqs (4) and (5) derived by Agarwal and Kachhava (Ref. [15]); ω_L (- - -) and ω_T (- - -) by Saxena et al (Ref. [13]); - . - . - due to molecular dynamics (Ref. [11]); . . . . model calculations of Tomanek (Ref. [12], Φ; experimental data from Suck et al (Ref. [16])

The elastic moduli E, B and G for glassy materials are given as [25]

$$E = (C_{11} - C_{12})(C_{11} + 2C_{12})/(C_{11} + C_{12}), \tag{18}$$

$$B = (C_{11} + 2C_{12})/3, \tag{19}$$

$$G = 3EB/(9B - E), \tag{20}$$

where $C_{11} = \rho V_L^2(0)$ and $C_{12} = C_{11} - 2C_{44}$ in which $C_{44} = \rho V_T^2(0)$. The Debye temperature is defined as [6]

$$\Theta_D = \frac{h}{k_B}\left[\frac{9n_i}{4\pi}\right]^{1/3}\left[\frac{1}{V_L^3} + \frac{1}{V_T^3}\right]^{-1/3}. \tag{21}$$

3. Calculations, results and discussion

To calculate the elastic moduli and Debye temperature of metallic glasses using the screening used by Bhatia and Singh (ABB–RNS) [7], the values of $V_L(0)$,

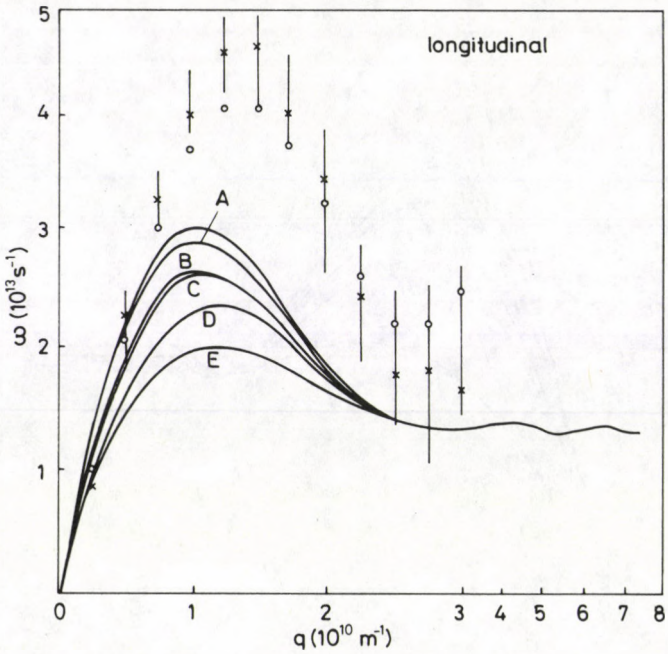

Fig. 3. $\omega_L - q$ dispersion relations for $Cu_{57}Zr_{43}$ on the basis of Eq. (4) derived by us (Ref. [18]). Vertical bars denote the positions of the first moment; crosses denote the peak positions (Ref. [17])

$V_T(0)$ and n_i for glasses $Ca_{70}Mg_{30}$ and $Mg_{70}Zn_{30}$ are taken from Hafner [6] and Vitek [26], respectively, while $V_L(0)$ $V_T(0)$ and ρ are taken from Kobayashi and Takeuchi [17] for $Cu_{57}Zr_{43}$ and from Golding et al [27] for $Pd_{77.5}Si_{16.5}Cu_6$. Relation $\rho = n_i M$ is used to calculate ρ or n_i, as the case may be. The nearest neighbour distance a is calculated by the relation $n_i a^3 = \sqrt{2}$ for FCC structure as for $Ca_{70}Mg_{30}$, $Cu_{57}Zr_{43}$ and $Pd_{77.5}Si_{16.5}Cu_6$ and by $n_i a^3 = (4/\sqrt{3})(c/a)$ for HCP structure as for $Mg_{70}Zn_{30}$. κ_e is calculated by using Eq. (3).

By substituting the values of ρ, $V_L(0)$, $V_T(0)$ and κ_e in Eqs (16) and (17), β and δ are found and hence the $\omega_L - q$ dispersion curves are obtained on the basis of Eq. (4) corresponding to various forms of screening given by Eqs (8, 12–15). $\omega_T - q$ dispersion curve is obtained on the basis of Eq. (5) which does not involve screening function.

To calculate elastic moduli and Debye temperature of glassy materials for various dielectric screenings due to conduction electrons, longitudinal sound velocity for a particular dielectric screening is obtained by taking slope of corresponding $\omega_L - q$ (longitudinal dispersion relations) curve whereas transverse dispersion relations are screening independent and transverse sound velocity is obtained by taking slope of $\omega_T - q$ (transverse dispersion relations) curve, in the higher wavelength region. The results for elastic moduli (E, B and G) and Debye temperature (Θ_D) for these

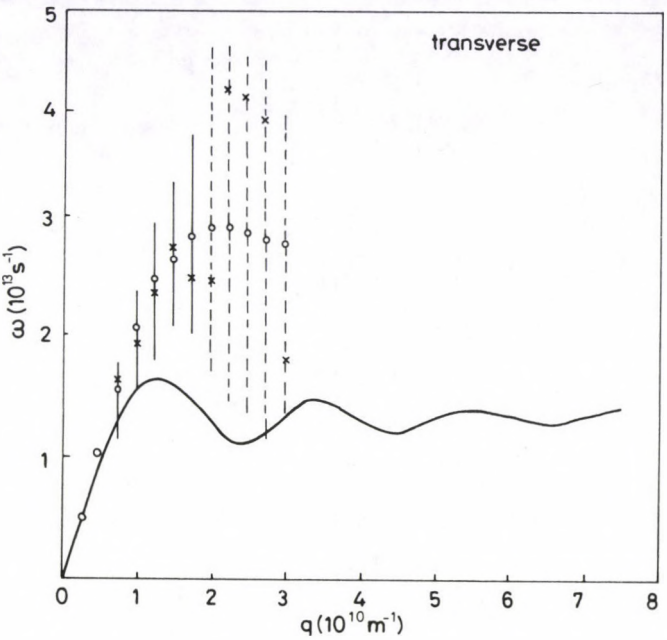

Fig. 4. $\omega_T - q$ dispersion relations for $Cu_{57}Zr_{43}$ on the basis of Eq. (5) derived by us (Ref. [18]). Vertical bars denote the positions of the first moment; crosses denote the peak positions (Ref. [17])

different screenings are calculated using Eqs (18–21) and are given in Table I.

Figure 1 gives $\omega - q$ relations for the metallic glass $Ca_{70}Mg_{30}$ both for longitudinal and transverse phonons. In this Figure as well as in Figs 2, 3 and 5, curves A, B, C, D and E represent $\omega_L - q$ dispersion relations on the basis of Eq. (4) with Hartree, Hubbard, Overhauser, Geldart–Vosko and self-consistent dielectric screening due to conduction electrons, respectively. It is apparent from the Figure that no experimental data are available for lower momentum ($q \to 0$) region. Figure 2 gives $\omega - q$ relations for $Mg_{70}Zn_{30}$ and shows that no experimental data are available at lower q values. Figures 3–4 give $\omega - q$ relations for $Cu_{57}Zr_{43}$ and Fig. 5 gives $\omega - q$ relations for $Pd_{77.5}Si_{16.5}Cu_6$; while no experimental data are available for these two glasses.

It is apparent from $\omega_L - q$ curves of the glassy materials that they are screening sensitive in low momentum region. The difference in $\omega_L - q$ relations begins right from the starting value of q and it becomes maximum at the first peak of the $\omega_L - q$ curve, again it tends to decrease and all the $\omega_L - q$ relations seem to converge at the q values, where the first peak of static structure factor calculation is found as is obvious in $Ca_{70}Mg_{30}$ at $q = 2.0 \times 10^{10}$ m^{-1} and in $Mg_{70}Zn_{30}$ at $q = 2.6 \times 10^{10}$ m^{-1}. After this q value $\omega_L - q$ relations are screening independent. The position of the first peak is independent of the screening; however, the height of the peak strongly

Table I

Elastic moduli (E, B and G) and Debye temperature (Θ_D) for metallic glasses $Ca_{70}Mg_{30}$, $Mg_{70}Zn_{30}$, $Cu_{57}Zr_{43}$ and $Pd_{77.5}Si_{16.5}Cu_6$ using different dielectric functions $\epsilon(q)$ including that used by Bhatia and Singh (ABB–RNS) [7]

	$Ca_{70}Mg_{30}$				$Mg_{70}Zn_{30}$				$Cu_{57}Zr_{43}$				$Pd_{77.5}Si_{16.5}Cu_6$			
	E	B	G	Θ_D	E	B	G	Θ_D	E	B	G	Θ_D	E	B	G	Θ_D
$\epsilon(q)$	(10^{10} Nm^{-2})			(K)	(10^{10} Nm^{-2})			(K)	(10^{10} Nm^{-2})			(K)	(10^{10} Nm^{-2})			(K)
ABB–RNS	1.90	2.40	0.69	261.87	6.01	8.25	2.17	351.11	5.79	5.81	2.17	339.26	9.60	18.30	3.39	312.05
H	1.89	2.26	0.69	261.36	5.99	8.04	2.17	350.83	5.49	3.93	2.16	338.16	9.57	17.26	3.39	311.67
HB	1.86	1.98	0.69	260.24	5.87	6.40	2.17	348.25	5.51	3.98	2.17	333.39	9.41	13.66	3.39	309.78
OH	1.85	1.85	0.69	259.58	5.81	4.37	2.17	347.06	5.78	5.79	2.16	333.08	9.38	13.06	3.39	309.44
GV	1.77	1.35	0.69	256.29	5.48	3.76	2.17	340.88	4.48	1.59	2.17	320.23	9.06	9.06	3.39	305.69
SCS	1.75	1.23	0.69	255.28	5.22	2.89	2.17	336.82	4.91	2.22	2.16	325.17	8.88	7.62	3.40	303.60

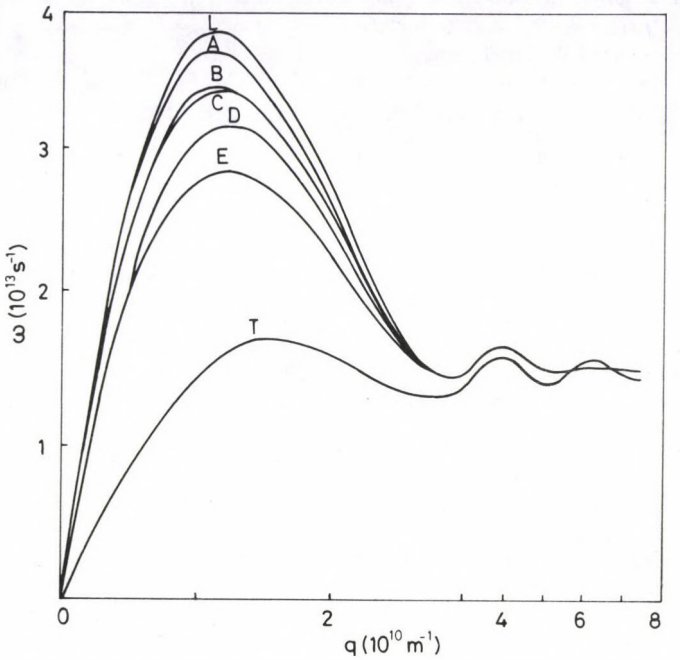

Fig. 5. Dispersion relations for $Pd_{77.5}Si_{16.5}Cu_6$ derived by Agarwal and Kachhava (Ref. [19])

depends on the screening. Most of the thermodynamical, transport and elastic properties of the substance are derived from this part of the curve. Therefore, to determine the appropriateness of particular screening due to conduction electrons, accurate experimental data of phonon frequencies are needed in this low momentum region and specially around the first peak of the $\omega_L - q$ curve.

Acknowledgements

We are thankful to Prof. R. N. Singh (Bhagalpur University, Bihar) for his valuable suggestions and discussion. One of us (P. C. Agarwal) acknowledges with gratitude the Senior Research Fellowship (NET) offered to him by CSIR, New Delhi.

References

1. W. Klement, R. H. Willens and P. Duwez, Nature, *187*, 869, 1960.
2. T. R. Anantharaman, Metallic Glasses: Production, Properties and Applications, Trans. Tech. Publications, Aedermannsdorf, Switzerland, 1984.
3. A. Hernando, M. Vázquez and J. M. Barandiarán, J. Phys. E *21*, 1129, 1988.

4. H. A. Rafizadeh, Can. J. Phys. *68*, 23, 1990.
5. Guang-Lin Zhao, Yi He and W. Y. Ching, Phys. Rev. B, *42*, 10887, 1990.
6. J. Hafner, Phys. Rev. B, *27*, 678, 1983.
7. A. B. Bhatia and R. N. Singh, Phys. Rev. B *31*, 4751, 1985.
8. N. S. Saxena, Arun Pratap, Deepika Bhandari and M. P. Saksena, Materials Science and Engineering, A *134*, 927, 1991.
9. J. Hubbard and L. Beeby, J. Phys. C *2*, 556, 1969.
10. J. B. Suck, H. Rudin, H.-J. Güntherodt, D. Tomanek, H. Beck, C. Morkel and W. Gläser, J. Phys. (Paris) Collq. *41*, C8-175, 1980.
11. L. von Heimendahl, J. Phys. F *9*, 161, 1979.
12. D. Tomanek, Diplomarbeit, Universität Basel, 1979.
13. N. S. Saxena, Deepika Bhandari, Arun Pratap and M. P. Saksena, J. Phys. C *2*, 9475, 1990.
14. S. Takeno and M. Goda, Prog. Theor. Phys., *45*, 331, 1971.
15. P. C. Agarwal and C. M. Kachhava, Physica B, *179*, 43, 1992.
16. J. B. Suck, H. Rudin, H.-J. Güntherodt and H. Beck, J. Phys. C *13*, L1045, 1980.
17. S. Kobayashi and S. Takeuchi, J. Phys. C *13*, L969, 1980.
18. P. C. Agarwal, K. A. Azez and C. M. Kachhava, Acta Phys. Hung., *71*, 211, 1992.
19. P. C. Agarwal and C. M. Kachhava, Phys. Stat. Sol. (b), *170*, K87, 1992.
20. P. C. Agarwal, K. A. Azez and C. M. Kachhava, Physica B, (communicated).
21. L. J. Sham and J. M. Ziman, Solid State Phys. Vol. *15*, eds F. Seitz and D. Turnbull, Academic, New York, 1963, p. 259.
22. C. M. Kachhava, Physica, *65*, 63, 1973.
23. C. M. Kachhava, Solid State Commun., *11*, 1439, 1972.
24. R. W. Shaw, J. Phys. *C3*, 1140, 1970.
25. Glassy Metals II, eds H. Beck and H.-J. Güntherodt, Springer Verlag, Berlin, 1983, p. 170.
26. J. Hafner, Amorphous Materials, ed. V. Vitek, American Institute of Mining, Metallurgical and Petroleum Engineers, New York, 1983, p. 217.
27. B. Golding, B. G. Bagley and F. S. L. Hsu, Phys. Rev. Lett., *29*, 68, 1972.

Acta Physica Hungarica 72 (2-4), pp. 193–202 (1992)

TRAVELLING WAVE SOLUTIONS OF DENSITY DEPENDENT DIFFUSION EQUATIONS

E. V. KRISHNAN

Department of Mathematics and Computing, Sultan Qaboos University
Alkhod, Muscat, Sultanate of Oman

(Received 4 August 1992)

Travelling wave solutions for two nonlinear diffusion equations have been found by a direct method. The behaviour of solutions for these equations with c and the parameter α in the problem varying have been investigated numerically as a boundary value problem. The equilibrium solutions ($c = 0$) of these equations have been found in terms of Weierstrass elliptic functions.

1. Introduction

The prototype for the spatial diffusion of biological populations in population dynamics is taken as [1]

$$u_t = (u^2)_{xx} + F(u). \tag{1.1}$$

The first term on the right-hand side of Eq. (1.1) represents density dependent diffusion and the second term describes population supply due to births and deaths. The phenomena like flow of liquids in porous media, the transport of thermal energy in plasma etc. have also (1.1) as the governing equation. The exact solutions for Eq. (1.1) have been presented by Gurtin and MacCamy [2], Newman [3] and Hosono [4]. Gurtin and MacCamy considered the case $F(u) = \mu u$ and then by variable transformations, $w = e^{\mu t} \cdot w$ and $\tau = (e^{\mu t} - 1)/\mu$ reduced (1.1) to

$$w_\tau = (w^2)_{xx}, \tag{1.2}$$

for which similarity solutions are known. Newman considered the case with $F(u) = u(u-1)$ and Hosono showed that the travelling wave solutions $u = u(x - ct)$ of Eq. (1.1) with $F(u) = u(u-1)(\alpha - u)$ varies its profile with the sign of the velocity c. Satsuma [5] chose the same $F(u)$ as that of Hosono and found an explicit expression for the travelling wave solution using Painlevé analysis. Ablowitz and Zeppetella [6] used the same method to obtain a travelling wave solution of Fisher's equation

$$u_t = u_{xx} + u(1-u). \tag{1.3}$$

In this paper, we have found explicit travelling wave solutions of

$$u_t = vu_{xx} + su(1-u), \tag{1.4}$$

$$u_t = vu_{xx} + su(1-u)(\alpha - u). \tag{1.5}$$

by a direct method [7]. Here, v is the coefficient of diffusion and s is the advantageous selection intensity in the propagation of a mutant gene. Also, we have investigated the numerical solutions of these equations as a boundary value problem using a deferred correction technique and Newton iteration. We have investigated the analytical solutions of these equations in terms of Weierstrass elliptic functions when $c = 0$, that is, the travelling wave solutions in an equilibrium state.

Here, we have taken the diffusion term as a linear one which is the case in Fisher's equation. We intend to consider the nonlinear case $(u^2)_{xx}$ elsewhere.

2. Direct method and Fisher's equation

In the direct method the solution is expressed as the sum of hyperbolic functions in the form

$$u(z) = \sum_{i=0}^{m} a_i \tanh^i \mu z, \tag{2.1}$$

where the expansion coefficient $\{a_i\}_0^m$, order of expansion m, and wave number μ are to be determined. The essential idea is that we balance the highest nonlinear term and derivative term for the above combination and then equate the like powers of the function on both sides of the equation. It can be immediately seen that a derivative term u_{nz} of n^{th} order has highest power in $\tanh \mu z$ of $m+n$. Therefore, for equations in u possessing a highest derivative term of order d and highest nonlinear term u^h, we have,

$$m = \frac{d}{h-1}. \tag{2.2}$$

The coefficients $\{a_i\}$ are found by solving a coupled set of nonlinear algebraic equations. To be exact, consider the case that the nonlinear differential equation for u has highest derivative term of order d. There result $m + d + 1$ equations for the $(m+1)$ a_i's, single wave number μ and any constants of integration.

The equation proposed by Fisher to describe the propagation of a mutant gene with an advantageous selection intensity s is given by [8]

$$u_t = vu_{xx} + su(1-u), \tag{2.3}$$

where v is the coefficient of diffusion. Considering the travelling wave solution

$$u = u(z) = u(x - ct), \tag{2.4}$$

Eq. (2.3) reduces to

$$v u_{zz} + c u_z + s u(1-u) = 0. \tag{2.5}$$

Consistent with Eq. (2.2), we have $m = 2$ and so we assume a solution of Eq. (2.5) in the form

$$u(z) = a_0 + a_1 \tanh(\mu z) + a_2 \tanh^2(\mu z), \tag{2.6}$$

where a_0, a_1, a_2 and μ are parameters to be determined later.

Substituting (2.6) in Eq. (2.5) and equating like powers of $\tanh(\mu z)$ on both sides, we get

$$6a_2\mu^2 v - s a_2^2 = 0 \tag{2.7}$$

$$2a_1\mu^2 v - 2a_2 c\mu - 2s a_1 a_2 = 0, \tag{2.8}$$

$$-8a_2\mu^2 v - a_1 c\mu + s a_2 - s a_1^2 - 2s a_0 a_2 = 0, \tag{2.9}$$

$$-2a_1\mu^2 v + 2a_2 c\mu + s a_1 - 2s a_0 a_1 = 0, \tag{2.10}$$

$$2a_2\mu^2 v + a_1 c\mu + s a_0 - s a_0^2 = 0. \tag{2.11}$$

From Eq. (2.7)–(2.11), we get

$$\mu = (s/24v)^{1/2}, \tag{2.12}$$

$$a_0 = \frac{1}{2} - \frac{4\mu^2 v}{s} - \frac{c^2}{50vs}, \tag{2.13}$$

$$a_1 = -\frac{6\mu c}{5s}, \tag{2.14}$$

$$a_2 = \frac{6\mu^2 v}{s}, \tag{2.15}$$

$$c = 10\mu v. \tag{2.16}$$

Therefore, for the existence of the travelling wave solution of (2.5) in the form (2.6), the parameters s and v should be of the same signs. Now, using expressions (2.12)–(2.16) it may easily be seen that

$$a_0 = \frac{1}{4}, \tag{2.17}$$

$$a_1 = -\frac{1}{2}, \tag{2.18}$$

$$a_2 = \frac{1}{4}. \tag{2.19}$$

Hence, our required solution is,

$$u(z) = \frac{1}{4} - \frac{1}{2}\tanh\left(\frac{s}{24v}\right)^{1/2} z + \frac{1}{4}\tanh^2\left(\frac{s}{24v}\right)^{1/2} z. \tag{2.20}$$

So, the Fisher's equation (2.3) has the explicit solution

$$u(x,t) = \frac{1}{4} - \frac{1}{2}\tanh\left(\frac{s}{24v}\right)^{1/2}(x-ct) + \frac{1}{4}\tanh^2\left(\frac{s}{24v}\right)^{1/2}(x-ct), \tag{2.21}$$

where

$$c = \left(\frac{25sv}{6}\right)^{1/2}. \tag{2.22}$$

3. Equation with higher nonlinearity

The equation under consideration is

$$u_t = vu_{xx} + su(1-u)(\alpha - u), \tag{3.1}$$

which is assumed to have a travelling wave solution in the form

$$u = u(z) = u(x - ct), \tag{3.2}$$

so that (3.1) reduces to

$$vu_{zz} + cu_z + su(1-u)(\alpha - u) = 0. \tag{3.3}$$

Here, $m = 1$ and so we assume a solution of Eq. (3.3) in the form

$$u(z) = a_0 + a_1\tanh(\mu z), \tag{3.4}$$

where a_0, a_1 and μ are parameters which will be determined later. Substituting (3.4) in (3.3) and equating like powers of $\tanh(\mu z)$ on both sides, we get

$$sa_1^3 + 2v\mu^2 a_1 = 0, \tag{3.5}$$

$$3a_0a_1^2 s - s(\alpha+1)a_1^2 - ca_1\mu = 0, \tag{3.6}$$

$$3a_0^2a_1 s - 2sa_0a_1(\alpha+1) + \alpha sa_1 - 2v\mu^2 a_1 = 0, \tag{3.7}$$

$$sa_0^3 - s(\alpha+1)a_0^2 + \alpha sa_0 + ca_1\mu = 0. \tag{3.8}$$

From Eq. (3.5)–(3.8) we get

$$\mu^2 = \frac{-sa_1^2}{2v}, \tag{3.9}$$

$$a_0 = \frac{\alpha+1}{3} + \frac{c}{3s}\sqrt{-s/2v}, \tag{3.10}$$

$$a_1^2 = 2a_0(\alpha+1) - 3a_0^2 - \alpha, \tag{3.11}$$

$$8a_0^3 - 8(\alpha+1)a_0^2 + 2(\alpha^2+3\alpha+1)a_0 - \alpha(\alpha+1) = 0. \tag{3.12}$$

Expressions (3.9) and (3.10) clearly indicate that for a solution in the form (3.4) to exist, s and v should be of opposite signs.

The quadratic expression in a_0 on the R. H. S. of (3.11) takes both negative and positive values. But since it is an expression for a_1^2, it should take only positive values and the condition for it is

$$\frac{\alpha+1}{3} - \frac{1}{3}\sqrt{\alpha^2-\alpha+1} < a_0 < \frac{\alpha+1}{3} + \frac{1}{3}\sqrt{\alpha^2-\alpha+1}. \tag{3.13}$$

For different values of α, one can find the domain for the function $f(a_0)$ given by

$$f(a_0) = -3a_0^2 + 2a_0(\alpha+1) - \alpha. \tag{3.14}$$

For any value of α, one can easily see that the cubic equation (3.12) in a_0 has three real roots because the maximum and minimum of the cubic expression in (3.12) have different signs for all values of α. Now, corresponding to the three values of a_0, provided they lie in the domain of $f(a_0)$, we can write down explicit solutions in the form (3.4). We shall try a simple case when $\alpha = 2$, say. When $\alpha = 2$, we can see that a_0 should be between $1 - 1/\sqrt{3}$ and $1 + 1/\sqrt{3}$, i.e. between 0.423 and 1.577. Now, the cubic equation (3.12) becomes

$$4a_0^3 - 12a_0^2 + 11a_0 - 3 = 0, \tag{3.15}$$

which has 3 real roots 1/2, 1 and 3/2, all of them lying between 0.423 and 1.577. When $a_0 = 1$, we get $c = 0$ which is the case of standing waves. When $a_0 = 1/2$, we obtain

$$a_1^2 = \frac{1}{4}, \tag{3.16}$$

$$\mu = \sqrt{-s/8v}, \tag{3.17}$$

$$c^2 = \frac{-9sv}{2}. \tag{3.18}$$

For $a_0 = 3/2$, we get

$$a_1^2 = \frac{1}{4}, \tag{3.19}$$

$$\mu = \sqrt{-s/8v}, \tag{3.20}$$

$$c^2 = -\frac{9sv}{2}. \tag{3.21}$$

The pairs of values $a_0 = 1/2$, $a_1 = 1/2$ and $a_0 = 3/2$, $a_1 = -1/2$ will yield the same solution with $\mu = \sqrt{-s/8v}$ and $c^2 = -9sv/2$ given by

$$u(x,t) = \frac{1}{2} + \frac{1}{2}\tanh\left(\frac{-s}{8v}\right)^{1/2}(x-ct). \tag{3.22}$$

Table I
Solutions with $c = 2.1$ to 2.9

z	$u(c=2.1)$	$u(c=2.3)$	$u(c=2.5)$	$u(c=2.7)$	$u(c=2.9)$
−5.00	1.0	1.0	1.0	1.0	1.0
−4.38	0.360	0.304	0.261	0.226	0.197
−3.75	0.143	0.100	0.730×10^{-1}	0.542×10^{-1}	0.407×10^{-1}
−3.13	0.578×10^{-1}	0.337×10^{-1}	0.207×10^{-1}	0.132×10^{-1}	0.850×10^{-2}
−2.50	0.246×10^{-1}	0.115×10^{-1}	0.593×10^{-2}	0.320×10^{-2}	0.178×10^{-2}
−1.88	0.104×10^{-1}	0.390×10^{-2}	0.169×10^{-2}	0.771×10^{-3}	0.368×10^{-3}
−1.25	0.437×10^{-2}	0.132×10^{-2}	0.472×10^{-3}	0.177×10^{-3}	0.655×10^{-4}
−0.625	0.184×10^{-2}	0.449×10^{-3}	0.134×10^{-3}	0.435×10^{-4}	0.148×10^{-4}
0	0.771×10^{-3}	0.153×10^{-3}	0.384×10^{-4}	0.105×10^{-4}	0.316×10^{-5}
0.625	0.321×10^{-3}	0.523×10^{-4}	0.112×10^{-4}	0.279×10^{-5}	0.802×10^{-6}
1.25	0.132×10^{-3}	0.178×10^{-4}	0.327×10^{-5}	0.715×10^{-6}	0.163×10^{-6}
1.88	0.534×10^{-4}	0.606×10^{-5}	0.959×10^{-6}	0.185×10^{-6}	0.410×10^{-7}
2.50	0.210×10^{-4}	0.204×10^{-5}	0.281×10^{-6}	0.484×10^{-7}	0.103×10^{-7}
3.13	0.786×10^{-5}	0.666×10^{-6}	0.824×10^{-7}	0.131×10^{-7}	0.257×10^{-8}
3.75	0.266×10^{-5}	0.204×10^{-6}	0.240×10^{-7}	0.381×10^{-8}	0.778×10^{-8}
4.38	0.711×10^{-6}	0.557×10^{-7}	0.770×10^{-8}	0.161×10^{-8}	0.468×10^{-9}
5.00	0.0	0.00	0.0	0.0	0.0

4. Numerical solution

In this Section we consider the two equations

$$\frac{d^2u}{dz^2} + c\frac{du}{dz} + u(1-u) = 0, \tag{4.1}$$

$$\frac{d^2u}{dz^2} + c\frac{du}{dz} + u(1-u)(\alpha - u) = 0, \tag{4.2}$$

and solve them numerically as boundary value problems using a deferred correction technique and Newton iteration. For these equations the solutions of biological interest satisfy $u(-\infty) = 1$ and $u(+\infty) = 0$. In our analysis, we have observed that the dependent variable u decays sufficiently rapidly from 1 to 0 when we take the values of z from -5 to 5.

First we considered the Eq. (4.1) and chose the values of c as 2.1, 2.3, 2.5, 2.7 and 2.9. The boundary conditions were $u(-5) = 1$ and $u(+5) = 0$. We could conclude that the solution decays faster when c increases. This is shown in Table I.

The second equation under consideration was (4.2) for which we took c to be 3.1 and 3.2 and varied α with values 1.5, 1.6, 1.7, 1.8 and 1.9. We could observe that the solution decays slower when α increases. This shown in Tables II and III.

Table I shows that as the travelling wave velocity increases, the solution decays faster.

Table II shows that as the parameter α increases, the decay is slower.

Table III also shows that as the parameter α increases, the decay is slower.

Table II
Solutions with $c = 3.1$ for $\alpha = 1.5$ to 1.9

z	$u(\alpha = 1.5)$	$u(\alpha = 1.6)$	$u(\alpha = 1.7)$	$u(\alpha = 1.8)$	$u(\alpha = 1.9)$
−5.00	1.0	1.0	1.0	1.0	1.0
−4.38	0.183	0.188	0.192	0.197	0.202
−3.75	0.373×10^{-1}	0.393×10^{-1}	0.415×10^{-1}	0.440×10^{-1}	0.469×10^{-1}
−3.13	0.163×10^{-2}	0.847×10^{-2}	0.926×10^{-2}	0.102×10^{-1}	0.113×10^{-1}
−2.50	0.163×10^{-2}	0.184×10^{-2}	0.208×10^{-2}	0.238×10^{-2}	0.275×10^{-2}
−1.88	0.344×10^{-3}	0.401×10^{-3}	0.471×10^{-3}	0.559×10^{-3}	0.673×10^{-3}
−1.25	0.832×10^{-4}	0.984×10^{-4}	0.118×10^{-3}	0.143×10^{-3}	0.177×10^{-3}
−0.625	0.188×10^{-4}	0.230×10^{-4}	0.285×10^{-4}	0.359×10^{-4}	0.461×10^{-4}
0	0.503×10^{-5}	0.613×10^{-5}	0.762×10^{-5}	0.967×10^{-5}	0.126×10^{-4}
0.625	0.112×10^{-5}	0.142×10^{-5}	0.184×10^{-5}	0.242×10^{-5}	0.329×10^{-5}
1.25	0.259×10^{-6}	0.336×10^{-6}	0.446×10^{-6}	0.607×10^{-6}	0.850×10^{-6}
1.88	0.580×10^{-7}	0.780×10^{-7}	0.107×10^{-6}	0.150×10^{-6}	0.218×10^{-6}
2.50	0.121×10^{-7}	0.172×10^{-7}	0.248×10^{-7}	0.365×10^{-7}	0.552×10^{-7}
3.13	0.236×10^{-8}	0.361×10^{-8}	0.552×10^{-8}	0.856×10^{-8}	0.136×10^{-7}
3.75	0.436×10^{-9}	0.719×10^{-9}	0.118×10^{-8}	$0.193 \times 1-^{-8}$	0.320×10^{-8}
4.38	0.778×10^{-10}	0.137×10^{-9}	0.236×10^{-9}	0.403×10^{-9}	0.691×10^{-9}
5.00	0.0	0.00	0.0	0.0	0.0

Table III
Solutions with $c = 3.2$ for $\alpha = 1.5$ to 1.9

z	$u(\alpha = 1.5)$	$u(\alpha = 1.6)$	$u(\alpha = 1.7)$	$u(\alpha = 1.8)$	$u(\alpha = 1.9)$
−5.00	1.0	1.0	1.0	1.0	1.0
−4.38	0.171	0.175	0.178	0.182	0.187
−3.75	0.322×10^{-1}	0.338×10^{-1}	0.356×10^{-1}	0.375×10^{-1}	0.397×10^{-1}
−3.13	0.619×10^{-2}	0.670×10^{-2}	0.728×10^{-2}	0.795×10^{-1}	0.872×10^{-1}
−2.50	0.119×10^{-2}	0.133×10^{-2}	0.150×10^{-2}	0.169×10^{-2}	0.193×10^{-2}
−1.88	0.228×10^{-3}	0.263×10^{-3}	0.306×10^{-3}	0.358×10^{-3}	0.424×10^{-3}
−1.25	0.499×10^{-4}	0.580×10^{-4}	0.684×10^{-4}	0.815×10^{-4}	0.986×10^{-4}
−0.625	0.554×10^{-5}	0.742×10^{-5}	0.997×10^{-5}	0.132×10^{-5}	0.177×10^{-5}
0	0.244×10^{-5}	0.285×10^{-5}	0.313×10^{-5}	0.386×10^{-5}	0.489×10^{-5}
0.625	0.146×10^{-6}	0.252×10^{-6}	0.494×10^{-6}	0.688×10^{-6}	0.965×10^{-6}
1.25	0.807×10^{-7}	0.962×10^{-7}	0.124×10^{-6}	0.166×10^{-6}	0.231×10^{-6}
1.88	0.158×10^{-7}	0.215×10^{-7}	0.259×10^{-7}	0.373×10^{-7}	0.545×10^{-7}
2.50	0.222×10^{-8}	0.381×10^{-8}	0.497×10^{-8}	0.801×10^{-8}	0.127×10^{-7}
3.13	0.381×10^{-9}	0.772×10^{-9}	0.110×10^{-8}	0.190×10^{-8}	0.319×10^{-8}
3.75	0.160×10^{-9}	0.279×10^{-9}	0.375×10^{-9}	0.617×10^{-9}	0.100×10^{-8}
4.38	0.141×10^{-9}	0.209×10^{-9}	0.251×10^{-9}	0.364×10^{-9}	0.526×10^{-9}
5.00	0.0	0.00	0.0	0.0	0.0

5. Analytical solution with $c = 0$

Here, we have considered the analytical solution of two equations

$$u_t = u_{xx} + u(1 - u), \tag{5.1}$$

$$u_t = u_{xx} + u(1 - u)(\alpha - u), \tag{5.2}$$

with $c = 0$, in terms of Weierstrass elliptic functions. This is more of mathematical interest because $c = 0$ means that we are dealing with standing waves. For Eq. (5.1), it is a straight-forward exercise but for (5.2) it is found that it is not possible to express the solution in terms of Weierstrass elliptic functions for certain values of α.

The equations under consideration, using the usual notation in variable z, can be written as

$$\frac{d^2u}{dz^2} + u(1-u) = 0, \tag{5.3}$$

$$\frac{d^2u}{dz^2} + u(1-u)(\alpha - u) = 0. \tag{5.4}$$

The solution of (5.3) can be written explicitly as [9]

$$u(z) = 6P(z) + \frac{1}{2}, \tag{5.5}$$

where $P(z)$ is the Weierstrass elliptic function with the invariants of the elliptic function given by

$$g_2 = \frac{1}{12} \quad \text{and} \quad g_3 < \frac{1}{216}. \tag{5.6}$$

Now, Eq. (5.4) can be shown to have solutions in terms of Weierstrass elliptic functions. For this purpose, we consider the $(2k)^{\text{th}}$ order ordinary differential equation

$$\frac{d^{2k}u}{dz^{2k}} = f(u; r+1), \tag{5.7}$$

where $f(u; r+1)$ is an $(r+1)$ degree polynomial in u.

We assume that

$$u = AQ^{(2s)}(z) \tag{5.8}$$

is a solution of (5.7) where A is an arbitrary constant and $Q^{(2s)}(z)$ is the $(2s)^{\text{th}}$ derivative of the elliptic function $Q(z) = 1/P(z)$, $P(z)$ being the Weierstrass elliptic function. One can easily prove that the $(2s)^{\text{th}}$ derivative of $Q(z)$ is a $(2s+1)$ degree polynomial in $Q(z)$ itself. So for (5.8) to be a solution of (5.7), we should have the relation

$$2k - r = 2rs. \tag{5.9}$$

So, it is necessary that $2k \geq r$ for us to assume a solution in the form (5.8). But it is in no way a sufficient condition for the existence of the periodic wave solution in the form (5.8). In the case of equation (5.4), we have, $k = 1$, $r = 2$ and so $s = 0$. Thus we can assume a solution of (5.4) in the form

$$u(z) = \frac{\lambda}{P(z)} + \mu, \tag{5.10}$$

where λ, μ are constants.

Substitution of (5.10) in (5.4) give rise to 4 equations

$$2\lambda = -\alpha\mu + (1+\alpha)\mu^2 - \mu^3, \tag{5.11}$$

$$0 = -\alpha + 2\mu(1+\alpha) - 3\mu^2, \tag{5.12}$$

$$-\frac{3}{2}g_2 = \lambda(1+\alpha) - 3\lambda\mu, \tag{5.13}$$

$$2g_3 = \lambda^2. \tag{5.14}$$

There are 4 equations in 4 unknowns λ, μ, g_2, g_3 which can be expressed in terms of the coefficient α in the equation (5.4):

$$\mu = \frac{(1+\alpha) + \sqrt{\alpha^2 - \alpha + 1}}{3}, \tag{5.15}$$

$$\lambda = \frac{(\alpha+1)(\alpha-2)(2\alpha-1) + 2(\alpha^2-\alpha+1)^{3/2}}{54}, \tag{5.16}$$

$$g_2 = \frac{(\alpha+1)(\alpha-2)(2\alpha-1)\sqrt{\alpha^2-\alpha+1} + 2(\alpha^2-\alpha+1)^2}{81}, \tag{5.17}$$

$$g_3 = \frac{(\alpha+1)^2(\alpha-2)^2(2\alpha-1)^2 + 4(\alpha^2-\alpha+1)^3}{5832} + \frac{4(\alpha+1)(\alpha-2)(2\alpha-1)(\alpha^2-\alpha+1)^{3/2}}{5832}. \tag{5.18}$$

The condition $g_2^3 - 27g_3^2 > 0$ requires that for positive α, it should be between 0.5 and 2.2 with the exception of 1 and for negative α, it should be less than -0.9.

Therefore, (5.10) is a solution of the Eq. (5.4) with the expressions for μ, λ, g_2 and g_3 given by (5.15)–(5.18) for the values of α specified as above.

6. Conclusion

We have derived the solutions expressed in terms of hyperbolic functions for two diffusion equations both of which satisfy the boundary conditions of biological interest, namely, $u(-\infty) = 1$ and $u(\infty) = 0$, and $u(x) > 0$. For the equation with cubic nonlinearity, this solution is identified with a kink solution.

The numerical solutions presented in the paper are an obvious confirmation of the asymptotic behaviour of the solutions of equations (2.3) and (3.1). We have found that as the travelling wave velocity increases, the solution decays faster and as the parameter α increases the decay is slower.

For the standing waves, the solution we have obtained in terms of the reciprocal of the Weierstrass elliptic function is a new one. For equations of the type (5.4) with third degree in u, it is not possible to represent the solution in positive powers of $p(z)$ and this seems to be the most direct representation.

References

1. W. S. C. Gurney and R. M. Nisbet, J. Theor. Biol., *52*, 441, 1975.
2. M. E. Gurtin and R. C. MacCamy, Math. Biosci., *33*, 35, 1977.
3. W. I. Newman, J. Theo. Biol., *85*, 325, 1980.
4. Y. Hosono, Jpn. J. Appl. Math., *3*, 163, 1986.
5. J. Satsuma, J. Phys. Soc. Jpn., *56*, 1947, 1987.
6. M. J. Ablowitz and A. Zeppetella, Bull. Math. Bio., *41*, 835, 1979.
7. L. Huibin and W. Kelin, J. Phys. A *23*, 3923, 1990.
8. R. A. Fisher, Ann. Eugen. *7*, 355, 1936.
9. E. T. Whittaker and G. N. Watson, A Course of Modern Analysis, Cambridge University Press, Cambridge, 1962.

Acta Physica Hungarica 72 (2-4), pp. 203–212 (1992)

CAN COSMIC STRINGS AND AN AXIAL MAGNETIC FIELD COEXIST IN A STATIONARY GODEL UNIVERSE

C. WOLF

Department of Physics, North Adams State College
North Adams, MA (01247), U.S.A.

(Received in revised form 18 August 1992)

A configuration of cosmic strings immersed in an axial magnetic field is studied in a stationary Godel cosmology. Strings oriented along the z direction require an axial magnetic field to support the resultant geometry while radially directed strings and azimuthal wrapped strings do not require an axial magnetic field to support the geometry but lead to a state of compression in the absence of the magnetic field.

1. Introduction

Modern cosmology has flowered greatly in the past two decades because of the host of new phenomena and topological defects that arise from spontaneously broken gauge theories [1]. It was Coleman's [2] great insight in observing that a radiatively corrected Higgs potential could serve as a source to drive inflation that led Guth [3] to propose inflation as a cure for the cosmological puzzles of flatness, horizon and absence of monopoles from the present universe. With the attention directed towards the Higgs sector of particle theories, it was soon apparent that topological defects such as domain walls [4], monopoles [5] and strings [6] all would figure into such major questions as the origin of large scale structure and the baryon asymmetry of the universe. With all these developments it seems imperative to ask what topological defects in cosmology can support a given cosmological metric. Topological defects such as strings and domain walls destroy local isotropy "unless there is a cloud of them having random orientation" and it seems of particular importance to ask what isometry in the metric can support a specific orientation of the defects. In this note we confine our attention to cosmic strings and ask what direction of orientation of the strings is allowed in an axial magnetic field with the metric having the isometry of the stationary Godel metric. The Godel metric represents a cylindrically symmetric rotating geometry with the matter rotating relative to the compass of inertia [7]. In the present case the matter is the energy density of the matter attached to strings. Panov has pointed out that due to bulging in the equatorial plane of the universe it might be difficult to observe rotation, he also pointed out that too much rotation would prevent inflation and certain rotating Bianchi type IX cosmologies approach the de Sitter inflationary cosmology for long times [8]. In subsequent investigations Panov has studied rotating Bianchi type

VIII cosmologies with a perfect fluid and heat flow [9] along with the problem of spontaneous symmetry breaking in a Godel universe with rotation [10]. Along the same line of investigation, Patel [11] has studied a rotating cosmology with a source-free electromagnetic field and a cosmology admitting shear and bulk viscosity along with heat flow and a scalar field [12]. Koijam [13] has demonstrated how a scalar field in a rotating cosmology with perfect fluid will damp the rotation and Dunn [14] has found homogeneous and inhomogeneous solutions to a Godel metric containing two fluids plus an electromagnetic field. Observational limits on rotation in the universe were first pointed out by Birch [15] and Soleng [16] has remarked that higher order terms in the aberration might be used to detect rotation.

If we turn to the problem of galaxy formation J. Silk [17] has shown that rotation in a Godel universe prevents gravitational instability at large scales, thus an upper limit is set for scale of large scale structure with the Jeans length providing a lower limit for the scale of larger scale structure.

Since both rotation and cosmic strings could figure into the dynamical state of affairs prior to inflation we will in this paper study how different orientations of strings effect the stationary Godel metric in the presence of an axial magnetic field. Israel [18] has given arguments for why strings should not be curved although circular loops of strings have been studied in the literature [19] and Tsoubelis [20] has studied a cylindrically symmetric shell of straight strings in general relativity. In what follows we represent the uniform distribution of strings by a specific form for the energy momentum tensor, we also allow for an axial magnetic field. Our analysis might also apply to the primitive structure of a super-cluster if in fact strings are instrumental in generating large scale structure. If certain orientations of strings are allowed in a stationary Godel cosmology, it suggests that the resulting structure of the configuration will have specific characteristics that may determine its influence on light propagation and gravitational effects produced exterior to the configuration. Korotkii and Obukhov [21] have discussed the rotation of the plane of polarization of electromagnetic waves produced by cosmological rotation which might provide an observational test for our above model. As a preliminary study to any work on light propagation in rotating cosmologies, as well as work on structure formation, we discuss and derive criteria specifying which orientation of strings are permitted in an axial magnetic field in a stationary Godel space time.

2. Cosmic strings and an axial magnetic field in a stationary Godel space time

We begin our analysis by writing the following form for the stationary Godel metric

$$(ds)^2 = (dt)^2 - dr^2 - dz^2 - l(d\phi)^2 + 2m(dt)(d\phi), \tag{2.1}$$

$(l, m =$ functions of $r)$, for the Ricci components of the metric we have calculated them to be $(x^0 = t,\ x^1 = r,\ x^2 = z,\ x^3 = \phi)$, $(c = 1)$,

$$R_{00} = -\frac{(m')^2}{2D^2}, \tag{2.2}$$

$$R_{11} = \frac{D''}{D} - \frac{(m')^2}{2D^2}, \tag{2.3}$$

$$R_{22} = 0, \tag{2.4}$$

$$R_{33} = -\frac{1}{2}(m')^2 - \frac{(mm')^2}{2D^2} + \frac{D'mm'}{D} + DD'' - mm'', \tag{2.5}$$

$$R_{03} = \frac{D'm'}{2D} - \frac{(m')^2 m}{2D^2} - \frac{m''}{2}, \tag{2.6}$$

here

$$D^2 = l + m^2 \quad \text{and} \quad g^{11} = g^{22} = -1, \quad g^{00} = \frac{l}{l+m^2},$$
$$g^{33} = -\frac{1}{l+m^2}, \quad g^{03} = \frac{m}{l+m^2}. \tag{2.7}$$

For the energy momentum tensor of the cosmic strings we have [22]

$$T_{\mu\nu} = (\rho + \lambda)U_\mu U_\nu - \lambda X_\mu X_\nu, \tag{2.8}$$

where λ = string tension, ρ = energy density of particles attached to strings, U_μ = four velocity of strings, X_μ = vector specifying direction of strings.

For an axial magnetic field we have $F_{13} = rB_z$, where

$$F_{\mu\nu} = \frac{\partial A_\mu}{\partial x^\nu} - \frac{\partial A_\nu}{\partial x^\mu},$$

here A_μ is the electromagnetic four potential, the Maxwell equations give using

$$F_{13} = rB_z, \quad \sqrt{-g} = (l+m^2)^{1/2},$$

$$\frac{\partial}{\partial r}(\sqrt{-g}F^{\mu\nu}) = 0,$$

$$\frac{\partial}{\partial r}\left(-\frac{rB_z\sqrt{l+m^2}}{l+m^2}\right) = 0 \tag{2.9}$$

for the (31) component, this gives

$$rB_z = \overline{K}\sqrt{l+m^2}, \quad (\overline{K} = \text{constant}). \tag{2.10}$$

For the energy momentum tensor of the electromagnetic field we have

$$T_{\mu\nu} = \frac{2}{\sqrt{-g}}\frac{\partial}{\partial g^{\mu\nu}}\left[-\frac{1}{16\pi}F_{\mu\nu}F^{\alpha\beta}\sqrt{-g}\right] = \frac{g_{\mu\nu}}{16\pi}F_{\alpha\beta}F^{\alpha\beta} - \frac{1}{4\pi}F_{\mu\alpha}F^\alpha_\nu,$$

using Eq. (2.10) we find

$$T_{00} = \frac{(rB_z)^2}{8\pi(l+m^2)}, \quad T_{11} = \frac{1}{8\pi}\frac{(rB_z)^2}{l+m^2}, \quad T_{22} = -\frac{(rB_z)^2}{8\pi(l+m^2)},$$

$$T_{33} = \frac{(rB_z)^2}{16\pi}\left[4 - \frac{2l}{l+m^2}\right], \quad T_{03} = \frac{m}{8\pi}\frac{(rB_z)^2}{(l+m^2)}, \tag{2.11}$$

$$T = T_{\mu\nu}g^{\mu\nu} = 0.$$

For the cosmic strings we first choose

$$U^\mu = (1,0,0,0), \quad X^\mu = (0,0,1,0) \tag{2.12}$$

(strings co-moving oriented in the z direction).

Using Eq. (2.7), Eq. (2.8) and Eq. (2.1) we find for the string component of the energy momentum tensor

$$T_{00} = (\rho+\lambda), \quad T_{11} = 0, \quad T_{22} = -\lambda, \quad T_{33} = (\rho+\lambda)m^2,$$
$$T_{03} = (\rho+\lambda)m, \quad T = T_{\mu\nu}g^{\mu\nu} = \rho + 2\lambda. \tag{2.13}$$

We now add together the components in Eq. (2.11) and Eq. (2.13) for cosmic strings in an axial magnetic field and insert them into the Einstein equations using Eq. (2.2), Eq. (2.3), Eq. (2.4), Eq. (2.5) and Eq. (2.6), we take the form of the Einstein equations to read

$$R_{\mu\nu} = -k\left[T_{\mu\nu} - \frac{1}{2}Tg_{\mu\nu}\right], \quad \left(k = \frac{8\pi G}{c^4}\right)c = 1. \tag{2.14}$$

The result is

$$-\frac{(m')^2}{2D^2} = -k\left[\rho + \lambda + \frac{(rB_z)^2}{8\pi(l+m^2)} - \frac{1}{2}(\rho+2\lambda)(1)\right], \tag{2.15}$$

$$\frac{D''}{D} - \frac{(m')^2}{2D^2} = -k\left[\frac{1}{8\pi}\frac{(rB_z)^2}{l+m^2} - \frac{1}{2}(\rho+2\lambda)(-1)\right], \tag{2.16}$$

$$0 = -k\left[-\lambda - \frac{(rB_z)^2}{8\pi(l+m^2)} - \frac{1}{2}(\rho+2\lambda)(-1)\right], \tag{2.17}$$

$$-\frac{(m')^2}{2} - \frac{(mm')^2}{2D^2} + \frac{D'mm'}{D} + DD'' - mm''$$
$$= -k\left[\frac{(rB_z)^2}{16\pi}\left(4 - \frac{2l}{l+m^2}\right) + (\rho+\lambda)m^2 - \frac{1}{2}(\rho+2\lambda)(-l)\right], \tag{2.18}$$

$$\frac{D'}{2D}m' - \frac{(m')^2 m}{2D^2} - \frac{m''}{2} = -k\left[(\rho+\lambda)m + \frac{m}{8\pi}\left(\frac{(rB_z)^2}{l+m^2}\right) - \frac{1}{2}(\rho+2\lambda)m\right]. \quad (2.19)$$

From Eq. (2.17) we have

$$\rho = \frac{(rB_z)^2}{4\pi(l+m)} = \rho_c. \quad (2.20)$$

Using Eq. (2.10) this gives

$$\rho = \frac{(\overline{K})^2}{4\pi} = \rho_c \quad \text{(a constant)} \quad (2.21)$$

inserting $(\rho+2\lambda)$ from Eq. (2.17) into Eq. (2.15) and using ρ_c from Eq. (2.21) gives

$$-\frac{(m')^2}{2D^2} = -k(\rho_c) = -k\rho_c. \quad (2.22)$$

Eq. (2.16) becomes

$$\frac{D''}{D} - \frac{(m')^2}{2D^2} = -k[\lambda + \rho_c]$$

or

$$\frac{D''}{D} = -k\lambda \quad \text{after using Eq. (2.22).} \quad (2.23)$$

If no magnetic field is present, we have $B_z = 0$, $\rho_c = 0$ from Eq. (2.21) and $m' = 0$, inserting $m' = 0$ and $\rho_c = 0$ into Eq. (2.18) gives again

$$\frac{D''}{D} = -k\lambda. \quad (2.24)$$

Since the mass density of particles attached to strings is zero, the only logical choice for λ is $\lambda = 0$ since otherwise we would have massless strings which is an unlikely possibility.

Thus if the magnetic field is zero it implies $\rho_c = \lambda = 0$ which in turn implies $D = r$ from Eq. (2.24), $D^2 = r^2$, $m = 0$ from Eq. (2.21) and Eq. (2.22) and we have the Minkowski metric with no rotation. If, however, $B_z \neq 0$ have upon substituting

$$\lambda = -\frac{D''}{D}$$

from Eq. (2.23) into Eq. (2.18)

$$-\frac{(m')^2}{2} - \frac{(mm')^2}{2D^2} + \frac{D'mm'}{D} + DD'' - mm'' = -k[\rho_c D^2 + \rho_c m^2] + DD'', \quad (2.25)$$

where we have used $l = D - m^2$, inserting

$$m' = \sqrt{2}D\sqrt{k\rho_c},$$

$$m = \int^{r} \sqrt{2} D \sqrt{k\rho_c} dr + C_0$$

(C_0 = integration constant) into Eq. (2.25) we may obtain a solution for D in terms of a power series

$$D = \sum_{i=0}^{\infty} a_1 r^i,$$

$$m = \sqrt{2k\rho_c} \sum_{i=0}^{\infty} \frac{a_i r^{i+1}}{i+1} + C_0 \tag{2.26}$$

with non-zero coefficients.

To obtain the string tension we use the relation

$$\lambda = -\left(\frac{D''}{D}\right)\frac{1}{k}$$

after the solution for D is found. The power series for D will start with a constant term and the higher powers of the series will be calculated in terms of a_0 and C_0. Thus cosmic strings in the presence of an axial magnetic field when the strings are pointed in the z direction can support a Godel metric with solution given by Eq. (2.26). When the axial magnetic field vanishes both the string tension and the energy density of the particles attached to the string vanishes and the metric is that of Minkowski space time. Thus the axial magnetic field is needed to support the string.

We now turn to the case of cosmic strings oriented along the radial direction, for this configuration we have

$$X^\mu = (0,1,0,0), \quad U^\mu = (1,0,0,0).$$

Using Eq. (2.7) and Eq. (2.8) we find for the cosmic string components of the energy momentum tensor

$$\begin{gathered} T_{00} = (\rho + \lambda), \quad T_{11} = -\lambda, \quad T_{22} = 0, \\ T_{33} = (\rho + \lambda)m^2, \quad T_{03} = (\rho + \lambda)m, \\ T = T_{\mu\nu} g^{\mu\nu} = \rho + 2\lambda, \end{gathered} \tag{2.27}$$

the components of the energy momentum tensor due to the axial magnetic field are the same as in Eq. (2.11), adding together the components of the energy momentum tensor in Eq. (2.11) and Eq.(2.27) for the axial magnetic field and the strings pointing in the r direction and inserting them into the Einstein equations we have

$$-\frac{(m')^2}{2D^2} = -k\left[(\rho + \lambda) + \frac{(rB_z)^2}{8\pi(l+m^2)} - \frac{1}{2}(\rho + 2\lambda)(1)\right], \tag{2.28}$$

$$\frac{D''}{D} - \frac{(m')^2}{2D^2} = -k\left[-\lambda + \frac{(rB_z)^2}{8\pi(l+m^2)} - \frac{1}{2}(\rho+2\lambda)(-1)\right], \tag{2.29}$$

$$0 = -k\left[-\frac{(rB_z)^2}{8\pi(l+m^2)} - \frac{1}{2}(\rho+2\lambda)(-1)\right], \tag{2.30}$$

$$\begin{aligned} &-\frac{1}{2}(m')^2 - \frac{(mm')^2}{2D^2} + \frac{D'mm'}{D} + DD'' - mm'' \\ &= -k\left[\frac{(rB_z)^2}{16\pi}\left(4 - \frac{2l}{l+m^2}\right) + (\rho+\lambda)m^2 - \frac{1}{2}(\rho+2\lambda) - l\right], \end{aligned} \tag{2.31}$$

$$\frac{D'}{2D^2}m' - \frac{(m')^2 m}{2D^2} - \frac{m''}{2} = -k\left[(\rho+\lambda)m + \frac{m}{8\pi}\left(\frac{(rB_z)^2}{l+m^2}\right) - \frac{1}{2}(\rho+2\lambda)(m)\right], \tag{2.32}$$

from Eq. (2.30) we have

$$(\rho+2\lambda) = \frac{(rB_z)^2}{4\pi(l+m^2)} \tag{2.33}$$

inserting Eq. (2.33) into Eq. (2.28) and Eq.(2.29) we obtain

$$-\frac{(m')^2}{2D^2} = -k\left[-\lambda + \frac{(rB_z)^2}{4\pi(l+m^2)}\right], \tag{2.34}$$

$$\frac{D''}{D} - \frac{(m')^2}{2D^2} = -k\left[-\lambda + \frac{(rB_z)^2}{4\pi(l+m^2)}\right]. \tag{2.35}$$

Equating (2.34) and Eq. (2.35) we find

$$\frac{D''}{D} = 0 \quad \text{or} \quad D = ar + b, \tag{2.36}$$

for an empty Godel universe we have $a = 1$, $b = 0$, $m = 0$, $\rho = \lambda = B_z = 0$, however, for $a \neq 1$, $b \neq 0$, m may have other solutions, from Eq. (2.34) and Eq. (230) we have using Eq. (2.10)

$$\lambda = \frac{(\overline{K})^2}{4\pi} - \frac{1}{k}\left(\frac{(m')^2}{2D^2}\right), \tag{2.37}$$

$$\rho = -\frac{(\overline{K})^2}{4\pi} + \frac{2}{k}\left(\frac{(m')^2}{2D^2}\right). \tag{2.38}$$

Inserting Eq. (2.33), Eq. (2.37) and Eq. (2.38) into Eq. (2.31) we have using Eq. (2.36)

$$-\frac{(m')^2}{2}-\frac{1}{2}\frac{(mm')^2}{(ar+b)^2}+\frac{amm''}{ar+b}+0-mm''$$
$$=-k[\rho(m^2+(ar+b)^2)+\lambda m^2+2\lambda(ar+b)^2], \tag{2.39}$$

with λ, ρ given by Eq. (2.37) and Eq. (2.38) in terms of $D = ar + b$ and m'. A non-zero solution for m can be obtained from Eq. (2.39) by a power series expansion for $a \neq 1$, $b \neq 0$.

Thus cosmic strings in the presence of an axial magnetic field can exist pointing in the r direction and serve as a source to the stationary Godel metric. We would find that Eq. (2.39) would also have a non-trivial solution for m if the magnetic field vanishes also, only in that case from Eq. (2.37) the string tension would be negative which is highly unphysical which suggests and necessitates compressive forces within the string.

For strings wrapped in the ϕ direction have

$$X^\mu=\left(0,0,0,\frac{1}{l^{\frac{1}{2}}}\right), \tag{2.40}$$

$$T_{00}=\frac{(\rho+\lambda)l-\lambda m^2}{l},$$
$$T_{11}=T_{22}=0, \quad T_{33}=\rho m^2+\lambda(m^2-l), \quad T_{03}=\lambda m,$$
$$T=\frac{\rho(l-m^2)+\lambda(2l)}{l+m^2}. \tag{2.41}$$

The Einstein equations read in this case

$$-\frac{(m')^2}{2D^2}=-k\left[\frac{l(\rho+\lambda)-\lambda m^2}{l}+\frac{(rB_z)^2}{4\pi(l+m^2)}-\frac{1}{2}(T)\right], \tag{2.42}$$

$$\frac{D''}{D}-\frac{(m')^2}{2D^2}=-k\left[\frac{(rB_z)^2}{8\pi(l+m^2)}-\frac{1}{2}(T)(-1)\right], \tag{2.43}$$

$$0=-k\left[-\frac{(rB_z)^2}{4\pi(l+m^2)}-\frac{1}{2}(T)(-1)\right], \tag{2.44}$$

$$-\frac{(m')^2}{2}-\frac{(mm')^2}{2D^2}+\frac{D'mm'}{D}+DD''-mm'' \tag{2.45}$$
$$=-k\left[\rho m^2+\lambda(m^2-l)+\frac{(rB_z)^2}{16\pi}\left(4-\frac{2l}{l+m^2}\right)-\frac{1}{2}T(-l)\right],$$

$$\frac{D'm'}{2D}-\frac{(m')^2m}{2D^2}-\frac{m''}{2}=-k\left[(\rho+\lambda)m+\frac{m(rB_z)^2}{8\pi(l+m^2)}-\frac{1}{2}(T)(m)\right]. \tag{2.46}$$

From Eq. (2.44) and Eq. (2.42) we may solve for ρ, λ in terms of m', D and $\overline{K}$, by substituting these values of ρ, λ into Eq. (2.43) and Eq. (2.45) we have two independent differential equations for D and m that have non-trivial power series solutions about $r = 0$. They also have the trivial solution $D = r$, $m = 0$, $\rho = \lambda = B_z = 0$. Thus cosmic strings can coexist with an axial magnetic field when they are wrapped in azimuthal direction. Also, Eq. (2.43) and Eq. (2.45) possess non-trivial solutions when $B_z = 0$, only in this case the string tension would be negative requiring a state of compression within the string.

3. Conclusion

Our analysis has demonstrated that only strings oriented in the z direction require an axial magnetic field to support the geometry while radially wrapped and azimuthally wrapped strings do not require a magnetic field to support the geometry. If cosmological rotation exists the z oriented strings would be most likely since they do not require a detailed dynamical mechanism to generate them except that a z component magnetic field must be present. As mentioned earlier any rotation of the universe as a whole would lead to a rotation of the plane of polarization of electromagnetic waves [20] and studying higher order terms in the aberration of light might also provide a probe to cosmological rotation [16]. It would be interesting to study models with a non-stationary Godel metric admitting bulk and shear viscosity in the presence of an axial magnetic field and cosmic strings to see what static and dynamic effects would be generated as well as the effect that such cosmologies would have on the propagation of light and the generation of density perturbations to seed large scale structure.

Recently Monteiro [23] has discussed stable causal Godel type models generated by a spin fluid with a strong spin vorticity coupling and Obukhov [24] has discussed new observational data pointing to rotation of the universe with more direct inference coming from observational data. Lastly, Singh et al [25] have recently discussed spin generated torsion in a cylindrically symmetric space-time with a z component magnetic field and it is hoped that studies of torsion in a Godel space-time may reveal an intimate connection between torsion, rotation in the universe and the avoidance of closed time-like curves in cosmology.

Acknowledgement

I'd like to thank the Physics Departments at Williams College and Harvard University for the use of their facilities.

References

1. I. J. R. Aitchison and A. J. G. Hey, Gauge Theories in Particle Physics, Adam Hilger Ltd., Bristol, 1982.

2. S. Coleman, Phys. Rev. D, *15*, 2929, 1977.
3. A. Guth, Phys. Rev. D, *23*, 347, 1981.
4. A. Vilenkin, Phys. Lett., *133B*, 177, 1983.
5. A. Albrecht and N. Turok, Phys. Rev. Lett., *54*, 1868, 1985.
6. L. Kawano, Ph. D. Thesis, Univ. of Chicago, 1989.
7. K. Godel, Rev. Mod. Phys., *21*, 447, 1949.
8. V. F. Panov, Sov. Phys. J. (U. S. A.) Vol. 32 (No. 6), 465, 1989.
9. V. F. Panov, Sov. Phys. J. (U. S. A.) Vol. 32 (No. 5), 403, 1989.
10. V. F. Panov, Sov. Phys. J. (U. S. A.) Vol. 32 (No. 2), 94, 1989.
11. L. K. Patel, Lett. Math. Phys. (Netherlands), *18*, (No. 1), 61, 1989.
12. L. K. Patel, Lett. Math. Phys. (Netherlands), *18*, (No. 4), 347, 1989.
13. M. S. Koijam, Astrophysics and Space Science (Netherlands), *161*, (No. 1), 111, 1989.
14. K. Dunn, Gen. Rel. and Grav., *21*, 137, 1989.
15. P. Birch, Nature, *298*, 451, 1982.
16. H. H. Soleng, Ann. Phys. (East Germany), *45*, 507, 1988.
17. J. Silk, Ph. D. Thesis, Harvard Univ. Astron. Dept., 1968.
18. W. Israel, Ann. Phys. (France), *14*, (No. 1), 109, 1989, Meeting on Relativity, Tours, France, 27–29 Ap. 1989.
19. R. J. Scherrer, J. M. Quashnock, D. N. Spergel and W. H. Press, Phys. Rev. D, *42*, 1908, 1990.
20. D. Tsoubelis, Class. and Quantum Grav., *6*, 101, 1989.
21. V. A. Korotkii and Yu. N. Obukhov, Sov. Phys. (J.E.T.P.) *72*, (No. 1), 11, 1991.
22. K. D. Krori and D. Goswami, Can. J. of Phys., *68*, 361, 1990.
23. W. Monteiro S., Jr., J. of Math. Phys., *32*, (No. 11), 3223, 1991.
24. Yu. N. Obukhov, Proc. of XXXII Semester in the Stefan Banach Int. Math. Center, Gauge Theory of Fund. Interactions, Warsaw, Poland, Sept. 19 – Dec. 3, 1988, World Scientific, Singapore, 1990, p. 341.
25. T. Singh, R. S. Srivastava, A. M. Helmi, Astrophysics Spa. Sci. (Netherlands), *178*, (No. 2), 227, 1991.

Acta Physica Hungarica 72 (2-4), pp. 213–221 (1992)

LATTICE DYNAMICAL STUDY OF SOME fcc METALS CENTERED AROUND A NEW SCHEME

M. K. MISHRA, PAWAN SRIVASTAVA* and VIKAS MISHRA*

Department of Physics, S. A. V. College, Kanpur, India
**D. B. S. College, Kanpur, India*

(Received in revised form 22 September 1992)

The present investigation used modified generalised Morse potential to explain the lattice dynamical behaviour of some fcc metals. This potential is controlled by factor P, used in the above modification. Theoretical and experimental findings are very close to each other and this agreement provides a satisfactory explanation of the above model.

1. Introduction

In the recent past, a number of authors [1–9] have put much emphasis on lattice dynamical studies based on Morse potential [10]. These studies [1–9] explain excellently the lattice dynamical behaviour of all types of cubic metals. It has now been proved that the Morse potential has a peculiar nature to explain these properties well, i.e. elastic, lattice dynamical and thermal. The three body forces derived by Mishra et al [3–5] explain the above properties in a broad manner. Mishra [6] used a modified empirical Morse potential and applied it on fcc cobalt. Theories given by Agarwal et al [7] and Aradhana and Rathore [9] added a new dimension to this type of study. But it is yet to know how they have developed a modified Born–Mayer potential [11] and then added to the Morse potential.

In the present communication, we have dealt with the specific nature of the generalised Morse potential which will be controlled by factor P also in the paired part of the potential. Then this two body part has been added to the modified three body generalised part. We have found that factor P is very important and may provide us a correct scheme to predict the lattice dynamical behaviour of Cu, Al, Ag and Pt. The subject matter of the present investigation is important and useful in many respects. The present scheme uses a minimal number of parameters for expressing two and three body forces. The results obtained are excellent and surprising to report and are very close to the experimental findings.

2. Theoretical formulation

2.1. Two body part

Following Milstein [12], the attractive and the repulsive character of the two body potential are blended to form a generalised exponential pair potential which assumes the following forms for the atoms located at r

$$\phi^x_{(r)} = D(P-1)^{-1}\left[\exp\{-P\alpha(r_0-r)\} - P\exp\{-\alpha(r_0-r)\}\right], \tag{1}$$

where D is the dissociation energy, α the parameter which measures the hardness of the potential, r_0 the equilibrium distance and P is the exponent acquiring values within the different ranges.

The average interaction energy cohesive due to the potential may be expressed as

$$\phi^x_{(r_j)} = D\{2(P-1)\}^{-1}\sum_J \left[\exp\{-P(r_0-r_J)\alpha\} - P\exp\{-(r_0-r_J)\alpha\}\right]. \tag{2}$$

The quotient 2 in Eq. (2) takes care of the double counts. Putting

$$\beta = \exp(\alpha r_0) \tag{3}$$

we have a more compact form of the potential, i.e.

$$\phi^x_{(r_j)} = D\{2(P-1)\}^{-1}\sum_J \left[\beta^P \exp(-P\alpha r_j) - \beta P\exp(-\alpha r_J)\right]. \tag{4}$$

This distance r_j may be written as

$$r_j = (m_1^2 + m_2^2 + m_3^3)^{1/2} a = M_j a, \tag{5}$$

where (m_1, m_2, m_3) are integers denoting the co-ordinates of the J-th atom of the solids and a is the semi lattice constant. We have evaluated the present $\phi^x_{(r_j)}$ up to eight nearest neighbours (140 atoms) for the fcc metals Cu, Al, Ag and Pt.

2.2. Three body part of the generalised and modified Morse potential

For the present purpose, the three body potential signifies an extra interaction energy affecting the pair owing to the presence of the third particle. In essence it is a distance dependent three body potential, which arises due to the deformation of the electron shells caused by (s–d) hybridisation. The short range three body exponential potential, capable of expressing the repulsive as well as attractive nature,

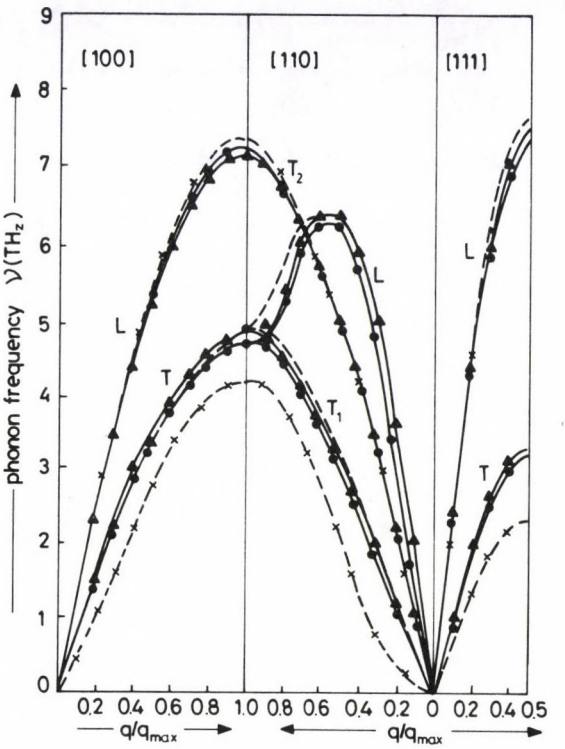

Fig. 1. Phonon dispersion curve for Cu ($P = 2.25$); (———) present study, (• – • – • – •) study due to Verma [22], ($x - x - x - x$) prediction due to Animalu [15], (– – ––) prediction due to Sharma and Joshi [16], (▲▲▲▲) experimental points [14]

coupling the atom (m, k) with its two common nearest neighbours ($r_1 = r_2$) may easily be written as

$$\phi^{y}_{(r_1,r_2)} = Q\{2(P-1)\}^{-1} \sum_{\substack{m'k' \\ m''k''}}^{1} \sum_{mk} \left[\beta^P \exp\{-\alpha P(r_1 + r_2)\} - P\beta \exp\{-\alpha(r_1 - r_2)\}\right] . \tag{6}$$

where r_1 and r_2 are the separations of the atoms $(m'k')$ and $(m''k'')$ from the atom (mk), Q is the deformation parameter. Prime on the first summation denotes, $m'k' \neq m''k''$.

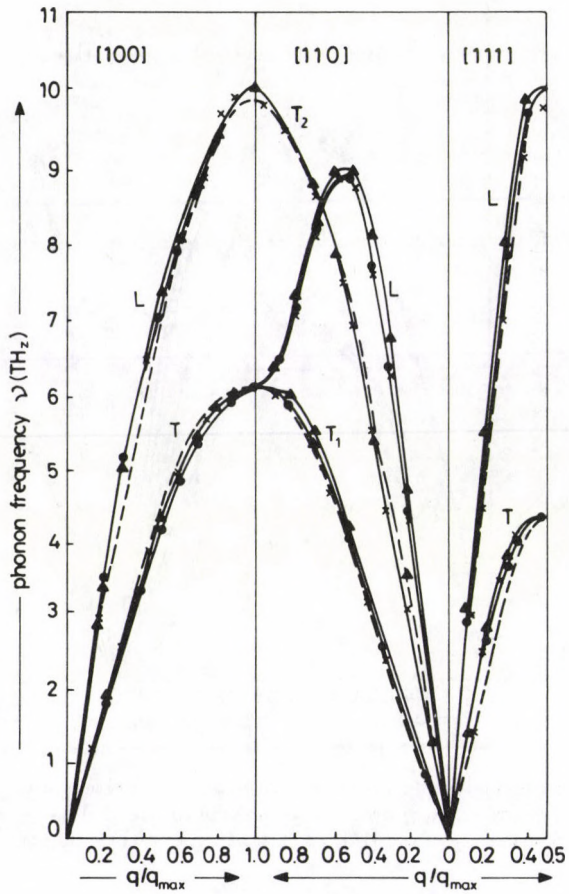

Fig. 2. Phonon dispersion curve for Al ($P = 2.25$); (———) present study, (• – • – • – •) study due to Verma [22], ($x - x - x - x$) Behari and Tripathi scheme [18], (– – ––) prediction due to Wang and Overhauser [19], (▲▲▲▲) experimental points [20]

2.3. The total potential

The total potential, responsible for the resultant interactions coupling the atoms of the crystalline solids may now be written as

$$\phi^{xy}(r_J, r_1, r_2) = \phi^{x}_{(r_J)} + \phi^{y}_{(r_1, r_2)}. \tag{7}$$

3. Parameter evaluation

Singh and Rathore [2] have studied the lattice dynamics of some cubic metals based on the generalised Morse potential. According to this study, cohesive energy,

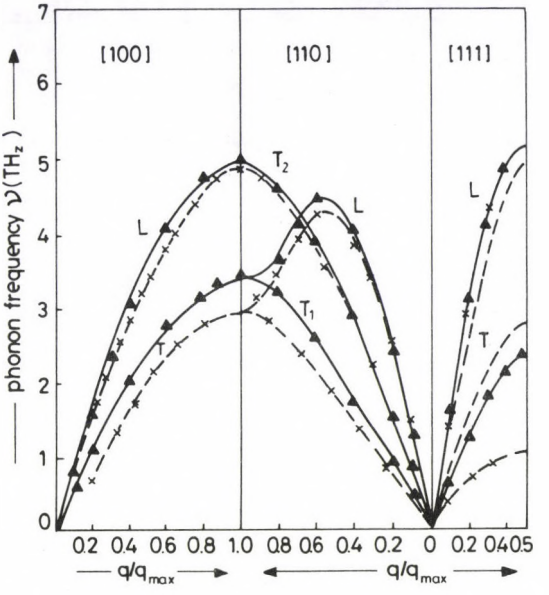

Fig. 3. Phonon dispersion curve for Ag ($P = 2.25$); (———) present study, ($x-x-x-x$) prediction due to Animalu [15], (– – ––) prediction due to Mohammad et al [1], (▲▲▲▲) experimental points [23]

lattice constant and compressibility are the input data for the empirical Morse potential. Compressibility and cohesive energy are, respectively, the sum of ionic interactions and interactions due to the electrons. Mishra and Rathore [3] have separated two and three body parts for compressibility. Mishra [6] has recently succeeded in elaborating the ionic behaviour and the behaviour due to electrons on the most significant contribution to the binding energy, which arises from the interaction between the metal ions and the electrons are not included in the potential [3], even though the potential is fitted to the total cohesive energy. In this note the following procedure has been adopted to separate the ionic interaction and the interaction due to electrons in terms of cohesive energy

$$\phi^{xy} = \phi^x + \phi^y, \tag{8}$$

where ϕ^{xy} is the total cohesive energy, ϕ^x the energy due to the ions and ϕ^y the energy due to electrons.

Further

$$\phi^y = E_f + E_n + E_c, \tag{9}$$

where E_f (Fermi energy) $= -2.21/r^2$ Rydberg, E_n (exchange energy) $= -0.916/r$ Rydberg, E_c (correlation energy) $= [0.0622 \ln r - 0.096]$ Rydberg, while 1 Rydberg $= 21.79 \times 10^{-12}$ erg.

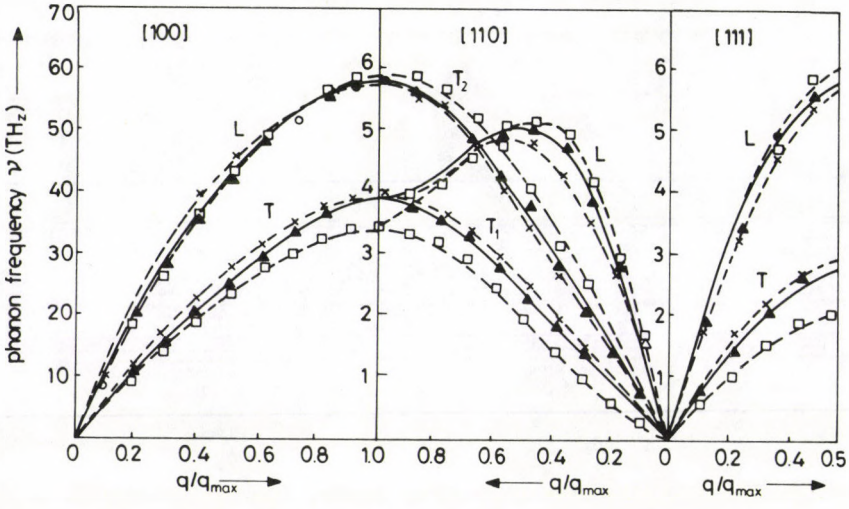

Fig. 4. Phonon dispersion curve for Pt ($P = 2.25$); (———) present study, ($x-x-x-x$) Rajput study [27], (□ – □ – □ – □) Vrati study [24], (▲▲▲▲) experimental points [25]

Table I
Input data used in the paper

Metals	Two body bulk modulus $k^x(\times 10^{12}$ dyne/cm^2)	Ionic part of cohesive energy $\phi(\times 10^{12}$ erg)	Semi lattice constant (a) (nm)	P . .
Cu	0.927	2.472	0.1805	2.25
Al	0.368	2.386	0.2025	2.25
Ag	0.645	2.076	0.2045	2.25
Pt	1.085	4.111	0.1960	2.25

Hence the energy due to electrons

$$\phi^y = \left[\frac{2.21}{r^2} - \frac{0.916}{r} + (0.0622 \ln r - 0.096)\right] \text{ Rydberg.} \tag{10}$$

Here r is the dimensionless quantity and may be varied like 2, 3, 4 or 5 while ln is the natural log. (Table I).

The three parameters (D, α and r_0) depending on the two body potential with the appropriate value of P are evaluated by the procedure laid down by Girifalco and Weizer [13]. The deforming parameter Q is evaluated from the knowledge of measured Cauchy's discrepancy in the second order elastic constants (Table II).

Table II
Computed parameters

Metals	D ($\times 10^{12}$ erg)	α $(\text{nm})^{-1}$	r_0 (nm)	Cauchy's discrepancy ($\times 10^{12}$ dyne/cm^2)
Cu	5.201	0.1331	0.2848	0.443 Ref. [21]
Al	5.709	0.1111	0.3324	0.354 Ref. [21]
Ag	4.070	0.1250	0.3140	0.362 Ref. [21]
Pt	0.468	0.0789	0.3501	1.742 Ref. [26]

Table III
Computed force constants ($\times 10^4$ dyne/cm)

Metals	α_1	β_1	α_2	β_2	β_3
Cu	−0.194	2.693	0.074	−0.091	0.072
Al	−0.201	2.150	0.037	−0.016	0.064
Ag	−0.122	2.211	0.033	−0.113	0.069
Pt	−2.507	0.278	18.300	0.801	2.530

4. Dynamical matrix

The elements of the diagonal and off diagonal matrix may be given, after solving the usual secular determinant, as

$$\begin{aligned} D_{\alpha'\alpha'}(\mathbf{q}) =& 4(\beta_1 + 2\alpha_1) - 2(\beta_1 + \alpha_1)C_{\alpha'}(C_{\beta'} + C_r) \\ & - 4\alpha_1 C_{\beta'}(r' + 4\beta_2 S_{\alpha'} + 4\alpha_2(S^2_{\beta'} + S^2_{r'}), \\ D_{\alpha'\beta'}(\mathbf{q}) =& 2(\beta_1 - \alpha_1)S_{\alpha'}S_{\beta'} + 4\beta_3[(C_{\alpha'} + C_{r'}) - 2], \end{aligned} \tag{11}$$

where $C_{\alpha'} = \cos(\frac{aq\alpha'}{2})$, $S_{\alpha'} = \sin(aq\alpha'/2)$. Hence α_1, α_2 are the first and β_1, β_2 are the second derivatives of the potential $\phi^x_{r_J}$ while β_3 is the second derivative of $\phi^y_{(r_1,r_2)}$ (Table III).

5. Discussion

The findings on Cu very close to the experimental points [14] in comparison to the theoretical studies given by Animalu [15] using the TMMP model and another study due to Sharma and Joshi [16]. The above theories are inefficient on the several grounds which are well explained by Prakash and Upadhyaya [17].

For the metal Al we have better results than the other recent studies given by Behari and Tripathi [18] and Wang and Overhauser [19]. Experimental points [20] are in good agreement with this approach for Al. The curves (1 and 2) have been compared with the recent study of Verma [22] also, which is lacking on the ground of parameter evaluation.

The dispersion curve of Ag is very close to the experimental points [23] in comparison to the theoretical studies given by Animalu [15] and by Mohammad et

al [1]. The deficiencies of the these studies [1 and 5] have already been pointed out by Mishra et al [3–5]. Again the phonon dispersion curve for Pt has been compared with the theoretical study of Rajput [27] and with the study of Vrati [24] also. Experimental points [25] are very well satisfied. We find that our calculations are in better agreement than others.

Finally we have drawn the conclusion that the present investigation provides us the satisfactory type of scheme which is centered around a more correct procedure. In actual practice, the lattice dynamical properties based on Morse potential have been computed in a proper manner for the first time, free from all deficiencies. The used input parameters are purely ionic for the two body part while the deforming parameter Q is explaining the three body part satisfactorily.

One more interesting conclusion has also been drawn that the variation of P for different values in the generalised Morse potential gives a very resonable ionic as well as three body part. If the value of P is varied, the results obtained are suddenly disturbed.

Acknowledgement

The authors are thankful to Dr. K. Singh, BHU, Varanasi, for providing computer facilities. One of the authors (MKM) is very grateful to his wife Smt. Aneeta for her cooperation.

References

1. K. Mohammad, M. M. Shukla, F. Milstein and J. L. Merz, Phys. Rev. (B), *29*, 3117, 1984; Solid Stat. Commun., *48*, 147, 1983.
2. G. Singh and R. P. S. Rathore, Phys. Stat. Sol. (b), *135*, 513, 1986; Phys. Stat. Sol. (b), *136*, 57, 1986; Ind. J. Pure and Appld. Phys., *24*, 303, 1986.
3. M. K. Mishra and R. P. Rathore, Acta Phys. Pol. (A), *75*, 525, 1989.
4. M. K. Mishra, A. K. Bajpai and S. K. Mishra, Ind. J. Pure and Appld. Phys., *29*, 510, 1991.
5. M. K. Mishra, A. K. Bajpai and R. P. S. Rathore, Acta Phys. Hung., *71*, 67, 1992.
6. M. K. Mishra, Phys. Stat. Sol. (b), *162*, K-73, 1990.
7. R. M. Agrawal, K. Aradhana and R. P. S. Rathore, Ind. J. Pure and Appld. Phys., *29*, 517, 1991.
8. R. P. S. Rathore, A. Singh and R. M. Agrawal, Phys. Stat. Sol. (b), *165*, 95, 1991.
9. K. Aradhana and R. P. S. Rathore, Czech. J. Phys., *B-40*, 686, 1990.
10. P. M. Morse, Phys. Rev., *34*, 57, 1929.
11. M. Born and J. E. Mayer, Z. Phys., *75*, 1, 1932.
12. F. Milstein, J. Appld. Phys., *44*, 3825, 3832, 1973.
13. L. A. Girifalco and V. G. Weizer, Phys. Rev., *114*, 687, 1959.
14. L. A. Savensson, B. N. Brockhouse and J. M. Rowe, Phys. Rev., *155*, 169, 1967.
15. A. O. E. Animalu, Phys. Rev., *B-8*, 4542, 1973.
16. K. C. Sharma and S. K. Joshi, Ind. J. Pure and Appld. Phys., *3*, 329, 1965.
17. D. Prakash and J. C. Upadhyaya, J. Phys. Chem. Solids, *49*, 91, 1988.
18. J. Behari and B. B. Tripathi, Aust. J. Phys., *23*, 311, 1970.
19. Y. R. Wang and A. W. Overhauser, Phys. Rev., *B-35*, 501, 1987.
20. R. Stedman and G. Nillson, Phys. Rev., *145*, 492, 1966.
21. C. Kittel, Introduction to Solid State Physics, John Wiley and Sons, New York, 1971, p. 149.

22. A. K. Verma, A. U. Thesis, 1990.
23. W. A. Kamitwakahare and B. N. Brockhouse, Phys. Lett., *29*, 639, 1969.
24. S. C. Vrati, Agra Univ. Thesis, 1980.
25. D. H. Dutton, B. N. Brockhouse and A. P. Miller, Can. J. Phys., *50*, 2915, 1972.
26. R. F. MacFarlane, J. A. Rayne and C. K. Jones, Phys. Lett. (A), *18*, 91, 1965.
27. A. Rajput, Phys. Stat. Sol. (b), *128*, 411, 1985.

Acta Physica Hungarica 72 (2-4), pp. 223–234 (1992)

MAGNETIC EFFECT ON LOW REYNOLDS NUMBER FLOW IN A HEATED TUBE OF SLOWLY VARYING SECTION*

A. OGULU and M. A. ALABRABA

Department of Physics, Rivers State University of Science and Technology
Port-Harcourt, Nigeria

(Received 22 September 1992)

A mathematical model is advanced for blood flow in an axisymmetric heated tube in the presence of a uniform magnetic field. The radius of the tube is assumed to to vary slowly in the axial direction. Using asymptotic series analysis about a small parameter, ϵ, solutions are obtained for the velocity components, temperature and pressure. The effect of the magnetic field on the axial velocity is discussed quantitatively.

1. Introduction

The study of physiological fluid dynamics is growing in popularity because the flow of blood through arteries gives an indication of the presence of cardiovascular diseases.

Unsteady low Reynolds number flow in a heated tube of slowly varying section was studied by [2]. Fluid motion established by an oscillatory pressure gradient superimposed on a mean, in a tube of slowly varying section was studied in that paper when the temperature of the tube wall varied with the axial distance. Mishra and Chauhan [8] proposed a mathematical model for pulsatile blood flow in a small diameter tube whose walls pulsated. In their study they modelled blood as a two layered fluid by considering core fluid as a micro-polar covered by a very thin cell free layer of Newtonian fluid. Blood flow through blood vessels under the action of a periodic accelerating field was the object of [9].

More recently Ogulu and Bestman [10, 11] studied blood flow in a heated tube of slowly varying section in the presence of radiative heat transfer; first considering blood as a Newtonian viscous fluid with constant viscosity and later the viscosity was varied as the temperature. They showed that the variation of blood viscosity had no appreciable effect on the velocity and temperature distributions.

In all the literature cited none considered the effect of a magnetic field on blood flow so it is the object of this study to look at the effect of a uniform magnetic field on blood flow. Magnetic resonance imaging (MRI) [7] is a well established technique for blood flow measurements where a static magnetic field is obtained by the flow of a current driven through large copper coils. This is one area of application of this study.

*This work is dedicated to the memory of Prof. A. R. Bestman.

The subsequent analysis is divided into four sections. In Section 2 the problem is put in mathematical terms. In Section 3 the leading approximations are presented with solutions. This is followed in Section 4 by the higher approximations. Finally, a quantitative discussion of the results is presented in Section 5.

2. Mathematical formulation

We consider blood flow in cylindrical polar coordinates (r', ϕ, z') with corresponding velocity components (u', v', w') such that $r' = 0$ is the axis of symmetry of the tube. The tube wall is defined as

$$r' = a_0 s(\epsilon z'/a_0). \tag{2.1}$$

Here ϵ is a small parameter and a_0 a suitable constant. Also we apply a uniform magnetic field $(0, 0, H_z)$. The equations of continuity, momentum and energy are therefore

$$\frac{1}{r'}\frac{\partial}{\partial r'}(r'u') + \frac{1}{r'}\frac{\partial v'}{\partial \phi} + \frac{\partial w'}{\partial z'} = 0, \tag{2.2a}$$

$$\rho_\infty \left(u'\frac{\partial u'}{\partial r'} + \frac{v'}{r'}\frac{\partial v'}{\partial \phi} + \frac{v'^2}{r'} + w'\frac{\partial u'}{\partial z'}\right) = -\frac{\partial p'}{\partial r'} + \\ + \mu\left(\nabla'^2 u' - \frac{u'}{r'^2} - \frac{2}{r'^2}\frac{\partial v'}{\partial \phi} + \frac{\partial^2 u'}{\partial z'^2}\right) + \rho g \cos\phi, \tag{2.2b}$$

$$\rho_\infty \left(u'\frac{\partial v'}{\partial r'} + \frac{v'}{r'}\frac{\partial v'}{\partial \phi} + \frac{u'v'}{r'} + w'\frac{\partial v'}{\partial z'}\right) = -\frac{1}{r'}\frac{\partial p'}{\partial \phi} + \\ + \mu\left(\nabla'^2 v' - \frac{v'}{r'^2} - \frac{2}{r'}\frac{\partial u'}{\partial \phi} + \frac{\partial^2 v'}{\partial z'^2}\right) - \rho g \sin\phi, \tag{2.2c}$$

$$\rho_\infty \left(u'\frac{\partial w'}{\partial r'} + \frac{v'}{r'}\frac{\partial w'}{\partial \phi} + w'\frac{\partial w'}{\partial z'}\right) = -\frac{\partial p'}{\partial z'} + \mu\left(\nabla'^2 w' + \frac{\partial^2 w'}{\partial z'^2}\right) - H_z w', \tag{2.2d}$$

$$\rho_\infty c_p \left(u'\frac{\partial T'}{\partial r'} + \frac{v'}{r'}\frac{\partial T'}{\partial \phi} + w'\frac{\partial T'}{\partial z'}\right) = k\left(\nabla'^2 T' + \frac{\partial^2 T'}{\partial z'^2}\right) + \\ + \frac{16\sigma}{3\alpha}\left[\frac{1}{r'}\frac{\partial}{\partial r'}\left(r'T'^3\frac{\partial T'}{\partial r'}\right) + \frac{1}{r'}\frac{\partial T'}{\partial \phi}\left(T'^3\frac{1}{r'}\frac{\partial T'}{\partial \phi}\right) + \frac{\partial}{\partial z'}\left(T'^3\frac{\partial T'}{\partial z'}\right)\right], \tag{2.2e}$$

where

$$\nabla'^2 = \frac{\partial^2}{\partial r'^2} + \frac{1}{r'}\frac{\partial}{\partial r'} + \frac{1}{r'^2}\frac{\partial}{\partial \phi^2},$$

and p' is the pressure, σ is the Stefan–Boltzmann constant, α is the absorption coefficient, μ is the molecular viscosity and c_p is the specific heat capacity. The undisturbed fluid density is denoted by ρ_∞, T' is temperature, H_z the magnetic field vector and $(\rho g \cos\phi, -\rho g \sin\phi, 0)$ the buoyancy force terms.

In (2.2) we have assumed that the density of the fluid is constant and equal to its value in the undisturbed fluid except in the buoyancy force terms, that is, we have made the Boussinesq approximation. Also we can assume that the induced magnetic field is negligible and in the energy equation (2.2e) viscous dissipation is neglected since the low Reynolds assumption necessarily entails low flow velocities.

The differential approximation for the radiative flux adopted here is that proposed by Cheng for a grey gas. It is

$$\frac{d}{dr}\left(\frac{1}{\alpha}\frac{dq'_r}{dr}\right) - 3\alpha q'_r - 16\alpha T'^3 \frac{dT}{dr} = 0. \tag{2.3}$$

The boundary condition on the velocity at the wall is the conventional no-slip condition, while for the magnetic field we assume that the wall is a perfect insulator. Thus

$$u' = v' = 0 = w' = H_z; \quad T' = T_w \quad \text{on} \quad r' = s(z) \tag{2.4a}$$

$$u',\ v',\ w',\ T',\ H_z < \infty \quad \text{on} \quad r = 0. \tag{2.4b}$$

It is now convenient to introduce the following non-dimensional quantities:

$$r = \frac{r'}{a_0},\ z = \frac{\epsilon z'}{a_0},\ (u, v, w) = \frac{(u', v', \epsilon w')}{\epsilon U_\infty},\ \Theta = \frac{T'}{T_\infty},\ R_e = \frac{U_\infty a_0}{\nu},$$
$$p = \frac{(p' - p_\infty)}{\mu U_\infty},\ G_r = \frac{g\beta T_\infty a_0^2}{\nu U_\infty},\ P_r = \frac{\mu c_p}{k},\ \nu = \frac{\mu}{\rho_\infty},$$
$$R_a = \frac{16\sigma a_0 T_\infty^3}{3\alpha k},\ M^2 = \frac{H_z^2 a_0^2}{\mu}. \tag{2.5}$$

We only consider the optically thin limit of Eq. (2.3) since blood can be regarded as an optically thin fluid ($\alpha \ll 1$). Bestman [3] showed that the optically thin limit of (2.3) in suitable non-dimensional variables is

$$\frac{dq}{dr} = \frac{3}{4} R_a(\Theta^4 - 1). \tag{2.6}$$

With the help of (2.5) Eqs (2.2a–e) incorporating (2.6) become

$$\frac{1}{r}\frac{\partial}{r}(ru)+\frac{1}{r}\frac{\partial v}{\partial\phi}+\frac{\partial w}{\partial z}=0, \tag{2.7a}$$

$$R_e\epsilon^2\left(u\frac{\partial u}{\partial r}+\frac{v}{r}\frac{\partial u}{\partial\phi}-\frac{v^2}{r}+w\frac{\partial u}{\partial z}\right)=-\frac{\partial p}{\partial r}+\epsilon\left\{\nabla^2-\frac{1}{r^2}\right\}u-\frac{2\epsilon}{r}\frac{\partial v}{\partial\phi}+$$
$$+\epsilon^2\frac{\partial^2 u}{\partial z^2}-G_r\epsilon\Theta\cos\phi, \tag{2.7b}$$

$$R_e\epsilon\left(u\frac{\partial v}{\partial r}+\frac{v}{r}\frac{\partial v}{\partial\phi}+\frac{uv}{r}+w\frac{\partial v}{\partial z}\right)=-\frac{1}{r}\frac{\partial p}{\partial\phi}+\epsilon\left\{\nabla^2-\frac{1}{r^2}\right\}v+$$
$$+\frac{2\epsilon}{r}\frac{\partial u}{\partial\phi}+\epsilon^2\frac{\partial^2 v}{\partial z^2}+G_r\epsilon\Theta\sin\phi, \tag{2.7c}$$

$$R_e\epsilon\left(u\frac{\partial w}{\partial r}+\frac{v}{r}\frac{\partial w}{\partial\phi}+w\frac{\partial w}{\partial z}\right)=-\epsilon\frac{\partial p}{\partial z}+\nabla^2 w+\epsilon^2\frac{\partial^2 w}{\partial z^2}-M^2 w, \tag{2.7d}$$

$$P_r R_e\epsilon\left(u\frac{\partial\Theta}{\partial r}+\frac{v}{r}\frac{\partial\Theta}{\partial\phi}+w\frac{\partial\Theta}{\partial z}\right)=\nabla^2\Theta+\epsilon^2+\epsilon^2\frac{\partial^2\Theta}{\partial z^2}-\frac{3}{4}R_a(\Theta^4-1), \tag{2.7e}$$

subject to the boundary conditions

$$v=u=0=w=M \qquad \text{on} \quad r=s(z) \tag{2.8a}$$
$$u,v,w,\Theta,M<\infty \qquad \text{on} \quad r=0. \tag{2.8b}$$

In these equations R_e is the Reynolds number, P_r the Prandtl number and G_r the Grashof number or free convection parameter.

If the pressure gradients are eliminated from Eqs (2.7b,c) we get

$$R_e\epsilon\left[\frac{1}{r}\frac{\partial}{\partial r}\left\{r\left(u\frac{\partial v}{\partial r}+\frac{v\partial v}{r\partial\phi}+\frac{uv}{r}+w\frac{\partial v}{\partial z}\right)\right\}-\frac{1}{r}\frac{\partial}{\partial\phi}\left(u\frac{\partial u}{\partial r}+\frac{v\partial u}{r\partial\phi}-\frac{v^2}{r}+w\frac{\partial u}{\partial z}\right)\right]$$
$$=\nabla^2\left\{\frac{1}{r}\frac{\partial}{\partial r}(rv)-\frac{1}{r}\frac{\partial u}{\partial\phi}\right\}+G_r\left\{\frac{\partial\Theta}{\partial r}\sin\phi+\frac{1}{r}\frac{\partial\Theta}{\partial\phi}\cos\phi\right\}$$
$$+\epsilon^2\frac{1}{r^2}\frac{\partial^2}{\partial z^2}\left\{\frac{\partial}{\partial r}(rv)-\frac{\partial u}{\partial\phi}\right\}. \tag{2.9}$$

Equation (2.9) will be found useful in subsequent analysis.

3. Leading approximate solutions

The mathematical statement of the problem is to solve (2.7) and (2.9) subject to (2.8). This problem is nonlinear and coupled and not amenable to closed form analytical treatment. We are interested in low Reynolds number situations such that $\epsilon R = o(1)$ rather than $\epsilon R = O(1)$ and larger. We therefore adopt an asymptotic analysis similar to that in [1] by expanding the velocity components and temperature in the form

$$v = v^{(0)} + \epsilon u^{(1)} + \epsilon^2 u^{(2)} + \ldots, \tag{3.1a}$$

$$u = u^{(0)} + \epsilon v^{(1)} + \epsilon^2 v^{(2)} + \ldots, \tag{3.1b}$$

$$w = w^{(0)}(r, z) + \epsilon w^{(1)}(r, \phi, z) + \epsilon^2 w^{(2)} + \ldots, \tag{3.1c}$$

while the pressure is expanded as

$$p = \frac{1}{\epsilon} p^{(0)} + p^{(1)} + \epsilon p^{(2)} + \ldots. \tag{3.2}$$

For the temperature we have

$$\Theta = \Theta^{(0)}(r, z) + \epsilon \Theta^{(1)}(r, \phi, z) + \epsilon^2 \Theta^{(2)} + \ldots. \tag{3.2a}$$

Bestman [4] has shown that approximate solutions in the form (3.1) and (3.2) agree well with numerical results when the Reynolds number is fairly low.

When (3.1) and (3.2) are substituted in (2.7) we find that the leading terms satisfy the equations

$$\begin{aligned}
&\frac{1}{r}\frac{\partial}{\partial r}(r u^{(0)}) + \frac{1}{r}\frac{\partial v^{(0)}}{\partial \phi} + \frac{\partial w^{(0)}}{\partial z} = 0, \\
&\frac{\partial p^{(0)}}{\partial r} = 0 = \frac{1}{r}\frac{\partial p^{(0)}}{\partial \phi}, \\
&0 = \frac{\partial^2 \Theta}{\partial r^2} + \frac{1}{r}\frac{\partial \Theta}{\partial r} - \frac{3}{4} R_a (\Theta^{(0)4} - 1), \\
&\frac{\partial p^{(0)}}{\partial z} = \nabla^2 w^{(0)} - M w^{(0)}.
\end{aligned} \tag{3.3}$$

$\frac{\partial p^{(0)}}{\partial z}$ is the externally applied pressure gradient which is constant for a healthy person. Suppose we call this constant K, then (3.3e) becomes

$$(\nabla^2 - M^2) w^{(0)} = K. \tag{3.4}$$

In the light of (3.1c) (3.4) becomes

$$\frac{\partial^2 w^{(0)}}{\partial r^2} + \frac{1}{r}\frac{\partial w^{(0)}}{\partial r} - M^2 w^{(0)} = K. \tag{3.5}$$

(3.5) is a modified Bessel equation of order zero whose solution is elementary. It is

$$w^{(0)} = \frac{K}{M^2}\left(\frac{I_0(Mr)}{I_0(Ms)} - 1\right), \tag{3.6}$$

where I_n is a modified Bessel function of the first kind of order n. Subsequently, k_n will represent a modified Bessel function of the second kind of order n.

Next we substitute (3.1) in (2.7a), the result is

$$\frac{1}{r}\frac{\partial}{\partial r}(ru^{(0)}) + \frac{1}{r}\frac{\partial v^{(0)}}{\partial \phi} = -\frac{\partial w^{(0)}}{\partial z}. \tag{3.7a}$$

To obtain another equation linking $u^{(0)}$ and $v^{(0)}$ we substitute (3.1) in (2.9), the leading term of which subject to (3.2a) is

$$\nabla^2\left\{\frac{1}{r}\frac{\partial}{\partial r}(rv^{(0)}) - \frac{1}{r}\frac{\partial u^{(0)}}{\partial \phi}\right\} = -G_r\frac{\partial \Theta^{(0)}}{\partial r}\sin\phi. \tag{3.7b}$$

Putting $v^{(0)} = V^{(0)}(r,z)\sin\phi$, $u^{(0)} = U^{(0)}(r,z)\cos\phi$ in (3.7a,b) we get

$$\frac{1}{r}\frac{\partial}{\partial r}(rU^{(0)}) - \frac{1}{r}V^{(0)} = -\frac{\partial w^{(0)}}{\partial z}, \tag{3.8a}$$

$$\nabla^2\left\{\frac{1}{r}\frac{\partial}{\partial r}(rV^{(0)}) + \frac{1}{r}U^{(0)}\right\} = G_r\frac{\partial \Theta^{(0)}}{\partial r}. \tag{3.8b}$$

The solution for $\Theta^{(0)}$ is given in [11], it is

$$\Theta^{(0)} = \frac{\Theta_w}{I^{1/2}(\frac{3}{2}R_a^{1/2}s)} \cdot I_0^{1/2}(\frac{3}{2}R_a^{1/2}r). \tag{3.9}$$

Solving (3.8a,b) simultaneously, the final results are

$$V^{(0)} = \frac{K}{2M^2}(s - 3r^2)\left(1 - \frac{I_1(Ms)}{I_0(Ms)}\right),$$

$$U^{(0)} = \frac{K}{2M^2}\left(s - \frac{r}{s^2}\right)\left(1 - \frac{I_1(Ms)}{I_0(Ms)}\right).$$

Subsequently subscript w will represent condition at the wall. The leading solutions are now complete.

4. Higher approximations

The equations governing the next approximations are

$$\frac{1}{r}\frac{\partial}{\partial r}(ru^{(1)}) + \frac{1}{r}\frac{\partial v^{(1)}}{\partial \phi} + \frac{\partial w^{(1)}}{\partial z} = 0, \tag{4.1a}$$

$$\frac{\partial p^{(1)}}{\partial r} = 0 = \frac{1}{r}\frac{\partial p^{(1)}}{\partial \phi}, \tag{4.1b}$$

$$R_e\left(u^{(0)}\frac{\partial w^{(0)}}{\partial r} + w^{(0)}\frac{\partial w^{(0)}}{\partial z}\right) = -\frac{\partial p^{(1)}}{\partial z} + \nabla^2 w^{(1)} - M^2 w^{(1)}, \tag{4.1c}$$

$$R_e P_r\left(u^{(0)}\frac{\partial \Theta^{(0)}}{\partial r} + w^{(0)}\frac{\partial \Theta^{(0)}}{\partial z}\right) = \nabla\Theta^{(1)} - \frac{3}{4}R_a(\Theta^{(0)3}\Theta^{(1)} - 1), \tag{4.1d}$$

subject to the conditions

$$v^{(1)} = u^{(1)} = 0 = w^{(1)} = M;\ \Theta^{(1)} = \Theta_w \quad \text{on} \quad r = s(z), \tag{4.2a}$$

$$u^{(1)},\ v^{(1)},\ w^{(1)},\ \Theta^{(1)},\ M < \infty \quad \text{on} \quad r = 0. \tag{4.2b}$$

Also, an equation corresponding to (3.7b) is

$$\begin{aligned} &R_e\left[\frac{1}{r}\frac{\partial}{\partial r}\left\{r\left(u^{(0)}\frac{\partial v^{(0)}}{\partial r} + \frac{v^{(0)}}{r}\frac{\partial v^{(0)}}{\partial \phi} + \frac{u^{(0)}v^{(0)}}{r} + w^{(0)}\frac{\partial v^{(0)}}{\partial z}\right)\right\} - \right. \\ &\left. -\frac{1}{r}\frac{\partial}{\partial \phi}\left(u^{(0)}\frac{\partial u^{(0)}}{\partial r} - \frac{v^{(0)}}{r}\frac{\partial u^{(0)}}{\partial \phi} - \frac{v^{(0)}}{r} + w^{(0)}\frac{\partial u^{(0)}}{\partial z}\right)\right] = \\ &\nabla^2\left\{\frac{1}{r}\frac{\partial}{\partial r}(rv^{(1)}) - \frac{1}{r}\frac{\partial u^{(1)}}{r\partial \phi}\right\} + G_r\left\{\frac{\partial \Theta^{(1)}}{\partial r}\sin\phi + \frac{1}{r}\frac{\partial \Theta^{(1)}}{\partial \phi}\cos\phi\right\}. \end{aligned} \tag{4.3}$$

$p^{(1)}$ is independent of r and ϕ.

We put

$$w^{(1)} = w_1^{(1)}(r, z) + w_2^{(1)}(r, z)\cos\phi. \tag{4.4}$$

Substitute (4.4) in (4.1c) to get

$$R_e u^{(0)}\frac{\partial w^{(0)}}{\partial r} = -\frac{\partial p^{(1)}}{\partial z} + \nabla^2 w_2^{(1)} \tag{4.5a}$$

and

$$R_e w^{(0)}\frac{\partial w^{(0)}}{\partial z} = -\frac{\partial p^{(1)}}{\partial z} + \frac{\partial^2 w_1^{(1)}}{\partial r^2} + \frac{1}{r}\frac{\partial w_1^{(1)}}{\partial r} - M^2 w_1^{(1)}. \tag{4.5b}$$

We put $\partial p/\partial z = p_z^{(1)}$. Substitute for $u^{(0)}$ and $w^{(0)}$ in (4.5a) and after some algebra we obtain

$$w_1^{(1)} = \left\{ r^2 - \frac{s^2 I_0(Mr)}{I_0(Ms)} \right\} \left\{ \frac{p_z^{(1)}}{3} + \frac{R_e K I_1(Ms)}{3M^2 I_0^2(Ms)} - \frac{R_e K}{3M^2 I_0^2(Ms)} \right\} + \\ + \left(1 - \frac{I_0(Mr)}{I_0(Ms)} \right) \left\{ \frac{R_e K}{M^2 I_0^2(Ms)} - \frac{R_e K I_1(Ms)}{M^2 I_0^3(Ms)} \right\}. \tag{4.6a}$$

Next we substitute for $w^{(0)}$ in (4.5b) and after some algebra we get

$$w_2^{(1)} = \frac{p_z^{(1)}}{3} r(r-s) + \left\{ \frac{R_e K^2 rs}{32M^3 I_0(Ms)} - \frac{R_e K^2 I_1(Ms) r}{32M^3 I_0(Ms)} \right\} (r^2 - s^2). \tag{4.6b}$$

We put $\Theta^{(1)} = \Theta_1^{(1)}(r,z) + \Theta_2^{(1)}(r,z)\cos\phi$ and by a simple separation of variables technique (4.1e) becomes

$$R_e P_r w^{(0)} \frac{\partial \Theta^{(0)}}{\partial z} = \frac{\partial \Theta_1^{(1)}}{\partial r^2} + \frac{1}{r} \frac{\partial \Theta_1^{(1)}}{\partial r} - 4R_a \Theta^{(0)3} \Theta_1^{(1)} \tag{4.7a}$$

and

$$R_e P_r U^{(0)} \frac{\partial \Theta^{(0)}}{\partial r} = \frac{\partial^2 \Theta_2^{(1)}}{\partial r^2} + \frac{1}{r} \frac{\partial \Theta_2^{(1)}}{\partial r} - \frac{1}{r^2} \Theta_2^{(1)} - 4R_a \Theta^{(0)3} \Theta_2^{(1)}. \tag{4.7b}$$

Without giving a descriptive method of solution, we directly write the simplified solutions for the perturbed temperature as

$$\Theta_1^{(1)} = \frac{1}{3} \frac{R_e P_r K \Theta_w R_a^{1/2} s}{M^2} \left\{ 1 - \frac{I_1(2\xi r)}{I_1(2\xi s)} \right\},$$

where $\xi = R_a^{1/2} \Theta^{(0)3/2}$ and

$$\Theta_2^{(1)} = \frac{2}{9} \frac{R_e P_r \Theta_w s}{M^2 R_a} \left\{ \frac{I_1(\xi r)}{I_0^{1/2}(\xi s)} - \frac{I_1(\xi s)}{I_0^{1/2}(\xi s)} - \frac{I_1^{1/2}(\xi r) I_1(Ms)}{I_0^{1/2}(\xi s) I_0(Ms)} + \right. \\ \left. \frac{I_1^{1/2}(\xi s) I_1(Ms)}{I_0^{1/2}(\xi s) I_0(Ms)} \right\} + \frac{4}{9} \frac{R_e P_r K \Theta_w r}{M^2 R_a s} \left\{ \frac{I_1^{1/2}(\xi s)}{I_0^{1/2}(\xi s)} - \frac{I_1^{1/2}(\xi r)}{I_0^{1/2}(\xi s)} - \right. \\ \left. - \frac{I_1^{1/2}(\xi s) I_1(Ms)}{I_0^{1/2}(\xi s) I_0(Ms)} + \frac{I_1^{1/2}(\xi r) I_1(Ms)}{I_0^{1/2}(\xi s) I_0(Ms)} \right\} + \frac{R_e P_r K \Theta_w^2 r}{3M^2 R_a^{1/2} s} \cdot \\ \cdot \left\{ 1 - \frac{I_0^{1/2}(\xi r)}{I_0^{1/2}(\xi s)} - \frac{I_1(Ms)}{I_0(Ms)} + \frac{I_1(Ms) I_0^{1/2}(\xi r)}{I_0(Ms) I_0^{1/2}(\xi s)} \right\}, \tag{4.8a}$$

$$\xi = 3/2 R_a^{1/2}. \tag{4.8b}$$

Finally, we assume $G_r \gg R_e$ so that (4.3) now becomes

$$\nabla^2 \left\{ \frac{1}{r} \frac{\partial}{\partial r}(rv^{(1)}) - \frac{1}{r} \frac{\partial u^{(1)}}{\partial \phi} \right\} = -G_r \left\{ \frac{\partial \Theta^{(1)}}{\partial r} \sin\phi + \frac{1}{r} \frac{\partial \Theta^{(1)}}{\partial \phi} \cos\phi \right\}. \tag{4.9}$$

We now put

$$\Theta^{(1)} = \Theta_1^{(1)}(r,z) + \Theta_2^{(1)}(r,z)\cos\phi, \tag{4.10a}$$

$$w^{(1)} = w_1^{(1)}(r,z) + w_2^{(1)}(r,z)\cos\phi, \tag{4.10b}$$

$$u^{(1)} = U_0^{(1)}(r,z) + U_1^{(1)}(r,z)\cos\phi + U_2^{(1)}(r,z)\cos 2\phi, \tag{4.10c}$$

$$v^{(1)} = V_1^{(1)}(r,z)\sin\phi + V_2^{(1)}(r,z)\sin 2\phi. \tag{4.10d}$$

Substitute (4.10c) in (4.1a) to get

$$\frac{1}{r} \frac{\partial}{\partial r}(rU_0^{(1)}) = -\frac{\partial w_1^{(1)}}{\partial z}. \tag{4.11}$$

Integration of (4.11) subject to (4.2) gives

$$U_0^{(1)} = \frac{p_{zz}^{(1)}}{12} \left\{ 2s^2 - r^3 \right\} + \frac{p_z^{(1)}}{3} s s_z r - \frac{R_e K s_z r^3}{24M} \left(1 - 2s^2 \right). \tag{4.11a}$$

Imposition of the appropriate boundary condition on (4.11a) leads to Reynolds equation in lubrication theory. Integration of the Reynolds equation gives

$$p_z^{(1)} = \frac{R_e K s}{10M} - \frac{R_e K s^3}{7M}$$

and

$$p_{zz}^{(1)} = \frac{R_e K s_z}{10M} - \frac{3 R_e K s^2 s_z}{7M},$$

so to terms of order ϵ, the free convection currents have no effect on the pressure distribution.

To continue the solutions we substitute (4.10c,d) in (4.3) to obtain

$$\nabla_1^2 \left\{ \frac{1}{r} \frac{\partial}{\partial r}(rV_1^{(1)}) + \frac{1}{r} U_1^{(1)} \right\} = -G_r \frac{\partial \Theta_1^{(1)}}{\partial r}, \tag{4.12a}$$

where

$$\nabla_1^2 = \left(\frac{\partial^2}{\partial r^2} + \frac{1}{r} \frac{\partial}{\partial r} - \frac{4}{r^2} \right) \sin 2\phi.$$

Let us now say

$$\frac{1}{r} \frac{\partial}{\partial r}(rV_1^{(1)}) + \frac{1}{r} U_1^{(1)} = \Phi(r),$$

then (4.12a) becomes

$$\nabla_1^2\Phi(r) = -G_r\frac{\partial\Theta_1^{(1)}}{\partial r}.$$

After substitution we can show that

$$\Phi(r) = \frac{1}{r}\frac{\partial}{\partial r}(rV_1^{(1)}) + \frac{1}{r}U_1^{(1)} = A\cdot r^2 + \frac{R_eP_rG_r\Theta_w KsI_1(\zeta r)}{6M^2\Theta^{(0)3/2}I_1(\zeta s)} +$$
$$+ \frac{R_eP_rG_r\Theta_w KsI_0(\zeta r)}{12M^2\Theta^{(0)3/2}I_1(\zeta s)}\left\{\frac{1}{r} - \frac{1}{\zeta}\right\} + \frac{R_eP_rG_r\Theta_w KsI_1(\zeta r)}{12M^2\Theta^{(0)3/2}I_1(\zeta s)}\left\{\frac{2}{\zeta r} - \frac{1}{\zeta^2}\right\}. \tag{4.13a}$$

A is an arbitrary constant obtained on imposition of concomitant boundary conditions. To obtain another equation linking $U_1^{(1)}$ and $V_1^{(1)}$ we substitute (4.10c,d) in (4.1a). The result is

$$\frac{1}{r}\frac{\partial}{\partial r}(rU_1^{(1)}) - \frac{1}{r}V_1^{(1)} = -\frac{sI_0(Mr)}{3}\left\{\frac{I_0(Ms)p_{zz}^{(1)} - I_1(Ms)p_z^{(1)}}{I_0^2(Ms)}\right\}.$$

To simplify the algebra involved in the simultaneous solution of (4.13a,b) we appeal to [1] for limiting form for small argument. The results are

$$v_1^{(1)} = \left\{\frac{p_{zz}^{(1)}I_0(Ms) - p_z^{(1)}I_1(Ms)}{I_0^2(Ms)}\right\}\left(\frac{22sr}{45} - \frac{s^2}{27} + \frac{s^2}{9}I_0(Ms) - \frac{srI_0(Mr)}{3}\right) +$$
$$\frac{R_eP_rG_rK\Theta_wR_a^{1/2}}{3M^2I_1(\zeta s)}\left\{\frac{r}{6} + \frac{1}{16\Theta^{(0)3/2}R_a^{1/2}} - \frac{1}{2R_a\Theta^{(0)3/2}} - \frac{1}{4R_a\Theta^{(0)3}} - s\right\},$$
$$u_1^{(1)} = \left\{\frac{p_{zz}^{(1)}I_0(Ms) - p_z^{(1)}I_1(Ms)}{I_0^2(Ms)}\right\}\left(\frac{sr^3}{90} + \frac{2sr}{9} + \frac{sI_0(Ms)}{9} - \frac{4s^2}{27}\right) +$$
$$\frac{R_eP_rG_rK\Theta_wR_a^{1/2}s}{3M^2I_1(\zeta s)}\left\{\frac{125}{72R_a\Theta^{(0)3}} - \frac{s}{18} + \frac{r}{12} + \frac{1}{3R_a\Theta^{(0)3/2}}\right\}.$$

Finally, using the same method, we can show that

$$v_2^{(1)} = \frac{R_eP_rG_rK\Theta_wR_a^{1/2}}{M^2I(\zeta s)}\left\{\frac{13s^4}{2295} - \frac{s^2}{18} - \frac{3r^2}{18} - \frac{s^2r^2}{30} + \frac{2rs}{9} + \frac{4r^3s}{135}\right\},$$

$$u_2^{(1)} = \frac{R_eP_rG_rK\Theta_wR_a^{1/2}}{M^2I_1(\zeta s)}\left\{\frac{13s^4}{2295} - \frac{s^2}{18} - \frac{2r^2}{9} - \frac{s^2r^2}{90} + \frac{s}{9} + \frac{r^3s}{135}\right\}.$$

The solutions are now complete.

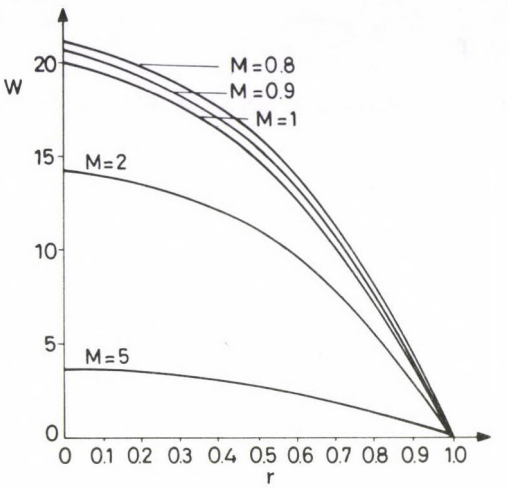

Fig. 1. Velocity profile; $M \geq 0.8$

5. Discussion

In this numerical discussion we present results of the effect of a uniform magnetic field on the axial velocity for flow in a locally dilating tube of the form $s = e^z$, where $z = 0$ is taken as the inlet to the aorta. We discuss only the axial velocity since in systematic flow the nutrients are convected in the axial direction.

Typical values of the parameters of the problem for blood are as follows; the constant pressure in the left ventricle of the heart, $K = -1$, Reynolds number for blood $= 40$, radiation parameter $= 0.5$ and the small parameter $\epsilon = 0.001$. These values are given in the literature, see for instance Ogulu and Bestman [10]. Figures 1 and 2 are plots at $z = 0$ of the axial velocity with radial distance with symmetry about $r = 0$.

We observe that the application of a uniform magnetic field has a definite effect on the velocity of blood flow. It induces a flow potential which is most pronounced in the major blood vessels around the heart and in the heart itself.

In Fig. 1, $M \geq 0.8$ and shows a steady decrease in velocity with increase in magnetic parameter. This means that the flow at the entrance of the aorta is reduced. For a normal flow, the heart does not experience a pressure differential since the inflow rate of blood equals the outflow rate and so for $M \geq 0.8$ more blood arrives at the heart than is leaving. This imposes extra burden on the heart which has to pump at a faster rate to nullify the pressure differential. In Fig. 2, $M \leq 0.5$ and shows a steady increase in velocity with increase in magnetic parameter within the range $0.25 < M \leq 0.5$. This means that the heart has to pump at a slower rate.

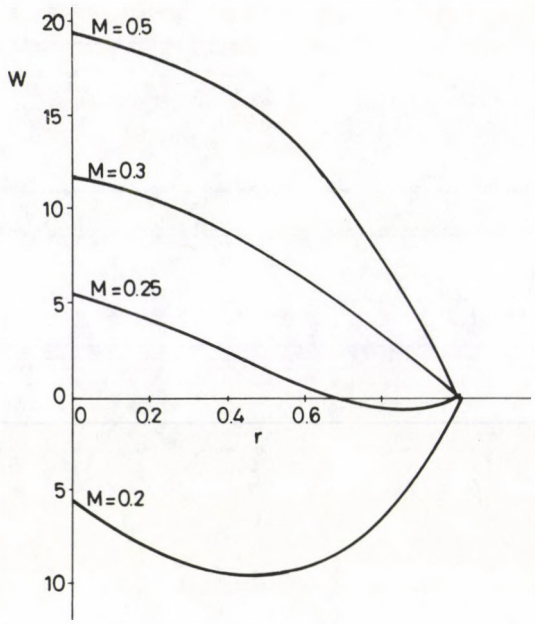

Fig. 2. Velocity profile; $M \leq 0.5$

$M = 0.25$ is a critical value where there is a flow reversal from $r \simeq 0.7$ to the wall where $r = 1$. For $m < 0.25$ the blood flow is completely reversed, this means a lot of pressure has to be applied to overcome the flow reversal.

References

1. M. Abramowitz and I. A. Stegun, Handbook of Mathematical Functions. Dover Publications Inc., New York, 1965.
2. A. R. Bestman, J. Austral. Math. Soc. Ser. B, *30*, 179, 1988.
3. A. R. Bestman, Int. J. Numerical Methods in Eng., *21*, 899, 1985.
4. A. R. Bestman, Numerical Methods in Thermal Problems, II, 790, 1981.
5. A. R. Bestman, Proc. 16th Midwestern Fluid Mechanics Conf., 10, 1979.
6. P. Cheng, AIAAJ, *2*, 1662, 1964.
7. M. A. Hopf and G. M. Bydder, eds, Magnetic Resonance Imaging and Spectroscopy. European Soc. of Magnetic Resonance in Medicine and Biology. Geneva, Switzerland, 1985.
8. J. K. Misra and R. S. Chauhan, Acta Phys. Hung., *67*, 123, 1990.
9. J. C. Misra and B. K. Sahu, Comput. Math. Applic., *16*, 12, 993, 1988.
10. A. Ogulu and A. R. Bestman, ICTP preprint, IC/92/43.
11. A. Ogulu and A. R. Bestman, ICTP preprint, IC/92/44.

Acta Physica Hungarica 72 (2-4), pp. 235–242 (1992)

WIDE ANGLE INTERFERENCE OF COHERENTLY SCATTERED LIGHT

P. VARGA, G. KISS and VERA SCHILLER

Institute for Materials Science
1525 Budapest, Hungary

(Received 29 September 1992)

A classical experiment, which can easily be performed in the classroom is reported here showing that light scattered in all directions is coherent whereas the usual interferometers offer interference within a restricted spatial angle only. The historical background of this experiment is given together with a brief survey of the early experiments and experimentators among whom is Schrödinger.

1. Introduction

Early quantum theory dealt with a concept, the so-called "Nadelstrahlung" (needle radiation), the existence of which was denied by the same authors who had used it [1]. According to this idea the light emitted by an atom (at rest) is a wave, but it is concentrated in a narrow, directed bundle. This picture enabled the dual nature of light to be explained in a simple way: on one side the wave nature remained thereby allowing interference phenomena to be interpreted, on the other side the energy, concentrated in the cone, accounted for local effects, e.g. the photoeffect. This working hypothesis was immediately rejected by Jordan referring to the experiments described in Section 2.

Though the nonexistence of Nadelstrahlung was proven its ghost has started to haunt again. On a previous occasion [2] it helped to explain certain optical phenomena without introducing the concept of the photon but it was also used [3] to prove the existence of the photon.

In most cases Einstein's paper [4] published in 1917 is mentioned as the source of the concept. In this work Einstein continued his previous article [5] in which he had deduced the law of black-body radiation. He had, in his earlier work, assumed the existence of spontaneous and induced atomic transitions and had required that the energy distribution of excited molecules should obey Boltzmann's law. Now he wanted to find full equilibrium between radiation and absorbing/emitting molecules. He showed that the momentum distribution of molecules remains Maxwellian if the exchange of energy $h\nu$ between the radiation field and the molecule is followed by momentum exchange of value $h\nu/c$. As the momentum change of the molecule has a definite direction an opposite one is to be attributed to the emitted light.

This assumption by no means contradicts the main body of experience: two-beam interference of quasimonochromatic light can be observed if the size of the

light source is small and the cone within the interfering light emerging from the source is limited. In the case of Young's interferometer if the source is relatively far from the screen with a double-slit, the lateral size Δx of the source and the angle $\Delta\alpha$ under which the double slit is seen from the source must obey the relation

$$\Delta x \cdot \Delta\alpha \leq \lambda/2, \tag{1}$$

where λ is the wavelength. This relation was known long ago [6], nowadays it is interpreted as the uncertainty relation between location and momentum. For a source of 0.1 mm width (i.e. for a fairly open exit slit of a monochromator) and visible light the opening of the light cone must be less than 10 minutes of arc.

2. Early experiments

Some years prior to Einstein's statement on the directed nature of emitted light Selényi showed [7] that interference can be observed for angles up to 100 degrees. This wide angle interference (WAI) experiment was performed with an interferometer developed by Selényi himself. This interferometer was more similar to a Fizeau type device (i.e. interferometer with amplitude division), and for this configuration Eq. (1) is not applicable. In Selényi's experiment the light source was a thin layer (less than $\lambda/4$ thick) either of sulphur particles or of fluorescein, coating the surface of a thin mica sheet, illuminated by the focused beam of an arc lamp. In the former case the light was coherently scattered, in the latter incoherently. The sheet was attached to a 45° glass prism by immersion liquid (see Fig. 1), the coating layer faced the prism.

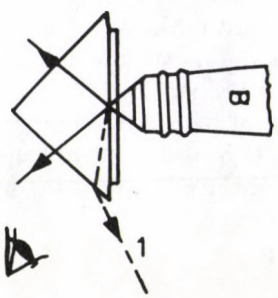

Fig. 1. Selényi's experimental setup

Interference took place between the light emitted directly from the scattering/luminating secondary source and the light reflected from the rear side of the sheet (see insert on Fig. 2). The prism coupled out the light reflected from the rear surface of the sheet even when the light was totally reflected on this surface. The interference pattern was observed through the side of the prism with the naked eye or by a telescope. It was photographed or studied by means of a spectroscope.

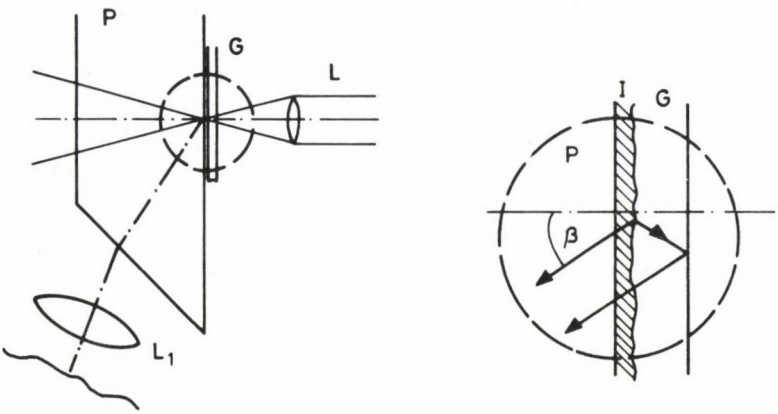

Fig. 2. Experimental setup. L — incident beam, P — rhombic prism, G — glass plate, I — bromonaphthalene fluid, L_1 — lens for observing interference field and imaging of the light spots

In the following Section we show that this experiment with coherently scattered light can easily be repeated by contemporary means and can be demonstrated in the classroom.

Schrödinger's [8] name cannot be overlooked in the history of WAI experiments: he performed another experiment. He was unaware of Selényi's work but knew of Einstein's. Schrödinger observed WAI using a Young's interferometer and a platinum wire of $2-4$ μm thickness as a light source.[1] Interference was measured up to 29°.

WAI was found for X-rays, too. Kossel and Woges [9] excited X-ray luminescence in a monocrystal of copper (for the K_α line $\lambda = 0.15$ nm) and studied the scattering in the same crystal. The exciting electron beam was focused therefore the source of X-rays could be regarded as a point; for a point source the diffraction pattern forms rings. In the experiment the rings occurred in pairs, each black ring was followed by a white one. The first was explained as the location of maximum intensity fringes caused by the interference between the direct and scattered wave, the second by minimum intensity. The interfering waves correspond to those in Selényi's experiment.

[1] There was no electronic control at that time and the thin wire often burned out. No wonder Schrödinger preferred theoretical physics!

Some decades later WAI was applied for enhancing the intensity of Raman scattered light [10], where valuable gain was achieved for measuring very weak light signals.

We started to perform WAI experiments in which any interaction between radiating molecules can be excluded up to the limit when a single molecule radiates. The reason for these novel experiments is that the early ones had been performed with macroscopic light sources: the number of simultaneously emitting molecules was high, but the mean intensity was low, i.e. the probability of observing a light quantum was very small. However, our attention was drawn to an unsuccessful repetition of Selényi's experiment [11], so we started to repeat them with contemporary tools. In the present paper we show that light scattered by a rough surface interferes at wide angles, too. The result of the experiment seems to be trivial from the point of view of the dominating theories. However, we feel that this experiment may help people to understand the meaning of the wave nature of light or, at least, the profound sense of Huygens' principle.

3. The recent experiment

The experimental arrangement is shown in Fig. 2. The geometry of the measurement is the same as that used by Selényi. The beam of a 20 mW He–Ne laser is focused by the lens L onto a ground glass scattering surface, which was produced by slight etching of one surface of a glass plate ($n = 1.52$, nominal thickness 180 microns). The mean diameter of the scattering objects is about one micron. This plate is attached to a 45° rhombic prism ($n = 1.57$) by bromonaphthalene fluid ($n = 1.66$). Because of the different indices of refraction the light is scattered in all directions by the rough surface. Scattered light is observed through the 45° tilted plane of the rhombus. The interference arises from the light scattered forward into the direction of the observer (see insert) and that reflected from the back surface into the same direction. The path difference is given by

$$\Delta s = 2nd\cos\beta,$$

where n is the refractive index of the plate, d its thickness, and β the angle between the surface normal and the direction of observation defined by the laws of geometrical optics. The angle between the interfering rays is $180° - 2\beta$. If the interference is observed perpendicularly to the prism surface and observation is perfected in the focal plane of a lens, the fringe spacing is given by

$$\Delta x = \frac{\lambda f}{2d\sin 45°}, \tag{2}$$

f being the focal length of the lens L_1.

In principle, focusing of the incident laser light by the lens L is not necessary: in this geometry interference can also be observed for an extended light spot. Focusing is used because the thickness d of the glass plate is not constant, therefore

a spot of 10 microns diameter is used. Moreover, the coherence area is limited by the speckle due to the rough surface.

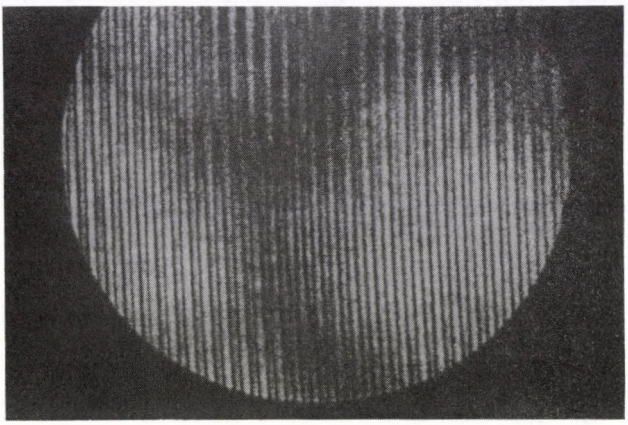

a)

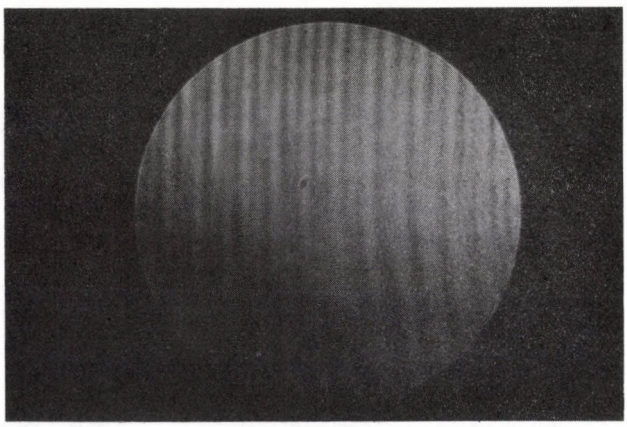

b)

Fig. 3. a – Interference pattern when the angle between interfering waves was 90°, b – the same for 136°

Interference was observed for $0° < \beta < 135°$. Observation under larger angles was hindered by the high intensity light pencil of unscattered light. The interference pattern shown in Fig. 3, photograph 3a was taken when the angle between the interfering rays was 90°, that of 3b for an angle of 134°. Figure 3a exhibits good contrast because the interfering beams were of the same intensity, for 134° the backward scattered beam is no longer totally reflected.

The scattering surface can be observed by a microscope. As a consequence of the reflection on the back surface two separate light spots must occur, A and

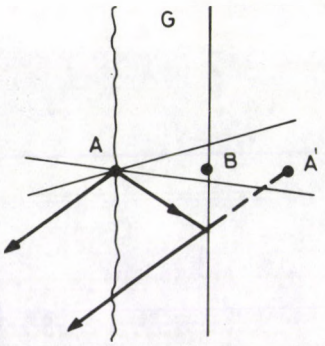

Fig. 4. Configuration of light spots in the near field: A illuminated spot, A' its virtual image, B the parasite spot

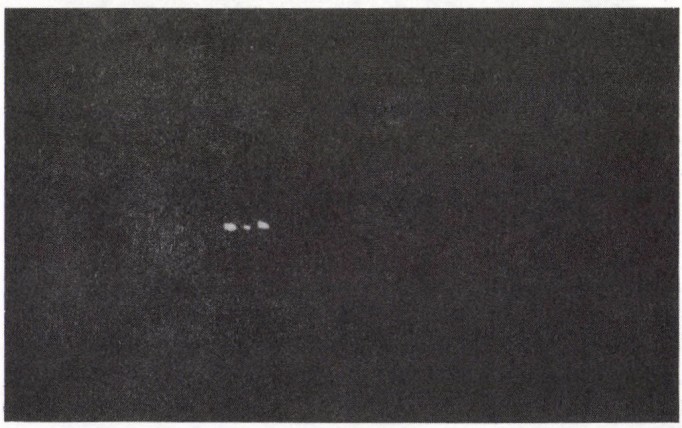

Fig. 5. Photograph of the near field

A' (Fig. 4), but a third one B appeared halfway between A and A' (Fig. 5). This spot was caused by the light scattered from the surface on which the light first impinges on the glass plate. Some scattering from this surface always takes place. The brightness of the spot changes when shifting the glass sheet, but this scattering can hardly be avoided even after the most thorough cleaning of the surface. The intensity of this parasitic source is often commensurable with that of sources A and A'. The occurrence of the third spot may lead one to doubt the correctness of

Table I
Measured and calculated fringe separation (in microns)

	Direct scan	Calculated
1^{st} run	243±2	241 ±0.6
2^{nd} run	241±2.5	244.5±1.3

Selényi's first experiment because purely the forward scattered light emerging from A and B can produce interference, too. (This was not the case for the fluorescent light of the second experiment of Selényi).

The fringe spacing does not differ from that given by (2) if the three spots are present; only the modulation of the interference field changes, the intensity of every even fringe is higher. If only A and B produced the interference, the fringe separation would be twice that given by (2). The interference pattern in the focal plane of lens L (Fig. 2) can be scanned and the fringe spacing established. Afterwards the separation of the two spots A and A' can be measured by a microscope, thus the distance d in Eq. (2) and the expected fringe separation can be calculated.

The results of two independent measurements are represented in Table I. From the very good coincidence of measured and calculated data it can be concluded that wide angle interference takes place when light is coherently scattered. We emphasize that the work reported here is the first step of a series of experiments on WAI. The next step will be performed using light incoherently scattered by a small number of atoms, for the last step a special light source is under development where only a single atom radiates. It is expected that the interference will not depend substantially on the intensity of the scattered light.

Note added in proof

The authors have been informed during the preparation of the manuscript that an article on WAI had been published (Ming Lai and J.-C. Diels, American J. Phys., *58*, 928, 1990). The authors of this article were unaware of the works of Selényi and Schrödinger and stated that it was the first experiment about WAI.

Acknowledgement

Thanks are due to Professor V. Telegdi who called our attention to the importance of repeating Selényi's experiments.

References

1. P. Debye, Physikalische Zeitschrift, *24*, 161, 1923; P. Jordan, Zeitschr. f. Phys., *30*, 297, 1924.
2. Trevor Marshall and Emilio Santos, Found. Phys., *18*, 185, 1988.
3. Christian Cormier-Delanoue, ibid. 1171, 1989.

4. A. Einstein, Mitteilungen der Physikalischen Gesellschaft Zürich, 1916. 47, also Physikalische Zeitschrift, *18*, 121, 1917.
5. A. Einstein, Strahlungs-Emission und -Absorption nach der Quantentheorie, Verhandl. Dtsch. Phys. Ges. *18*, 318–323, 1916.
6. E. Verdet, Vorlesungen über die Wellentheorie des Lichtes, Vieweg und Sohn, Braunschweig, 1881.
7. P. Selényi, Math. und Naturwiss. Berichte aus Ungarn, *27*, 76, 1909; in abbreviated form: Annalen d. Phys., *35*, 444, 1911.
8. E. Schrödinger, Annalen d. Phys., *61*, 69, 1920.
9. W. Kossel, H. Woges, ibid. *23*, 676, 1935.
10. G. A. N. Connel, R. J. Nemanich and C. C. Tsai, Appl. Phys. Lett., *36*, 31, 1980; J. Fortner, R. Q. Yu and J. Lannin, J. Vac. Sci. Technol., *A8*, 3493, 1990.
11. P. Selényi, Zeitschr. f. Phys., *108*, 401, 1938; ibid. *111*, 79, 1938; Phys. Rev., *56*, 477, 1939.

Acta Physica Hungarica 72 (2-4), pp. 243–248 (1992)

QUATERNIONIC TREATMENT OF THE ELECTROMAGNETIC WAVE EQUATION

S. KRISTYAN

California Institute of Technology, Division of Chemistry and Chemical Engineering
Pasadena, California 91125, USA

and

J. SZAMOSI

American Cyanamid Company, Research and Development Division
Princeton, New Jersey 08543, USA

(Received 6 October 1992)

After introducing the quaternions and some of their important properties the Maxwell Equations are translated by quaternion representation. The derivation of the wave equation is also discussed.

1. Introduction

The abstract structure of quaternions or hypercomplex numbers has been applied successfully in several disciplines, e.g. quantum theory [3], engineering and even teaching practice. Algebra must use a larger set of numbers than the real numbers in order to solve the simple second order equation $x^2 + 1 = 0$. For this G. Cardano and R. Bombelli, Italian mathematicians, introduced the complex numbers in the 16th century. The complex numbers have the form $a + bi$ where a and b are real numbers and the symbol i stands for $i^2 = -1$. The symbol i for the $(-1)^{0.5}$ was first used by L. Euler in the 18th century. It is obvious that the real numbers (R) constitute a subset of the complex numbers (C). It is worth noting that other types of numbers are also defined [1]. These are the hyperbolic complex numbers, $a + bE$ where $E^2 = 1$, and the Study numbers, $a + b\Omega$ where $\Omega^2 = 0$. The interesting property of the hyperbolic complex and Study numbers is that in some cases of nonzero (!) numbers ($a \neq 0 \neq b$ or at least one of these nonzero) the division (or multiplicative inverse) cannot be evaluated [1]. However, in case of complex numbers the division can always be evaluated. If we define the numbers $a + bi + cj$ where $i^2 = j^2 = -1$ then one has trouble with the division in the set again. But introducing a new term with symbol k, the

$$Q = a + bi + cj + dk \tag{1}$$

type numbers allow us to evaluate the division in the set again [1]. The most interesting representatives of this set are the quaternions ("quadruple numbers"). These quaternions have the following sum and product properties: Sum of two quaternions is like the sum of two four dimensional vectors. The product is like the product of two four term sums but applying the following definition: $i^2 = j^2 = k^2 = -1$, $ij = k$, $ji = -k$, etc. The product rule between the i, j, k symbols of quaternions can be kept in mind with the help of Fig. 1. Following the arrows the product of two symbols in that order is the third symbol and the opposite order in the product yields the negative (additive inverse) of the third symbol.

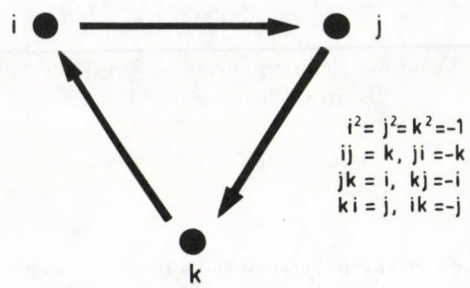

Fig. 1. The product rule of the quaternions

It can be proven that the quaternions obey additive commutativity, additive associativity and multiplicative associativity, this latter being

$$(Q_1 * Q_2) * Q_3 = Q_1 * (Q_2 * Q_3) \tag{2}$$

(multiplication is marked by asterisk), however, do not generally obey multiplicative commutativity (this can be understood by Fig. 1). Eq. (2) will have great importance in Section 2. The definition of the conjugate of a quaternion is analogous to the complex conjugate, i.e. the conjugate of a quaternion in Eq. (1) is noted by Q^c and in it the b, c and d values change sign but a is the same. It can be proved easily that $Q + Q^c = 2a$ and $Q * Q^c = a^2 + b^2 + c^2 + d^2$. The latter defines the square of the absolute value of the quaternions. Several properties similar to the case of complex numbers can be proven. If $\mathbf{e}_1$, $\mathbf{e}_2$, $\mathbf{e}_3$ are the Cartesian unit vectors, then $b\mathbf{e}_1 + c\mathbf{e}_2 + d\mathbf{e}_3$ are the general three dimensional vectors from the origin to the point (b, c, d). Formally a quaternion is a (Descartes) sum of the real number a and the vector $b\mathbf{e}_1 + c\mathbf{e}_2 + d\mathbf{e}_3$ (see Eq. (1)). The term a is called the real part (ReQ) of the quaternion and the rest in Eq. (1) is called the vectorial (or imaginary) part (ImQ or VeQ). Let us consider two purely imaginary quaternions $q_1 = b_1 i + c_1 j + d_1 k$ and $q_2 = b_2 i + c_2 j + d_2 k$. The product of these quaternions $q_1 * q_2 \equiv \mathrm{Re}(q_1 * q_2) + \mathrm{Im}(q_1 * q_2)$

where the real part is $\mathrm{Re}(q_1 * q_2) = -(b_1b_2 + c_1c_2 + d_1d_2)$ and the imaginary is $\mathrm{Im}(q_1 * q_2) = (c_1d_2 - d_1c_2)i + (d_1b_2 - b_1d_2)j + (b_1c_2 - c_1b_2)k$. From vector algebra the geometrical meaning of the right hand sides are known: the scalar or dot product of the two vectors $\mathbf{v}_1 = q_1$ and $\mathbf{v}_2 = q_2$ is $\mathbf{v}_1\mathbf{v}_2 = \mathrm{Re}(q_1 * q_2)$ and the vector product of these two is $\mathbf{v}_1 \times \mathbf{v}_2 = \mathrm{Im}(q_1 * q_2)$. (The $\mathbf{v}_i = q_i$ for $i = 1, 2$ is an equivalence relation between the three dimensional vectors (R^3) and the purely imaginary quaternions ($\mathrm{Im}\{Q\}$).) Finally, the product of two quaternions, having only imaginary parts , i.e. $a = 0$ in Eq. (1) (using the equivalence $\mathbf{v}_i = q_i$ again):

$$q_1 * q_2 = -\mathbf{v}_1\mathbf{v}_2 + \mathbf{v}_1 \times \mathbf{v}_2. \tag{3}$$

The associative property in Eq. (2) and the product property in Eq. (3) of the quaternions are powerful tools in those processes where vector fields are necessary for description. A typical example is the Maxwell equations of electromagnetism, which will be shown in the next Section.

The quaternions form a subalgebra of the Clifford algebra of the three-dimensional Euclidean space, and electrodynamics can be formulated in the powerful Clifford algebra language [6,7,8].

2. Applications

2.1. Quaternion representation of the Maxwell equations

When the operator Nabla or del, $\nabla \equiv \mathbf{e}_1(\partial/\partial x) + \mathbf{e}_2(\partial/\partial y) + \mathbf{e}_3(\partial/\partial z)$, operates on a scalar function (for example on the electric potential) $U(x, y, z)$, it gives the gradient of the function, ($\mathrm{grad}\ U \equiv \nabla U$) pointing to that direction at any considered point where the slope of the surface is the highest; and the "a physical flow" is $-(\mathrm{const.}\nabla U)$. On a vector function (for example on the electric field) $\mathbf{E} = (E_1, E_2, E_3)$, where $E_i = E_i(x, y, z)$ for $i = 1, 2, 3$, the Nabla can operate on two ways: $\mathrm{div}\mathbf{E} \equiv \nabla\mathbf{E}$ and $\mathrm{curl}\ \mathbf{E} \equiv \nabla \times \mathbf{E}$, i.e. the scalar and vector product of the two vectors (considering ∇ as a vector). Gauss's Theorem says that the flux integral of a vector function $\mathbf{E}$ extended over a closed surface S is equal to the volume integral of $\mathrm{div}\mathbf{E}$ extended over the volume bounded by the surface. Stokes's Theorem says that the circulation integral of a vector function $\mathbf{E}$ extended along a closed curve G is equal to the scalar surface integral of $\mathrm{curl}\ \mathbf{E}$ extended over any surface bounded by the curve. The sign of $\mathrm{div}\ \mathbf{E}$ tells if the vector space is a "fountain" or a "sink" at the given point. For example a rotating disc defines a velocity vector space, where the curl at the center of the disc is nonzero and is related to the angular velocity.

The Maxwell equations (named by Pauli) show the div and the curl of electric

field and magnetic induction. At constant permittivity these are [2]:

$$\nabla \mathbf{E} = \rho/\epsilon, \tag{4}$$

$$\nabla \mathbf{B} = 0, \tag{5}$$

$$\nabla \times \mathbf{E} = -\partial \mathbf{B}/\partial t, \tag{6}$$

$$\nabla \times \mathbf{B} = \mu \mathbf{J} + \mu\epsilon \partial \mathbf{E}/\partial t. \tag{7}$$

(The order of the above four equations is different with different authors, and the electric displacement vector ($\mathbf{D}$) and magnetic field vector ($\mathbf{H}$) can also be used in the above field equations. The integral representations of Eqs (4–7) are also used as counterpart.)

With Eq. (3) the above four equations can be written in more compact form:

$$\nabla * \mathbf{E} = -\rho/\epsilon - \partial \mathbf{B}/\partial t, \tag{8}$$

$$\nabla * \mathbf{B} = \mu \mathbf{J} + \mu\epsilon \partial \mathbf{E}/\partial t. \tag{9}$$

With Eqs (3–7) the products: $\mathbf{E} * \mathbf{E} = -\mathbf{E}\mathbf{E} + \mathbf{E} \times \mathbf{E} = -E^2$ and similarly $\mathbf{B} * \mathbf{B} = -B^2$ since the vector product of parallel vectors is zero and the dot product is the square of the absolute value. With these the energy density of the electrostatic field is $w = -\epsilon \mathbf{E} * \mathbf{E}/2$ and of the magnetostatic field is $w = -\mathbf{B} * \mathbf{B}/2\mu$. Two excellent works [4,5] also point out the advantage of the compact forms in Eqs (8–9).

2.2. The electromagnetic wave equation (the consequences of the products $\nabla * \nabla * \mathbf{E}$ and $\nabla * \nabla * \mathbf{B}$)

From the associativity in Eq. (2) we have

$$\nabla * (\nabla * \mathbf{E}) = (\nabla * \nabla) * \mathbf{E}. \tag{10}$$

Applying the rule in Eq. (3) on the left hand side and Eq. (4) with no charge ($\rho = 0$) and Eq. (6)

$$\nabla * (\nabla * \mathbf{E}) = \nabla * (-\nabla \mathbf{E} + \nabla \times \mathbf{E}) = \nabla * (-\partial \mathbf{B}/\partial t). \tag{11}$$

Applying Eq. (3) again on the right hand side and using Eqs (5) and (7) with no current ($\mathbf{J} = 0$):

$$\nabla * (\nabla * \mathbf{E}) = -(-\partial(\nabla \mathbf{B})/\partial t + \partial(\nabla \times \mathbf{B}/\partial t) = -\mu\epsilon \partial^2 \mathbf{E}/\partial t^2, \tag{12}$$

where $\rho = 0$ and $\mathbf{J} = 0$ were used because we are considering the electromagnetic wave. Using Eq. (3) the right hand side of Eq. (10) becomes

$$(\nabla * \nabla) * \mathbf{E} = (-\nabla\nabla + \nabla \times \nabla) * \mathbf{E} = (-\nabla\nabla) * \mathbf{E} = -\Delta \mathbf{E}, \tag{13}$$

where we used that $\nabla \times \nabla = 0$ by the parallelity, and $\nabla^2 \equiv \Delta$ is the Laplacian. From Eqs (10), (12) and (13)

$$\mu\epsilon\partial^2\mathbf{E}/\partial t^2 = \Delta\mathbf{E}, \tag{14a}$$

which is the well-known wave equation with $c = (\mu\epsilon)^{-0.5}$, the speed of light. Similarly to Eq. (10) for $\mathbf{B}$ with Eqs (3), (4) and (7) with no current ($\mathbf{J} = 0$) and no charge ($\rho = 0$) again in the electromagnetic waves, one obtains

$$\mu\epsilon\partial^2\mathbf{B}/\partial t^2 = \Delta\mathbf{B}. \tag{14b}$$

Unfortunately the associativity property in Eq. (2) is strictly true for vectors, but generally not if differential operator(s) as imaginary quaternions are among the variables like in Eq. (10). Eq. (10) is accidentally true for any $\mathbf{E}$ vectors but for example $\mathbf{E} * (\nabla * \mathbf{B})$ and $(\mathbf{E} * \nabla) * \mathbf{B}$ are not equal generally. The relationships in that case are more complex [9]. The reason is the non-commutative property of the product of the differential operators with functions (which is not source of error in case of the product of function vector components being those commutative). In this manner a note must also be made on Eq. (10) since that holds only if in $\nabla * \mathbf{E}$ the vector product $\nabla \times \mathbf{E}$ in Eq. (11) is forced/defined to be not differential operator (i.e. not $E_1\partial/\partial x$), but $\partial E_1/\partial x$, etc.

Acknowledgement

Valuable suggestions by Prof. Géza Knapecz, Technical University of Budapest, Hungary, are greatly appreciated.

Notations

Although the notations are defined in the text, the following summary may make the reading of this paper easier:

$\mathbf{B}$	= magnetic induction
C	= set of complex numbers
c	= speed of light
$\mathbf{E}$	= electric field
$\mathbf{e}_1, \mathbf{e}_2, \mathbf{e}_3$	= Cartesian unit vectors in the three dimensional space
ϵ	= permittivity
i	= $(-1)^{0.5}$ imaginary unit or symbol of complex numbers, i – symbol of quaternions, respectively (sometimes subscript)
i, j, k	= i-, j- and k-symbol of quaternions, respectively, see Eq. (1)
$\mathbf{J}$	= electric current density
μ	= permeability
Q^c	= conjugate of quaternion Q
$Q_1 * Q_2$	= product of two quaternions Q_1 and Q_2
$\{Q\}$	= set of quaternions or hypercomplex numbers (notation for elements appearing in this work: Q, Q_1, Q_2, Q_3, q_1, q_2)

R = set of real numbers (notation for elements appearing in this work: a, b, c, d)
ρ = charge density
t = time
$\mathbf{v}_1\,\mathbf{v}_2$ = the scalar or dot product of two (three) dimensional vectors
$\mathbf{v}_1 \times \mathbf{v}_2$ = the vector product of two three dimensional vectors
∇ $\equiv \mathbf{e}_1(\partial/\partial x) + \mathbf{e}_2(\partial/\partial y) + \mathbf{e}_3(\partial/\partial z)$, the Nabla or del operator
Δ $\equiv \nabla^2 = (\partial^2/\partial x^2) + (\partial^2/\partial y^2) + (\partial^2/\partial z^2)$, the Laplacian

References

1. I. L. Kantor, A. Sz. Szolodovnyikov: Hiperkomplex számok (Hypercomplex Numbers), Gondolat, Budapest, 1985 (in Hungarian).
2. D. J. Griffiths, Introduction to Electrodynamics, Prentice-Hall, Inc., London, 1981.
3. W. Gough, Eur. J. Phys., *8*, 164, 1987.
4. P. R. Girard, Eur. J. Phys., *5*, 25, 1984 and references therein.
5. V. Majernik and M. Nagy, Lettere al Nuovo Cimento, *16*, N. 9. 265, 1976.
6. D. Hestenes, Space-Time Algebra, Gordon and Breach, New York, 1966.
7. B. Jancewicz, Multivectors and Clifford Algebra in Electrodynamics, World Scientific, Singapore, 1988.
8. J. S. R. Chisholm and A. K. Common.: Clifford Algebras and their Applications in Mathematical Physics, D. Reidel Publ., Dordrecht, 1986.
9. Similar case can be found in vector analysis, e.g. $\mathbf{A}(\mathbf{E} \times \mathbf{B}) = \mathbf{E}(\mathbf{B} \times \mathbf{A})$ holds for vectors but if differential operator(s) as vector(s) are among the vectors, for example the $\nabla(\mathbf{E} \times \mathbf{B}) = \mathbf{B}(\nabla \times \mathbf{E}) - \mathbf{E}(\nabla \times \mathbf{B})$ more complex relationship holds, etc.

Acta Physica Hungarica 72 (2-4), pp. 249–252 (1992)

EXAMPLES OF UNCONVENTIONAL DIMENSIONAL ANALYSIS*

Z. RÁCZ**

Department of Physics, Clarkson University
Potsdam, New York 13676, USA

(Received 20 October 1992)

It is shown that dimensional analysis can be used (i) to calculate the energy levels in a one-dimensional potential $V(x) \sim |x|^k$, and (ii) to estimate the value of the gravitational constant G.

1. Introduction

The end of the sixties and the beginning of the seventies was a good time to be a graduate student and to work on critical phenomena. Simple approaches to the theory of phase transitions such as the Landau theory or the high-temperature series were easily understandable, some of the exact solutions (e.g. the solution of the spherical model) were also manageable, and then there was the scaling theory that was technically simple but carried some mystique for a beginner. An important aspect of the good feelings was the fact that the problem was clearly formulated and sounded like what ambitious students wanted to hear: Give a method of calculating the critical exponents and you will be remembered forever. There was excitement in the air.

At the Eötvös University in Budapest, it was Péter Szépfalusy who generated the excitement. In the spring of 1971 he gave a course on phase transitions that was attended by a number of graduate and undergraduate students (Imre Kondor, László Sasvári, Pál Ruján, Gábor Forgács among them) who later made their name in statistical physics. In one of his lectures, Péter Szépfalusy made the side-remark that the scaling theory can be viewed as a generalized dimensional analysis. This remark set off a long debate among the students and in an attempt to understand it, we tried for a while to solve every problem by dimensional considerations. I remember vividly how Péter Gnädig showed us a dimensional-analyis proof of the Pythagorean theorem and how he calculated the deflection of light passing near the sun by the same method. Although our debates subsided with the appearence of Wilson's work [1] that showed how scaling and non-trivial scaling dimensions can emerge from a relatively simple mathematical structure, I remained addicted

*Dedicated to Prof. P. Szépfalusy on his 60th birthday

**Permanent address: Institute for Theoretical Physics, Eötvös University, 1088 Budapest, Puskin u. 5–7, Hungary.

to dimensional analysis. During the past 20 years, I collected [2] and made up many examples of naive dimensional analysis that were extremely helpful in both illuminating subtle points and enlivening long lectures. Below you will find two of my favorites that contain some unexpected twists. It is a great pleasure to dedicate them to Péter Szépfalusy on this auspicious occasion.

2. Energy levels in a potential $V(x) = g|x|^k$

Consider the quantum-mechanical problem of determining the energy of the stationary states of a particle of mass m in an attractive potential $V(x) = g|x|^k$. The task is to find the quantum-number dependence of the energy by using dimensional analysis. The unconventional feature of this problem is, of course, the fact that the quantum number is a dimensionless quantity so, in principle, dimensional analysis cannot help.

The first steps of our analysis go along the usual route. The relevant physical quantities that determine the energy are identified as the mass (m), the coupling constant (g), and since the problem is quantum-mechanical, the Planck constant (h). The dimensions of m and h are known to be $[m] = M$ and $[h] = ML^2T^{-1}$ where M, L, and T denote the dimensions of mass, length and time, respectively, and the dimension of g is obtained from the condition that $g|x|^k$ is energy

$$[g] = \frac{ML^{k-2}}{T^2}. \tag{1}$$

A short calculation leads to the conclusion that there is only one way to combine m, g and h into a quantity that has the dimension of energy. As a consequence, the expression for the energy of the n-th quantum level will necessarily have the following prefactor

$$E_n \sim \frac{g^{2/(k+2)}h^{2k/(k+2)}}{m^{k/(k+2)}}. \tag{2}$$

Of course, the above argument does not yield the quantum-number dependence of E_n. We can add, however, the following observation: In the quasi-classical limit (n is large), the Planck constant and the quantum number n enter the theory through the Bohr–Sommerfeld quantization rule for the action

$$\oint p dx = nh, \tag{3}$$

where $n = 1, 2 \ldots$. Since h and n appear only in the combination nh, it is clear that every quantity calculated in the quasi-classical limit will depend on n through nh. In particular, Eq. (2) then yields the desired result about the n-dependence of the energy

$$E_n \sim n^{2k/(k+2)}. \tag{4}$$

Familiar examples (harmonic oscillator: $k = 2$, $E_n \sim n$; square well: $k \to \infty$, $E_n \sim n^2$; Coulomb potential: $k = -1$, $E_n \sim n^{-2}$) are easily recovered. Using the WKB approximation [3], one can show that Eq. (4) gives the correct large-n asymptotics of E_n for arbitrary k, and furthermore, that the $E_n \sim n^{2k/(k+2)}$ behaviour sets in for small values of n.

3. An estimate of the gravitational constant G

A conventional dimensional analysis consists of two steps: (i) identification of the relevant physical constants, and (ii) construction of the desired physical quantity from given constants. Clearly, the physical constants are considered to be primary and given, and all the other quantities are assumed to be derivatives, i.e. expressable through the constants. One may try to reverse the above logic, however, and ask the following question: Which properties of the physical universe determine the known physical constants? Using this reversed logics we shall estimate the value of the gravitational constant G.

One expects that G depends on some very general features of the universe. The dimension of G is given by

$$[G] = \frac{L^3}{MT^2}, \tag{5}$$

thus we have to come up with some mass, length and time characterizing the universe. The mass and the length are obvious; we have to take the mass and the radius of the universe, respectively. Since $[G]$ contains M and L only in the combination M/L^3, actually we need only the density of the universe (ρ). As to the characteristic time, the only one that pertains to the present state of the universe is the inverse of the rate of the expansion or, in other words, the inverse of the Hubble constant (H^{-1}). (Alternatively, one could think of the lifetime, τ, of the universe but H^{-1} and τ are equal within a factor of the order 2.) Thus we arrive at the following expression for G:

$$G \approx \frac{H^2}{\rho}. \tag{6}$$

Estimates of H are in a narrow range [4]

$$1.6 \cdot 10^{-18}\ \mathrm{s}^{-1} < H < 3.2 \cdot 10^{-18}\ \mathrm{s}^{-1}, \tag{7}$$

but ρ is less well known (and its upper limit is rather speculative)

$$3 \cdot 10^{-28}\ \mathrm{kg/m}^3 < \rho < 5 \cdot 10^{-26}\ \mathrm{kg/m}^3. \tag{8}$$

Choosing H and ρ values appropriately from the above ranges, Eq. (6) reproduces the measured value of G ($6.67 \cdot 10^{-11}\ \mathrm{m^3 kg^{-1} s^{-2}}$). It is clear, however, that the

two orders of magnitude uncertainty in ρ translates into a two orders of magnitude uncertainty in G. Of course, one should not expect Eq. (6) to be exact (Note that dimensional analysis does not give the numerical coefficient in front of H^2/ρ). Nevertheless, it seems to be quite remarkable that a simple dimensional analysis can translate the large-scale properties of the universe into a constant, G, that is measured on the length-scale of a meter and the result turns out to be a correct order-of-magnitude estimate.

Acknowledgement

While writing this manuscript, I enjoyed the hospitality of Clarkson University where I was partially supported by NSF grant CHE-90 08033, and by the Donors of the Petroleum Research Fund, administered by the American Chemical Society.

References

1. K. G. Wilson and J. Kogut, Phys. Rep. *C12*, 76, 1974.
2. A rich source of interesting examples of dimensional analysis is the book Similarity, Self-similarity, and Intermediate Asymptotics by G. I. Barenblatt, Consultants Bureau, New York, 1979.
3. L. D. Landau and E. M. Lifshitz, Quantum Mechanics, Nonrelativistic Theory, Addison-Wesley Publishing Co., Reading, Mass. 1958.
4. See for example G. Börner, The Early Universe, Facts and Fiction, Springer-Verlag, Berlin-Heidelberg, 1988.

Acta Physica Hungarica 72 (2-4), pp. 253–258 (1992)

OPPENHEIMER–VOLKOFF EQUATION IN D SPACE-TIME DIMENSIONS

T. HARKO

Institutul Oncologic
3400 Cluj, Romania

(Received 26 October 1992)

The equations which describe the hydrostatic equilibrium of a relativistic stellar configuration in D space-time dimensions ($D \geq 4$) with a spherical symmetric gravitational field are obtained. With suitable transformations, the equations of mass continuity and of hydrostatic equilibrium are given in a non-dimensional form. With the obtained equations the homogeneous stellar model is studied and some stability criteria are obtained in D ($D \geq 4$) space-time dimensions.

1. Introduction

The Oppenheimer–Volkoff equation is the main theoretical tool in the study of astrophysical relativistic objects such as collapsing stars [1], neutron stars [2] or strange quark stars [3].

Lately, there has been an increasing interest in the study of gazeous spheres in D space-time dimensions. So, Krori et al [4] have extended the interior Schwarzschild solution with vanishing normal pressure of Florides [5] to D space-time dimensions in the presence of a cosmological constant. Wolf [6] has extended the binding energy calculations of Wright [7] to D space-time dimensions with the condition of vanishing normal pressure. He finds that a gazeous sphere with $D \geq 4$ is unstable in the post-Newtonian degree of approximation.

The purpose of the present paper is to obtain a generalization of the Oppenheimer–Volkoff equation in D space-time dimensions, $D \geq 4$ and to obtain its solution in the case of a homogeneous gaseous sphere.

The present paper is organized as follows. In Section 2, using the Einstein field equations we deduce the Oppenheimer–Volkoff equation in D space-time dimensions. A non-dimensional form of this equation is obtained in Section 3. The case of a homogeneous gaseous sphere is analysed in Section 4. The results are summarized in Section 5.

2. Oppenheimer–Volkoff equation in D space-time dimensions

In D space-time dimensions the spherically symmetric metric takes the form:

$$ds^2 = e^{\nu}(dx^0)^2 - e^{\lambda}dr^2 - r^2 d\Theta_1^2 - r^2 \sin^2\Theta_1 d\Theta_2^2 - r^2 \sin^2\Theta_1 \sin^2\Theta_2 d\Theta_3^2 - \ldots$$
$$- r^2 \sin^2\Theta_1 \ldots \sin^2\Theta_{D-3} d\varphi^2. \tag{2.1}$$

Here:

$$x^0 = ct,\ x^1 = r,\ x^2 = \Theta_1,\ x^3 = \Theta_2,\ \ldots,\ x^{D-2} = \Theta_{D-3},\ x^{D-1} = \varphi.$$

(r is the radial coordinate in D space-time dimensions) with domain:

$$0 \leq r < \infty,\ 0 \leq \Theta_i \leq \pi\ (i = 1,\ D-3),\ 0 \leq \varphi \leq 2\pi.$$

The Einstein equations are:

$$R_i^k - \frac{1}{2} R\, \delta_i^k = \frac{8\pi G}{c^4} T_i^k, \tag{2.2}$$

where the components of the energy-momentum tensor are:

$$T_0^0 = \rho c^2,\ T_1^1 = T_2^2 = \cdots = T_{D-1}^{D-1} = -p. \tag{2.3}$$

Using (2.1) the field equations become:

$$\frac{(D-2)\lambda' e^{-\lambda}}{2r} - \frac{(D-2)(D-3)(e^{-\lambda}-1)}{2r^2} = \frac{8\pi G\rho}{c^2}, \tag{2.4a}$$

$$\frac{(D-2)\nu' e^{-\lambda}}{2r} + \frac{(D-2)(D-3)(e^{-\lambda}-1)}{2r^2} = \frac{8\pi G p}{c^4}, \tag{2.4b}$$

$$e^{-\lambda}\left[\frac{\nu''}{2} + \frac{\nu'^2}{4} - \frac{\nu'\lambda'}{4} + \frac{(D-3)(\nu'-\lambda')}{4r}\right] + \\ + \frac{(D-3)(D-4)(e^{-\lambda}-1)}{2r^2} = \frac{8\pi G}{c^4} p. \tag{2.4c}$$

From $T_{i;k}^k = 0$ it follows:

$$\nu' = -\frac{2p'}{p + \rho c^2}. \tag{2.5}$$

From Eq. (2.4a) we obtain immediately:

$$\frac{d(r^{D-3} e^{-\lambda})}{dr} = (D-3) r^{D-4} - \frac{8\pi G}{c^2} \frac{2}{D-2} \rho\, r^{D-2} \tag{2.6}$$

or

$$e^{-\lambda} = 1 - \frac{8\pi G}{c^2} \frac{2}{D-2} \frac{1}{r^{D-3}} \int_0^r \rho\, r^{D-2} dr$$

and

$$e^{-\lambda} = 1 - \frac{2GF(D)M}{r^{D-3}}, \tag{2.7}$$

where:

$$F(D) = -\frac{1}{(D-2)2^{D-5}}, \tag{2.8}$$

$$M(r) = \frac{1}{c^2}\int_0^r \pi\, 2^{D-2}\rho\, r^{D-2} dr. \tag{2.9}$$

Using (2.9) and (2.5) in Eq. (2.4b) we obtain the Oppenheimer–Volkoff equation in D space-time dimensions:

$$\frac{dp}{dr} = -\frac{G(p+\rho c^2)[(D-3)F(D)M + (8\pi/c^4)(1/(D-2)r^{D-1}p]}{r^{D-2}\left(1 - \frac{2GF(D)}{r^{D-3}}\right)}. \tag{2.10}$$

3. Non-dimensional form of the Oppenheimer–Volkoff equation

To obtain the non-dimensional form of the Oppenheimer–Volkoff equation (2.10) and of the mass continuity equation:

$$\frac{dM}{dr} = \frac{1}{c^2}\pi\, 2^{D-2}\rho\, r^{D-2} \tag{3.1}$$

we shall introduce Ureche's [8] non-dimensional independent variable η and the non-dimensional functions $\Psi(\eta)$, $P(\eta)$, $m(\eta)$ by means of the transformations:

$$r = a\eta,\ \rho = \rho_c \Psi,\ p = \rho_c c^2 P,\ M = M^* m. \tag{3.2}$$

Here a is a scale factor (a characteristic length), ρ_c the central density and M^* a characteristic mass.

Using (3.2) in Eqs (3.1) and (2.10) we obtain:

$$\frac{dm}{d\eta} = \eta^{D-2}\Psi, \tag{3.3a}$$

$$\frac{dP}{d\eta} = -\frac{(\Psi + P)[(D-3)m + \eta^{D-1}P]}{\eta^{D-2}(1 - \frac{2m}{\eta^{D-3}})}, \tag{3.3b}$$

where we have taken:

$$M^* = \frac{1}{2}\,\pi\, 2^{D-2}\rho_c\, a^{D-1}, \tag{3.4a}$$

$$a^2 = \frac{c^2}{2^{D-2}\pi G\rho_c}. \tag{3.4b}$$

The system (3.3a)-(3.3b)must be integrated with the boundary conditions:

$$M(0) = 0,\ \rho(R) = 0,\ p(R) = 0, \tag{3.5}$$

where R is the radius of the gaseous sphere, together with an equation of state of the form:

$$p = p(\rho). \tag{3.6}$$

In the new variables, the equation of state (3.6) becomes

$$P = P(\Psi), \tag{3.7}$$

while the boundary conditions (3.5) will become:

$$m(0) = 0,\ \Psi(\eta_s) = 0,\ P(\eta_s) = 0, \tag{3.8}$$

where $\eta_s = R/a$ is the value of the non-dimensional radial coordinate η at the surface of the gaseous sphere.

If we suppose that m is an increasing (non-decreasing) function of η, while Ψ and P are decreasing (non-increasing) function of the same argument, then from the transformations (3.2) it follows that:

$$\Psi \in [0, 1],\ P \in [0, P_c], \tag{3.9}$$

where P_c is the value of P in the centre of the star.

4. Homogeneous gaseous sphere in D space-time dimensions

We shall consider now the case of a homogeneous gaseous sphere in D space-time dimensions, that is, we suppose ρ =const. In this case $\Psi \equiv 1$, $\eta \in [0, \eta_s]$.

The differential system (3.3a) and (3.3b)can be easily integrated, using the boundary conditions:

$$m(0) = 0,\ P(0) = P_c \tag{4.1}$$

to give the exact solution:

$$m(\eta) = \frac{\eta^{D-1}}{D-1}, \tag{4.2a}$$

$$P(\eta) = \frac{\frac{D-3}{D-1}(1+P_c) - (\frac{D-3}{D-1} + P_c)(1 - \frac{2}{D-1}\eta^2)^{1/2}}{(\frac{D-3}{D-1} + P_c)(1 - \frac{2}{D-1}\eta^2)^{1/2} - (1+P_c)}. \tag{4.2b}$$

The radius R of the gaseous sphere can be obtained from the condition $P(\eta_s) = 0$ and is given by:

$$R^{D-3} = \frac{[(D-3) + (D-1)P_c]^2}{4F(D)[(D-3) + (D-2)P_c]P_c} R_g, \tag{4.3}$$

where

$$R_g = 2GF(D)M_s \tag{4.4}$$

is the D-dimensional gravitational (Schwarzschild) radius of the sphere and M_s is the total mass of the sphere.

We can generalize the classical restriction for the upper limit of the general theory of relativity in D space-time dimensions in the form:

$$p \leq \frac{1}{D-1}\rho c^2, \tag{4.5}$$

which gives:

$$P_c \in [0, 1/3]. \tag{4.6}$$

If we use the restriction

$$p \leq \rho c^2, \tag{4.7}$$

then

$$P_c \in [0, 1]. \tag{4.8}$$

Using the restriction (4.5) we obtain the following criterion of stability for a homogeneous gaseous sphere in D space-time dimensions:

$$R^{D-3} \geq \frac{(D-2)^2(D-1)^2}{4F(D)[(D-1)(D-3)+(D-2)]}R_g, \tag{4.9}$$

while using the restriction (4.7) we obtain:

$$R^{D-3} \geq \frac{(D-2)^2}{F(D)(2D-5)}R_g. \tag{4.10}$$

This expression generalizes to D space-time dimensions the criteria given by Ureche [8].

From (2.7) it follows immediately:

$$e^{-\lambda} = 1 - \frac{\pi G\rho r^2}{4(D-1)(D-2)c^2} \tag{4.11}$$

and from (2.5) we obtain:

$$e^{\nu(\eta)} = \frac{[P_c + \rho c^2]^2}{[P(\eta) + \rho c^2]^2}. \tag{4.12}$$

So, the problem of the homogeneous sphere in D space-time dimensions is completely solved.

5. Conclusions

In the present paper we have obtained the Oppenheimer–Volkoff equation in D space-time dimensions and found some stability criteria for homogeneous gaseous spheres. This represents the starting point upon which calculations of the internal structure and stability in higher dimensions can be made. Other factors influencing stability and structure in D space-time dimensions such as cosmological constant, scalar or vector fields will be investigated in a future paper.

References

1. J. R. Oppenheimer and G. M. Volkoff, Phys. Rev., *55*, 374, 1939.
2. T. Overgaard and E. Ostgaard, Astron. Astrophys., *243*, 412, 1991.
3. A. Rosenhauer, E. F. Staubo, L. P. Csernai, T. Overgaard and E. Ostgaard, Nucl. Phys. A, *540*, 630, 1992.
4. K. D. Krori, P. Bargahani and K. Das, Gen. Rel. and Grav. , *21*, 1099, 1989.
5. P. S. Florides, Proc. R. Soc. (London) A, *337*, 529, 1974.
6. C. Wolf, Acta Phys. Hung., *70*, 288, 1991.
7. J. P. Wright, Phys. Rev., *136*, 288, 1964.
8. V. Ureche, Rev. Roum. de Phys., *25*, 301, 1980.

Acta Physica Hungarica 72 (2-4), pp. 259–263 (1992)

DILATATION ET FUSION DES METAUX

Y. THOMAS

Institut de Recherches Scientifiques et Techniques
49045 Angers Cédex (France)

(Reçu 3 Novembre 1992)

Une théorie thermocinétique de la fusion des métaux permet d'exprimer l'amplitude des vibrations thermiques responsables de la dilatation de coefficient linéaire α et la température de fusion T_f en fonction de caractéristiques du réseau. Le produit $\alpha \cdot T_f$ apparaît comme un invariant structural. Les résultats sont comparés à des données expérimentales.

Introduction

Poursuivons l'étude du phénomène complexe de fusion, pour lequel il n'existe que diverses approches souvent anciennes et incomplètes [1], par une théorie thermocinétique qui, à partir de l'expérience, considère le point de fusion comme le point à partir duquel l'énergie thermique apportée à un réseau cristallin n'augmente plus que l'énergie potentielle W des atomes et non leur énergie cinétique moyenne.

Pour cela, on reprend le modèle du solide constitué d'oscillateurs anharmoniques identiques où la force rappelant chaque atome vers sa position d'équilibre est:

$$F_{(r)} = -\frac{dW(r)}{dr} = -K_1(r - r_0) + K_2(r - r_0)^2 + \ldots$$

avec K_1 et K_2 constants ($K_2 \ll K_1$), r: distance interatomique et r_0 cette distance à l'équilibre ($r - r_0 = x$) [2]. Nous considérons essentiellement les métaux.

Amplitude des oscillations atomiques

Exprimons les constantes K_1 et K_2 en fonction de caractéristiques des métaux.

Pour des petits déplacements atomiques, on se limite au second ordre du développement et on admet que les valeurs moyennes des énergies cinétique et potentielle sont les mêmes que pour un oscillateur harmonique. Loin du zéro absolu, ce principe de l'équipartition de l'énergie s'écrit:

$$\frac{1}{2}k_1\overline{(r - r_0)}^2 = \frac{1}{2}KT, \quad \overline{x^2} = KT/K_1$$

où K est la constante de Boltzmann et T la température absolue. Une solution de la forme:

$$x_{(t)} = r - r_0 = (\overline{r} - r_0) + a_1 \cos \omega t + a_2 \cos 2\omega t$$

de l'équation de mouvement $md^2(r-r_0)/dt^2 = F_{(r)}$ pour un oscillateur de masse m donne, avec $\omega = (K_1/m)^{1/2}$, comme dans le cas harmonique pour un seul degré de liberté

$$a_1^2 = 2x^2 = 2KT/K_1$$

avec une bonne approximation.

Le carré de l'amplitude a_1 de la fréquence fondamentale est proportionnelle à KT (et dépend des conditions initiales du mouvement).

La dilatation ou élongation moyenne constante de l'oscillateur est:

$$\overline{x} = \overline{r} - r_0 = a_1^2 K_2 / \, 2\, K_1 \, .$$

On sait que la compressibilité (considérée comme indépendante de la température) est:

$$X = -\frac{1}{V}\frac{dV}{dP} = 3(1-2G)/E$$

si G et E sont les modules de Poisson et d'Young, respectivement. Considérons une chaîne de n oscillateurs constituant un échantillon (section r_0^2, largeur $l = nr_0$) d'une substance polycristalline quasi isotrope. Son allongement Δl est dû à une force $K_1 \frac{\Delta l}{n} = E\, r_0^2 \frac{\Delta l}{l}$ soit $K_1 = E\, r_0$. Avec une bonne approximation: $3(1-2G) \simeq 1$ (car dans les structures compactes $G > \frac{1}{3}$ et le nombre d'atomes croît alors que c'est l'inverse dans les structures non compactes) d'où $K_1 = r_0/\chi$ (r_0 étant le diamètre atomique) et $a_1 = (2KT\chi/r_0)^{1/2}$ exprimant l'amplitude des oscillations thermiques des noyaux du réseau cristallin.

La valeur de a_1 est une valeur moyenne comme les autres constantes macroscopiques des métaux. Les valeurs ainsi calculées sont en accord satisfaisant avec celles déduites de l'étude expérimentale aux rayons X [3] comme le montre les exemples de KCl (cubique simple): $r_0 = 0.628$ nm, $\chi = 5,7 \cdot 10^{13}$ m^2·N^{-1} et de Al (cubique à faces centrées): $r_0 = 0.284$ nm, $\chi = 1,37 \cdot 10^{13}$ m^2·N^{-1}.

a (nm)

	KCl		Al	
T K	calculé	expéri.	calculé	expéri.
86	0.0146	0.0149	0.0107	0.0110
290	0.0265	0.0255	0.0190	0.0175

Des résultats analogues sont obtenus à l'aide de la formule de Debye–Waller:

$$\overline{a_1^2} = 4,364 \cdot 10^{-18} \frac{T}{Na \cdot m \cdot \Theta_D^2}[\Phi(u) + \frac{u}{4}]m^2,$$

où Na est le nombre d'Avogadro et $u = \frac{\Theta_D}{T}$ avec Θ_D la température de Debye difficile à déterminer avec précision [4]. Notre expression précédente de a_1, équivalente dès que T est assez élevée (u petit) à l'avantage d'être indépendante de Θ_D.

Si α est le coefficient de dilatation linéaire du métal: $\alpha = \frac{1}{T}\frac{\overline{x}}{r_0}$, les expressions précédentes de $\overline{x}_1$, K_1 et a_1 permettent de calculer la seconde constante $K_2 = r_0 \alpha K_1^2/K = \alpha r_0^3/K\chi^2$.

Fusion à la température T_f

L'annulation de la force $F_{(x)}$ entre un couple d'atomes à la fusion montre que $|x| \leq K_1/K_2$. Le mouvement stable d'un chaîne d'oscillateurs anharmoniques est d'ailleurs limité à $|x| \leq K_1/2K_2$, car $dF_{(x)}/dx = 0$ pour $x = K_1/2K_2$. On ne peut jamais avoir $x > K_1/2K_2$ où les atomes ne seraient plus rappelés à leur position d'équilibre stable (dF/dx serait négatif). En conséquence pour $T = T_f$: $|x|_{MAXI} = K_1/2K_2 = (4/3)\overline{x} + a_{1f}$ d'après la solution $x_{(t)}$ adoptée précédemment. En remplaçant $\overline{x}$, K_1 et K_2 en fonction des grandeurs caractéristiques du métal:

$$a_{1f} = \frac{K\chi}{2\alpha r_0^2} - \frac{4}{3} r_0 \alpha T_f,$$

où le second terme $\frac{4}{3} r_0 \alpha T_f$ est très petit. Soit, en première approximation:

$$T_f = \frac{3K\chi}{40\alpha^2 r_0^3}.$$

Comparons quelques résultats expérimentaux moyens avec les valeurs de T_f calculées à l'aide de cette expression [4,5] (tableau I).

Nos résultats sont toujours supérieures aux valeurs expérimentales par un facteur $\Gamma = T_f$ calculé$/T_f$ expérimental qui dépend de la symétrie cristalline et croît avec elle (1,66 pour les cubiques à corps centrés; 1,16 pour les cubiques à faces centrées et 1,36 pour les hexagonaux). En effet, notre détermination de T_f résulte de la distribution statistique de Maxwell des amplitudes de vibration des atomes puisque nous avons posé à la fusion $a_{1f} = \frac{K}{2K_2} - \frac{4}{3}\overline{x}$ soit environ 57 % des noeuds du réseau cristallin ayant atteint (ou dépassé) la valeur de l'amplitude critique a_{1f} précédente. Or la fusion doit se produire pour un nombre plus faible d'oscillateurs vibrant à l'amplitude critique, ceci d'autant plus que la symétrie du réseau est grande. On doit donc écrire avec le facteur Γ de la symétrie cristalline:

$$T_f = \frac{1}{\Gamma} \cdot \frac{3K\chi}{40\alpha^2 r_0^3}.$$

(M_0 donne une valeur discordante due à une transformation allotropique).

Conséquences

Adoptons à nouveau pour l'énergie potentielle l'expression $W(r) = -a/r^m + b/r^n$ [1]. On peut alors considérer que la force élémentaire $F(r)$ résulte du développement en série de Taylor de $F(r) = -a'/r^{m'} + b'/r^{n'}$ avec $F(r_0) = 0$, $m' = m+1$, $n' = n+1 \ldots$).

Tableau I

Comparaison des valeurs de T_f et valeurs de $\alpha \cdot T_f$

Métaux	$\alpha \cdot 10^6$ K^{-1}	$\chi \cdot 10^{13}$ m$^2 \cdot$ N^{-1}	$r_0 \cdot 10^{10}$ m	T_f K		$\Gamma = \frac{T_f \text{ calculé}}{T_f \text{ expérimental}}$	$\alpha \cdot T_f$ expé %
				calculé	expérimental		
Na	70,5	15,9	3,7	620	371	1,67	2,60
K	85	33	4,59	512	337	1,52	2,86
Fe	12,4	0,55	2,49	3245	1808	1,79	2,24
Mo	5,5	0,36	2,72	7402	2890	(2,61)	(1,56)
Al	26	138	2,86	1160	933	1,24	2,42
Ni	16	0,54	2,48	2140	1726	1,24	2,76
Cu	16,6	0,75	2,56	1682	1356	1,24	2,25
Pd	11,5	0,54	2,74	2105	1825	1,15	2,09
Ag	18,6	1,01	2,88	1165	1235,5	0,95	2,29
Zn	31	1,72	2,74	972	693	1,40	2,14
Cd	32	2,25	3,04	785	594	1,32	1,90

Il en résulte:

$$K_1 = \frac{n' - m'}{r_0^{m'+1}} a' \quad \text{et} \quad K_2 = \frac{n'(n'+1) - m'(m'+1)}{2r_0^{m'+2}} a',$$

$$\frac{K_1}{K_2} = \frac{2r_0}{1 + n' + m'} = \frac{r_0/\chi}{\alpha r_0^3 / K\chi^2} = \frac{K\chi}{\alpha r_0^2} = \frac{40}{3} \Gamma \alpha T_f r_0.$$

D'où: $\alpha T_f = \frac{6}{40} \frac{1}{\Gamma(1+n'+m')}$, c'est une constante qui dépend de la symétrie du réseau que multiplie la constante γ de Grüneisen [5]. Le produit $\alpha \cdot T_f$ apparaît comme une constante pour chaque type de structure en accord avec des résultats précédents [6] car l'expression de T_f est aussi égale à $\frac{12}{40\Gamma} \frac{1}{(1+n'+m')^2} \frac{r_0^3}{K\chi}$. En effet, les exposants n' et m' sont caractéristiques de chaque structure cristalline en accord avec la théorie de Wigner et Seitz.

On vérifie (tableau I) que de produit αT_f, représentant le pourcentage total de la dilatation linéaire jusqu'à T_f est sensiblement constant pour chaque structure. Il croît avec la symétrie de la structure: 2,57 % pour les cubiques à corps centrés, 2,36 % pour les cubiques à faces centrées et 2,02 % pour les hexagonaux. Ceci est en accord avec le fait que γ dépend plus de la symétrie que de la température à laquelle les valeurs de r_0, χ et α sont considérées et avec le fait que la fusion intervient pour des vibrations atteignant, comme nous l'avons montré [1], une certaine fraction de l'écart interatomique indépendamment de la nature de l'atome. Ceci est également en accord avec des invariants connus pour des structures de même type: $V/\chi T_f$, $\alpha V/\chi$, $V/\chi L$ où V est le volume atomique et L la chaleur de sublimation.

Il en résulte toutefois une légère dispersion des valeurs par l'influence de la température (surtout sur α) et des valeurs plus discordantes se rapportant vraisemblablement à des transformations allotropiques qui peuvent être ainsi détectées (cas de M_0) ou à des effets magnétiques (cas de Ni).

References

1. J. E. Lennard-Jones, Devonshire, Proc. Roy. Soc. A, *170*, 464, 1939; M. Born, J. Chem. Phys., *7*, 591, 1939; R. Furth, Proc. Roy. Soc. A, *183*, 87, 1939; Phil. Mag., *40*, VII, 1227, 1949; Y. Thomas, Acta Phys. Hung., *71*, 207, 1992.
2. Y. Thomas, Phys. Lett., *66A*, 2, 131, 1978.
3. J. K. Roberts and A. R. Miller, Heat and Thermodynamics, N. Y., 5th ed., 1960.
4. Y. Thomas et G. Goureaux, C. R. Acad. Sc., Paris, *268*, 1518, 1969.
5. N. F. Mott and H. Jones, The Theory of the Properties of Metals and Alloys, Dover Inc., N. Y., 1958.
6. J. Frenkel, Kinetic Theory of Liquids, Oxford, Clarendon Press, 1946; M. E. Straumanis, J. Appl. Phys., *21*, 936, 1950.

Acta Physica Hungarica 72 (2-4), pp. 265–273 (1992)

THERMAL-FIELD DYSON MAPPING FOR HOT ODD NUCLEI

E. M. GALINSKY

Laboratory of Neutron Physics, Joint Institute for Nuclear Research
141980 Dubna, Moscow Region, Russia

and

R. B. BEGZHANOV

Institute of Nuclear Physics
Ulugbec, Tashkent 702132, Uzbekistan

(Received in revised form 3 November 1992)

Two possibilities of Dyson fermion–boson realization for two-particle operators at finite temperature are derived using the thermal-field dynamic formalism. The nature of spurious states appearance in an odd-particle system is investigated. It is further observed that the matrix element of the pairing interaction between the fermion–boson basis is identical to the corresponding fermion matrix element.

Recently, very excited nuclei can be produced in heavy-ion collision and their properties can be studied experimentally as function of temperature. Experimental evidences have suggested that a nuclear system is thermally equilibrated rapidly after the formation of a compound nucleus from heavy-ion reactions [1]. The large nuclear state density equally populates individual highly-excited states. Consequently, average properties of the system are usually measured. This is why the statistical extension of different approaches can be appropriate to be applied to study collective states at finite temperature. One of such extensions is thermal-field Dyson mapping (TFDM) [2].

The Dyson boson mapping [3] is quite applicable to the description of nuclear collective motion, especially to the analysis of mode–mode coupling in cold nuclei [4]. The Dyson boson mapping has a big merit that a mapped operator is written in a form of a finite series of boson operators and then there is no ambiguity in the mapped operator. On the other hand, it has an outward demerit in that the transformation is non-unitary and the mapped Hamiltonian is not Hermitean, thus unphysical (spurious) states appear. Recently, it has been shown [2] that while carrying out the calculations of the matrix elements with a physical Hamiltonian, in even-particle hot system (the particle in the single particle shell model state), in the ideal thermal boson basis state one can separate the physical an unphysical components and need not worry about the spurious state using the TFDM. The purpose of the present paper is to generalize the TFDM to be applicable to an odd-particle hot system.

There are two ways to formulate the TFDM: 1) thermalization after Dyson mapping (TFDM-I); 2) Dyson mapping after thermalization (TFDM-II). Thermal-field boson realization applied to an even - A hot system has been worked out in [2] and [5]. We start with the two-particle operators

$$\begin{aligned} A^+(jj';\lambda\mu) &= \sum_{mm'} C^{\lambda\mu}_{jmj'm'} a^+_{jm} a^+_{j'm'}, \\ A(jj';\lambda\mu) &= \sum_{mm'} C^{\lambda\mu}_{jmj'm'} a_{j'm'} a_{jm}, \\ B(jj';\lambda\mu) &= \sum_{mm'} C^{\lambda\mu}_{jmj'm'} a^+_{jm} \tilde{a}_{j'm'}, \end{aligned} \tag{1}$$

where a^+_{jm}, a_{jm} are single-particle creation and annihilation operators, respectively, satisfying the usual commutation relations for fermions, λ denotes multipolarity excitation and μ denotes z-projection in the laboratory system of λ. The usual time-reversed notation ($\sim$) is used for the annihilation operator, $\tilde{a}_{jm} = (-1)^{j-m} a_{j-m}$.

Applying the ansatz thermalization [6] and Dyson mapping for odd-particle system [7], we obtained TFDM-I and TFDM-II for the operators (1)

$$\begin{aligned} [A^+(jj';\lambda\mu)]^{\text{odd}}_{\text{TFDM-I}} &= [A^+(jj';\lambda\mu)^{\text{even}}_{\text{TFDM-I}} - \sum_{J_1 J_2 j_1} G^{\lambda}_{J_1 J_2}(jj' j_1) * \\ &* \{\sqrt{(1-n_{J_1})(1-n_{j_1})(1-n_{j'})}[b^+_{J_1}(jj_1)_T [\beta^+_{j_1}(T)\tilde{\beta}_{j'}(T)]_{J_2}]_{\lambda\mu} - \\ &- \sqrt{(1-n_{J_1})(1-n_{j_1})n_{j'}}[b^+_{J_1}(jj_1)_T [\beta^+_{j_1}(T)\beta^+_{j'}(T)]_{J_2}]_{\lambda\mu} + \\ &+ \sqrt{(1-n_{J_1})n_{j_1}(1-n_{j'})}[b^+_{J_1}(jj_1)_T [\beta_{j_1}(T)\tilde{\beta}_{j'}(T)]_{J_2}]_{\lambda\mu} - \\ &- \sqrt{(1-n_{J_1})n_{j_1}n_{j'}}[b^+_{J_1}(jj_1)_T [\beta_{j_1}(T)\beta^+_{j'}(T)]_{J_2}]_{\lambda\mu} - \\ &- \sqrt{n_{J_1}(1-n_{j_1})(1-n_{j'})}[\tilde{b}_{J_1}(jj_1)_T [\beta^+_{j_1}(T)\tilde{\beta}_{j'}(T)]_{J_2}]_{\lambda\mu} - \\ &- \sqrt{n_{J_1}(1-n_{j_1})n_{j'}}[\tilde{b}_{J_1}(jj_1)_T [\beta^+_{j_1}(T)\beta^+_{j'}(T)]_{J_2}]_{\lambda\mu} + \\ &+ \sqrt{n_{J_1}n_{j_1}(1-n_{j'})}[\tilde{b}_{J_1}(jj_1)_T [\beta_{j_1}(T)\tilde{\beta}_{j'}(T)]_{J_2}]_{\lambda\mu} - \\ &- \sqrt{n_{J_1}n_{j_1}n_{j'}}[\tilde{b}_{J_1}(jj_1)_T [\beta_{j_1}(T)\beta^+_{j'}(T)]_{J_2}]_{\lambda\mu}\}, \end{aligned} \tag{2}$$

$$\begin{aligned} [A(jj';\lambda\mu)]^{\text{odd}}_{\text{TFDM-I}} &\equiv [A(jj';\lambda\mu)^{\text{even}}_{\text{TFDM-I}} = \\ &= \sqrt{1-n_\lambda}\, b_{\lambda\mu}(jj')_T + \sqrt{n_\lambda}\, \tilde{b}^+_{\lambda\mu}(jj')_T, \end{aligned} \tag{3}$$

$$\begin{aligned} [B(jj';\lambda\mu)]^{\text{odd}}_{\text{TFDM-I}} &= [B(jj';\lambda\mu)^{\text{even}}_{\text{TFDM-I}} + \sqrt{(1-n_j)(1-n_{j'})} * \\ &* [\beta^+_j(T)\tilde{\beta}_{j'}(T)]_{\lambda\mu} - \sqrt{(1-n)n_{j'}}[\beta^+_j(T)\beta^+_{j'}(T)]_{\lambda\mu} + \sqrt{n_j(1-n_{j'})} * \\ &* [\tilde{\beta}_j(T)\beta_{j'}(T)]_{\lambda\mu} - \sqrt{n_j n_{j'}}[\tilde{\beta}_j(T)\beta^+_{j'}(T)]_{\lambda\mu}, \end{aligned} \tag{4}$$

$$[A^+(jj';\lambda\mu)]^{\text{odd}}_{\text{TFDM-II}} = [A^+(jj';\lambda\mu)^{\text{even}}_{\text{TFDM-II}} - \sqrt{(1-n_j)(1-n_{j'})}*$$
$$* \sum_{J_1 J_2 j_1} G^{\lambda}_{J_1 J_2}(jj'j_1)[b^+_{J_1}(jj_1)_T[\beta^+_{j_1}(T)\tilde{\beta}_{j'}(T)]_{J_2}]_{\lambda\mu} - \tag{5}$$
$$- \sqrt{(1-n_J)n_{j'}}[\beta^+_j(T)\tilde{\beta}_{j'}(T)]_{\lambda\mu} - \sqrt{(1-n_{J'})n_j}[\tilde{\beta}^+_{j'}(T)\beta_j(T)]_{\lambda\mu},$$

$$[A(jj';\lambda\mu)]^{\text{odd}}_{\text{TFDM-II}} = [A(jj';\lambda\mu)^{\text{even}}_{\text{TFDM-II}} - \sqrt{n_j n_{j'}}*$$
$$* \sum_{J_1 J_2 j_1} G^{\lambda}_{J_1 J_2}(jj'j_1)[b^+_{J_1}(jj_1)_T[\beta^+_{j_1}(T)\tilde{\beta}_{j'}(T)]_{J_2}]_{\lambda\mu} - \tag{6}$$
$$- \sqrt{(1-n_J)n_{j'}}[\tilde{\beta}^+_{j'}(T)\beta_j(T)]_{\lambda\mu} - \sqrt{(1-n_{J'})n_j}[\beta^+_j(T)\tilde{\beta}_{j'}(T)]_{\lambda\mu},$$

$$[B(jj';\lambda\mu)]^{\text{odd}}_{\text{TFDM-II}} = [B(jj';\lambda\mu)^{\text{even}}_{\text{TFDM-II}} + \sqrt{(1-n_j)(1-n_{j'})}*$$
$$* [\beta^+_j(T)\tilde{\beta}_{j'}(T)]_{\lambda\mu} - \sqrt{(1-n_j)n_{j'}} \sum_{J_1 J_2 j_1} G^{\lambda}_{J_1 J_2}(jj'j_1)* \tag{7}$$
$$* [b^+_{J_1}(jj_1)_T[\beta^+_{j_1}(T)\tilde{\beta}_{j'}(T)]_{J_2}]_{\lambda\mu} - \sqrt{n_j n_{j'}}[\tilde{\beta}^+_{j'}(T)\beta_j(T)]_{\lambda\mu},$$

where

$$[A^+(jj';\lambda\mu)]^{\text{odd}}_{\text{TFDM-I}} = \sqrt{1-n_\lambda}\, b^+_{\lambda\mu}(jj')_T + \sqrt{n_\lambda}\, \tilde{b}^+_{\lambda\mu}(jj')_T -$$
$$- \sum_{\substack{J_1 J_2 J_3 \\ J_4 j_1 j'_1}} C^{\lambda}_{J_1 J_2 J_3 J_4}(jj'j_1 j'_1) * \{\sqrt{(1-n_{J_1})(1-n_{J_2})(1-n_{J_3})}*$$
$$* [[b^+_{J_1}(jj_1)_T b^+_{J_2}(j'j'_1)_T]_{J_4}\tilde{b}_{J_3}(j_1 j'_1)_T]_{\lambda\mu} + \sqrt{(1-n_{J_1})(1-n_{J_2})n_{J_3}}*$$
$$* [[b^+_{J_1}(jj_1)_T b^+_{J_2}(j'j'_1)_T]_{J_4} b^+_{J_3}(j_1 j'_1)_T]_{\lambda\mu} + \sqrt{(1-n_{J_1})n_{J_2}(1-n_{J_3})}*$$
$$* [[b^+_{J_1}(jj_1)_T \tilde{b}_{J_2}(j'j'_1)_T]_{J_4}\tilde{b}_{J_3}(j_1 j'_1)_T]_{\lambda\mu} + \sqrt{(1-n_{J_1})n_{J_2}n_{J_3}}*$$
$$* [[b^+_{J_1}(jj_1)_T \tilde{b}_{J_2}(j'j'_1)_T]_{J_4} b^+_{J_3}(j_1 j'_1)_T]_{\lambda\mu} + \sqrt{n_{J_1}(1-n_{J_2})(1-n_{J_3})}*$$
$$* [[\tilde{b}_{J_1}(jj_1)_T b^+_{J_2}(j'j'_1)_T]_{J_4}\tilde{b}_{J_3}(j_1 j'_1)_T]_{\lambda\mu} + \sqrt{n_{J_1}(1-n_{J_2})n_{J_3}}*$$
$$* [[\tilde{b}_{J_1}(jj_1)_T b^+_{J_2}(j'j'_1)_T]_{J_4} b^+_{J_3}(j_1 j'_1)_T]_{\lambda\mu} + \sqrt{n_{J_1}n_{J_2}(1-n_{J_3})}*$$
$$* [[\tilde{b}_{J_1}(jj_1)_T \tilde{b}_{J_2}(j'j'_1)_T]_{J_4}\tilde{b}_{J_3}(j_1 j'_1)_T]_{\lambda\mu} + \sqrt{n_{J_1}n_{J_2}n_{J_3}}*$$
$$* [[\tilde{b}_{J_1}(jj_1)_T \tilde{b}_{J_2}(j'j'_1)_T]_{J_4}\tilde{b}_{J_3}(j_1 j'_1)_T]_{\lambda\mu}\},$$

$$[B(jj';\lambda\mu)]^{\text{odd}}_{\text{TFDM-I}} = -\sum_{J_1J_2j_1} D^{\lambda}_{J_1J_2}(jj'j_1)\{\sqrt{(1-n_{J_1})(1-n_{J_2})}*$$
$$*\,[b^{+}_{J_1}(jj_1)_T\tilde{b}_{J_2}(j'j'_1)_T]_{\lambda\mu} + \sqrt{(1-n_{J_1})n_{J_2}}[b^{+}_{J_1}(jj_1)_T b^{+}_{J_2}(j'j'_1)_T]_{\lambda\mu} +$$
$$+\sqrt{n_{J_1}(1-n_{J_2})}[\tilde{b}_{J_1}(jj_1)_T\tilde{b}_{J_2}(j'j'_1)_T]_{\lambda\mu} + \sqrt{n_{J_1}n_{J_2}}[\tilde{b}_{J_1}(jj_1)_T b^{+}_{J_2}(j'j'_1)_T]_{\lambda\mu}\},$$
$$[b^{+}_{J_1}(jj')_T\tilde{b}_{J_2}(jj'_1)_T]_{J_3M_3} = \sum_{M_1M_2} C^{J_3M_3}_{J_1M_1J_2M_2} b^{+}_{J_1M_1}(jj_1)b_{J_2M_2}(j'j'_1)_T.$$

$b^{+}_{JM}(jj_1)_T$, $b_{JM}(jj_1)_T$, $\beta^{+}_{jm}(T)$, $b_{jm}(T)$ are the creation and annihilation operators of thermal bosons and fermions, respectively. Expressions $[A^{+}(jj';\lambda\mu)]^{\text{odd}}_{\text{TFDM-II}}$, $[A(jj';\lambda\mu)]^{\text{odd}}_{\text{TFDM-II}}$, $[B(jj';\lambda\mu)]^{\text{odd}}_{\text{TFDM-II}}$ are given in [2], but the explicit forms for the coefficients $C^{\lambda}_{J_1J_2J_3J_4}(jj'j_1j'_1)$, $G^{\lambda}_{J_1J_2}(jj'j_1)$ and $D^{\lambda}_{J_1J_2}(jj'j_1)$ are given in [8,9], n_j in the occupation number of fermions with energy $\mathcal{E}_j$ at temperature T

$$n_j = [\exp(\mathcal{E}/T)+1]^{-1}$$

and n_λ is the occupation number of bosons with energy ω_λ at temperature T

$$n_\lambda = [\exp(\omega_\lambda/T)-1]^{-1}.$$

It is clear from (5)–(7) that in the zero-temperature limit $T \to 0$. These formulae transform completely into the usual Dyson mapping for these operators given in [9]. Then, we consider a system consisting of $P+1$ identical nucleons, where P is the number of nucleon pairs, each of which occupies time-reversed orbits, the unpaired nucleon occupying one j-shell. Namely, we will deal with the simple case of three-level (three-j) model, where P nucleon pairs occupying two j-levels which can have the same or different degeneracies are available. Let ΔE be the distance between the levels. As a residual interaction, we use a pairing force with constant matrix elements G. For this case the algebraic expressions for the same matrix are available. This model is an extension of the model for an even-particle system [10]. The Hamiltonian of the system is

$$\begin{aligned} H_F &= \hat{E}_1 j_1 B(j_1j_1;00) + \Delta E[\hat{j}_3 B(j_3j_3;00) - \hat{j}_2 B(j_2j_2;00)] - G/4* \\ &*\{[\hat{j}_1 A^{+}(j_1j_1;00) + \hat{j}_2 A^{+}(j_2j_2;00)][\hat{j}_1 A(j_1j_1;00) - \hat{j}_2 A(j_2j_2;00)] + \\ &+[\hat{j}_1 A^{+}(j_1j_1;00) + \hat{j}_3 A^{+}(j_3j_3;00)][\hat{j}_1 A(j_1j_1;00) + \hat{j}_3 A(j_3j_3;00)] + \\ &+[\hat{j}_2 A^{+}(j_2j_2;00) + \hat{j}_3 A^{+}(j_3j_3;00)][\hat{j}_2 A(j_2j_2;00) - \hat{j}_3 A(j_3j_3;00)]\}, \end{aligned} \tag{8}$$

where $\hat{j} = \sqrt{2j+1}$. We can introduce an orthonormal basis for this system

$$\begin{aligned} |S, P-S> &= 1/(\sqrt{S!(P-S)!})a^{+}_{j_1m_1}(A^{+}(j_2j_2;00))^{s}* \\ &*(A^{+}(j_3j_3;00))^{P-S}|0>, \end{aligned} \tag{9}$$

where $a_{jm}|0>=0$, i.e. $|0>$ is fermion vacuum, the unpaired nucleon occupying the j_1-level, S nucleon pair occupying the j_2-level.

The thermal fermion–boson basis states corresponding with these states (9) are

$$|S, P-S) = 1/(\sqrt{S!(P-S)!})\beta^{+}_{j_1 m_1}(T)(b^{+}_{00}(j_2 j_2)_T)^S * \\ * (b^{+}_{00}(j_3 j_3)_T)^{P-S}|\tilde{0}>|\tilde{0}), \tag{10}$$

where $\beta_{jm}(T)|\tilde{0}>$, $b_{00}(jj)_T|\tilde{0}) = 0$, i.e. $|\tilde{0}>$ and $|\tilde{0})$ are thermal fermion and thermal boson vacuum, respectively.

Using the expressions (2)–(8), (10) we can receive the matrix element of the thermal fermion–boson image H_{FB} Hamiltonian of the system H_F in this basis (10), for the case of TFDM-I and TFDM-II, respectively,

$$H^I_1 = \{E_1 + \Delta E[3P - 2(S-1)]\}\delta_{ss'}, \tag{11}$$

$$H^I_2 = -G/2\{S[\hat{j}_2 + (1-n^{(2)})^2(1-S)] + (P-S)[\hat{j}^2_3 + (1-n^{(3)})^2(1-P+S)] - \\ - 4n^{(2)}S(S+1) + n^{(3)}[4(P-S)(P-S+1)-1] + n^{(2)^2}(5S^2 - S - 3) + 3n^{(3)^2} * \\ * [(P-S)^2 - 1]\}\delta_{ss'},$$

$$H^I_3 = -G/4\{[\sqrt{(1-n)^{(2)})(1-n^{(3)})} + \sqrt{n^{(2)}n^{(3)}}]\sqrt{S(P-S+1)}\hat{j}_2\hat{j}_3 - \\ - [\sqrt{(1-n^{(2)})(1-n^{(3)})}[n_{j_3} + P - S + n^{(3)}(P-S+3)]\hat{j}_2\hat{j}_3^{-1} + \sqrt{n^{(2)}n^{(3)}} * \\ [n_{j_2} + 2S - 1 + n^{(3)}(2-S)]\hat{j}_3\hat{j}_2^{-1}]\sqrt{S(P-S+1)}\}\delta_{s',s-1}, \tag{12}$$

$$H^I_4 = -G/4\{[\sqrt{(1-n^{(2)})(1-n^{(3)})} + \sqrt{n^{(2)}n^{(3)}}]\sqrt{(S+1)(P-S)}\hat{j}_2\hat{j}_3 - \\ - [\sqrt{(1-n^{(2)})(1-n^{(3)})}[n_{j_2} + S + n^{(2)}(S+3)]\hat{j}_3\hat{j}_2^{-1} + \sqrt{n^{(2)}n^{(3)}} * \\ * [n_{j_3} + 2(P-S) + n^{(3)}(S-P+2)]\hat{j}_2\hat{j}_3^{-1}]\sqrt{(S+1)(P-S)}\}\delta_{s',s+1},$$

$$n^{(2,3)} \equiv n^{(j_2,j_3)}_{\lambda=0},$$

$$(S', P-S'|H^{II}_{FB}|S, P-S) = H^{II}_1 + H^{II}_2 + H^{II}_3 + H^{II}_4, \tag{13}$$

where

$$H_1^{II} = \{E_1 + \Delta E[3(1-2n_{j_3})(P-S) - (1-2n_{j_2})S + 2(1-2n_{j_1})]\}\delta_{ss'},$$
$$H_2^{II} = -G/2\{S(\hat{j}_2^2 + 1 - S)(1-n_{j_2})^2 + (P-S)(\hat{j}_3^2 + 1 - P - S)(1-n_{j_3})^2 +$$
$$+ (S+1)(\hat{j}_2^2 - S)n_{j_2}^2 + (P-S+1)(\hat{j}_3^2 - P - S)n_{j_3}^2 + 4[S\sqrt{n_{j_2}(1-n_{j_2})} + (P-S)*$$
$$* \sqrt{n_{j_3}(1-n_{j_3})}]^2 + n_{j_1}(5n_{j_1} - 4)\}\delta_{ss'}, \tag{14}$$
$$H_3^{II} = -G/4\{(1 - n_{j_2} - n_{j_3} + 2n_{j_2}n_{j_3})\sqrt{S(P-S+1)}\hat{j}_2\hat{j}_3 -$$
$$- (1 - n_{j_2} - n_{j_3} - 2n_{j_2}n_{j_3})(P-S)\sqrt{S(P-S+1)}\hat{j}_2\hat{j}_3^{-1}\}\delta_{s',s-1},$$
$$H_4^{II} = -G/4\{(1 - n_{j_2} - n_{j_3} + 2n_{j_2}n_{j_3})\sqrt{(S+1)(P-S)}\hat{j}_2\hat{j}_3 -$$
$$- (1 - n_{j_2} - n_{j_3} - 2n_{j_2}n_{j_3})S\sqrt{(S+1)(P-S)}\hat{j}_2\hat{j}_3^{-1}\}\delta_{s',s+1}.$$

Here after the brackets $< \cdots >$ denote the average value over the grand canonical ensemble [11]. It is clear from (11)–(14) that due to the nonunitary character of the Dyson mapping, the matrix elements $H_{ss'} \neq H_{s's}$ for $S = S'$, thus spurious states appear.

Using the expressions (2)–(8), the Hermitization prescription [12] and introducing bi-orthonormal fermion–boson basis (for the even-particle system bi-orthonormal boson basis was introduced [13])

$$|S, P-S)_R = \gamma_{S,P-S}\frac{\beta^+_{j_1m_1}(T)(b^+_{00}(j_2j_2)_T)^S(b^+_{00}(j_3j_3)_T)^{P-S}}{\sqrt{S!(P-S)!}}|\tilde{0}> |\tilde{0}),$$
$$_L(S, P-S| = \gamma^{-1}_{S,P-S}(\tilde{0}|<\tilde{0}|\frac{(b_{00}(j_3j_3)_T)^{P-S}(b_{00}(j_2j_2)_T)^S\beta_{j_1m_1}(T)}{\sqrt{S!(P-S)!}}, \tag{15}$$

where

$$\gamma_{S,P-S} = \sqrt{\frac{(\hat{j}_2^2 - S)!\hat{j}_2^{2S}\hat{j}_3^2!}{(\hat{j}_3^2 - P + S)!\hat{j}_3^{2(P-S)}\hat{j}_2^2!}}$$

we receive the matrix element of the thermal fermion–boson image Hamiltonian (8) in this basis (15), for the case of TFDM-I and TFDM-II, respectively,

$$_L(S', P-S'|H^I_{FB}|S, P-S)_R = H_1^I + H_2^I + H_3^I, \tag{16}$$

where

$$H_1^I = \{E_1 + \Delta E[3P - 2(S-1)]\}\delta_{SS'},$$

$$H_2^I = -G/2\{S[\hat{j}_2^2 + (1-n^{(2)})(1-S)] + (P-S)[\hat{j}_3^2 + (1-n^{(3)})(1-P+S)] +$$
$$+ n^{(2)}[(2S+1)^2 + n^{(2)}(3S^2+S+1) - 1] + n^{(3)}[(2P-2S+1)^2 + n^{(2)}*$$
$$* [3(P-S)^2 + P - S - 1]\}\delta_{ss'}, \tag{17}$$

$$H_3^I = -G/4[\sqrt{(1-n^{(2)})(1-n^{(3)})} +$$
$$+ \sqrt{n^{(2)}n^{(3)}}][\sqrt{S(\hat{j}_2^2 - S + 1)(P-S+1)(\hat{j}_3^2 - P + S)}*$$
$$* \delta_{s',s-1} + \sqrt{(S+1)(\hat{j}^2 - S)(P-S)(\hat{j}_3^2 - P + S + 1)}\delta_{s',s+1}]$$
$$_L(S', P-S'|H_{FB}^{II}|S, P-S)_R = H_1^{II} + H_2^{II} + H_3^{II}, \tag{18}$$

where

$$H_1^{II} = \{E_1 + \Delta E[3(1-2n_{j_3})(P-S) + (1-2n_{j_2})S + 2(1-n_{j_1})]\}\delta_{ss'},$$
$$H_2^{II} = -G/2\{S[\hat{j}_2^2 + 1 - S)(1-n_{j_2})^2 + (P-S)(\hat{j}_3^2 + 1 - P - S)(1-n_{j_3})^2 +$$
$$+ (S+1)(\hat{j}^2 - S)n_{j_2}^2 + (P-S+1)(\hat{j}_3^2 - P - S)n_{j_3}^2 + 4[S^2 n_{j_2}(1-n_{j_2}) +$$
$$+ (P-S)^2 n_{j_3}(1-n_{j_3})]\delta_{ss'}, \tag{19}$$
$$H_3^{II} = -G/4[1 - n_{j_2} - n_{j_3} + 2n_{j_2}n_{j_3}][\sqrt{S(\hat{j}_2^2 - S + 1)(P-S+1)(\hat{j}_3^2 - P + S)}*$$
$$* \delta_{s',s-1} + \sqrt{(S+1)(\hat{j}_2^2 - S)(P-S)(\hat{j}_3^2 - P + S + 1)}\delta_{s',s+1}.$$

Using the expressions (8)–(9) we receive the fermion matrix element

$$< S', P-S|H_F|S, P-S >= \{E_1 + \Delta E[3P - 2(S-1)] -$$
$$- G/2[S(\hat{j}_2^2 + 1 - S) + (P-S)(\hat{j}^2 + 1 - P - S)]\}\delta_{ss'} - G/4*$$
$$* [\sqrt{S(\hat{j}_2^2 - S + 1)(P-S+1)(\hat{j}_3^2 - P + S)}\delta_{s',s-1} + \tag{20}$$
$$+ \sqrt{(S+1)(\hat{j}_2^2 - S)(P-S)(\hat{j}_3^2 - P + S + 1)}\delta_{s',s+1}].$$

It is clear from (16)–(19) that in the zero-temperature limit $n \to 0$ and these formulae transform into (20). Therefore, the matrix element of the pairing interaction between the thermal fermion–boson basis states turns out to be equivalent to the corresponding fermion matrix element.

It should be noted that the above analysis shows some distinctions between the characteristic features of the TFDM-I and TFDM-II. Namely, in the case TFDM-I the thermal effect is taken into account only through the interactions between bosons, since the boson operators in this scheme are the image of the fermion pairs at $T = 0$. The bosons in the case TFDM-II already include the effect of

temperature, since they are the image of the thermal pair-operators. These two schemes (TFDM-I and TFDM-II) should be equivalent in principle, if one does not make any approximation. However, if one performs some approximation [12] to diagonalize the Hamiltonian, the results become different from each other, i.e. $H_K^I \neq H_K^{II}$, where $K = 1, 2, 3$. Furthermore, there is a conceptual difference in the nature of the boson Hilbert subspace of the fermion–boson Hilbert space. In fact, the thermal boson vacuum $|\tilde{0})$ must be defined in TFDM-I and the temperature plays a definite role through the Bose–Einstein distribution function in the thermal Bogoliubov transformation [6]. One the other hand, the boson part image of the system in TFDM-II has nothing to do with the boson version of thermal field dynamics (TFD). In other words, the Hamiltonian in TFDM-II is not a thermal Hamiltonian in the sense of TFD although it is a faithful representation of the thermal Hamiltonian H_F: the Bose–Einstein distribution function never appears in TFDM-II.

In conclusion, in this paper we derived the Dyson fermion–boson realization for two-particle operators at finite temperature, in an odd-particle system, for the TFDM-I and TFDM-II. Due to the nonunitary character of the Dyson mapping the spurious states appear. Using the Hermitization prescription [12] it was shown that the physical subspace does not mix with the unphysical one. Thus, one need not worry about the spurious states while carrying out the calculations in the fermion–boson basis states, for an odd-particle system, at $T \neq 0$. Let us note that in the description of features of the giant multipole resonance (GMR), in hot odd nuclei, such as an enhancement in the broadening of the resonance and down shift of its centroid energy with increasing temperature [14], TFDM can be applied. It should be very desirable to investigate the influence of the effects of the quantal and thermal fluctuations [15], as well as shape changes [16] on the GMR, energy centroid in these nuclei. The calculations of these features of GMR and the influence of these effects on the GMR, in realistic hot odd nuclei, within the framework TFDM are the goal for our future study.

Acknowledgement

The authors thank Professor R. V. Jolos for his interest in the work and useful suggestions.

References

1. J. O. Newton, B. Herskind, R. M. Diamond, E. L. Dines, J. E. Draper, K. H. Lindenberger, C. Schuck, S. Shin and F. Stephens, Phys. Rev. Lett., *46*, 1383, 1981.
2. R. B. Begzhanov and E. M. Galinsky, Europhys. Lett., *12*(7), 617, 1990.
3. F. J. Dyson, Phys. Rev., *102*, 1217, 1956.
4. K. Takada and S. Tazaki, Nucl. Phys., *A448*, 56, 1986.
5. T. Hadsuda, Nucl. Phys., A, *492*, 187, 1989.
6. H. Umezawa, H. Matsumoto and M. Tachiki, Thermal Field Dynamics and Condensed States, North Holland, Amsterdam, 1982.

7. D. Janssen, F. Donau, S. Fraundorf and R. V. Jolos, Nucl. Phys. A, *172*, 145, 1971.
8. T. Marumori, K. Takada and F. Sakata, Prog. Theor. Phys. Suppl. Chap. 1, 71, 1981.
9. Nguyen Dinh Dang, Mod. Phys. Lett., *A3*, 1041, 1988.
10. R. A. Broglia, C. Riedel and B. Sorenson, Nucl. Phys. A, *107*, 1, 1968.
11. K. Tanabe, Phys. Rev. C, *37*, 2802, 1988.
12. Y. K. Gambhir, G. Basavaraju, Pramana, *13*, 47, 1979.
13. Y. K. Gambhir, J. A. Sheikh, P. Ring and P. Schuck, Phys. Rev. C, *31*, 1519, 1985.
14. K. A. Snover, Nucl. Phys. A, *482*, 13, 1988.
15. A. L. Goodman, Phys. Rev. C, *29*, 1887, 1984.
16. S. Levit and Y. Alhassid, Nucl. Phys. A, *413*, 439, 1984.

Acta Physica Hungarica 72 (2-4), pp. 275–293 (1992)

CORRECTIONS FOR GRAD AND MARKOVIAN APPROXIMATIONS IN STATISTICAL DERIVATION OF NONEQUILIBRIUM THERMODYNAMICS

R. E. NETTLETON and E. S. FREIDKIN

Department of Physics, University of the Witwatersrand
Johannesburg 2050, South Africa

(Received 10 November 1992)

In previous work, non-linear phenomenological equations exhibiting reciprocity have been derived as first moments of a kinetic equation obtained from the Liouville equation via Grabert projection operators. In the derivation, a Markovian approximation and Grad-type ansatz based on information theory were used to derive self-consistent first-moment equations. It is possible to generalize the Grabert operators so that the previous derivation, after replacement of the old by the new operators, is free of these approximations.

1. Introduction

The Grad approach [1] to solution of the Boltzmann equation [2] in a dilute gas expands the singlet distribution function $f(\mathbf{c})$, for $\mathbf{v}$ the particle velocity and $\mathbf{c} \equiv \mathbf{v} - \langle \mathbf{v} \rangle$, in tensor Hermite functions with coefficients which are tensor moments of f. This involves an approximation, since only finite numbers of moments and polynomials are used. On substituting the expansion back into the Boltzmann equation and taking moments of the result, one obtains a self-consistent set of generalized hydrodynamic equations for the moments in question. The latter may include the heat flux and viscous pressure, and so these self-consistent equations have the form of kinetic equations derived from extended thermodynamics[3]. The latter appears, therefore, [4,5] to receive a statistical basis from the coincidence in form between its equations and those of Grad theory.

To establish a statistical basis for non-equilibrium thermodynamics in dense fluids, in contrast to the dilute gas, we replace the gas-kinetic Boltzmann equation with an equation derived via projection operators from the classical Liouville equation. The derivation starts [6] with the operator identity,

$$\exp(i\hat{L}t) = \exp(i\hat{L}t)\hat{P} + i\int_0^t du\{\exp(i\hat{L}_u)\}\hat{P}\hat{L}(1-\hat{P})\cdot \exp\{i\hat{L}(1-\hat{P})(t-u)\} + (1-\hat{P})\exp\{i\hat{L}(1-\hat{P})t\}, \tag{1}$$

where $\hat{L}$ is the self-adjoint Liouville operator and $\hat{P}$ an arbitrary time-independent projection operator. The solution of the Liouville equation is

$$f(t) = \exp(-i\hat{L}t)f(0), \tag{2}$$

where $f(0)$ is the phase-space distribution at $t = 0$. We define a set of state variables

$$\alpha_1 \equiv \int f\hat{A}_i(x)dx \quad (i = 1, \ldots, n), \tag{3}$$

where the $\{\hat{A}_i\}$ are dynamical functions of phase, x. The values $\{\alpha_i\}$ can also be calculated from

$$\alpha_k \equiv \int g(\{a_j\})a_k\, da, \tag{4a}$$

$$g \equiv \int f\psi_a\, dx, \tag{4b}$$

$$da \equiv \prod_j da_j, \tag{4c}$$

$$\psi_a \equiv \prod_j \delta(\hat{A}_j - a_j) \equiv \delta(\hat{A} - a). \tag{4d}$$

According to the maximum entropy formalism [7,8]

$$f(0) = Z^{-1} \exp\left(-\beta\hat{H} - \sum_j \overline{\lambda}_j \hat{A}_j\right), \tag{4e}$$

where $\hat{H}$ is the Hamiltonian and the bar in $\{\lambda_j\}$ denotes initial ($t = 0$) values, chosen to satisfy (3) identically when $\alpha(t) = \alpha(0)$. Z is a normalization factor. With (4e) as initial state, we can use these results to derive from (1) the equations

$$\partial g/\partial t = -\sum_k (\partial/\partial a_k)(v_k^* g) + \int_0^t ds \sum_{kj} (\partial/\partial a_k) \cdot$$

$$\cdot \int da' D_{kj}(a, a', s)(\partial/\partial a'_j)[g(a', t-s)/p_\beta(a')], \tag{5a}$$

$$\dot{A}_k \equiv i\hat{L}\hat{A}_k, \tag{5b}$$

$$p_\beta \equiv \int \rho_\beta \psi_a dx,\ \rho_\beta \equiv Z_c \exp(-\beta\hat{H}),\ \beta \equiv (\kappa T)^{-1}, \tag{5c}$$

$$v_k^* \equiv p_\beta^{-1} \int \rho_\beta \psi_a \dot{A}_k\, dx, \tag{5d}$$

$$D_{kj}(s) \equiv \int dx \rho_\beta \psi_{a'} \dot{A}_j (1 - \hat{P}) \exp[i\hat{L}(1 - \hat{P})s]\psi_a \dot{A}_k. \tag{5e}$$

Z_c is the canonical partition function and κ the Boltzmann constant. Previous derivations [6] of (5a) have used $f(0) = \rho_\beta p_\beta^{-1}(\overline{\alpha})\delta(\hat{A} - \overline{\alpha})$, corresponding to initial value $\overline{\alpha} = \alpha(0)$, but the derivation can be carried through with (4e) instead. Eq. (5a) serves to replace the kinetic theory Boltzmann equation when we discuss

the statistical basis for non-equilibrium thermodynamics in dense fluids. It can hold, of course, as well for gases.

A set of generalized hydrodynamic equations can be derived for the set $\{\dot{\alpha}_k\}$ by multiplying (5a) by each a_k in turn and integrating over a-space. To obtain equations having the structure [3] of non-equilibrium thermodynamics, i.e. closed equations for the moments $\{\alpha_k\}$, two more approximations have been made in existing derivations [9]. One is the Markovian approximation:

$$g(a', t - s) \simeq g(a', t), \tag{6}$$

which rests on the assumption that the time-correlation in D decays rapidly with increasing s. The other approximation introduces an ansatz for g which depends parametrically on $\{\alpha_k\}$ into the right-hand member of (5a). This is what Grad [1] does in the kinetic theory Boltzmann equation. To obtain an ansatz for $g(t)$, we have extended [9] the maximum entropy distribution (4e) to arbitrary states and times, replacing $\overline{\lambda}_j \to \lambda_j(\{\alpha_k\})$ for $t > 0$. Thus, in the right-hand side of (5a), we have introduced [9]

$$\begin{aligned} g \simeq \overline{g} \equiv Z^{-1} \int dx\, \psi_a \exp\left(-\beta \hat{H} - \sum_j \lambda_j \hat{A}_j\right) \\ = Z_c p_\beta \exp\left[\beta F(\alpha) + \sum_j \lambda_j(\alpha)(\alpha_j - a_j)\right]. \end{aligned} \tag{7}$$

This ansatz resembles a similar exponential expression proposed in the "modified moment method" [10] to extend the gas-kinetic Grad theory [1] to the non-linear regime.

With the foregoing approximations, it has been shown [9] that the terms in the kinetic equations for $\{\dot{\alpha}_k\}$ can be grouped in the general, non-linear case so that they exhibit reciprocity. While the approximations appear reasonable, $\overline{g}$ is not an exact solution to (5a), and the s-dependence of the D-matrix is not known. This makes arbitrary any assumptions about rapidity of decay of the time-correlation. We seek here to show that validity of Onsager reciprocity does not depend on (6) and (7). To do this, we exploit the flexibility which we shall show to exist in the definition of $\hat{P}$. The earliest derivation using projection operators of this kind was by Zwanzig [11,12] who assumed a micro-canonical shell ensemble. His projection operator was extended by Grabert [6] for use in a canonical ensemble. A further generalization has been found [13] which adds terms to the exponents in (4e) and (7). The coefficients in these terms can be adjusted to satisfy conditions such as the requirement that the trace of thermodynamic pressure equals the trace of the momentum flux. Such conditions characterize particular phenomenologies and apply to non-linear terms. They are not sufficiently general for our present purposes. In the following sections we develop a new, generalized $\hat{P}$. This is constructed to make the functions $\{\alpha_k(t)\}$ calculated from (5a), (6), and (7) agree with a result which is free of the Grad and Markovian approximations. This implies that exact

equations for $\{\dot{\alpha}_k\}$ can be cast in a form which is identical, except for definitions of the projection operators, to the one used in earlier proofs [9] of Onsager reciprocity.

In the following Section, we discuss the form assumed by (5a) when the functions $\{\hat{A}_k\}$ include a function $\hat{A}$ even under $\mathbf{p}_j \to -\mathbf{p}_j$ $(j = 1, \ldots, N)$, with N the total number of particles, plus higher derivatives $\hat{A}_p \equiv (i\hat{L})^p \hat{A}$ $(p > 1)$. We develop an exact solution in powers of t to a generalized version of (5a). The first moment of this solution yields an exact t-expansion of $\alpha_j \equiv \langle \hat{A}_j \rangle$. In Section 3, we generalize the projection operator of Grabert [6] so that arbitrary functions with adjustable parameters appear therein. The parameters can be adjusted to make as many terms as desired in the t-expansion for α agree with the exact result, calculated as in Section 2 without the Markovian approximation and Grad-type ansatz for $\overline{g} \simeq g$. The procedure is illustrated in Sections 4 and 5 to $O(t^4)$ for a particular model involving a binary mixture of particles of types A and B, with $\hat{A}$ proportional to the mass centre of component A. Algebraic equations are derived whose solution yields projection operators which compensate to this order for effects produced by Grad and Markovian approximations in the calculation of α. In Section 4, $\alpha = \langle \hat{A} \rangle$ is the only variable. In Section 5, $\eta = \langle \dot{A} \rangle$ is added. The new projection operator for the latter case is shown to differ from the one used in Section 4. In Section 6 a summary is given with references to applications of reciprocity to linear and nonlinear transport and to chemical reactions. This provides background to show the importance of the present results.

2. Generalized Grabert equation and solutions

In the present Section, we generalize (5a) by supposing that, if $\hat{A}(x)$ is a function even under reversal of signs of particle momenta, we have a set of derivative functions

$$\hat{A}_r(x) \equiv (i\hat{L})^{r-1} \hat{A}(x) \quad (r = 1, \ldots, n). \tag{8}$$

With $\psi_a = \prod_r \delta(\hat{A}_r - a_r)$, a product of Dirac deltas, (5a) becomes:

$$\frac{\partial g}{\partial t} = -\sum_i (\partial/\partial a_i)(v_i^* g) + \int_0^t ds \sum_{ij} (\partial a_i) \int da' D_{ij}(a, a', t-s) \cdot \cdot (\partial/\partial a'_j)[g(a', s)/p_\beta(a')], \tag{9a}$$

$$v_1^* \equiv p_\beta^{-1} \int dx\, \rho_\beta(x) \dot{A}_i(x) \psi_a(x), \tag{9b}$$

$$D_{ij} = 0 \quad (i \neq n \neq j), \tag{9c}$$

$$D_{nn}(a, a', s) = \int dx \rho_\beta \psi_{a'} \hat{A}_{n+1}(1 - \hat{P}) \exp[i\hat{L}(1 - \hat{P})s] \psi_a \hat{A}_{n+1}. \tag{9d}$$

Eq. (9a) has previously been derived [9] for the case $n = 2$ which corresponds to most existing cases considered in extended thermodynamics.

We can find an exact solution to (9a) of the form

$$g(a,t) = \sum_{m\geq 0} G_m(a)t^m. \tag{10}$$

Such an expansion is not of practical use when we describe the approach to a steady state where $t \to \infty$. Here, however, we want only to show that we can find a $\hat{P}$ such that a solution using $\overline{g}$ and the Markovian approximation will have the same first moment as Eq. (10) when the latter is calculated using the projection operator of Grabert and no approximations. If this case can be shown for the first few terms in (10), we can easily see that the result can be generalized to higher order in t. However, the general case, involving high powers of t, would be intractably messy if we tried to carry it out in practice.

Substitution of (10) into (9a) and comparison of powers of t yields:

$$-p_\beta^{-1}(\partial/\partial a_j')D_{ij}(a,a',t-s) \equiv \sum_{k\geq 0} \Omega_i^{(k)}(a,a')(k!)^{-1}(t-s)^k, \tag{11a}$$

$$G_{m+1}(a) = -\sum_i (\partial/\partial a_i)[(m+1)^{-1}v_i^* G_m] +$$

$$+\sum_i \sum_{m'+k+1=m} \int da' \Omega_i^{(k)}(a,a')m'!\{(m+1)!\}^{-1}G_{m'}(a). \tag{11b}$$

Eq. (11a) defines the functions $\Omega_i^{(k)}$. Eq. (11b) can be contrasted with the result of using the Markovian approximation (6), but not the ansatz (7). This result is:

$$G_{m+1}^{(M)}(a) = -\sum_i (\partial/\partial a_i)[(m+1)^{-1}v_i^* G_m] + \sum_i \sum_{k+1+n=m} [(m+1)(k+1)!]^{-1} \cdot$$

$$\cdot (\partial/\partial a_i) \int da' \Omega_i^{(k)}(a,a')G_n(a'). \tag{12}$$

Depending on n, the first few $G_m^{(M)}(a)$ have the same first moments as the corresponding exact functions, G_m. We can assert that

$$\alpha_k = \sum_{j\geq 0} \alpha_{kj} t^j, \tag{13a}$$

$$\alpha_{kj} = \int G_j(a) a_k \, da, \tag{13b}$$

$$\alpha_{kj}^{(M)} = \int G_j^{(M)}(a) a_k \, da = \alpha_{kj} \ (j+k-2 \leq n). \tag{13c}$$

In Section 4, we consider the case where $n = 1$ and $\hat{A}$ is proportional to the position of the mass centre of one of the components of a binary mixture of A and B

particles. The criterion (13c) asserts that $\alpha_{kj} = \alpha_{kj}^{(M)}$ if $j \leq 2$. Thus the Markovian approximation has no effect on the calculation of α to $O(t^2)$. If we use this approximation to derive a generalized hydrodynamic equation for α, the $O(t^4)$ term in the solution of the latter will differ from the corresponding term in the exact, non-Markovian result. The $O(t^2)$ term can also differ from the exact result because we use the Grad-type ansatz. To make the Markovian result (11b) yield an $O(t^4)$ term which agrees with the one calculated from (12), we need to modify the projection operator $\hat{P}$ in (12) so that it differs from the Grabert projection operator, $\hat{P}_g$, used in (11b). The necessary modification is developed in Section 3 and a detailed illustration of its use described in Section 4. Section 5 describes an extension of this calculation to the case $n = 2$, with $\hat{A}$ and $\dot{A}$ the two functions designated $\hat{A}_1$ and $\hat{A}_2$ in (8). For that case, the criterion (13c) says that the Markovian approximation has no effect if $j \leq 3$ ($k = 1$) or $j \leq 2$ ($k = 2$). It is again necessary to modify the projection operator in (12) to make $\alpha_{k4}^{(M)} = \alpha_{k4}$.

It should be remembered at this point that in derivations [9] of extended thermodynamics we use the maximum entropy $\overline{g}$ of (7) as well as the Markovian approximation (6) in the right-hand member of (5a). The projection operators $\hat{P}$ developed in Section 4 and 5 are designed to compensate to $O(t^4)$ for the use of this additional approximation as well as for the Markovian approximation. Since this procedure can be extended to higher orders in t, the illustrations in Sections 4 and 5 argue strongly that an approximate generalized hydrodynamic equation for $\alpha(t)$ based on (6) and (7) can yield an exact result for α to any desired order in t if we redefine $\hat{P}$ properly.

3. Generalized projection operators

We consider here how we can define a projection operator $\hat{P}$ which has all the mathematical properties of the operator $\hat{P}_g$ defined by Grabert [6] but which also contains adjustable parameters. The parameters can be determined so that the first moment α of g calculated using (5a), (6), and (7) agrees to any desired order in t with the result of using $\hat{P}_g$ in (5a) without either the Markovian approximation (6) or the maximum entropy ansatz (7). If this can be done, we can construct an exact equation for $\alpha(t)$ in which the coefficients depend on the new operator $\hat{P}$ in the same way as in an earlier demonstration [9] of Onsager reciprocity which appeared to rest on (6) and (7).

In the notation of Eqs (3) and (4a–d), we define [6] the Grabert $\hat{P}_g$ by:

$$\hat{P}_g \chi(x) \equiv \int da\, p_\beta^{-1}(a) \psi_a(x) Tr(\rho_\beta \psi_a \chi), \tag{14}$$

where χ is an arbitrary function of the phase co-ordinates x. The transposed operator has the form:

$$\hat{P}_g^T \chi \equiv \rho_\beta \int da\, \psi_a(x) p_\beta^{-1}(a) Tr(\psi_a \chi). \tag{15}$$

One can demonstrate that these operators have the mathematical properties:

$$\hat{P}_g^2 = \hat{P}_g, \tag{16a}$$

$$\hat{P}_g \psi_a = \psi_a, \tag{16b}$$

$$P_g^T(\rho_\beta \chi) = \rho_\beta \hat{P}_g \chi, \tag{16c}$$

$$\alpha = \int g a da = \int \hat{P}_g^T f(x) \hat{A}(x) dx, \tag{16d}$$

where $f(x)$ is the solution (2) of the Liouville equation. The derivation [9] of kinetic equations for $\dot{\alpha}$ in which the coefficients exhibit reciprocity depends only on the fact that $\hat{P}$ has properties (15) and (16a–d). It can go through unchanged with any other projection operator which exhibits these same properties. We can thus look for generalizations of $\hat{P}_g$ which obey (16a–d).

One generalization already developed [13] replaces ρ_β in the definition (14) of $\hat{P}_g$ with

$$\tilde{\rho}_\beta \equiv \tilde{Z}^{-1} \exp\left(-\beta \hat{H} - \sum_i \gamma_i \hat{B}_i(x)\right), \tag{17}$$

where $\tilde{Z}$ is a normalizing factor, and the functions $\hat{B}_i(x)$ are constants of the motion. The $\{\gamma_i\}$ are functions which vanish in equilibrium so that $\tilde{\rho}_\beta$ approaches the equilibrium canonical distribution. Such a generalization of $\hat{P}_g$ yields corrections to higher-order terms in the generalized hydrodynamic equations for $\dot{\alpha}$. The set $\{\gamma_i\}$ can be determined e.g. to make the thermodynamic pressure equal the trace of the momentum flux tensor. The latter condition characterizes certain statistical and phenomenological treatments [10] and so it must be imposed when we discuss the statistical foundations of the latter.

In the present paper, we explore a different generalization of $\hat{P}_g$ which is not designed like (17) to make corrections to small, non-linear terms. We define $\hat{P}$ so that

$$\hat{P}\chi(x) \equiv \int da \int dx' \, \delta(\phi(x) - \phi(x')) \rho_\beta(x') \chi(x') \psi_a(x') \psi_a(x) \cdot \tag{18a}$$

$$\cdot \left\{ \int dx'' \, \delta(\phi(x) - \phi(x'')) \rho_\beta(x'') \psi_a(x'') \right\}^{-1},$$

$$\hat{P}^T\chi(x) \equiv \rho_\beta \int da \int dx' \, \delta(\phi(x) - \phi(x')) \chi(x') \psi_a(x') \psi_a(x) \cdot$$

$$\cdot \left\{ \int dx'' \, \delta(\phi(x) - \phi(x'') \rho_\beta(x'') \psi_a(x'') \right\}^{-1}. \tag{18b}$$

$\phi(x)$ is an arbitrary phase function. One can readily verify that $\hat{P}$ and $\hat{P}^T$ obey (16a–d). One can therefore use $\hat{P}$ instead of $\hat{P}_g$ in (1) and (5a–e).

We can exploit the arbitrariness of the $\phi(x)$ by determining them so that the first moment equations derived from (5a), after application of (6) and (7), are

in fact exact equations for $\dot{\alpha}$ in the sense that their solutions agree with (10). These equations can thus be cast in a form in which the coefficients have the same dependence on $\hat{P}$ they would have when (6) and (7) are used. In Sections 4 and 5, we choose $\phi(x)$ to be a linear combination of a set $\{\phi_i(x)\}$ of independent functions:

$$\Phi(x) = \sum_i d_i \phi_i(x). \tag{19}$$

The coefficients $\{d_i\}$ are evaluated so that the set $\{a_{kj}\}$ defined in (13b), when G is calculated from (6), (7), and the new $\hat{P}$ operator, will be exact to any desired value of j. If there are several variables, with $\alpha_i = \langle \hat{A}_i(x) \rangle$, where i indexes the members of the set, we can understand $\delta(\phi(x) - \phi(x'))$ to mean

$$\delta(\phi(x) - \phi(x')) = \prod_j \delta(\phi_j(x) - \phi_j(x')). \tag{20}$$

The number of factors in the product depends on the number of independent state variables. We replace (19) in this case by

$$\phi_j(x) = \sum_k d_{jk} \tilde{\phi}_k(x). \tag{21}$$

The tilde distinguishes the functions in the argument of the δ-functions in (20) from those appearing in the right-hand member of (21), corresponding to ϕ_i in (19). It is seen in Sections 4 and 5 that the set $\{\phi_i\}$ will not be the same when there are both odd and even variables as they are when all the variables are even under time-reversal.

4. Illustration for single relaxing variable

We proceed here to consider a simple model belonging to unextended thermodynamics for which we evaluate the d-parameters in (19). Two such parameters only are introduced. Adjustment of these serves to make $\alpha(t)$, calculated from the first moment of (5a) when (6) and (7) are used, agree to $O(t^4)$ with the exact t-expansion of $\alpha(t)$ calculated without approximations by the scheme described in (11b). In practice, we want to obtain phenomenological equations for α which are valid at long times, and so the first two powers of t do not interest us. However, we illustrate via this calculation a procedure which, in principle, can be extended to all orders. The illustration given here shows that, if a finite number of d-parameters are used, then the coefficients in the t-expansion of α are all algebraic functions of finite order. Calculations analogous to those given here can be carried out to any specified order in t.

The model for which we describe this illustration is a binary mixture of N_A particles of type A and N_B of type B with pairwise interactions and masses m_A

and m_B. The system is contained in finite volume V which exchanges heat with a reservoir at temperature T. We have just one thermodynamic state variable,

$$\hat{A} = \sum_{i=N_B+1}^{N} x_i, \tag{22}$$

$$\alpha = \int f\hat{A}\, dx = \int g(a) a\, da, \tag{23}$$

N_A times the x-component of the mass centre of the A particles. Here $N = N_A + N_B$, and the particles are numbered in sequence: $1, \ldots, N_B, N_B + 1, \ldots, N$. All the B particles are enumerated at the beginning of the sequence. The configuration coordinates of particle i are $\mathbf{r}_i = (x_i, y_i, z_i)$. This choice permits exact evaluation of the integrals in $\hat{P}\dot{A}$.

To define a suitable ϕ for this case, introduce:

$$\tilde{P}_i \equiv p_{ix}/m_i^{\frac{1}{2}} \quad (i = 1, \ldots, N), \tag{24a}$$

$$\phi(x) = \tilde{P}_N + d_1\tilde{P}_{N-1} + d_2\tilde{P}_{N-2}. \tag{24b}$$

The coefficient of $\tilde{P}_N$ can be equated to unity without loss of generality, since the $\{\alpha_k\}$ depend on ratios of the other coefficients to this one. The ϕ defined in (24b) is used in calculating the D defined in (5e) which in turn is used in (5a) together with (6) and (7) to obtain an equation for $\dot{\alpha}$ in which the coefficients depend on d_1 and d_2. To calculate D, we need initially to evaluate $\hat{P}\dot{A}$ which is done easily if we can express ρ_β and $\dot{A}$ in terms of ϕ. By taking ϕ to depend only on momenta, we choose the simplest form which leads to a dependence of D on d_1 and d_2.

To calculate $\hat{P}\dot{A}$, we use:

$$\dot{A} = m_A^{-\frac{1}{2}} \sum_{i \epsilon A} \tilde{P}_i, \tag{25a}$$

$$\begin{aligned} K_x &\equiv \frac{1}{2}\sum_{j=1}^{N-3} \tilde{P}_j^2 + \frac{1}{2}(\tilde{P}_{N-2}^2 + \tilde{P}_{N-1}^2 + \tilde{P}_N^2) \\ &= \frac{1}{2}\sum_{j=1}^{N-3} \tilde{P}_j^2 + \frac{1}{2}[\tilde{P}_{N-2}(1+d_2^2)^{\frac{1}{2}} + d_2\phi(1+d_2^2)^{-\frac{1}{2}} + d_1 d_2 (1+d_2^2)^{-\frac{1}{2}}\tilde{P}_{N-1}]^2 \\ &+ \frac{1}{2}[\tilde{P}_{N-1}\{1 + d_1^2 - d_1^2 d_2^2 (1+d_2^2)^{-1}\}^{\frac{1}{2}} - \phi d_1 (1+d_2^2)^{-1} \cdot \\ &\cdot \{1 + d_1^2 - d_1^2 d_2^2 (1+d_2^2)^{-1}\}^{-\frac{1}{2}}]^2 + \frac{1}{2}\phi^2 (1 + d_1^2 + d_2^2)^{-1}. \end{aligned} \tag{25b}$$

We have, on putting $\psi_a = \delta(\hat{A} - a)$ into (18a):

$$\begin{aligned} \hat{P}\dot{A} &= \int \prod_{i \leq N-2} d\tilde{P}_i\, \dot{A} \exp(-\beta K_x) \Big/ \int \prod_{i \leq N-2} d\tilde{P}_i \exp(-\beta K_x) \\ &= m_A^{-\frac{1}{2}} \phi (1 + d_1 + d_2)/(1 + d_1^2 + d_2^2). \end{aligned} \tag{26}$$

These results are used in calculating the coefficients in the kinetic equation for $\dot{\alpha}$. Substitute for g from (6) and (7) into the right-hand member of (5a), multiply by a, and integrate over a-space. We get [for λ cf. 30b]

$$\dot{\alpha} = \lambda(\alpha) \int_0^t ds \int da\, da' D(a, a', s) = \lambda(\alpha)[D_1 t + D_3 t^2 + \ldots]. \tag{27}$$

From (5e), we see after some lengthy calculations that

$$\begin{aligned} D_1 &= (2\pi m_A \kappa T)^{-N_A/2} (2\pi m_B \kappa T)^{-N_B/2} \int \exp\{-\beta K_x\} \dot{A}(1-\hat{P})\dot{A} \prod_{i \in A} dp_{xi} \\ &= m_A^{-1} \kappa T [N_A - (1 + d_1 + d_2)^2/(1 + d_1^2 + d_2^2)]. \end{aligned} \tag{28}$$

When the exponent in $D(a, a', s)$ as defined in (5e) is expanded, the second non-vanishing term, with an integrand of second-order in $\hat{L}$ which is even under momentum reversal, is $O(s^2)$. This yields after another lengthy calculation:

$$\begin{aligned} D_3 &= (1/3) \int \rho_\beta \dot{A}(1-\hat{P}) i\hat{L}(1-\hat{P})\dot{A} dx \\ &= (1/3) m_A^{-1} \kappa T (1 + d_2^2)^{-\frac{1}{2}} \{1 + d_1^2 - d_1^2 d_2^2 (1 + d_2^2)^{-1}\} [\sum_{i=N_B+1}^{N-3} B_i \qquad (29a) \\ &\quad + (1 - d_2)(1 + d_2^2)^{-1}(B_{N-2} + d_2 B_N) + \{1 - d_1 - d_1 d_2 (1 - d_2)(1 + d_2^2)^{-1}\} \cdot \\ &\quad \cdot \{1 + d_1^2 - d_1^2 d_2^2 (1 + d_2^2)^{-1}\} \{B_{N-1} + d_1 B_N - d_1 (B_{N-2} + d_2 B_N)(1 + d_2^2)^{-1}\}], \end{aligned}$$

$$B_i \equiv -m_A^{-1} \beta \langle F_1^2 \rangle, \quad N_{B+1} \leq i \leq N - 3, \tag{29b}$$

$$\begin{aligned} B_{N-2} &\equiv -\beta m_A^{-1} \langle F_1^2 \rangle (1 + d_2^2)^{-1} [1 - d_2 - d_1 d_2 \{1 - d_1 - d_1 d_2 (1 - d_2) \cdot \\ &\quad \cdot (1 + d_2^2)^{-1}\} \{1 + d_1^2 - d_1^2 d_2^2 (1 + d_2^2)^{-1}\}^{-1}], \end{aligned} \tag{29c}$$

$$\begin{aligned} B_{N-1} &\equiv -\beta m_A^{-1} \langle F_1^2 \rangle (1 + d_2^2)^{-1} [(1 - d_1)(1 + d_2^2) + (1 - d_2)^2 d_1 \qquad (29d) \\ &\quad - d_1^2 \{1 - d_1 - d_1 d_2 (1 - d_2)(1 + d_2^2)^{-1}\} \{1 + d_1^2 - d_1^2 d_2^2 (1 + d_2^2)^{-1}\}^{-1}], \\ B_N &\equiv -\beta m_A^{-1} \langle F_1^2 \rangle (1 + d_2^2)^{-1} [d_2 (1 - d_2) + d_1 \{1 - d_1 - d_1 d_2 (1 - d_2)(1 + d_2^2)^{-1}\} \cdot \\ &\quad \cdot \{1 + d_1^2 - d_1^2 d_2^2 (1 + d_2^2)^{-1}\}^{-1}]. \end{aligned} \tag{29e}$$

F_1 here denotes the force on particle 1 and $\langle F_1^2 \rangle$ an equilibrium canonical average.

To obtain the coefficient α_n of t^n in (13a), we require the corresponding

coefficient λ_n in the t-expansion of λ from a self-consistency condition:

$$\alpha = Z^{-1} \int dx\, \hat{A} \exp(-\beta \hat{H} - \lambda \hat{A}), \tag{30a}$$

$$\lambda = \sum_{j \geq 1} \lambda_{(j)} (\alpha - \alpha_0)^j, \tag{30b}$$

$$\lambda_{(1)} = -(\langle \hat{A}^2 \rangle_0)^{-1}, \tag{30c}$$

$$\lambda_{(2)} = 0, \tag{30d}$$

$$\lambda_{(3)} = \frac{1}{2} \lambda_{(1)}^4 \{\langle \hat{A}^4 \rangle_0 - (1/3)(\langle \hat{A}^2 \rangle_0)^2\}. \tag{30e}$$

The subscript zero in (30c,e) indicates equilibrium averages calculated with the equilibrium canonical distribution, ρ_β, defined in (5c). From (27) after integration with respect to t, we find:

$$\alpha = \overline{\alpha} + \frac{1}{2} \overline{\lambda} D_1 t^2 + (1/4) t^4 (\lambda_2 D_1 + \overline{\lambda} D_3) + \ldots, \tag{31a}$$

$$\overline{\lambda} = \sum_{j \geq 1} \lambda_{(j)} (\overline{\alpha} - \alpha_0)^j, \tag{31b}$$

$$\lambda_2 = \sum_{j \geq 1} \lambda_{(j)} j (\overline{\alpha} - \alpha_0)^{j-1} \alpha_2, \tag{31c}$$

where $\overline{\alpha}$ is the arbitrary initial value of α, and $\overline{\lambda} = \lambda(\alpha)$ at $t = 0$. These equations yield [(cf. (13a)]:

$$\alpha_2 = \frac{1}{2} \overline{\lambda} D_1, \tag{32a}$$

$$\alpha_4 = (1/4)(\lambda_2 D_1 + \overline{\lambda} D_3). \tag{32b}$$

D_1 and D_3 in (32a,b) are functions of d_1 and d_2 given by (28) and (29a-e). We can evaluate d_1 and d_2 to make (32a,b) agree with the exact expression, calculated without the Markovian approximation and Grad ansatz from (10) and (11b). The exact calculation gives:

$$\alpha_2^e = \frac{1}{2} N_A \kappa T \overline{\lambda} / m_A, \tag{33a}$$

$$\alpha_4^e = (N_A \kappa T \overline{\lambda} / 12 m_A)[-m_A^{-1} \beta \langle F_1^2 \rangle_i + \frac{1}{2} \overline{\lambda}^2 N_A \kappa / T m_A^{-1} - \frac{1}{2} (m_A / N_A \kappa T) \langle \hat{P}_g A^\dagger \hat{P}_g A^\dagger \rangle_i]. \tag{33b}$$

$A^\dagger \equiv (i\hat{L})^2 \hat{A}$, and subscript i indicates an average over the initial ($t = 0$) ensemble characterized by the $t \to 0$ limit of (7). The equation $\alpha_2 = \alpha_2^e$ has the solution

$d_1 = -(1 + d_2)$. Putting this into the equation $\alpha_4 = \alpha_4^e$, we find

$$d_2 = d_{20} + O(N_A^{-1}), \tag{34a}$$

$$\rho \equiv \frac{1}{2} m_A^2 \langle \hat{P}_g A^\dagger \hat{P}_g A^\dagger \rangle / N_A \langle F_1^2 \rangle, \tag{34b}$$

$$(1 + \rho)^2 (1 + d_{20}^2)^3 = (1 + d_{20} + d_{20}^2)^2. \tag{34c}$$

(34c) has a real solution for ρ small. ρ should be small because $m_A \hat{P}_g A^\dagger$ is the mean force on A resulting from displacement of the mass centre and large equilibrium fluctuations in the latter are not probable. From these calculations, it is clear that we can go to higher order by adding terms to ϕ in (24b) with additional coefficients d_i for $i > 2$.

5. Example of coupled odd and even variables

In the statistical derivation [9] of reciprocity in non-linear extended thermodynamics, one assumes a set of variables of type $\alpha = \langle \hat{A} \rangle$ which are even under time-reversal plus a set of type $\eta = \langle \dot{A} \rangle$ which are odd. We proceed here to consider the model of Section 4 with just two such variables, $\hat{A}$ being given by (22). For this case, the amplitude g for the probability that $\hat{A}$ have a numerical value within da of a and $\dot{A}$ a value within dv of v is:

$$g(a, v) = \int f(x) \psi_a(x) dx, \tag{35a}$$

$$\psi_a \equiv \delta(\hat{A} - a) \delta(\dot{A} - v), \tag{35b}$$

$$\alpha = \int a g(a, v) da\, dv, \tag{35c}$$

$$\eta = \int v g(a, v) da\, dv. \tag{35d}$$

Eq. (5a) is replaced by:

$$\partial g / \partial t = -(\partial / \partial a)(vg) - (\partial / \partial v)(qg) + \int_0^t ds (\partial / \partial v) da' dv' D(a, a', t - s) \cdot \cdot (\partial / \partial v')[g(a', s) / p_\beta(a')], \tag{36a}$$

$$D(a, a', s) = \int dx\, \rho_\beta \psi_{a'} A^\dagger (1 - \hat{P}) \exp[i \hat{L} (1 - \hat{P}) s] \psi_a A^\dagger, \tag{36b}$$

$$q \equiv \int dx\, p_\beta^{-1} \rho_\beta \psi_a A^\dagger, \tag{36c}$$

where $A^\dagger \equiv (i\hat{L})^2 \hat{A}$ replaces $\dot{A}$ in (5e) in accord with (9a). $\hat{P}$ is an arbitrary projection operator for which we use (18a) plus (34b). This definition will satisfy (16a–c). The derivation of (36a) assumed $g = \overline{g}$ as in (7) or (3) below, at $t = 0$.

In order to derive a phenomenological equation of extended thermodynamics for $\dot{\eta}$ which can be integrated to yield $\alpha(t)$, since $\eta = \dot{\alpha}$, we need again to make the Markovian approximation (6) and invoke the Grad-type ansatz which replaces with F the Helmholtz free energy (cf. [9]):

$$g \to \overline{g} = Z_c p_\beta \exp[\beta F(\alpha, n) + \lambda(\alpha)(\alpha - a) + \tilde{\lambda}(\eta)(\eta - v)] \tag{37}$$

in the right-hand side of (36a). $\lambda(\alpha)$ is given by (30a-e) and $\tilde{\lambda}$ by an analogous condition [cf. 46a-d below] which implies $\tilde{\lambda} = 0$ at $t = 0$ if $\eta(0) = 0$. p_β and all other functions in this Section are calculated using (35b) in place of (4d). Otherwise definitions such as (5c) and (14) remain intact. The equation for $\dot{\eta}$ is the first moment of (36a), with (36b) for D. The question again arises whether we can find ϕ in (18a) so that the approximations (6) and (37) will yield a first moment equation for $\dot{\eta}$ which is exact. That is, the solution of this equation for $\alpha(t)$ agrees, to an arbitrary given order in t, with the first moment equation obtained by using $\hat{P}_g$ and no approximations in (36a).

We shall seek a function $\phi(x)$ which contains a single adjustable parameter $\tilde{d}_1$. This is adjusted to make $\alpha(t)$, calculated via (6) and (37), agree to $O(t^4)$ with the exact result. As in Section 4, the method can be extended to higher order in t by introducing parameters $\tilde{d}_i$ with $i \geq 2$ into ϕ, but doing this in practice is more difficult in the present case. By considering coupled odd an even parameters here, we accomplish two objectives: (1) We show that earlier demonstrations [9] of reciprocity in extended thermodynamics are not limited by the Markovian approximation and Grad ansatz for g. (2) We see that the choice of ϕ depends drastically on the choice of variables and can differ radically in the present Section from its form in Section 4.

The reason for this difference stems from the fact that D in (36b) depends on [cf. (9)]

$$A^\dagger = m_A^{-1} \sum_{i \epsilon A} F_i, \tag{38}$$

where F_i is the force on particle i stemming from interactions with the remaining particles. If we took ϕ to be a function of momenta as in (24b) and $\hat{P}$ from (18a), then $\hat{P}A^\dagger$ would not depend on ϕ which would also be true of D. To introduce adjustable parameters into the t-expansion of α, we must have a ϕ which depends on configuration co-ordinates and not solely on momenta.

We choose

$$\phi(x) = F_N + \tilde{d}_1 F_{N-1}. \tag{39}$$

To calculate $\hat{P}A^\dagger$, one must calculate averages $\langle F_N \rangle$, $\langle F_{N-1} \rangle$, and $\langle F_j \rangle$ for $j < N-1$ subject to the restriction that ϕ and $\hat{A}$ have specified values imposed by the δ-factors in $\hat{P}$. To do this, we invoke fluctuation theory. Let ψ_1 represent the numerical value of A, and ψ_j $(j = 2, \ldots, N_{A+1})$ the values of F_{N-j+2}, respectively. We introduce

the distribution function:

$$\rho_f(\{\phi_i\}) = C_\psi \exp[-\sum_{ij} \mu_{ij}\psi_i\psi_j], \tag{40a}$$

$$\Delta \equiv \det(\mu_{ij}), \tag{40b}$$

$$C_\psi = \Delta^{\frac{1}{2}}\pi^{-\frac{1}{2}(N+1)}. \tag{40c}$$

According to fluctuation theory, the argument of the exponent should be $\Delta S/\kappa$, ΔS being the entropy fluctuation at constant internal energy. In practice, the coefficients μ_{ij} should be evaluated so that, e.g.

$$\langle F_i F_j\rangle_0 = \int \rho_f \psi_{N-i+2}\psi_{N-j+2}\, d\psi, \tag{41}$$

where subscript zero denotes an equilibrium canonical average. The elements of μ_{ij} fall into four groups, according to whether they couple $\hat{A}$ to itself, $\hat{A}$ to members of the set $\{F_i\}$, or the forces F_i to one another. Thus

$$\sum_{ik}\mu_{ik}\psi_i\psi_k = \mu_{aa}\psi_1^2 + \sum_{k>1}\mu_{af}\psi_1\psi_k + \sum_{k>1}\mu^d_{ff}\psi_k^2 + \sum_{1<k\neq j>1}\mu^0_{ff}\psi_j\psi_k. \tag{42}$$

In taking ϕ to be a sum of terms whose values have a Gaussian distribution, we set up a calculation formally analogous to the one in Section 4 where momenta played a mathematical role similar to the one played by the F's here.

Into Eq. (42) substitute

$$\psi_2 = \phi - \tilde{d}_1\psi_3. \tag{43}$$

The values $\overline{\psi}_3$ and $\overline{\psi} = \overline{\psi}_k$ $(k > 3)$ which make (42) an extremum subject to fixed ψ_1 and ϕ are given by:

$$\begin{aligned}
&2\overline{\psi}_3[-(\mu^0_{ff})^2(N_A-2)\tilde{d}_1(1+\tilde{d}_1) + (\mu^d_{ff})^2(1+\tilde{d}_1^2) + \\
&+\mu^0_{ff}\mu^d_{ff}\{(N_A-2)(1+\tilde{d}_1^2) - 2\tilde{d}_1\}] = \\
&= -\psi_1\mu_{af}\mu^d_{ff}(1-\tilde{d}_1) + 2\phi[-\tilde{d}_1(N_A-2)(\mu^0_{ff})^2 + (\mu^d_{ff})^2\tilde{d}_1 \\
&+\mu^0_{ff}\mu^d_{ff}\{(N_A-2)\tilde{d}_1 - 1\}],
\end{aligned} \tag{44a}$$

$$\begin{aligned}
&2\overline{\psi}[(\mu^d_{ff})^2(1+\tilde{d}_1^2) - (\mu^0_{ff})^2(N_A-2)\tilde{d}_1(1+\tilde{d}_1) + \\
&+\mu^d_{ff}\mu^0_{ff}\{(N_A-2)(1+\tilde{d}_1^2) - 2\tilde{d}_1\}] = \\
&= \psi_1\mu_{af}[-\mu^d_{ff}(1+\tilde{d}_1^2) + \mu^0_{ff}\tilde{d}_1(1+\tilde{d}_1)] + \\
&+2\phi[(\mu^0_{ff})^2\tilde{d}_1(1+\tilde{d}_1) - \mu^0_{ff}\mu^d_{ff}(1+\tilde{d}_1^2)].
\end{aligned} \tag{44b}$$

When (42) is expressed in terms of ψ_1, ϕ, $\overline{\psi}_3$ and $\overline{\psi}$, we get a new distribution in which the values (44a,b) give respectively $\langle F_{N-1}\rangle$ and $\langle F_j\rangle$ for $j < N-1$ subject to fixed ψ_1 and ϕ. We thus obtain:

$$\hat{P}A^{\dagger} = m_A^{-1}(N_A - 2)\overline{\psi} + m_A^{-1}[\phi + (1 - \tilde{d}_1)\overline{\psi}_3]. \tag{45}$$

Eq. (45) is used to calculate the leading term in D which has a simple algebraic dependence on $\tilde{d}_1$.

When D is calculated using (45), we obtain a corresponding first moment equation for $\dot{\eta}$ by multiplying (36a) by v and integrating over a and v space. We introduce the notation:

$$\tilde{\lambda} = \sum_{j\geq 1} \tilde{\lambda}_{(j)} n^j, \tag{46a}$$

$$\tilde{\lambda}_{(1)} = -(\langle \dot{A}^2\rangle_0)^{-1} = -m_A/(N_A \kappa T), \tag{46b}$$

$$\tilde{\lambda}_{(2)} = 0, \tag{46c}$$

$$\tilde{\lambda}_{(3)} = \frac{1}{2}\tilde{\lambda}_{(1)}^{-4}(\langle \dot{A}^4\rangle_0 - (1/3)(\langle \dot{A}^2\rangle_0)^2), \tag{46d}$$

where (46b-d) follow from a consistency condition analogous to (30a). Subscript zero on an angular bracket denotes an equilibrium canonical average. Similarly, $\lambda_{(j)}$ are defined as in (30c-e). If $\overline{\lambda}$ is the $t \to 0$ limit of λ as in Section 4, we can write the solution of the first-moment equation for $\alpha(t)$ in the form (assuming $\dot{\alpha} = 0$ at $t = 0$):

$$\alpha(t) = \overline{\alpha} + \alpha_2 t^2 + \alpha_4 t^4 + O(t^6), \tag{47c}$$

$$\alpha_2 = \frac{1}{2}\overline{\lambda}(N_A \kappa T/m_A), \tag{47b}$$

$$\alpha_4 = (1/12)\,\overline{\lambda}[\frac{1}{2}\lambda_{(1)}(N_A\kappa T/m_A)^2 - \langle A^{\dagger}(1-\hat{P})A^{\dagger}\rangle_i + (3/2)\lambda_{(3)}(N_A\kappa T/m_A)^2\overline{\alpha}^2]. \tag{47c}$$

Subscript i denotes an average in the $t = 0$ initial ensemble, given by setting $\lambda = \overline{\lambda}$ and $\tilde{\lambda} = 0$ in (37).

Using result (45), we find that:

$$\langle A^{\dagger}(1-\hat{P})A^{\dagger}\rangle_i = (N_A/m_A^2)\langle F_N^2\rangle_i + (2N_A/m_A^2)\langle F_N F_{N-1}\rangle_i + m_A^{-2}[(\mu_{ff}^d)^2(1+\tilde{d}_1^2) - (\mu_{ff}^0)^2\tilde{d}_1(1+\tilde{d}_1)(N_A-2) + \mu_{ff}^d\mu_{ff}^0\{(N_A-2)(1+\tilde{d}_1^2) - 2\tilde{d}_1\}]^{-1} \cdot \left(\frac{1}{2}N_A\kappa T(\overline{\lambda}\overline{\alpha}-1)[(1-\tilde{d}_1)^2\mu_{af}\mu_{ff}^d + (N_A-2)\mu_{af}\{\mu_{ff}^d(1+\tilde{d}_1^2) - \mu_{ff}^0\tilde{d}_1(1+\tilde{d}_1)\}] + \kappa T(1+\tilde{d}_1)[\overline{\lambda}N_A\langle F_N\rangle_i - \beta N_B\langle F_{N_B}F_N\rangle_i][(N_A-2)\{\mu_{ff}^d\mu_{ff}^0(1+\tilde{d}_1^2) - (\mu_{ff}^0)^2\tilde{d}_1(1+\tilde{d}_1)\} + (2-\tilde{d}_1)\{(\mu_{ff}^0)^2(N_A-2)\tilde{d}_1 - (\mu_{ff}^d)^2\tilde{d}_1 + \mu_{ff}^0\mu_{ff}^d(1-(N_A-2)\tilde{d}_1)\}]\right). \tag{48}$$

On substitution from (48) into (47c), we obtain an explicit dependence of α_4 on $\tilde{d}_1$, and we can evaluate $\tilde{d}_1$ to make this expression for α_4 agree with an exact result, α_4^e, calculated using $\hat{P}_g$ and without (6) and (37).

We do not have to calculate an exact α_2^e, since (42a) is exact by the criterion in (13c). To calculate α_4^e we use

$$\alpha_4^e = (1/4)\int vG_3 da\, dv \tag{49}$$

from the fact that $\dot{\alpha}$ is the first v-moment of g, and we obtain $\alpha(t)$ from it by integration. According to (11b), with $\overline{F} = F(\alpha, 0)$, we have

$$G_1 = -v(\partial/\partial a)G_0 - (\partial/\partial v)(qG_0), \tag{50a}$$

$$G_0 = Z_c p_\beta \exp\left[\beta\overline{F} - \overline{\lambda}(\overline{\alpha} - a)\right], \tag{50b}$$

$$\begin{aligned} 2G_2 &= -(\partial/\partial a)(vG_1) - (\partial/\partial v)(qG_1) \\ &\quad + (\partial/\partial v)\int da'dv' D_1(a,a')(\partial/\partial v')[G_0(a')/p_\beta(a')], \end{aligned} \tag{50c}$$

$$\begin{aligned} 3G_3 &= -(\partial/\partial a)(vG_2) - (\partial/\partial v)(qG_2) \\ &\quad + \frac{1}{2}(\partial/\partial v)\int da'dv' D_1(a,a')(\partial/\partial v')[G_1(a')/p_\beta(a')]. \end{aligned} \tag{50d}$$

Using (50a-d) in (49), we can simplify the latter. Useful intermediate results are:

$$\int qv^2 G_0\, da\, dv = \langle \dot{A}^2 A\rangle_i = (N_A\kappa T/m_A^2)\langle A^\dagger\rangle_i, \tag{51a}$$

$$\begin{aligned} \langle A^\dagger\rangle_i &= \int A^\dagger \rho_\beta \exp(-\lambda_i \hat{A}) dx \Big/ \int \dot{\rho}_\beta \exp(-\lambda_i \hat{A})\, dx \\ &= \overline{\lambda}\int \rho_\beta \dot{A}^2 dx = N_A\kappa T\overline{\lambda}/m_A, \end{aligned} \tag{51b}$$

$$p_\beta^{-1}\partial p_\beta/\partial a = (m_a/N_A\kappa T)q, \tag{51c}$$

$$p_\beta^{-1}\partial p_\beta/\partial v = -\beta m_A v/N_A. \tag{51d}$$

After lengthy calculations, we obtain:

$$\alpha_4^e = (N_A/24\,\beta m_A)\overline{\lambda}^2\langle A^\dagger\rangle_i - (\overline{\lambda}/24)\langle A^\dagger \hat{P}_g A^\dagger\rangle_i + (\overline{\lambda}/24)\langle A^\dagger(1-\hat{P}_g)A^\dagger\rangle_i. \tag{52}$$

The subscript i denotes averages carried out as in (50b) with the initial distribution $g(t=0)$. When $\tilde{\lambda} = 0$, the initial distribution is obtained by setting $\lambda = \overline{\lambda}$; $\alpha = \overline{\alpha}$; $\eta = 0$ in (3).

Equating α_4 given by (47c) and (48) to α_4^e in (52), we evaluate $\tilde{d}_1$ to make them agree. The equation for $\tilde{d}_1$ is cubic and should have a real root provided μ_{af}, μ_{ff}^d and μ_{ff}^0 do not vanish. We can extend this work to higher order by adding values of spatial derivatives of the $\{F_i\}$ to the set $\{\psi_i\}$ in (40a).

6. Summary and discussion

We have sought here to deal with a possible objection to attempts [4,5,9] to base a statistical derivation of non-equilibrium thermodynamics on the Grad approach to solution of the gas-kinetic Boltzmann equation. In the latter, one introduces an ansatz for the distribution, the latter being the function g in the present paper. This ansatz depends parametrically on a number of moments. The form of the ansatz $\overline{g}$ is chosen to satisfy a consistency condition such as (30a) which gives the first moments exactly. However, if $\overline{g}$ depends on only a finite number of moments, it cannot solve exactly the equation for g. On substituting $\overline{g}$ for g in (5a) or (36a) and taking first moments, one obtains closed, self-consistent generalized hydrodynamic equations for these moments. When there are several variables, e.g. α and η in Section 5, the coefficients in the coupled equations for $\dot{\alpha}$ and $\dot{\eta}$ have been shown [9] to exhibit Onsager reciprocity in the non-linear regime.

These coefficients, calculated from (5a) and (36a), depend on the projection operator $\hat{P}$ which is arbitrary save for the requirement that it satisfies (16a-c). We seek to show, accordingly, that we can determine $\hat{P}$ defined in (18a) so that the solution $\alpha(t)$ of the first-moment generalized hydrodynamic equation agrees exactly to any desired order in t with the first moment of a solution to (5a) or (36a) obtained without approximation and with use of the Grabert $\hat{P}_g$ of (14). Alternatively, one could use as "exact solution" a t-expansion for $\alpha(t)$ fitted to the result of a molecular dynamic simulation. If this is done, the Markovian approximation (6) and the use of a Grad-type ansatz for $\overline{g}$ do not affect the validity of the demonstration [9] of reciprocity. The latter demonstration does not depend on the precise form of $\hat{P}$ so long as it satisfies (16a-c).

To generalize the Grabert $\hat{P}_g$, we determine $\phi(x)$ in (18a) so that the coefficient α_j $(j = 0, \ldots, \nu)$ of the $O(t^j)$ term, to any given order ν, in the solution of the generalized hydrodynamic equation agrees with the coefficient α_j^e in the t-expansion of the exact result. If there are several variables, $\{\alpha_k(t)\}$, one can introduce a set $\{\phi_k(x)\}$ of more than one undetermined function in (18a), with $\delta(\phi(x) - \phi(x'))$ representing a product of factors $\delta(\phi_k(x) - \phi_k(x'))$.

The process of choosing the function ϕ is illustrated in Section 4 for the case where there is one variable $\alpha = \langle \hat{A} \rangle$, with $\hat{A}$ proportional to the mass centre of one component of a binary mixture. Such a model may appear artificial, but the integrals to be evaluated can be done exactly, and one obtains algebraic equations of finite order for the parameters d_1 and d_2 in ϕ. This model belongs to classical unextended thermodynamics and adds weight to the use of reciprocity in classical nonlinear problems.

In extended thermodynamics, we require at least two state variables, α and $\eta = \dot{\alpha}$. We take in Section 5 the same model for $\hat{A}$ used in Section 4. However, D in (36a) depends on $A^\dagger \equiv (i\hat{L})^2 \hat{A}$ rather than on $\dot{A}$ as in (5a) and in the unextended model of Section 4. If $\hat{P}A^\dagger$ is to depend on ϕ, then ϕ must depend on configuration co-ordinates and not solely on momenta as in Section 4. Otherwise, the ϕ-dependence cancels between numerator and denominator in $\hat{P}$. Since $A^\dagger$ is a sum

of forces F_i, the integrals in $\hat{P}A^{\dagger}$ can be evaluated using a Gaussian fluctuation-theoretic distribution for the values of the forces. This is justifiable because in $\hat{P}$ we are calculating averages of fluctuations in a constrained equilibrium state. As argued in Section 2, $\alpha_2 = \alpha_2^e$ automatically, and so we need only one parameter $\tilde{d}_1$ to make $\alpha_j = \alpha_j^e$ for $j = 2, 4$.

The foregoing calculations are the latest in a series designed to show that the original formulation of de Groot [14], which postulated a Gibbs equation and reciprocity, can be carried over to the extended and non-linear regimes. These papers began by generalizing the work of Zwanzig [12] to the linear extended case [15]. A similar procedure was used [16] to justify use of reciprocity in the non-linear extended regime for a microcanonically-distributed system. By making use of the work of Grabert, the latter calculation was generalized [9] to the case of a system in equilibrium with a heat bath. In the present paper, we show that one can relax the Markovian approximation and the ansatz (37) of [9]. This paves the way for re-erecting reciprocity to the status of a basic postulate of non-equilibrium thermodynamics.

The resulting formalism, starting with an application [17] to viscoelasticity, was used to calculate liquid transport coefficients from molecular models [18]. More recent applications [19–22] have estimated the magnitude of non-linear effects in chemical reactions and steady-state transport. The aims of these applications differ from those in alternative formulations [3] which do not use reciprocity. There one is interested in the rigorous derivation of rheological kinetic equations with coefficients fitted to experiment rather than estimated from microscopic models.

References

1. H. Grad, Commun. Pure Appl. Math., *2*, 331, 1949.
2. S. Chapman and T. G. Cowling, The Mathematical Theory of Non-Uniform Gases, Cambridge University Press, Cambridge, 1952.
3. D. Jou, J. Casas-Vázquez and G. Lebon, Repts. Progr. Phys., *51*, 1105, 1988.
4. G. Lebon, Bull. R. Soc. Belg. Class. Sci., *64*, 456, 1978.
5. L. S. Garcia-Colin, Far from Equilibrium (Lecture Notes in Physics 132) ed. L. Garrido, Springer, Berlin, 1980.
6. H. Grabert, Projection Operator Techniques in Nonequilibrium Statistical Mechanics, Springer, Berlin, 1982.
7. E. T. Jaynes, Phys. Rev., *106*, 620, 1957.
8. E. T. Jaynes, Phys. Rev., *108*, 171, 1957.
9. R. E. Nettleton and E. S. Freidkin, Physica A, *158*, 672, 1989.
10. B. C. Eu, J. Chem. Phys., *73*, 2958, 1980.
11. R. Zwanzig, J. Chem. Phys., *33*, 1338, 1960.
12. R. Zwanzig, Phys. Rev., *124*, 983, 1961.
13. R. E. Nettleton, Phys. Rev., A *42*, 4622, 1990.
14. S. R. de Groot, Thermodynamics of Irreversible Processes, North-Holland, Amsterdam, 1951.
15. R. E. Nettleton, J. Chem. Phys., *40*, 112, 1964.
16. R. E. Nettleton, Physica A, *132*, 143, 1985.
17. R. E. Nettleton, Phys. Fluids, *2*, 256, 1959.
18. J. Casas-Vázquez, D. Jou and G. Lebon, Recent Developments in Nonequilibrium Thermodynamics, Springer, Berlin, 1984; Chapter I.

19. R. E. Nettleton, J. Phys. A: Math. Gen., *20*, 4017, 1987.
20. R. E. Nettleton, J. Non-Equilib. Thermodyn., *12*, 273, 1987.
21. R. E. Nettleton, Il Nuovo Cimento, *101*B, 53, 1988.
22. R. E. Nettleton, J. Phys. A: Math. Gen., *22*, 5281, 1989.

Acta Physica Hungarica 72 (2-4), pp. 295–301 (1992)

SHELL MODEL CALCULATIONS FOR ALKALI HALIDE MOLECULES

S. Y. YOUSIF and A. N. IMTANI

Department of Physics, College of Science, University of Basrah
Basrah, Iraq

(Received 1 December 1992)

This work applies the shell model to study the behaviour of the internuclear interactions of diatomic alkali halide molecules from data given by the dynamical models for alkali halide crystals. Our interest is to test the breathing shell model when core holes have been introduced. This will provide another source of information on the nature of the interaction potential between anion and cation systems and give insight into the rate of relaxation in determining shifts in Auger and photoelectron spectroscopy.

Introduction

It is well known that environmental shifts in photoelectron (PES) and Auger (AES) spectroscopies are due both to chemical shifts characterising the initial state and to final state relaxation shifts [1–5]. In specifying shifts in elemental solids and related compounds the free atom is often used as reference; then PES and AES are combined to isolate the so called extra-atomic relaxation, a quantity which is independent of experimental energy reference [6–10]. The modified Auger parameter α' [11–15] gives similar information.

Alkali halide molecules are attractive systems for investigation, because the interatomic forces are well understood in the initial state, and it appears that chemical shift and relaxation are of comparable importance in their electron spectroscopy. Recently Banna et al [16–19] have made elegant measurements of the binding energies of various Cs halide molecules in gas phase, while Aksela et al [20–21] have performed innovative experiments to provide corresponding Auger data. The Cs binding energies and Auger shifts are small relative to the free Cs atom, but show a distinctive trend through the molecular series. It is the objective of this paper to gain insight into the interactions in inner core ionised alkali halide molecules through a hierarchy of potential models, (1) rigid ion models with no electronic polarisation; (2) Rittner potential models [1]; (3) a shell model of the type previously used by Sangster [12–15] in evaluating initial state properties.

It will be shown that repulsive and polarisation potentials are intimately linked, and that an understanding of how repulsive interactions change in the presence of core holes is of crucial importance in interpreting the electron spectroscopic data.

(a) Rittner model

The influential Rittner potential [1] assumes the ions to be polarisable spherical charge distributions with full ionicity, and it is usually of the form:

$$U(r) = -\frac{1}{4\pi\epsilon_0}\left[\frac{1}{r} + \frac{\alpha_+ + \alpha_-}{2r^4} + \frac{2\alpha_+\alpha_-}{r^7}\right] - \frac{C}{r^6} + R(r), \tag{1}$$

where α_+ and α_- are the polarisabilities of the alkali ion and halogen ion, respectively, $R(r)$ is a two parameter repulsion term (usually Born–Mayer). The second and third terms represent a dipole–dipole and a quasi-elastic energy stored in the induced dipole moments, and are valid for internuclear separation large compared with ion dimension.

The Rittner model and its modified version have been employed by a number of investigators in the calculation of the molecular properties (dissociation energies, vibrational frequencies, and other physical properties) through analytical modelling of the interionic forces in diatomic ionic molecules and by using formulae such as those of Dunham [2] and Varshni and Shukla [3].

In spite of the success of the Rittner model and its related modifications, however, the model is inconsistent in that it does not include the higher order polarisabilities, while the exponential form of the repulsion interaction may lead to an inaccurate representation to the attractive potential as was discussed by Brewer and Brackett [4]. Another question concerns the value of the polarisability of the alkali halide ions used, since it is known that the polarisability of an anion is decreased in the Coulomb field of a cation, while that of a cation increased in the Coulomb field of an anion. Shanker et al [5] used values calculated for ions in molecular alkali halides. Recently Szymaski and Matthew [6] compared various different sets of the polarisabilities in different environments, and found that binding energy predictions are relatively intensive to the polarisability value chosen. The more rapidly varying repulsive potential is capable of compensating for changes in the attractive polarisation term. On the other hand, Szymanski and Matthew found that the use of various models for the repulsive term leads to a wide variation in calculated binding energies.

(b) The shell model

In order to analyse the interactions in alkali halide molecules in a more consistent way, it is important to go beyond the Rittner model. A quantum mechanical calculations has been attempted by Brumer and Karplus [7], and also by Matcha [8]. Another approach is to use what is called the shell model. The simplest form of the shell model was first formulated by Dick and Overhauser [9] to account for dielectric properties of alkali halides. It separates the ion into a core and a shell coupled by a spring and has proved a very useful classical parameterisation of inter-ionic force

constants. Cochran [10] has reviewed the use of such model in the parameterisation of the lattice dynamics of ionic crystals, while Schroder [11] has extended the model by introducing shell breathing. Sangster [12], however, used the breathing shell model to study the properties of diatomic molecules. The information required to parameterise the model is available from data of elastic and dielectric constants from dynamical models of alkali-halide crystals. The diatomic molecule was considered to contain a positive ion, which to first order can be considered as a point charge $(+e)$ and a negative ion contains a rigid shell of charge (Ye) and a core of charge (Xe), where $X+Y=-1$. In the presence of an electric field the shell centre will be displaced by distance w, and the total potential $\Phi(R,w,\zeta)$ can be described by the different contributions; electrostatic, polarisation, deformation, and short range interactions:

$$\Phi(R,w,\zeta)=\phi_{\text{es}}(r,w)+\phi_{\text{pol}}(w)+\phi_{\text{def}}(\zeta)+\phi_{\text{int}}(R,\zeta), \tag{2}$$

where $\phi_{\text{pol}}(w)=\frac{1}{2}kw^2$, $\phi_{\text{def}}(\zeta)=\frac{1}{2}h_2\zeta^2$ for anisotropic deformation, $\phi_{\text{def}}(b)=\frac{1}{2}G_2(\rho-\overline{\rho}_0-b)^2$ for anisotropic deformation and

$$\phi_{\text{int}}(R,\zeta)=B_{+-}\exp(-\alpha_{+-}r)-\frac{C_{+-}}{r^6}-\frac{D_{+-}}{r^8}.$$

(See Sangster [15] for details of the various parameters).

Results and discussion

The main objective of this work is to apply the Rittner model and the shell model to the problem where the alkali ion in a diatomic molecule has one core hole (XPS final state, Auger initial state), or two core holes (Auger final state). Recent experimental and theoretical data [16–21] make it possible to test both these models for XPS and Auger transitions. The excited states involved are very short lived so that change in nuclear position during the transitions may be neglected. The different parameters of the shell model (d_0, w_0, R_0 and D) for some alkali halide molecules are shown in Tables I and II with the alkali ion having one or two core holes. In the various different contributions to Eq. (2), the Coulomb charge is now increased by one or two, while for the short range interaction three assumptions have been considered: (i) full repulsion as in the ground state; (ii) half repulsion i.e. B^{+-} in Eq. (2) reduced to half the ground state value; (iii) zero repulsion.

Table III shows the calculated binding energies for CsX structure obtained using both the shell model with the same assumption as discussed above, and the Rittner model. These are compared with the experimental data of Mathews et al [17]. In general there is 0.5 eV shift between the Rittner model values and the experimental ones, while the shell model values suggest that CsCl and CsBr have lost some of the repulsion in the final state, while for CsF and CsI full repulsion gives better agreement with experiment. However, in the shell model calculations

Table I

Shell model values for internuclear distances and binding energies for some alkali halide molecules when the alkali ion has one core hole

	d_0 (nm)	w_0 (nm)	R_0 (nm)	D (eV)
		(a) full repulsion		
NaCl	0.243	0.031	0.212	13.60
LiF	0.156	0.042	0.114	20.45
KI	0.307	0.040	0.267	11.03
NaBr	0.253	0.049	0.204	13.61
NaI	0.276	0.067	0.209	12.86
KBr	0.286	0.032	0.254	11.55
CsF	0.234	0.013	0.221	11.48
CsCl	0.304	0.022	0.282	9.79
CsBr	0.318	0.027	0.291	9.57
CsI	0.342	0.033	0.309	9.20
		(b) half repulsion		
NaCl	0.243	0.039	0.204	14.51
KI	0.307	0.048	0.259	11.81
NaBr	0.253	0.069	0.184	15.24
KBr	0.286	0.039	0.247	12.30
CsF	0.234	0.018	0.216	12.33
CsCl	0.304	0.027	0.277	10.30
CsBr	0.318	0.034	0.284	10.10
CsI	0.342	0.041	0.301	9.70
		(c) zero repulsion		
NaCl	0.243	0.054	0.189	15.78
KI	0.307	0.062	0.245	12.74
KBr	0.286	0.050	0.236	13.34
CsF	0.234	0.027	0.207	13.42
CsCl	0.304	0.033	0.271	10.84
CsBr	0.318	0.044	0.274	10.72
CsI	0.342	0.054	0.288	10.35

it was assumed that only the negative ions are polarisable and an extension of the Sangster model is needed for dealing with the Cs halides.

For the Auger transition, Aksela and Aksela [20] have reported a theoretical relativistic Auger energy for free Cs^+: $M_4\ N_{4,5}\ N_{5,5}(^1G_4) = 552.52$ eV. This calculated value exceeds the experimental value by approximately 1.7 eV. Using a corrected Auger energy estimated (550.8 eV), we have calculated Auger energies for CsX molecules using both the Rittner model and the shell model. For the shell model the binding energy values listed in Tables I, II have been used. For the Rittner model, full repulsion in assumed in these calculations. These results are shown in Table IV together with the theoretical and experimental data of Aksela et al [21]. It is clear from these data that the relaxation energies calculated in the shell model are similar to the ionic model if the same repulsion assumptions are assumed, but for detailed comparison to gain insight into the various interaction

Table II
Shell model values for internuclear distances and binding energies for some alkali halide molecules when the alkali ion has two core holes

	d_0 (nm)	w_0 (nm)	R_0 (nm)	D (eV)
		(a) full repulsion		
NaCl	0.243	0.053	0.190	23.40
KI	0.307	0.074	0.233	19.75
KBr	0.286	0.057	0.229	20.15
CsF	0.234	0.026	0.208	18.54
CsCl	0.304	0.038	0.266	15.90
CsBr	0.318	0.047	0.271	15.70
CsI	0.342	0.057	0.285	15.30
		(b) half repulsion		
NaCl	0.243	0.069	0.174	25.75
KI	0.307	0.101	0.206	21.93
KBr	0.286	0.073	0.213	21.96
CsF	0.234	0.034	0.200	19.74
CsCl	0.304	0.046	0.258	16.70
CsBr	0.318	0.060	0.258	16.70
CsI	0.342	0.073	0.269	16.40
		(c) zero repulsion		
CsF	0.243	0.052	0.182	21.60
CsCl	0.307	0.064	0.240	17.90

Table III
Calculated ($Cs3d_{5/2}$) binding energies in CsX (X = F, Cl, Br or I) (eV)

	Shell model			Rittner	Expt.
	(a)	(b)	(c)	model	(d)
CsF	731.1	730.2	729.1	730.6	731.1
CsCl	732.0	731.6	731.0	731.2	731.7
CsBr	732.1	731.6	731.0	731.4	731.7
CsI	732.3	731.8	731.1	731.6	732.2

(a) using full repulsion
(b) using half repulsion
(c) using zero repulsion
(d) Experimental values of Mathews et al [17]

terms in the Auger transition, more experimental data and theoretical calculations are required.

Summary

In this work two models of the environmental shift in the photoelectron and Auger spectra of alkali halide molecules have been compared:
(1) the ionic model;
(2) the shell model.

Table IV
Calculated Auger energies E_{AUG} ($M_4N_{4,5}N_{5,5}$:$^1G_4$) (eV)

	Shell model					Rittner model		
	(a)	(b)	(c)	(d)	(e)		(f)	(g)
Cs(CsF)	557.9	559.1	560.9	558.2	560.0	557.8	557.2	558.64
Cs(CsCl)	556.9	557.7	558.9	557.2	557.0	557.1	556.0	558.59
Cs(CsBr)	557.0	558.0	–	557.4	–	556.8	555.8	558.77
Cs(CsI)	557.0	558.0	–	557.5	–	556.6	555.4	559.00

(a) using full repulsion initial state and full repulsion final state
(b) using full repulsion initial state and half repulsion final state
(c) using full repulsion initial state and zero repulsion final state
(d) using half repulsion initial state and half repulsion final state
(e) using half repulsion initial state and zero repulsion final state
(f) theoretical data of Aksela et al [21]
(g) experimental data of Aksela et al [21]

Though very similar in many ways the basic difference between them is that for the Rittner model the polarisation/relaxation contribution to the binding energy is independent of the repulsive contribution, while in the shell model the repulsion energy between shell changes when a shell is displaced in an electric field. For the ground state the two models give comparable predictions of binding energy, even so the shell model has been parameterised from crystal data.

In the final state of photoelectron emission or Auger emission the difficulty is in estimating the residual repulsion energy between ions. The ion with the core hole shrinks, decreasing overlap, but the neighbouring ion deforms tending to increase overlap. The excited states are short lived so that changes in nuclear positions are not involved. From the work by Brewer and Brackett [4] and Szymanski and Matthew [6] on the ground state it is clear that the repulsive potential is not wholly repulsive, but mops up deficiencies in the attractive components in the potential. This may happen to an even greater extent in the excited states, where higher order polarisabilities, not considered explicitly in the potential, will become increasingly important (see Matthew and Szymanski [22]).

The various different possibilities considered in the shell model suggest that repulsive energy is still of some importance even in the highly compressed Auger final state, but more work needs to be done on the question.

It is worth pointing out that when one or two core holes are introduced the displacement w of the shell relative to the core may be quite large (Tables I, II), and indeed divergence occurs in the calculation for some molecules not listed. This reflects the fact that higher order polarisability terms, neglected in the formalism, are not important.

References

1. E. S. Rittner, J. Chem. Phys., *19*, 1030, 1951.
2. J. L. Dunham, Phys. Rev., *41*, 713, 1932.
3. Y. P. Varshini and R. C. Shukla, J. Mol. Spect., *16*, 63, 1965.
4. L. Brewer and E. Brackett, Chem. Rev., *61*, 425, 1961.
5. J. Shanker, H. B. Arawal and G. G. Agrawal, J. Chem. Phys., *73*, 4056, 1980.
6. J. E. Szymanski and J. A. D. Matthew, Can J. Phys., *62*, 583, 1984.
7. P. Brumer and M. Karplus, J. Chem. Phys., *58*, 3903, 1973.
8. R. L. Matcha, J. Chem. Phys., *48*, 335, 1968; *63*, 4490, 1970.
9. B. G. Dick and A. W. Overhauser, Phys. Rev., *112*, 90, 1958.
10. W. Cochran, Proc. R. Soc. (London), *A253*, 495, 1959.
11. U. Schroder, Sol. State Comm., *4*, 347, 1966.
12. M. J. L. Sangster, J. Phys. Chem. Solids, *34*, 355, 1973.
13. M. J. L. Sangster, J. Phys. Chem. Solids, *35*, 195, 1974.
14. M. J. L. Sangster, Sol. Stat. Comm., *18*, 67, 1976.
15. M. J. L. Sangster, Sol. Stat. Comm., *15*, 471, 1974.
16. R. D. Mathews, R. J. Key, A. Sur, C. S. Ewing and M. S. Banna, J. Chem. Phys. *74*, 5407, 1981.
17. R. D. Mathews, A. R. Slaughter, R. J. Key and M. S. Banna, J. Electr. Spectr., *26*, 271, 1982.
18. R. D. Mathews, A. R. Slaughter, R. J. Key and M. S. Banna, J. Chem. Phys., *78*, 62, 1983.
19. M. S. Banna, R. J. Key and C. S. Ewing, J. Electr. Spectr., *26*, 259, 1982.
20. S. Aksela and H. Aksela, Chem. Phys. Lett., *94*, 592, 1983.
21. S. Aksela, H. Aksela and S. Leinoneu, J. Electr. Spect., *35*, 1, 1984.
22. J. A. D. Matthew and J. E. Szymanski, J. Electr. Spect., *33*, 73, 1984.

Acta Physica Hungarica 72 (2-4), p. 303 (1992)

BOOK REVIEWS

George de Hevesy, 1885–1966, Festschrift. Ed. György Marx
Akadémiai Kiadó, Budapest, 1988

The George de Hevesy's centennial was celebrated at an international conference held in Budapest in 1985. Hevesy, one of the most outstanding scientists of Hungarian origin, received the Nobel Prize from chemistry in 1943 "for his work on the use of isotopes as tracers in the study of chemical processes" and was famous also for the discovery of hafnium (1923) and for neutron activation analysis (1934). He was born in Budapest. In 1918–19, for a short period of time, he became Professor of Physics at the Budapest University. After 1920 he worked in Copenhagen, Freiburg and Stockholm, died in Freiburg in 1966.

The thin (165 pages) volume the texts of some of the lectures delivered at the Conference, together with the chronology of Hevesy's life and the bibliography of his printed works which consists of 397 items. The significance of the book and the event was underlined by the list of the distinguished authors, including two Nobel prize winners: Rudolf L. Mössbauer and Kai Siegbahn. The former wrote about the history of his gamma resonance method, the latter about electron spectroscopy with special regard to the purpose of chemical analysis. Vitalii I. Goldanski's paper also discusses the Mössbauer spectroscopy, but its more advanced form. Ferenc Mezei spoke and wrote about his major work on the neutron spin echo.

All these papers are more or less connected to Hevesy's favourite subjects (particularly, spectroscopy), while the one, co-authored by Gustav Arrhenius and Hilde Levi, is connected to Hevesy not only by the subject (cosmochemistry and geochemistry) but by the authors' personality also. Levi was Hevesy's collaborator for a while, and Arrhenius is his son-in-law. The volume contains two papers on George de Hevesy himself: by György Marx on his scientific achievements of highest significance, and by Gábor Palló on his times and works in Hungary.

G. Palló

Acta Physica Hungarica 72 (2-4), p. 305 (1992)

CORRIGENDA

EVALUATION OF EXPLICIT EXPRESSIONS FOR MEAN CHARACTERISTICS OF ATOMIC SPECTRA

R. KARAZIJA

Institute of Theoretical Physics and Astronomy
2600 Vilnius, Lithuania

(Acta Phys. Hung., *70*, pp. 367–379, 1991)

The equation (28) for N multiplier should read:

$$\mathcal{N} = (-1)^{h+\sum_i t_i} \prod_i \binom{\Omega_i}{N_i}^{-1} \binom{\Omega_i - p_i}{N_i - t_i}, \quad N_i \geq t_i, \tag{28}$$

where h is the number of loops in the diagram.

CONTENTS

Volume 72

CONDENSED MATTER

ASTROPHYSICS

CLASSICAL AND APPLIED PHYSICS

INTERDISCIPLINARY

Physics

Spacetime without Reference Frames

by
T. MATOLCSI

In the concept of this book spacetime is the fundamental notion; the points of spacetime are structured with the assumption of absolute time and absolute velocity of light resulting in the non-relativistic and special relativistic case, respectively. This gives the possibility of developing both the non-relativistic and the special relativistic chapters along the same notions: world line, observer, splitting of spacetime to space and time, reference frames, splitting of classical fields to spacelike and timelike components, the symmetry groups of spacetime (the Galilean and the Poincaré group).
The book contains lots of examples with detailed calculations through which the reader can clearly understand the connection between the traditional way of thinking and the new way of handling the problems presented in the book; the well-known special relativistic paradoxes are treated in detail. In the general relativistic case, only the basic thoughts are expressed.
The mathematics involved is rather simple and it is summarized in the second part of the book.

This book is an enlarged and revised version of "A concept of Mathematical Physics — Models for Space-Time" by T. Matolcsi

In English. 1992. Approx. 400 pages. Numerous figures. 17 x 25 cm. Hardbound.
Approx. $ 50.00

Akadémiai Kiadó, Budapest

Manuscript received by Akadémiai Kiadó:
3 November 1992
Manuscript received by TYPOTEX Ltd for TEX typesetting:
9 November 1992
Date of publication: 30 March 1993
PRINTED IN HUNGARY
Akadémiai Kiadó és Nyomda Vállalat
Budapest

NOTES TO CONTRIBUTORS

I. PAPERS will be considered for publication in Acta Physica Hungarica only if they have not previously been published or submitted for publication elsewhere. They may be written in English, French, German or Russian.

Papers should be submitted to

Prof. I. Kovács, Editor
Department of Atomic Physics, Technical University
1521 Budapest, Budafoki út 8, Hungary

Papers may be either articles with abstracts or short communications. Both should be as concise as possible, articles in general not exceeding 25 typed pages, short communications 8 typed pages.

II. MANUSCRIPTS

1. Papers should be submitted in three copies.
2. The text of papers must be of high stylistic standard, requiring minor corrections only.
3. Manuscripts should be typed in double spacing on good quality paper, with generous margins.
4. The name of the author(s) and of the institutes where the work was carried out should appear on the first page of the manuscript.
5. Particular care should be taken with mathematical expressions. The following should be clearly distinguished, e.g. by underlining in different colours: special founts (italics, script, bold type, Greek, Gothic, etc.); capital and small letters; subscripts and superscripts, e.g. x^2, x_3; small *l* and l; zero and capital O; in expressions written by hand: *e* and *l*, *n* and *u*, *v* and v, etc.

A List of Symbols on a separate sheet should be attached to each paper.

6. References should be numbered serially and listed at the end of the paper in the following form: J. Ise and W. D. Fretter, Phys. Rev., *76*, 933, 1949.

For books, please give the initials and family name of the author(s), title, name of publisher, place and year of publication, e.g.: J. C. Slater, Quantum Theory of Atomic Structures, I. McGraw-Hill Book Company, Inc., New York, 1960.

References should be given in the text in the following forms: Heisenberg [5] or [5].

7. Captions to illustrations should be listed on a separate sheet, not inserted in the text.
8. In papers submitted to Acta Physica all measures should be expressed in SI units.

III. ILLUSTRATIONS AND TABLES

1. Each paper should be accompanied by three sets of illustrations, one of which must be ready for the blockmaker. The other sets attached to the copies of the manuscript may be rough drawings in pencil or photocopies.
2. Illustrations must not be inserted in the text.
3. All illustrations should be identified in blue pencil by the author's name, abbreviated title of the paper and figure number.
4. Tables should be typed on separate pages and have captions describing their content. Clear wording of column heads is advisable. Tables should be numbered in Roman numerals (I, II, III, etc.).

IV. RETURN OF MATERIAL

Owing to high postage costs, the Editorial Office cannot undertake to return *all* material not accepted for any reason for publication. Of papers to be revised (for not being in conformity with the above Notes or other reasons) only *one* copy will be returned. Material rejected for lack of space or on account of the Referees' opinion will not be returned to authors outside Europe.